Durham E-Theses

Development of Targeted Therapeutics for the Treatment of Glioblastoma

JAIN, MOHIT,LAXMILAL

Development of Targeted Therapeutics for the Treatment of Glioblastoma

Assessment of expression and activity of Matrix Metalloproteinases (MMPs) in human gliomas and rationalised computer-aided design of peptide-conjugated chemotherapeutics as probes for evaluating MMP mediated tumour-selective drug release from nanostructure implants

Mohit Laxmilal Jain

Submitted for the degree of Doctor of Philosophy

School of Medicine, Pharmacy and Health

Durham University

2017

Abstract

Development of Targeted Therapeutics for the Treatment of Glioblastoma

Mohit Jain

Glioblastoma is the most aggressive cancer of the brain. Despite recent advances in cancer biology and multimodality therapies, such as surgery, radiotherapy and chemotherapy, the outcome of patients with high grade glioma remains fatal. The major drawback of current glioma chemotherapeutics is their inability to cross the blood brain barrier, lack of tumour specificity agents and their consequent side effects. Matrix metalloprotease (MMP) activity is central to cancer development, angiogenesis and invasion. They are highly active in the tumour environment and absent or inactive in normal tissues, therefore they represent viable targets for cancer drug discovery. A better understanding of the role of MMPs in human gliomas could potentially have diagnostic, prognostic and therapeutic implications. This study aims to assess the expression of specific MMPs in preclinical human glioma models and clinical glioma samples; evaluate *in silico* docking to rationalise substrate binding preferences of homologous MMPs; rationally design MMP-subtype-selective tumour activated prodrugs; and determine the feasibility of targeting MMP-selective anticancer prodrugs conjugated to graphene oxide as a local drug delivery approach for glioblastoma.

This study found significant overexpression of MMP-10 in glioma relative to histologically normal brain tissues. Strong correlation was observed between MMP-10 protein and gene expression of glioma cell lines relative to low expression in a normal brain cell line. MMP-10 activity, as measured by fluorogenic substrate cleavage assay, also demonstrated a strong correlation between MMP-10 activity and gene expression levels.

Following demonstration of selective overexpression of MMP-10 in glioma, a reiterative *in silico* proteolytic docking coupled *in vitro* biochemical assessment was utilised to rationalise functional similarity and differentiate substrate binding selectivity of homologous MMPs. The binding modes of MMP-substrates within the active site of closely related MMPs were able to accurately predict the cleavage subsites by specific MMPs, as confirmed by *in vitro* cleavage assay. The success of computational and experimental methodology provided a robust tool for identifying MMP-subtype differences and subsequent development of MMP-10 selective peptide prodrugs.

MMP-subtype selective and MMP-10 selective prodrugs were designed by rational exploitation of MMP-docked complexes of substrates. Peptide residues were modified to achieve selectivity for MMP-2 and MMP-10 (over MMP-3 and MMP-9) demonstrating predicted cleavage at distinct subsites. This selectivity was further exploited to attain MMP-10 selectivity, over MMP-2, MMP-3 and MMP-9. The

rationally designed peptide prodrugs were synthesised and were shown to be preferentially cleaved by MMPs at predicted subsites and demonstrated no activation by engineered-out MMPs, as predicted. Compared to MJ02 (MMP-2 and MMP-10 selective doxorubicin prodrug), MJ04 (MMP-10 selective doxorubicin prodrug) demonstrated selective metabolism by glioma cell lines to release chemotherapeutic agents. This therapeutic approach against glioma cell lines depended upon the involvement of MMPs, confirmed using pharmacological inhibition. MJ04 demonstrated negligible activity in the presence of an MMP-10 selective inhibitor, suggesting MMP-10 selective activation of the prodrug in glioma cells relative to normal glial cells.

Following successful development of MMP-10 selective prodrugs, the feasibility of targeting glioma tumour with local delivery of chemotherapeutics from functionalised graphene-oxide tethered prodrug implants, was assessed as a therapeutic strategy to circumvent the blood brain barrier. Graphene oxide conjugated prodrug was synthesised which is shown to be preferentially cleaved in MMP expressing glioma cell lines relative to normal glial cells. This study demonstrates that MMP-10 is overexpressed in glioblastoma and can be used to metabolise anticancer prodrugs that can be activated selectively by local tumour environment.

Table of Contents

List of Abbreviations

1321N1	Grade II Human Astrocytoma cell line
ABC	ATP-binding Cassette
AGT	O^6-alkylguanine DNA-alkyltransferase
AMBER	Assisted Model Building with Energy Refinement force field
AQP4	Aquaporin 4
BBB	Blood Brain Barrier
BCNU	Bis-chloroethynitrosourea
cDNA	Complimentary Deoxyribonucleic Acid
CFF	Consistent Force Field
CHARMM	Chemistry at HARvard Macromolecular Mechanics force field
CNS	Central Nervous System
CSCs	Cancer Stem Cells
CSF	Cerebrospinal Fluid
DCM	Dichloromethane
DIPEA	N,N-Diisopropylethylamine
DMEM	Dulbecco's Modified Eagle Medium
DMF	Dimethylformamide
ECM	Extracellular Matrix
EGFR	Epidermal growth Factor Receptor
EMEM	Eagle's Minimal Essential Medium
Et2O	Diethyl Ether

GBM	Glioblastoma Multiforme
H460	Human Non-Small Cell Lung Carcinoma cell line
HCO2H	Formic Acid
HNSCC	Head and Neck Squamous Cell Carcinoma
Hof	Homophenylalanine
HPLC	High Performance Liquid Chromatography
HT1080	Human Fibrosarcoma
ICP	Intracranial Pressure
IHC	Immunohistochemistry
LCMS	Liquid Chromatography - Mass Spectrometry
MCF7	Human Breast Cancer cell line
MD	Molecular Dynamics
MDR	Multidrug Resistance protein
MeCN	Acetonitrile
MGMT	O6-methyl guanine DNA-methyltransferase
MM	Molecular Mechanics
MMFF	Merck Molecular Force Field
MMPIs	Matrix metalloprotease Inhibitors
MMPs	Matrix Metalloproteases
M-MuLV	Moloney Murine Leukaemia Virus
MT-MMPs	Membrane Type-Matrix Metalloproteases
MTT	3-(4,5-Dimethylthiazol-2-yl)-2,5-diphenyltetrazolium Bromide
NF-KB	Nuclear Factor Kappa-light-chain-enhancer of activated B cells
NSC	Non-Crystallographic Symmetry

NSCLC	Non-Small Cell Lung Carcinoma
OAPs	Orthogonal Array of Particles
PDB	Protein Data Bank
P-gp	P-Glycoprotein
PKC	Protein Kinase C
PNET	Primitive Neuroectodermal tumour
PyBOP	benzotriazol-1-yloxytripyrrolidinophosphonium hexafluorophosphate
QSAR	Quantitative Structure Activity Relationship
RPMI	Roswell Park Memorial Institute medium
RT-PCR	Reverse Transcription-Polymerase Chain Reaction
SVG-P12	Human Foetal Glial cell line
TFA	Trifluoroacetic Acid
TIMPs	Tissue Inhibitor of Metalloproteases
TMZ	Temozolomide
U87-MG	Grade IV Human Glioblastoma Astrocytoma cell line
VEGF	Vascular Endothelial Growth Factor
WHO	World Health Organisation

Statement of Copyright

The copyright of this thesis rests with the author. No quotation from it should be published without the author's prior written consent and information derived from it should be acknowledged.

Acknowledgements

I would like to express my sincere appreciation and gratitude towards my supervisors Dr. Jason Gill, Dr. David Berry and Dr. Jonathan Harburn, for giving me the opportunity to work with them, and for providing continued support, encouragement, collegiality, mentorship and invaluable suggestions throughout this exciting project.

I would also like to thank all my research colleagues who helped me in difficult times and gave me motivation to complete this project. I would like to thank all the members of staff at the School of Medicine, Pharmacy and Health for their assistance and helpful feedback throughout my project.

Special thanks to my parents and close friends for their unconditional support and love over the years. Completion of this project would not have been possible without you.

Dedication

This thesis is dedicated to the memory of my mother Chanda Jain, who I miss every day. Throughout her lifetime she taught me the value of education and helping people in need.

This thesis is dedicated to my father Laxmilal Jain, a selfless person who always placed my happiness first. Thank you for teaching me to believe in myself and in my dreams.

This thesis is dedicated to my sister Divya, a smart woman, who I hope, would be proud of my achievement.

Chapter 1: Introduction

1.1 Cancer

Cancer is a complex and heterogenic disease that can exhibit a broad range of physiological, genetic and histological perturbations in all of the body systems. Cancer develops from normal cells that acquire the ability to proliferate uncontrollably and ultimately become malignant.[1] Malignancy, by definition, allows the cancer cells to invade surrounding normal tissue and metastasise to vital organs resulting in disseminated disease state. Unlike many other diseases, in its early stages cancer is often asymptomatic and remains hidden, with the problem only being identified later in the process once the cancer has become symptomatic and noticeable by the patient. Unfortunately, by this stage the cancer is commonly aggressive and in many cases, has disseminated to other sites within the body. As a consequence cancer is often life-threatening with patients having a poor prognosis and significantly reduced life expectancy.[2]

In terms of development and progression towards life-threatening disease, cancer has been characterised as having six well-defined hallmarks. More recently a further four enabling characteristics have been identified; these account for the specific requirements of the cancers existence and thus can be exploited as targets for therapeutic cancer treatment.[3, 4] The first four of the hallmarks comprising of sustained proliferative signalling, enabling replicative immortality, evading growth suppressors and resisting cell death; relate to the cancer cells ability to proliferate and survive. Whereas, the latter two hallmarks comprising of inducing angiogenesis, and activating invasion and metastasis; relate to gain of malignant potential and revolve around the central roles of extracellular proteases.[3, 4]

1.1.1 Angiogenesis

In order for the tumour to expand beyond 2-3 mm^3 it requires access to its own blood supply, before this point nutrient and oxygen are obtained from the surrounding normal vasculature which is close enough to facilitate diffusion. This physiological process by which new blood vessels are generated from existing ones is termed as angiogenesis. [3, 5, 6]

1.1.2 Invasion and metastasis

The defining factor of cancer is malignancy, the ability to disseminate from its original location to another area of the body. The invasion-metastasis cascade is a sequence of cellular biological changes of cancer cells, initiated with local invasion, intravasation into surrounding blood and lymphatic vessels, transfer through hematogenous and lymphatic systems, followed by extravasation into parenchyma of distant tissues, formation of small cancer nodules (micrometastases) and finally the progression of micrometastatic lesions into macroscopic tumours (termed as 'colonisation').[5-9] Several classes of proteins are found to be altered in cells possessing invasive and metastatic capabilities including cell-cell adhesion molecules, integrins and extracellular proteases. The activity of a set of proteases in cancer progression is known as cancer degradome. A great number of reports have suggested a strong correlation between the activity of extracellular proteases and, tumour progression, invasion and metastasis.[10, 11]

1.2   Cancer of the brain: Glioma

Malignant gliomas are the most common neoplasms of the central nervous system (CNS). They form a special group of neoplasias, with restricted tumour migration and increased tumour infiltration into normal brain tissues, for which no cure is currently available and only modest research progress has been made in understanding their biology. Their specific origin derives from the normal neural stem cells- the microglial cells, with which they share morphological characteristics and molecular markers, i.e., oligodendrocytes (oligodendrogliomas), astrocytes (astrocytomas) and ependymal cells (ependymomas).[12]

They account for 77% of all malignant primary CNS tumours. In adults, gliomas account for 29% of all brain tumours, 80% of all primary brain tumours occurring in patients 65-84 years of age. Gliomas also affect children and the most common types are astrocytomas (52%), medulloblastomas (21%), high grade gliomas (19%) and primitive neuroectodermal tumours (PNETs).[13] The World Health Organisation (WHO) developed a universally accepted system for the classification of brain tumours. This classification includes a grading system that distinguishes gliomas into different stages depending on the tumour size, the level of penetration and spread to the lymph nodes or to distant organs.[12] According to the malignancy, there are four different grades of glioma tumours: grades I (juvenile pilocytic), II (diffuse), III (anaplastic) and IV (glioblastoma multiforme) for astrocytoma; and grades II or III for oligodendrogliomas and oligoastrocytomas. Lower-grade glioma tumours (grades I and II) tend to be well-differentiated and possess few cellular atypias but in general they are closely similar to their non-neoplastic cellular counterparts. These tumour types contain specific genetic mutations with progressive initiation of additional genetic alterations.[14] This is

followed by the advancement of the tumour to higher malignancy and progression rates.[15] Higher grade tumours (grades III and IV) are anaplastic, demonstrating increased vessel density, high mitotic activity, cellular anomalies and elevated cell density. Grade IV astrocytoma, better known under the name of glioblastoma multiforme (GBM), is the most common and aggressive form of brain tumour. Glioblastomas contribute for about 60-70% of all gliomas, anaplastic astrocytomas for 10-15%; and anaplastic grade II and III type accounts for 10%. Glioblastoma samples are characterised by areas of necrosis, very high cell density, robust neoangiogensis and numerous atypical cells.[12] They are incurable, show a highly aggressive course and poor treatment response and, patients have short-term survival expectancies.[16]

1.3   Glioblastoma molecular pathophysiology

1.3.1 Epidermal growth factor receptor (*EGFR*)

The *EGFR* gene is a common driver of glioblastoma progression and is involved in the control of cell proliferation. The amplification of *EGFR* is found in nearly 40% of all glioblastoma cases and can occur by reverse transcription from RNA or insertion.[17] Essentially, all cases of *EGFR* amplification in glioblastoma are associated with EGFR overexpression, which is in contrast to the 97% of non-amplified *EGFR* glioblastomas that demonstrate no EGFR overexpression.[18]

EGFR amplification is accompanied with the presence of EGFR protein variants. 68% of EGFR mutants have deletions in the N-terminal ligand binding regions between 6 and 273 amino acids, termed EGFRvIII. Deletion in the ligand-binding regions can lead to ligand-independent activation of EGFR.[19] Common tyrosine

kinase inhibitors such as gefitinib have limited therapeutic use due to the specific nature of these exon 2-7 deletions in EGFRvIII.[20] Therefore, approaches to address the lack of extracellular receptor are currently being pursued. However, EGFRvIII is not indicative of overall median survival except in cases of ≥ 1year survival which may limit the therapeutic value of this target.[21]

1.3.2 p53 and PTEN

Tumour suppressor protein, p53, plays important role in the formation of high-grade tumours. P53 initiates DNA repair or apoptosis if the damage is irreparable.[22] There is significant correlation between the presence of mutant p53 and the advancement of low-grade astrocytoma to the high-grade glioblastoma. p53 mutant cells have the ability to expand to high-grade glioma as these cells proliferate expeditiously and overtake the non-p53 mutant cells population.[23] There is strong evidence that shows nuclear localisation is correlated with long-term survival rates since nuclear p53 is required for apoptotic induction limiting tumour expansion. Long-term survivors (>3 years) have tumours with high levels of nuclear p53 compared to short-terms survivors, and this is not caused by differences in the mutation rate.[24] Gene therapy experiments targeting glioblastoma and cancer stem cells with nanoparticle delivery of the p53 gene have showed induction of apoptosis after standard chemotherapy and improved survival in mouse models. This has not yet been tested in clinical trials.[25]

Multiple simultaneous tumour suppressor mutations are common in glioblastoma progression. Studies have found that primary tumours expressing mutant p53 had associated PTEN mutations or deletions in the majority of glioblastoma samples. PTEN is a phosphatase tumour suppressor that is mutated in glioblastomas and is

considered as prognostic indicator in patients >45 years old.[26] Under normal conditions, PTEN regulates cellular homeostasis by preventing cell cycle entry and maintaining the neural stem cell population. PTEN null mutants are sensitive to growth factors and more prone to proliferation than wild-type neural stem cells.[27] Bryostatin, an inhibitor of protein kinase C (PKC) downstream to PTEN, supressed the growth of tumours in non-sense PTEN background, suggesting that PTEN non-sense mutations can be indirectly targeted for glioblastoma therapy.[28]

1.4   Role of angiogenesis and invasion in glioma

Glioblastoma growth is closely linked with the formation of new blood vessels and one of the most serious clinical obstacles are the development of vasogenic brain oedema and intracranial pressure (ICP) due to blood brain barrier (BBB) leakage.[29] Glioblastomas are the most vascularised tumours in humans and the grade of malignancy is directly related to endothelial proliferation. The vessel formation is highly defective with abnormal morphology and function. Histological samples show vessels with heterogeneous distribution, irregular basal lamina, variable diameters and permeability.[30-32] One of the widely accepted arguments to explain disorganised vessel formation in GBM is the proportionately high amount of vascular epidermal growth factor (VEGF) present in the tumours.[33] VEGF is one of most studied molecules in angiogenesis and acts as a hypoxia-inducible factor; the areas expressing highest levels of VEGF are also the regions of necrotic core. VEGF overexpression in GBM is responsible for the crosstalk between the tumour and the endothelial cells in order to promote angiogenesis.[34]

Besides strong angiogenic potential of glioblastomas, they are also highly infiltrative and diffuse, with different degrees of invasiveness.[35] The tumours can penetrate the brain by colonising the entire organ and sending their invasive tumour cells far beyond the main tumour mass. The invasion of gliomas into the brain parenchyma is characterised by preferential migration along white matter tracts around neurons, blood vessels and spread in subpial region. Despite the considerable invasive potential of gliomas, they seldom leave the nervous tissue to metastasise into other organs, remaining restricted in the skull, with only little evidence of systemic spread.[12] The invasive properties of malignant brain tumours are of great clinical significance, as they are actively responsible for poor prognosis in patients. This invasive and infiltrative property of glioma tumours is primarily caused by the perturbation of factors and enzymes present in the extracellular matrix (ECM) of the brain. The ECM of the brain is dysregulated primarily due to the disruption of the blood-brain barrier which is the 'first line of defence' against impairment of central nervous system function.[36]

1.5   Pathophysiological barriers of glioblastoma

Solid tumours are commonly treated with surgical resection in conjunction with radiotherapy and systemic chemotherapeutic agents. A vast majority of chemotherapeutic agents used within the clinic are alkylating agents, anthracyclines and antimetabolites broadly termed as cytotoxic chemotherapy. These agents can be used at different stages of cancer progression and are generally directed at targeting nucleic acid replication or synthesis, many of which have been approved for clinical use since the 1960s.[37, 38] Mechanistically these agents do not exclusively target cancer cells, and will also attack any rapidly

proliferating cell type such as those in the digestive tract and bone marrow; resulting in systemic toxicity. A prerequisite for the effective delivery of any cancer drug is that it reaches the tumour-site in therapeutic concentrations. This is difficult to achieve in most solid tumours because of pathological factors such as abnormal tumour vasculature, intra-tumoural pressure gradients and variable hypoxia.[37, 38] In glioma, the situation is further complicated by the presence of the blood-brain barrier (BBB), which acts as a physiological and physical obstacle for delivery of drugs to the central nervous system.[36]

1.5.1 The healthy blood-brain barrier

The human brain is comprised of over 100 billion capillaries with a total length of 400 miles, a median inter-capillary distance of about 50 μm and a total surface area of 20 m^2, making it the most perfused organ in the body.[39] The normal function of the vasculature in the central nervous system (CNS) is essential not only for the adequate supply of oxygen and nutrients, but also to protect the brain from neurotoxic compounds. This protective physiologic blood barrier that strictly regulates the entry of molecules to the brain is known as the blood brain barrier (BBB). The BBB refers to both passive and active mechanisms used by the brain endothelium to regulate access to the brain. The BBB is a cellular barrier that controls the ionic composition for efficient synaptic signalling function, prohibits macromolecules and unwanted cells from entering the brain as well as insulates the CNS from neurotoxic molecules and ensures brain nutrition.[39-41] This barrier is modified in the context of glioma as evidenced by the penetration of gadolinium (Gd) through the BBB on magnetic resonance imaging (MRI) of patients with glioblastoma.[42, 43] Gd enhancement increases concomitantly with the WHO grade of astrocytomas.[44] Although BBB dysregulation is observed in many gliomas, the

disruption is often heterogeneous and the vasculature remains intact in regions where infiltrating cells are found, emphasising the need for tumour-selective methods to bypass the BBB. This section summarises the normal functioning of the BBB and the impact of brain tumours on BBB integrity.

1.5.1.1 Astrocytes and pericytes

The BBB is essentially formed by the endothelial cells that exert their barrier properties by the neurovascular unit comprising of astrocytes, pericytes and perivascular macrophages (Figure I.1).[45] Astrocytic endfeet provide cellular connection to neurons and cover the basal lamina of the brain capillaries. Astrocytes play an important role in maintaining the barrier properties of the endothelium.[46] Cerebral pericytes are additional components of the BBB, occupying the perivascular space. Pericytes cover the endothelium, provide structural integrity of the BBB and contribute to the induction of barrier properties during embryogenesis.[47, 48] There is growing evidence that astrocytes and pericytes secrete soluble developmental signals like retinoic acid, sonic hedgehog and Wnt that control the initiation of barrier properties.[49-52] Endothelial cells that form capillary-like structures in the presence of pericytes demonstrate apoptotic resistance, indicating a stabilising function of pericytes in angiogenesis.[53] Studies have also demonstrated the pericyte role in vascular stability and repair, and in modulation of astrocyte function.[54]
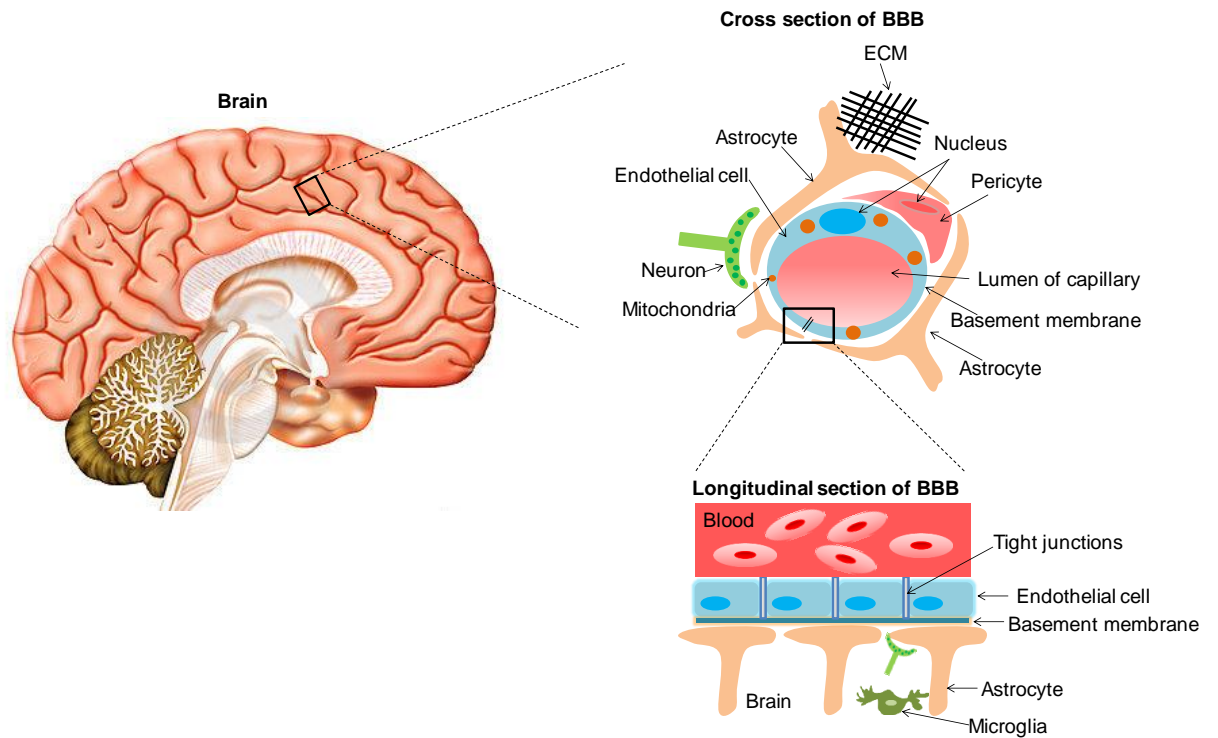
Figure I.1: A healthy blood-brain barrier (BBB): In the healthy brain, astrocytic endfeet surround blood vessels. Vascular endothelial cells form the BBB through tight junctions, trapping cells and blood serum components in the vascular lumen (Adapted from[55, 56]).

1.5.1.2 Endothelial cells and tight junctions

Brain endothelial cells are closely connected by intercellular tight junctions. Except for gaseous or very small molecules such as carbon dioxide and water, the tight junctions of the BBB are highly effective at prohibiting the exchange or influx of various toxins and regulating the fluctuations in ionic concentrations.[45] One importance feature of the brain endothelial cells is the presence of specific transport systems that regulate the ingress of compounds necessary for brain metabolism, and principal among these are ATP-binding cassette (ABC) transporters.[57, 58] A range of intracellular and extracellular enzymes also provide further resistance by metabolising molecules or substances ranging from peptides to neurotoxic compounds. Tight junctions are the links between capillary endothelial cells and are more complex in the brain than those found in peripheral tissues, and they serve to prevent paracellular diffusion. Tight junction affiliated proteins include claudin-1, claudin-5, occludin and junctional adhesion molecules (JAMs).[59, 60] Occludins and claudin-1 are linked via zona occludens (ZO) protein complexes to tight junction proteins (eg. Jacop, 7H6, Cingulin) that are capable of binding to the actin/myosin cytoskeletal systems, resulting in overall modification of tight junction properties and functions. The BBB's restriction of small ions is mainly contributed by claudin-3 and claudin-5 proteins of tight junctions. As a result of the integral structure of the endothelial cell layer and the lack of fenestrae, the BBB actively controls the transendothelial passage of soluble particles from the blood to the brain and *vice versa*.[39]

1.5.1.3 Extracellular matrix

The quality of BBB is directly related to the normal functioning of the microvascular endothelial tight junctions of the brain. Although it is well known that the

organisation and composition of the tight junctions depend on the brain microenvironment, it is still unknown which microenvironment components are directly associated with the maintenance of the tight junctions.[60] The brain microenvironment components include the basal lamina and the "second line of defence" consisting of astrocytes, pericytes and microglia. The astrocytic endfeet membrane is the main residence of the K^+ channel Kir4.1, which is adjacent to the water channel protein aquaporin-4 (AQP4).[61] Aquaporins are a family of integral membrane transport proteins that regulate water efflux across cell membranes in response to osmotic pressure gradients.[62] AQP4 is the molecular equivalent of the orthogonal array of particles (OAPs) which accumulates at the astroglial endfeet membranes. The accumulation of OAPs at this membrane domain is probably due to the presence of extracellular matrix (ECM) compounds such as fibronectin, laminins, collagens, and the heparansulphate proteoglycan (HSPG) agrin. Aquaporins participate in the buffering process of the brain extracellular space: synaptic activity induces the increase in the concentration of extracellular K^+ ions which are taken up by astrocytes. The uptake of K+ causes the osmotic entry of water through the water channels of AQP4. To avoid swelling of astrocytes the water is released into the extracellular spaces comprising of regions around the vessels and the surface of the brain. Therefore, the directed water flow is essential for brain physiology and is thought to be closely regulated by this BBB-ECM complex. There are at least two components of the BBB-ECM that have been identified to be expressed during BBB maturation, suggesting a specific role in the BBB induction: agrin and laminin.[63, 64] The HSPG agrin is present in the subendothelial basal lamina and is known to maintain the integrity of the BBB.[64] Laminin is situated in the basal lamina of the CNS vessels and demonstrates

elevated activity at the onset of BBB maturation.[65] The normal functioning of agrin and laminin on protein level is closely connected to its degradation by the matrix metalloproteases (MMPs).[29]

1.5.1.4 P-Glycoprotein

The integrity and polarity of the BBB is also maintained through an efflux pump known as permeability-glycoprotein (P-gp), also known as multidrug resistance protein 1 (MDR1). This transmembrane protein belongs to the ABC transporter family and is encoded by the *ABC1* or *MDR1* gene.[66] The P-gp is localised on the apical membrane that regulates transport in a single direction. The normal physiological role of P-gp is to protect the body from synthetic compounds by effluxing cytotoxic molecules into luminal spaces for elimination.[67, 68]

1.5.2 Tumour-associated changes in the BBB

The lost barrier function can be detected through MRI using a contrast medium (CM) application. The standard CM used in MRI for GBM diagnosis is gadolinium (Gd), which in normal conditions is not able to cross the intact BBB. In case of GBM, Gd can diffuse into the tissues of the compromised or disrupted barrier and characteristic ring enhancing lesions are seen.[43]

In low grade astrocytomas (grade I and II) there is no detectable disruption of the BBB; tumour vasculature looks mostly like normal brain vessels and the tumour mass is sustained by normal glial cells. As glioma progresses and becomes increasingly aggressive, the endothelial cells are separated from the normal vessel structure and form new tumour associated angiogenic spots. As these cells migrate, they disrupt normal brain vasculature to arrive at the tumour site (Figure I.2). In GBM, the BBB alterations involve the formation of blood vessel

fenestrations and tight junction disruption. In addition, the perivascular space is increased and the basal lamina is altered.[69, 70]

1.5.2.1 Tight junctions in glioblastoma

In human glioblastoma, it was found that a key component of BBB tight junctions, claudin-3, is absent. Claudin-3 is a promotor of glioblastoma vessel leakage.[71] In addition, the loss of claudin-1 in tumour microvessels, downregulation of occludin and claudin-5 in hyperplastic vasculature has also been implicated. These alterations result in a phenotypical change in BBB function due to hyperpermeable endothelial cells and leaky tight junctions.[72]

1.5.2.2 Aquaporins in glioblastoma

The altered aquaporin (AQP) expression in the astrocytic endfeet of the BBB has been strongly correlated to glioma progression. AQP4 redistribution is responsible for the loss of agrin in cerebral capillary basal laminae in glioblastoma. It has been reported that the distribution of AQP4 is shifted from the glial membrane to the entire surface of glioma cells and there is eventual loss of OAP arrangement in glioblastoma.[73]

1.5.2.3 Disruption of P-Glycoprotein activity

The overexpression of P-gp is also a common feature to many multidrug resistant tumours. P-gp expression levels in glioma were correlated with multi-drug resistance and glioma grade.[74, 75] In relation to the BBB, P-gp is disrupted at the necrotic region of glioblastoma but preserved at the tumour periphery. These residual border cells with an intact barrier can limit drug uptake and the tumour often relapse into larger and more aggressive tumours.[76, 77]

1.5.2.4 Dysregulation of brain ECM

Besides vasculature disruption, the ECM is also modulated by glioma tumours (Figure I.2). It was demonstrated that agrin, an essential component of the basal lamina of BBB, is absent if the tight junction proteins are downregulated.[53] The loss of agrin is a parallel event with the redistribution of the AQP4 over the surface of glioma cells. The loss of agrin and other ECM components on protein level is strongly linked to its degradation by matrix metalloproteases (MMPs).[29] These proteases are thought to be involved in BBB-impairment in the following ways: (1) Shedding of growth factors such as VEGF and fibroblast growth factors which have been stored in the ECM vessel contributing to the angiogenic process; (2) ECM remodelling via stimulation of integrin receptors by binding to the Arg-Gly-Asp (RDG) binding domains. In response, integrins are further upregulated in glioma endothelial cells causing induction of cell migration, invasion and angiogenesis;[78] (3) The cleavage of the basal lamina which disrupts the ECM component functionalities (including agrin) which are important for the BBB integrity.[79]

Cross section of disrupted BBB

ECM degradation

Invading glioma cells

Leakage of blood vessel

Astrocyte

Degradation of basement membrane

Longitudinal section of disrupted BBB

Loss of tight junctions

Blood

Invading glioma cell

Endothelial cell

Degradation of basement membrane

Astrocyte

Brain

Leakage of serum
into brain parenchyma
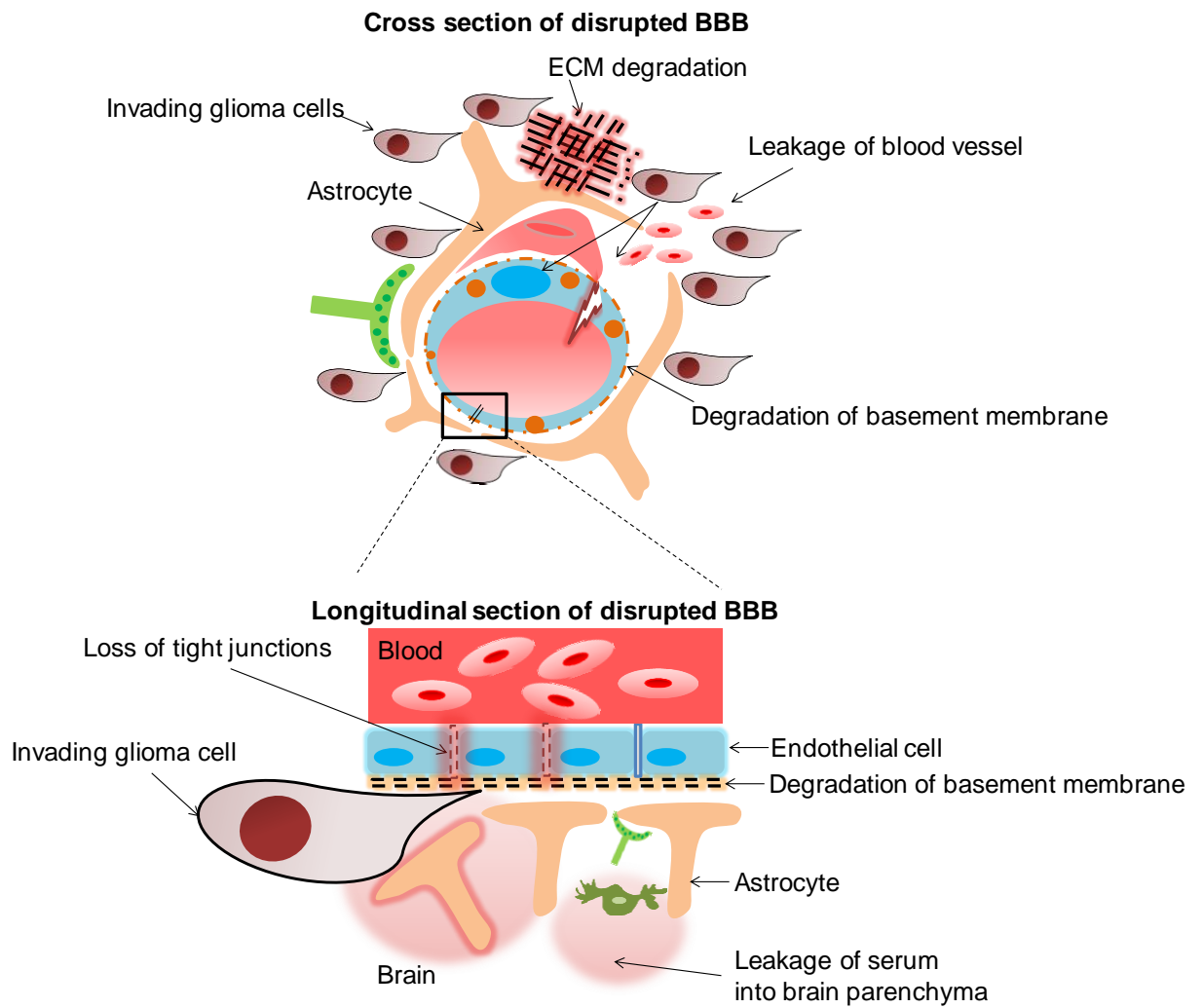
Figure I.2: Disrupted BBB in glioma: Glioma cells migrate along blood vessels, leading to degradation of the ECM and breakdown of basement membrane; displacement of astrocytic feet and complete loss of tight junctions leading to the extravasation of serum components into the neural parenchyma (Adapted from [55, 56]).

1.5.3 Disrupted BBB – A major obstacle to efficient drug delivery

The high metabolic requirement of high-grade glioma creates hypoxic areas that trigger increased expression of VEGF and angiogenesis, leading to the formation of a dysfunctional BBB and abnormal vessels.[80, 81] Moreover, the invasive potential of glioblastoma causes widespread proliferation of tumour cells outside regions of the disrupted BBB and inside areas of normal brain tissues where the function of the barrier is still intact. Essentially, this includes the areas that do not show Gd enhancement on MRI. As a result, the BBB dysfunction in both low-grade and high-grade glioma forms a major obstacle in brain tumour therapy by preventing the delivery of therapeutic agents selectively to the tumour site in sufficient amounts.[82, 83]

The disrupted BBB is formed by brain tumour capillaries and consists of a barrier that is variably distinct from the normal BBB. Brain tumour capillaries demonstrate overexpression of receptors, growth factors and proteases that mediate ligand dependent drug delivery, which can be exploited as a strategy to selectively enhance drug delivery to tumour tissues.[84, 85] Drug efflux transporters expressed at the normal BBB are also present in endothelial cells at the tumour BBB which can significantly impede drug delivery to the brain. In addition, ABC transporters present in tumour cells may confer chemoresistance to glioblastomas, thus forming another hurdle towards effective treatment.[86]

1.6 Current standard of care for glioblastoma

The treatment of glioblastoma currently consists of maximal surgical resection with combined radiotherapy and chemotherapy with temozolomide. The combination of

surgery and radiotherapy has been shown to increase patient survival upto 12 months. Depending on malignancy, the responsiveness of the tumour to radiotherapy varies. Typically, as previously stated, the glioma tumour recurs at the original tumour site in 90% of the patients within 1 year.[87-89]

1.6.1 Temozolomide

The addition of temozolomide (TMZ) to radiotherapy improves both the overall survival and progression-free survival by 2-3 months. TMZ is an orally active DNA alkylating agent and was approved by the US Food and Drug Administration (FDA) in 2005 for the treatment of glioblastoma (Figure I.3). TMZ is an imidazotetrazine derivative of dacarbazine that possesses strong antitumour activity against high grade glioma. It also has the ability to bypass the BBB by increasing the transport of P-glycoprotein across the microvascular endothelial cells.[87, 89]
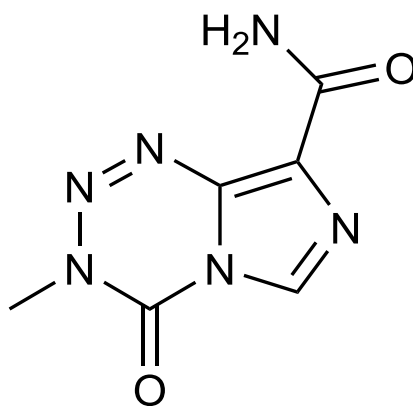
Figure I.3: Chemical structure of temozolomide, an alkylating antineoplastic agent

TMZ acts as a prodrug and is irreversibly converted into the linear triazine 5-(3-methyltriazel-1-yl) imidazole-4-carboxamide (MTIC), the antitumour effector. However, the tumour cells are able to reverse damage to DNA and subsequently become resistance to TMZ, by expressing O^6-alkylguanine DNA-alkyltransferase (AGT) enzyme encoded by an excision repair enzyme O^6-methylguanine DNA-

methyltransferase (MGMT).[90-92] Furthermore, the median survival of patients with radiotherapy and TMZ is only limited to 3 months with high rate of glioblastoma recurrence. Another disadvantage to TMZ use is the risk of DNA damage in healthy cells and lack of selectivity for glioblastoma cells, leading to systemic toxicities such as bone marrow suppression, nausea and vomiting. No doubt the improvement and success of TMZ regime is significant compared to radiotherapy alone, but remains unsatisfactory and inefficacious in comparison with the treatment of other tumour types.[93, 94]

1.6.2 Gliadel wafers

In order to circumvent the therapeutic difficulties of BBB, the insertion of Gliadel wafers into the tumour resection cavity for the treatment of recurrent malignant glioma has been extensively reported and is currently a controversial topic among the neurosurgeons. Gliadel wafer is a biodegradable polymer infused with 3.85% alkylating agent carmustine (1,3-bis[2-chloroethyl]-1-nitrosourea) (BCNU) and has been approved by the US Food and Drug Administration (FDA) for the treatment of brain tumours.[95-100] The mechanism of action of BCNU is mediated by its chloroethyl moieties, which can alkylate the reactive sites on nucleoproteins and interfere with DNA repair and synthesis. BCNU has a very short life, with the parent molecule not detectable after 5 minutes and its metabolites can rapidly enter the cerebrospinal fluid (CSF). However, the penetration of BCNU inside the brain tissue was observed for a very short distance. The implant of BCNU eliminates the need for the encapsulated drug to cross the BBB and allows for the sustained release of carmustine in the extracellular fluid of the brain.[95, 101-103] These wafers could supply a controlled dose of 7.7 mg BCNU for 5 days and has been reported to extend median survival of patients by 2-4 months with newly

diagnosed malignant glioma, resulting in median survival of 13 months after tumour resection. BCNU wafer in combination with TMZ can extend the overall survival to 14.6 months.[89, 96-98, 100, 101, 104] Since postoperative treatment with radiotherapy plus concomitant TMZ does not deliver chemotherapeutic agent to the debulked tumour during the 3-week period between surgery and radiotherapy, the BCNU wafer provides a theoretical 'therapeutic bridge' allowing continuous adjuvant therapy immediately after tumour resection. However, it remains to be known whether this therapeutic bridge is associated with clinical benefit.[87, 89]

It has been believed and emphasised that local chemotherapy with BCNU wafers offer a survival benefit compared to radiotherapy alone and is well tolerated in patients with glioblastoma. Contradictory results showed that BCNU wafers provided no significant clinical outcome relative to standard treatment. It was also suggested that neurotoxicity after Gliadel use was significantly higher in patients. Several complications have been associated with the implantation of BCNU wafers including cerebral oedema, convulsions, hydrocephalus, complications in wound healing and infection of the brain tissue.[96, 100, 101] For instance, intracranial hypertension was present in Gliadel implanted patients compared to placebo patients (9.2% vs 1.7%). This was observed at a late stage; typically at the time of tumour recurrence. CSF leakage was also found to be more common in Gliadel implanted patients. The efficacy of BCNU wafers is limited due to lack of tumour selective targeting and adverse side effects. Therefore, additional research strategies are critical for successful glioma therapy.[95, 101]

1.7   Novel therapies in clinical trials

Although current therapy regimes have improved over the past two decades, overall patient survival has not increased to the level obtained for other solid tumours. New therapies with novel empirical properties are currently in clinical trials (Table I.1). These therapies are designed for use in combination with current standard chemotherapeutics as a means to improve therapeutic efficacy and range from personalised medicine approaches targeting the tumour tissues to the disruption of tumour microenvironment.[105]

1.7.1 Monoclonal antibodies

One of the new classes of therapeutic agents is based on the use of monoclonal antibodies that identify cell surface receptors and ligands, to impede receptor signalling through disruption of receptor-ligand binding and downstream receptor activation. FDA approved Avastin (bevacizumab) is the mainstream antibody against VEGF. Avastin aims to block the response to VEGF in GBM and prevent the promotion of neoangiogenesis of the tumour.[106] Avastin is not specific to a tumour type as it does not target tumour-specific antigens or receptors and there are associated side effects such as deep vein thrombosis, caused by broad blockage of VEGF signalling.[107]

In contrast to the agnostic use of Avastin, AMG595 is currently being tested in phase I clinical trials. AMG595 is a non-cleavable immunoconjugate linker that specifically targets EGFRvIII. Once EGFRvIII is engaged by AMG595, receptor mediated internalisation occurs, thus targeting cytotoxic agent mertansine (DM1) to tumour cells. One potential limitation of AMG595 is that EGFR is mutated in

roughly 40% of GBM cases and of these mutated cases, 65% have EGFRvIII mutations, thus leaving only a limited percentage of total GBM cases that can potentially benefit from this approach.[108]

1.7.2 Innate immunotherapy

Some research groups are also attempting to reengineer the patient innate immune system in order to combat their own GBM tumours. DCVax-L is currently in phase III clinical trial for newly diagnosed GBM cases. This treatment uses the tumour cells and normal dendritic cells to improve the patient innate immune response to recognise GBM tumour for elimination. The clinical trials with DCVax-L in patients have showed an increase in median life expectancy by 3 years with lesser side effects than standard treatment.[109, 110]

1.7.3 Oncolytic viruses

Oncolytic viruses have also been tested for their potential use against GBM. Oncolytic virus is a virus that selectively infects and kills cancer cells. These viruses lack the capability of replication except in specific cell population such as tumour. Once the selected viruses reach the tumour, they undergo lytic expansion, thus destroying the tumour population and become replicative incompetent once the tumour is eradicated. GBM adenovirus trials using DNX-2401 are currently underway. This adenovirus is selective against the deregulated retinoblastoma protein in GBM.[111] The presence of RGD-4C peptide linker gives the virus an additional affinity for integrins. The mechanism of DNX-2401 remains unclear but it was found to promote cell death through autophagic activity and reduce the size of the tumour in mouse xenograft models.[112]

Treatment	Intervention	Molecular target	Clinical Phase
TRC105 + Bevacizumab (Avastin)	Antibody + Drug	Engoglin/VEGF	I
Amgen386	Antibody	Angiopoietin-1 and -2	I
AMG595	Antibody drug conjugate	EGFRvIII	I
DNX2401 and temozolomide	Virus + TMZ	-	I
Axitinib (Inlyta) + Radiotherapy	Drug + radiation	Tyrosine kinase receptors (multiple)	II
Bevacizumab (Avastin) + TPI 287	Drug	VEGF/Tubulin	II
AR-67	Drug	Topoisomerase 1	II
PD 0332991 (Palbociclib)	Drug	CDK 4/6	II
Aldoxorubicin	Drug	DNA	II
DC-Vax L	Immunotherapy	-	III
Rindopepimut	Immunotherapy	EGFRvIII	III

Table I.1: Treatment currently in clinical trials for their potential application in GBM (Adapted from[105]). As of January 2016 TRC105+Bevacizumab is in Phase-II clinical trials. In June 2016, DNX2401+pembrolizumab (a checkpoint inhibitor) entered Phase-II clinical trials for recurrent glioblastoma.

While therapeutic antibodies, viruses and innate immunotherapies carry a great potential due to inherent binding specificity, there are specific issues in the case of GBM (and other brain tumours). Any drug administered systemically would require selective transport through the BBB, which normally impedes access to the vast majority of drugs.[113]

1.8　Modification of existing drugs

Chemical modification of standard chemotherapeutics as an approach to deliver drugs across the BBB has also been studied with varying levels of success (Table I.2). These modifications are mostly nanoparticle-based and they refer to the process of making existing drugs smaller in size, more perfectly charged (low hydrogen bonding capabilities) and more lipid soluble, in order to cross the BBB. Nanosystems are colloidal carriers that consist of liposomes and polymeric nanoparticles. To minimise the interaction of nanosystems with the reticuloendothelial systems (RES), polyethylene glycol (PEG) surface modifications on the surface of nanosystems have been widely used as an approach. If the modifications are specific and suitable for BBB transport, then these colloidal systems encapsulated with drug molecules could improve targeting to brain tumours as drug carriers. Further studies are ongoing towards selective passage of nanosystems across the BBB.[114-117]

Drug name	Mode of action	Modification type	Examples	Route of administration	Targeted Brain tumour type
Carboplatin	Platinum-based antineoplastic agents	Liposomes	Liposomal carboplatin	IV	Glioma and medulloblastoma
Carmustine (BCNU)	Alkylating agent	Nanoparticles	Chitosan surface-modified poly(lactide-co-glycolide) nanoparticles loaded with BCNU BCNU-loaded poly(lactic acid) nanoparticle	Wafer implant/ IV/ oral	GBM, medulloblastoma and low grade astrocytoma
Cisplatin	Platinum-based anticancer drugs	Liposomes	Transferrin-modified cisplatin liposome Cis-lipo(Tf)	IV	Glioma and medulloblastoma
Doxorubicin (DOX)	Anthracyclines, inhibiting nucleic acid synthesis	Liposomes	Long-circulating PEGylated liposomes to cross BBB	IV	GBM
		Nanoparticles	Cationic solic nanoparticles, loaded with DOX Human serum albumin nanoparticles loaded with DOX		
Etoposide (ETP)	Topoisomerase inhibitor	Nanoparticle	ETP-encapsulated cationic lipid nanoparticles grafter with 5-HT moduline Liposomal etoposide	IV/oral	Malignant brain tumours
Irinotecan	DNA topoisomerase-I inhibitor	Liposome	Nanoliposomal irinotecan	IV	GBM
Lomustine (CCNU)	Alkylating nitrosourea compound	Liposomes or microcapsules	Administration of CCNU-Lips and inclusion complex solution of CCNU with hydroxypropyl-β-cyclodextrin	Oral	Oligodendroglioma; mixed oligoastrocytoma

Table I.2: Reported modifications of few important chemotherapeutics (Adapted from [117]).

Drug name	Mode of action	Modification type	Examples	Route of administration	Targeted Brain tumour type
Methotrexate	Antimetabolite and antifolate	Nanoparticle	Magnetic nanoparticle	Oral/injection	Malignant brain tumours, brain lymphoma
Paclitaxel (Taxol)	Taxanes	Chemical Liposomes	Tx-67,10-O-deacetylpaclitaxel 10-monosuccinyl ester Polysorbate 80 coated Paclitaxel plus artemether liposomes	IV	High grade glioma, oligodendroglioma
Temozolomide (TMZ)	Alkylating agent	Nanoparticle based	Polysorbate-80-coated nanoparticles as feasible carrier for TMZ delivery to the brain Transferrin-appended PEGylated nanoparticles for TMZ delivery to brain TMZ solid lipid nanoparticles TMZ loaded PLGA based supermagnetic nanoparticles TMZ loaded in chitosan/albumin nanoparticles	Oral	GBM
Vincristine (Oncovin)	Vinca alkaloid	Liposome	Vincristine sulphate liposomes, PEGylated liposome	IV	Anaplastic oligoastrocytoma; oligodendroglioma

Table I.2: Continued

1.9   Invasive potential of glioblastoma and the role of proteases

The modern era of brain tumour therapy is characterised by target specific drugs with efficient delivery strategies. However, the standard of care for GBM has not improved the overall patient survival and the prognosis remains poor. The annual incidence of glioblastoma is 5 in 100,000 individuals and from the time of diagnosis, the average survival of patients is 17 weeks without treatment and 30 weeks with a combination of surgery and radiotherapy. Although there are severe side effects to the use of chemotherapy, the mean survival can be increased to 15 months after diagnosis.[87-89] However, the current treatment regime is ultimately inadequate and ineffective for the treatment of glioblastoma. The reasons for poor prognosis in patients with GBM are due to the following therapeutic limitations: the presence of blood-brain barrier restricting the amount of systemic drug reaching the tumour-site; the lack of tumour-selective treatment options; intrinsic resistance of tumour cell to chemotherapeutic drugs;   severe neurotoxicity; restricted localisation and diffused infiltration of individual tumour cells into the surrounding normal brain tissue that prevents complete surgical tumour resection; and subsequent to this inevitable recurrence of glioblastoma. From a therapeutic standpoint, there is a critical need to understand the clinical hallmarks of GBM and their evolution from early stages of glioma.[71, 105, 118-121]

Recent efforts to understand GBM biology has led to the discovery of molecular gene signatures.[122, 123] Mutations in the p53 genes, genes regulating retinoblastoma (RB) protein function, EGFR signalling and MGMT promotor has also been identified to correlate with poor overall survival.[124] Beyond these abundant genetic and epigenetic alterations, there is another crucial characteristic preventing complete eradication GBM, which is infiltrative (or invasive) growth

pattern. This tumour event complicates complete surgical removal causing tumour regrowth and further invasion of surviving tumour in close proximity to the resection area.[125, 126]

The invasive capability of brain tumour cells has a clinical role in the ineffectiveness of current treatments, because the remaining tumour cells infiltrate into the surrounding brain tissue and lead to inevitable tumour recurrence. The invasion process includes the increased secretion and expression of several extracellular proteases such as serine, cysteine and metalloproteases, to further degrade the extracellular matrix (ECM) components selectively.[125, 127] These proteases have established roles in maintaining the microenvironment that supports tumour cell survival. The ECM components of the tissue is involved in dynamic regulation of cellular functions during normal and diseased remodelling process such as tissue repair, embryogenic development, inflammation, and tumour invasion and metastasis.[128-130] The invasion of brain tumour cells into the brain parenchyma is a biologically distinct process from invasion of tumour cells into other organ systems, because the ECM in the brain differs from that of most organs. Due to confinement of the brain into the skull and compact cellular assembly; the ECM is condensed to 20% of the tissue volume and the spread of tumour is restricted. Brain ECM is situated in intercellular spaces between glial and neuronal cells where it can be viewed as netlike feature on the neuronal surface and is therefore also known as perineuronal net (PNN).[36, 128] This ECM network is composed of proteoglycans of the lectican family and glycosaminoglycans. Advanced stages of glioblastoma has been known to express the protein components of lectican family which are usually absent from normal brain. The overexpression of lectican proteins is one of the main reasons

for the dissemination of gliomas along myelinated white fibre tracts resulting in distant invasion of tumour cells through the corpus callosum. The lectican protein members are endogenously cleaved for activation by various extracellular proteases such as serine proteases, cathepsins and matrix metalloproteases (MMPs).[127, 128] The extracellular proteases play an important role in degrading the ECM components, enhancing tumour invasion, affecting tumour cell behaviour, promoting tumour growth and proteolytically activating growth factors for cancer progression. Among these proteases, MMPs have been identified in the degradation of all the ECM macromolecules in the brain. They are overexpressed in many types of cancer including malignant brain tumours and significant research has focused on understanding this family of proteases in recent years.[125, 127, 129, 130]

1.10 Matrix metalloproteases (MMPs)

Matrix metalloproteases (MMPs) are zinc dependent endoproteases, comprising of 24 human genes divided into 5 main groups: collagenases, gelatinases, stromelysins, matrilysins and membrane-type MMPs (MT-MMPs) (Table I.3). They are a family of highly homologous endoproteases, capable of degrading most components of the basement membrane and ECM.[131] All the MMPs except MT-MMPs (cell membrane-bound) are secreted by the cell. MT-MMPs are activated intracellularly in the Golgi network by pro-protein convertases called furin and are therefore, already active at the extracellular surface. Secreted MMPs are mainly activated by MT1-MMP and plasmins, respectively.[132] Cell surface associated plasmin, produced by the activity of receptor-bound urokinase-like plasminogen activator (uPA), is a key initiator of MMP activation, particularly stromelysin-1 (MMP-3) and gelatinase B (MMP-9). Active MT1-MMP acts as a secondary

activator, cleaving gelatinase A (MMP-2) to potentiate downstream self-cleavage reactions (Figure I.4).[131, 132]
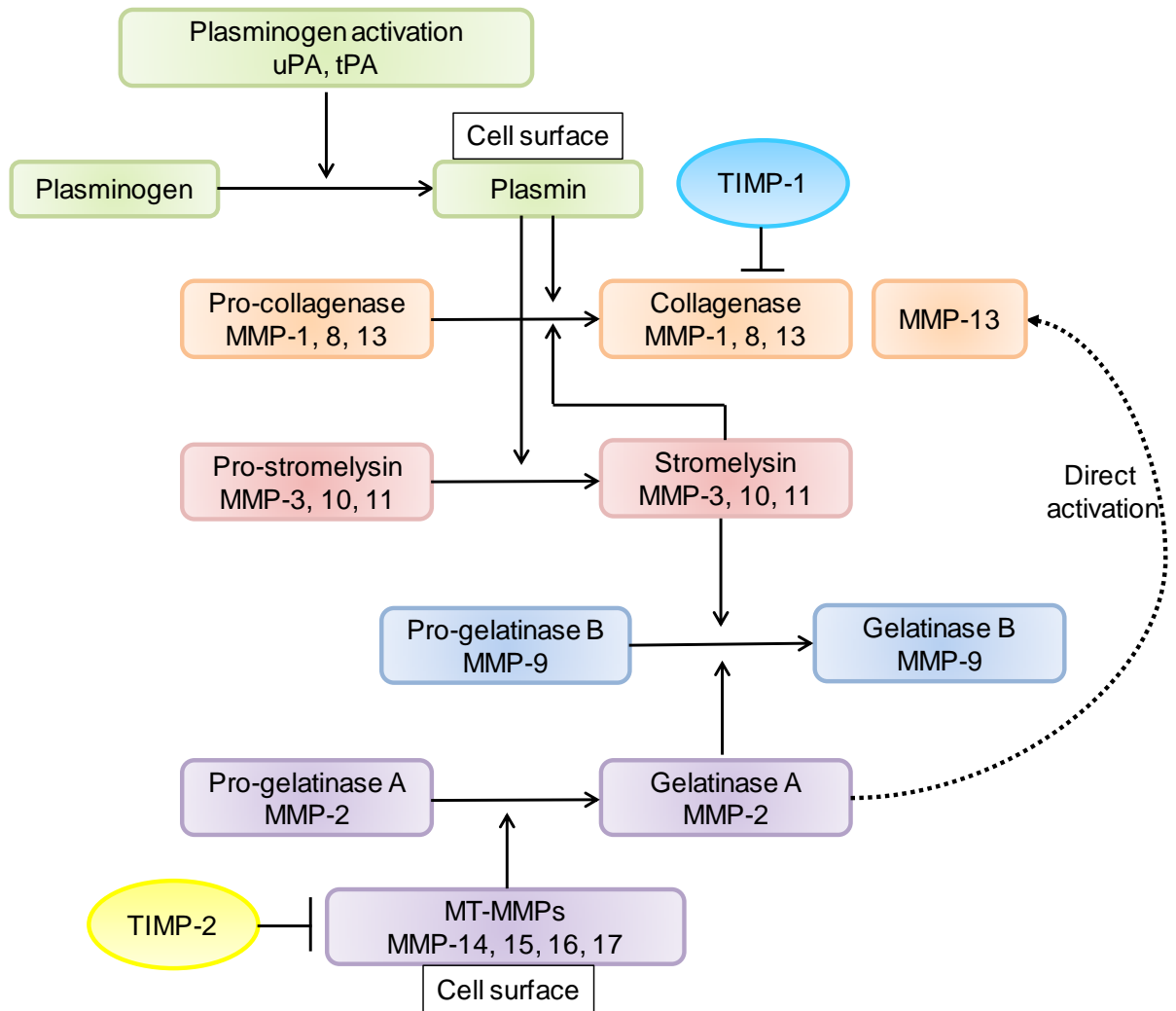
Figure I.4: MMP activation cascades. Cleavage by activator proteases is required for the conversion of inactive MMP zymogens into active MMP enzyme. Cascades involving upstream and downstream MMPs form a complex network in which TIMP-mediated checkpoints are present. Adapted from [131, 132]

MMPs typically have N-terminal signal peptide (pre-domain) to bind the enzyme to the endoplasmic reticulum and transport it out of the cell. Next to the pre-domain, there is a conserved pro-domain which contains a zinc-binding sequence. At the C-terminus end, most MMPs possess a hemopexin-like domain that regulates substrate recognition and is linked to the catalytic domain by a flexible hinge region.[133] Although MMPs are classified based on their substrate selectivity (that is, the substrates for which they show greater hydrolysis as a unit of time), it has been suggested that MMP catalytic domains share considerable sequence homology (55-65%) with a common residue motif, HExGHxxGxxH, consisting of three histidine residues that coordinate the catalytic Zn^{2+} ion. This sequence similarity may mean that certain MMPs can support the function of others during pathological processes such as tumour-related proteolysis.[133, 134]

Structural class	MMP designation	Common names (s)	Notable structural feature(s)
Simple Hemopexin Domain	1	Interstitial collagenase, Collagenase-1	Standard signal peptide, propeptide domain, catalytic domain, hinge region and C-terminal hemopexin domain
	3	Stromelysin-1	
	8	Neutrophil collagenase, Collagenase-2	
	10	Stromelysin-2	
	12	Macrophage elastase	
	13	Collagenase-3	
	18	Collagenase-4	
	19	Rheumatoid arthritis-associated MMP	
	20	Enamelysin	
	22	MMP-23B	
	27		
Gelatin-Binding	2	72 kDa Type IV gelatinase, Gelatinase A	Fibronectin type II repeats
	9	92 kDa Type IV gelatinase, Gelatinase B	
Minimal Domain	7	Matrilysin	No C-terminal hemopexin domain; no hinge region
	26	Endometase, matrilyson-2	
Furin-Activated and Secreted	11	Stromelysin-3	Furin recognition sites
	28	Epilysin	
Vitronectin-like Insert	21	MMP-23A	
Type I Transmembrane	14	MT1-MMP	Transmembrane domain; cytoplasmic tail; MT loop
	15	MT2-MMP	
	16	MT3-MMP	
	24	MT4-MMP	
Type II Transmembrane	23	Cystein array MMP	No C-terminal hemopexin domain; no hinge region
GPI-linked	17	MT5-MMP	Transmembrane domain; cytoplasmic tail
	25	MT6-MMP	

Table I.3: Classification of human MMPs, adapted from [135, 136]

1.11   Regulation of MMPs

MMP activity is regulated both at the transcriptional and post-transcriptional levels and is controlled at the protein level by pro-enzyme activators and inhibitors. The expression of MMPs is stimulated by growth factors, cytokines, tumour promoters, cell-cell interactions, oncogenic transformation and physical stress.[137, 138] The transcriptional binding sites involved in the regulation of MMP genes are: the polyomavirus enhancer-A binding protein-3 (PEA3) site, the activator protein (AP) -1 and -2 sites, the signal transducers and activators of transcription (STAT) site and the nuclear factor kappa B (NF-κB) site.[139] Interestingly, co-regulated MMP genes share several transcriptional binding sites in their promotor sequences whilst functionally regulated MMPs such as gelatinases (MMP-2 and MMP-9) or collagenases (MMP-1 and MMP-8), differ in the composition of cis-elements present in their promotor sequences.[140]

Secreted MMP zymogens are activated extracellularly, in a two-step process: an initial cleavage by an activator protease to destabilise the protein, followed by a final cleavage, generally by another MMP, releasing the N-terminal prodomain to produce a mature enzyme.[141] In contrast, the membrane bound MT-MMP zymogens are activated intracellularly and produced on the cell surface in a proteolytically active state. Tissue inhibitors of metalloproteases (TIMPs) are endogenous tissue inhibitors of MMPs and are consequently important regulators of tissue remodelling, ECM turnover and cell behaviour.[135] The balance between MMPs and the TIMPs is strictly regulated under physiological conditions and is critical in maintaining the net proteolytic activity. Malignant tumours have the ability to disrupt this balance and to produce uncontrolled proteolytic activity that accompanies tumour growth, invasion and metastasis. In malignancy, virtually all

MMPs are proteolytically active in the extracellular tumour microenvironment, incongruent from the lack of activity in normal tissues, but some are expressed at higher concentrations than others.[142]

1.12   MMPs and glioma

During development of carcinogenesis, tumour cells interact with the tumour microenvironment involving the ECM, growth factors and cytokines.[143] Critical enzymes in this process are MMPs because they contribute to the formation of tumour microenvironment by degrading most components of the ECM and the basement membrane, thus promoting tumour growth, migration, invasion, metastasis and angiogenesis.[144] Interactions of tumour cells with the basement membrane are thought to be the crucial event that initiates the metastatic signalling cascade. Several MMPs have been associated with tumour cell invasion as evidenced by the correlation between local tissue infiltration and increased MMP levels.[135, 143, 144] For example, MMP-7 deficient mice showed reduction in intestinal tumourigenesis.[127, 145] Tumour colonisation in the lungs was found to be decreased in the mice lacking MMP-2 or MMP-9.[146, 147] During cancer progression, increased shedding of the epidermal growth factor receptor (EGFR) ligands was observed with the increased expression of MMP-3 and MMP-7.[148, 149] MMPs are also associated with tumour angiogenesis and are required for 'angiogenic switch' that occurs during neovascularisation of tumours.[150] MMP-9 participates in angiogenic switch because it increases the production of vascular endothelial growth factor (VEGF), which is an important mediator of tumour vasculature.[150] MMPs possess the ability to cleave a wide range of non-matrix substrates such as Fas ligand (involved in apoptosis); integrin, cadherins and β-catenin (involved in cell dissociation); VEGF and TNF-α (involved in cell-cell communication); and

TGF-β and FGF (involved in cell division).[143, 151] In addition to MMP-2 and MMP-9, MT-MMPs have also been suggested as being overexpressed in many forms of cancer and the cause of malignant transformations.[152, 153] Extensive studies show frequent overexpression of several MMPs in many forms of human tumour, indeed MMP levels serve as both prognostic indicators of clinical outcome and markers of tumour progression in several human types including colon (MMP-1), non-small cell lung cancer (MMP-10 and MMP-13), breast (MMP-11), gastric (MMP-2 and MMP-9) and small-cell lung cancer (MMP-3, MMP-11 and MMP-14).[154-158] Due to these associations in cancer development, MMPs represent a significant therapeutic target.

Several MMPs are suggested to be overexpressed in malignant brain tumours, but due to the association of vascular basement membrane with the typical invasion route of glioma cells, a large number of studies have focused on illustrating the function of gelatinases, MMP-2 and MMP-9, as promoters of glioma cell invasion.[127] The ECM-bound cytokine TGF-β is an important cytokine regulator of the MMP-system because it induces MMP expression and suppresses TIMP expression thereby promoting invasion of glioma cells. TGF- β is secreted by various proteases such as furin, calpain and plasmin.[159] It has been reported that MMP-2 expression increases in glioma tumours compared to normal brain *in vivo*. In association with this, MT1-MMP, which is the endogenous activator of MMP-2, is also overexpressed in glioma tissues and the correlation was demonstrated with MMP-2 activation.[128] In addition, the neural stem cells demonstrating extensive tumour migration expressed MMP-2 but not MMP-9, suggesting that MMP-2 is closely linked to invasive character.[160-165] On the contrary, the inhibition of MMP-2 protein levels decreased tumour growth and invasion of glioma cells *in vitro*. MMP-

9 expression was detected at the sites of endothelial proliferation and at tumour margins, suggesting their prominent role in promoting tumour angiogenesis. Like MMP-2, MMP-9 expression has been shown to correlate with increasing malignancy of brain tumour cells.[162, 164-169]

Very few studies have focused on the role of MMPs, other than gelatinases and MT-MMPs, in glioblastoma tumours. Although most of them are expressed by glioma cells, MMP-1, MMP-3 and MMP-12 were reported to be localised in glioma cells;[130, 170, 171] and MMP-8 is expressed by neutrophils.[172] MMP-1, MMP-7, MMP-10 and MMP-19 were shown to cleave brevican, a proteoglycan of the lectican family of the brain ECM.[173, 174] Brevican cleavage products have been shown to increase glioma cell dispersion, invasion and EGF receptor activation.[175, 176] It has been suggested that the upregulation of extracellular proteases in glioma tumours is either associated with a compensatory mechanism or corresponding reduction of their endogenous inhibitors, enabling rampant or controlled proteolysis. In addition, divergent reports on the dual role of TIMPs in MMP inhibition and proMMP activation has either been linked to increased glioma invasion or increased survival time. A host of proteases found in glioblastoma have congruent functions but there are some with opposing functions.[177-182] Therefore, increased knowledge is necessary to clarify the role of MMPs and TIMPs in glioma development; and to detect the most important ones appropriate for tumour-selective targeting strategy.

1.13   Pharmacological targeting of MMPs for cancer therapy

On the basis of their clear role in several steps of cancer progression, MMPs were the first proteases to be considered as targets for cancer due to well-known functions in ECM degradation.[131] Over the past two decades significant drug discovery effort has focused on the inhibition of MMPs as a strategy to prevent tumour invasion and subsequent metastasis. As a result the pharmaceutical industry produced a number of well tolerated orally active MMP inhibitors (MMPIs), in an attempt to control the secretion, enzymatic activity and activation of MMPs. These agents were largely peptidomimetic zinc-binding hydroxamates, based upon MMP peptide substrate.[131, 133, 183, 184] By the early 2000s, many MMPIs had reached clinical trials with the majority of them representing a broad spectrum due to structural similarities between MMPs and lack of selective binding within the MMP active sites. The first MMPI that had entered the clinical development was batimastat (BB-94), a broad spectrum hydroxamate derivative with poor water solubility.[185] To circumvent the solubility problem, it was soon replaced by an orally administered analogue, marimastat. However, both batimastat and marimastat were associated with musculoskeletal side effects in patients and lack of efficacy at tolerated doses.[186, 187] In addition, preclinical studies with both these inhibitors showed that they can interact with TIMP-2 for direct activation of proMMP-2 by MT1-MMP, thus increasing the net proteolysis.[148, 188] The lack of efficacy could be attributed to the poor clinical trial design, in which inhibitors were administered to late stage cancer patients with extensively disseminated disease. In a similar trial to marimastat, a comparatively selective inhibitor of MMP-2, MMP3 and MMP-9; tanomastat, proved to be inefficacious than the standard treatment. Many such phase III clinical trials failed to reach the stage of increased survival probably as a

result of broad spectrum subtype specificity of MMPIs and insufficient knowledge about the complexity of the disease biology.[131, 189, 190]

As opposed to monotherapy with MMPIs, clinical studies combining temozolomide with marimastat in glioblastoma showed significant increase in patient survival by 5 months, compared to temozolomide alone. Although the combination therapy with MMPIs delayed the progression of glioblastoma, the treatment itself resulted in severe normal tissue toxicity. A better outcome is expected with more selective and less toxic inhibitors targeting mostly the tumour-associated proteases.[191]

Altogether the failure of MMPIs could be attributed to two factors; i) naivity regarding the MMP family and subsequent lack of enzyme specificity, and ii) poor clinical trial design, in which inhibitors were administered to late stage cancer patients with extensively disseminated disease. The generation of MMP selective inhibitors still proves mostly elusive however, because of broad MMP structural similarity of their catalytic site, substrate complexity and identification of specific MMPs as anti-targets. The overlap of different MMPs in substrate specificity, functions and expression pattern along with a multitude of factors that regulate their activation, stimulation and inhibition also pose tremendous challenge in the design of selective, effective and safe MMPIs. It is also important to identify which MMPs are therapeutic targets (pro-tumourigenic) and which ones are anti-targets (anti-tumourigenic). Inhibiting the activity of anti-targets counterbalances the efficiency of target inhibition thus causing the failure of MMPIs.[133, 141, 192-194]

These rationale hypotheses have now prompted re-evaluation of research strategies in understanding of protease specificity and identification of specific protease targets to improve therapeutic efficacy and reduce side effects. Several

additional strategies have been evaluated over recent years, including development of inhibitors exploiting the enzymatic transition state, inhibitors binding enzyme cavity subsites or alternative zinc chelation groups. As the research in the pathological role of MMPs continue, careful consideration in rationalised pharmacological and biochemical design of MMPIs for selective treatment of cancers may prove to be clinically beneficial.[133, 192, 195-197]

In contrast to inhibition of MMP function, exploitation of MMP-mediated proteolysis within diseased tissues has been heavily investigated as a diagnostic, therapeutic and prognostic approach.[198, 199] These studies used activity-based probes comprising of a broad-spectrum or selective MMP-cleavable peptide labelled with a quenched fluorophore or imaging moiety. In this approach, elevated MMP activity in the diseased tissue results in activation of the probe via selective cleavage of the peptide and release of the contrast agent, facilitating imaging and quantification of MMP activity.[198, 199] In line with the MMP-activated probe-based approaches, elevated activity of MMPs within diseased tissue has also been explored as strategy for conversion of a non-toxic peptide-conjugated prodrug into a potent therapeutic entity within the tumour microenvironment. These prodrugs are drug delivery molecules where a potent chemotherapeutic is coupled to a peptide sequence which inactivates the therapeutic and serves to provide selective cleavage by MMPs expressed within the tumour microenvironment.[200-204]

1.14   Exploitation of tumour microenvironment for the treatment of cancer

Based on the distinct role of MMPs in natural and pathologic states, MMPs are well known to cleave the components of the ECM by degrading proteins and contribute to the formation of tumour microenvironment. When specific MMPs are identified as pharmacologic targets for therapeutic intervention, they can either be

inhibited or their proteolytic activity can be used to cleave prodrugs and thus release the drug selectively in the tumour tissue overexpressing MMPs. The advantage of prodrug approach is dose intensification and reduced systemic exposure. A requirement for success in this approach is the incorporation of peptide sequence selectively cleaved by MMPs overexpressed within the tumour microenvironment, relative to normal tissue.[203, 205]

A small number of studies have focused on developing MMP-activated prodrugs, most commonly directed towards gelatinases MMP-2 and MMP-9 with varying levels of success.[206-211] One of the initial studies assessed MMP-2 mediated tumour-selective activation of the prodrug comprising of an alkylating agent melphalan incorporated within the MMP-2 cleavable hexapeptide.[211] The *in vitro* cytotoxicity of this prodrug proved disappointing however, but the melphalan warhead was successfully released in MMP-positive tumour cells, thereby suggesting the therapeutic potential of MMP-activated prodrugs.[211] Subsequent studies were based on conjugating the drug molecule to the terminus of peptide sequence rather than incorporating within it. One such strategy involved the incorporation of albumin as a macromolecular carrier with the peptide-doxorubicin conjugate to increase the tumour accumulation of doxorubicin.[209, 210] The albumin-prodrug demonstrated efficient activation by MMP-2 tissue homogenates to release doxorubicin.[209] The maximum tolerated dose was substantially higher than free doxorubicin *in vivo* and subsequent studies showed superior anticancer activity against A375 melanoma at equitoxic doses.[209] Several other studies have also investigated the concept of macromolecular drug delivery of MMP-activated prodrugs with varying success rates.[212-214]

Contrary to the use to macromolecular drug carriers, the use of MMP-activated prodrugs conferring to a simple 'endcap-peptide-warhead' structure have shown significant potential as tumour targeted therapeutics. One study involved the development of an anthraquinone linked to the C-terminus of MMP-9 cleavable heptapeptide and the N-terminus was 'endcapped' with fluorescein isothiocyanate (FITC).[206] The FITC allowed for prodrug cleavage to be observed fluorescently, as the FITC is chemically quenched by anthraquinone in the intact prodrug. Using tissue homogenates of a murine myeloma model, the prodrug metabolism was higher in MMP-9 expressing tumours (bone marrow, spleen) relative to other tissues (heart, lung, kidney), as determined by FITC fluorescence release. There was however, a significant level of prodrug cleavage in non-diseased tissues, suggesting the prodrug lacked specificity towards MMP-9.[206] In an attempt to further increase MMP-selectivity, peptidomimetic analogues of peptide-prodrugs were also developed, incorporating doxorubicin, duocarmycins and auristatins.[208] However, these peptidomimetic MMP-prodrugs were either not selective against MMP-positive versus MMP-negative models or demonstrated no activation by MMPs. Therefore, careful consideration of the peptide sequence selectivity and the choice of effector molecule are crucial for enhancing the tumour targeting of these MMP-activated prodrugs.

In one of the most detailed studies reported to date, MMP-activated prodrugs of doxorubicin were demonstrated to have a higher therapeutic index than doxorubicin alone, using the pan-MMP expressing HT1080 preclinical tumour model.[207] In this study, the length of peptide chain was suggested to be important for both MMP-cleavage efficiency and compound stability, with a heptapeptide comprising three or four amino acid to the carboxy-end of the scissile bond being

optimal. The optimised peptide-prodrugs examined were preferentially activated by the secreted MMP-2 and MMP-9, as well as membrane-bound MT1-MMP, but not by the endoprotease neprilysin; supporting their selectivity towards MMP family.[207] These prodrugs demonstrated pharmacological stability *in vivo* and preferential metabolism in MMP-positive tumours relative to heart and plasma. In addition, the administration of optimised prodrug in mice resulted in 80% cure rate compared to only 10% with doxorubicin alone. One limitation of this approach was that a considerable fraction of Leu-doxorubicin produced in the tumour was not readily metabolised to release doxorubicin, allowing for free circulation of Leu-doxorubicin from the tumour into other tissues before its conversion to doxorubicin.[207]

The prodrug of vascular disrupting agent (ICT2588) with rationalised modification of peptide sequence for selective activation by MT1-MMP has also been demonstrated.[203, 215] ICT2588 was shown to be preferentially hydrolysed to its active metabolite (colchicine derivative) in tumour homogenates of MT1-MMP expressing HT1080 relative to MT1-MMP-negative model and normal tissues. In addition the administration of prodrug in HT1080 tumour-bearing mice resulted in the production of active metabolite, diminution of tumour vasculature and haemorrhage necrosis of the tumour; with reduced toxicity, higher therapeutic index and increased pharmacodynamic effect relative to the active metabolite.[215] Co-administration of ICT2588 with doxorubicin resulted in tumour growth delay by 22.6 days and complete tumour regressions, which was superior to monotherapeutic administration of ICT2588 or doxorubicin.[215] ICT2588 achieved clinical cure in 60% of treated animals and is currently in Phase I clinical trial.

The development of anticancer agents activated by the increased proteolytic activity of endoproteases, such as MMPs, is an area of drug development showing

tremendous potential and great promise. Several studies on MMP-prodrug strategies to date have endeavoured to exploit the proteolytic activity of MMP-2 and MMP-9 based on the significant levels of data on their tumour expression. In many cases, these attempts have not proved as fruitful as anticipated. The likely cause for this is the primary focus of strategies is directed towards peptide conjugation of the chemotherapeutic and inactivation of this agent to form a prodrug rather than improving the selectivity of the peptide sequence. It is also important to realise that many MMP-activated prodrug systems are bound to face similar difficulties as MMPIs in the clinic.[194, 205] Therefore, the clinical expression profile of the MMP system must be clear for individual cancers so that specific MMPs overexpressed in malignancy can be targeted by choosing selectively cleavable substrates as linkers. In addition, certain MMPs may be targets in one disease and anti-targets in another, so identifying the appropriate MMPs will be one of key steps in the development of targeted drug delivery systems. For example, choice of multi-MMP targeting should be carefully validated. MMP-2 and MMP-9 have very identical substrate specificity and usually difficult to differentially target. These two MMPs have been determined as targets as well as anti-targets for cancer. Identifying substrates specific towards MMP-2 (validated target) over MMP-9 (suggested anti-targets) for prodrug systems would be beneficial. Similarly, peptide substrates that target MMP-10 (validated target) but not others would be beneficial since it has been identified as a target. Determination of the optimal peptide sequence to facilitate selective cleavage of the prodrug by a specific MMP family (or even a sub-family member) is now known to be the most important and difficult step in the design of MMP-activated prodrugs.[194, 205] The correct identification of an MMP as a viable drug target and MMP substrate selectivity

requirement is extremely crucial in the future development of tumour targeted prodrugs.

1.15   Project Aims and objectives

The aim of this study is to investigate the potential for the development of novel MMP-activated prodrugs as a strategy for the targeted treatment of glioma.

Specific objectives of this research project include:

1. To identify and characterise specific MMPs as targets for protease activated anticancer prodrugs.

2. To rationalise functional similarity of MMP subfamily substrate selectivity utilising *in silico* proteolytic docking coupled to *in vitro* biochemical assessment for enabling progress towards subsequent development of MMP-selective anticancer prodrugs.

3. Rationalised design, synthesis and preclinical screening of peptide-prodrugs conjugated to potent chemotherapeutics, for evaluating MMP-mediated tumour selective drug release.

4. Development of graphene-oxide tethered prodrug implants as a therapeutic strategy for localised drug delivery following tumour resection, with an aim to halt the recurrence of glioblastoma.

These objectives will form the chapters within this work with the thesis as a whole addressing the overall aim of the project.

Chapter 2: Preclinical and Clinical Expression of MMPs

II.1   Drug target validation

Rational drug discovery is a multidisciplinary and stepwise process. The preliminary phase in drug development is the identification and validation of a suitable molecular target. Tumour drug targets can be identified by proteomic, genomic and genetic-linkage studies, but these approaches only relate to a certain gene, protein or mutation with disease. The expression levels of therapeutic targets might change in response to a disease, so these alterations must be elucidated to focus on those that are truly pathogenic. In the targeting of signalling pathways, it is crucial to establish that the downregulation of target is not compensated by changes in other pathways mediators. Therefore a validation process is required to determine whether a drug target has a role in tumour maintenance.[194]

When protein family members have a high degree of structural and functional homology, it is likely that the drugs targeted at one family member will also affect other proteins in the family that are not involved in disease pathogenesis – these are called 'family counter-targets'.[194] It is also important to identify which family members are also anti-targets – molecules that could have severe side-effects on the patients if inhibited or disrupted.[194] A molecule classified both as an anti-target in one disease and a target in the other supersedes its classification as a target from the viewpoint of drug development. For example, millions of patients who took cyclooxygenase 2 (COX2) inhibitors for the treatment of osteoarthritis and other inflammatory diseases, experienced rare anti-target side effects indicating COX2 was an anti-target in these patients.[216] Therefore, human safety concerns

must be carefully considered before drug development without prior knowledge of the drug target. The ability to chemically inhibit a target specifically is an important criterion in assessing whether to proceed with the development of a drug against the validated target – An issue that also applies to the development of MMPIs for cancer therapy.[194]

In selecting MMPs as targets, it is important to understand whether the function and activity of MMPs correlate with malignancy and tumour lesion location, and whether the expression is congruent with substrates that are involved in pathogenesis. Furthermore, the expression and proteolytic activity of MMPs in normal tissues should also be low to avoid drug side effects. When an MMP is upregulated in a tumour, it is also important to determine whether the MMP is actually contributing to the pathogenesis or is a secondary effect of the disease where MMP regulation might actually be a host-protective response.[193, 194, 205] If the MMP function is involved in reversing the tumour progression or mediating the immune-response against the tumour then the MMP is an anti-target.[194]

As discussed in chapter 1, MMPs represent a valid biological source of potential drug targets for the treatment of cancers. Due to their degradative capacity, MMPs can be chemically exploited for anti-tumour prodrugs, to allow selective activation of a non-potent prodrug to a toxic chemotherapeutic agent within the tumour microenvironment.[204] The following section of work demonstrates the utilisation of techniques by which the genetic and protein expression of the MMPs can be identified in preclinical *in vitro* glioma models. The rationale for viewing these MMPs as potential molecular targets for anti-tumour therapy is demonstrated by their involvement in various cancer types and is supported by a wealth of literature.

II.2   Aims and objectives

To identify and characterise specific MMPs as targets for protease-activated anticancer prodrugs

Specific objectives of this section include:

1. To determine the genetic expression of MMPs in preclinical human glioma cell models and rationally identify MMP expression profiles for further evaluation as drug targets.

2. To evaluate protein expression and activity of key MMPs in preclinical glioma tumour models, as putative targets for drug development

3. To assess the clinical expression of key MMPs human glioma relative to histologically normal brain tissues, to verify their potential as clinically relevant targets.

II.3   Materials and Methods

All reagents were supplied by Sigma-Aldrich (UK) unless otherwise stated. Sterile plastic cell culture ware was obtained from Sarstedt (UK).

II.3.1 Cell lines

All cell lines were purchased from ATCC (Manassas, Virginia, USA) or ECACC (Salisbury, Wiltshire, UK) and grown *in vitro*. Human cell lines used in these studies include: U87-MG (grade IV glioma), 1321N1 (grade II glioma), SVG-P12 (normal glial cells), H460 (NSCLC) and MCF7 (breast carcinoma) (See Appendix 1).

II.3.2 Tissue culture

1.3.2.1   Passaging of cells

Tissue culture procedures were performed in a sterile MSC-Advantage Class II biological safety cabinet (Thermo Fisher Scientific, Massachusetts, US). Cell lines were grown in monolayer culture in complete Roswell Park Memorial Institute (RPMI) 1640 media, Dulbecco's Modified Eagle Medium (DMEM) or Eagle's Minimum Essential Media (EMEM) (containing 1% NEAA); all containing 10% fetal bovine serum (FBS) and 2 mM L-glutamine (See Appendix 1). Cells were incubated in a humidified atmosphere of 5% CO_2 at 37°C. The medium was replaced every 3 to 4 days. The cells were routinely passaged when they attained 70 to 80% confluence. The medium was discarded and the contents of the flask rinsed twice with 10 ml Hanks Balanced Salt Solution (HBSS). Cells were detached from the surface of the flask by the action of 2 to 4 ml 0.25% trypsin/ethlyenediaminetetracetic acid (EDTA) followed by incubation at 37°C for 5 minutes. The cells were then resuspended in 10 ml of fresh medium and

centrifuged at 1000 x g for 5 minutes at room temperature in Heraeus Megafuge16 (Thermo Fisher Scientific, Massachusetts, US). The medium was discarded and the cell pellet resuspended in 10 ml fresh media. Between 0.5-1 ml of the resuspended cells were transferred to a new non-vented flask containing 10 ml fresh medium. After 10 passages, cells were discarded and replaced with fresh stocks.

1.3.2.2 Cell counting

Cells were lifted using 0.25% trypsin-EDTA solution and resuspended in 10 ml fresh medium. A 10 µl sample of the cell suspension was then placed into a haemocytometer chamber. Cell counts were taken from 5 grids of the haemocytometer chamber and calculated as the mean of 5 counts. Cell numbers were expressed as (mean cell count) x 10^4/ml medium.

13.2.3 Harvesting of cells for gene and protein expression analysis

Harvesting of cells occurred whilst still within their exponential growth phase. Cells were lifted using trypsin/EDTA as described above. Following centrifugation, the pellet was resuspended in 1 ml of fresh medium, placed in a 1.5 ml microcentrifuge tube and centrifuged again at 1000 x g for 5 minutes. The supernatant was discarded and the remaining pellet was snap frozen in liquid nitrogen and then stored at -80°C.

II.3.3 Reverse transcription-polymerase chain reaction (RT-PCR) for detection of MMP gene expression

II.3.3.1 Total RNA extraction

Total RNA extraction was performed using the QIAshredder and RNeasy Mini kits according to manufacturer's instructions (Qiagen, Hilden, Germany). Briefly, cell lines were grown as described in section II 2.2, and cell pellets collected following centrifugation at 10,000 x g. Excess media was removed from cell pellets and 350 µl buffer RLT (See Appendix 2) was added to each pellet (in RNase-free centrifuge tubes) and vortexed to mix. Resultant lysates were homogenised by transferring buffer RLT contents into Qiashredder spin columns and centrifuging for 2 min at 10,000 x g. Equal volumes of ethanol (70%) were added to the homogenised lysate, and the resulting lysate transferred to RNeasy spin column and centrifuged for 15 s at 10,000 x g. The flow-through was discarded and, buffer RW1 (See Appendix 3) was added to the spin columns and the column centrifuged for 15 s at 10,000 x g. Buffer RPE (See Appendix 4) was added to the RNeasy spin column and centrifuged at 10,000 g. To elute the RNA, RNase-free water (30-50 µl) was added directly into the spin column membrane and centrifuged for 1 min at 10,000 x g to collect the RNA. All RNA samples were stored at -80°C until required for use.

II.3.3.2 Analysis of RNA concentration

RNA samples were diluted in RNase-free water. Purity of RNA was analysed by measuring the relative absorbance spectrophotometrically at 260 nm and 280 nm using semi-micro polystyrene cuvettes (RNA purity shown by ratio of absorbance between 1.7 and 2.0). The concentration of RNA samples was analysed by

measuring their absorbance at 260 nm (assuming absorbance of 1.0 is equivalent to 40 µg/ml RNA (Warburg & Christian, 1942)).

II.3.3.3   cDNA Synthesis: Reverse transcription

Synthesis of cDNA from RNA was performed using Protoscript First Strand cDNA Synthesis Kit (New England Biolabs, Massachusetts, USA) according to manufacturer's instructions. Briefly, random Primer Mix (60 µM) was added to 1 µg of RNA and the volume adjusted to 8 µl using nuclease-free water in 0.2 ml microcentrifuge tube. RNA samples were denatured at 70°C for 5 minutes and then rapidly cooled on ice to ensure primer annealing. To each RNA sample a cDNA synthesis mix was added consisting of: M-MuLV (Moloney Murine Leukaemia Virus) reaction mix and M-MuLV enzyme mix. The sample was mixed and incubated at 25°C for 5 minutes followed by incubation at 42°C for 1 h to facilitate cDNA synthesis. Samples were diluted 1:1 with nuclease-free water (final volume 40 µl). cDNA samples were stored at -20°C. Appropriate negative controls (RT-) were prepared by treating RNA samples with the reagents described above but without the addition of M-MuLV enzyme mix in the cDNA synthesis mix, to highlight any genomic DNA contamination in subsequent PCR analyses.

II.3.3.4   Primer design

MMP and GAPDH primer design were based on the findings of Kohrmann *et al.*,[217] and provided by Invitrogen Life Technologies (Massachusetts, USA). MMP primer sequences (Table II.1) were evaluated by BLAST search (http://www.ncbi.nlm.nih.gov/tools/primer-blast/) to confirm agreement with human DNA sequence. On delivery, primers were reconstituted to 10 µM stock solutions in nuclease-free water, and stored at -20°C.

II.3.3.5 Polymerase chain reaction (PCR) of MMP expression

PCR reactions were performed using the Protoscript *Taq* RT-PCR kit (New England Biolabs, Massachusetts, USA). All reaction reagents and samples were kept on ice throughout. To each cDNA sample (5 µl) a PCR reaction mix was added consisting of: *Taq* 2X Master mix (10 µl) (See Appendix 5), sense primer (10 µM), antisense primer (10 µM) and the volume adjusted to 20 µl using nuclease-free in 0.2 ml PCR centrifuge tubes. The contents of each tube were mixed well and centrifuged briefly. All samples underwent the following PCR programme, 94°C for 5 minutes followed by cycles of 94°C for 30 s, primer annealing for 30 s and elongation at 68°C for 1 minute (Table II.2). Each program finished with 10 minutes incubation at 68°C to ensure complete elongation of newly synthesised cDNA.

After the reaction was complete, all PCR samples were stored at 4°C ready for analysis. The additional following controls were included in the PCR reaction described above: Positive controls consisted of sample cDNA with known expression profiles whilst negative (RT-) controls consisted of PCR products from cDNA samples created without the addition of M-MuLV enzyme mix (as detailed in section II.3.3.3).

Gene	Primer	Primer sequence
MMP-2	Forward	F-5'-TTTCCATTCCGCTTCCAGGGCAC-3'
	Reverse	5'-TCGCACACCACATCTTTCCGTCACT-3'
MMP-3	Forward	5'-GGCTTTCCCAAGCAAATAGC -3'
	Reverse	5'-GTGCCCATATTGTGCCTTCT -3'
MMP-9	Forward	5'-CCTGCCAGTTTCCATTCATC-3'
	Reverse	5'-GCCATTCACGTCGTCCTTAT-3'
MMP-10	Forward	5'-GTCACTTCAGCTCCTTTCCT-3'
	Reverse	5'-ATCTTGCGAAAGGCGGAACT-3'
MMP-12	Forward	5'-ACAGATGATGGACCCTGGTT-3'
	Reverse	5'-AGAGTCAAGCAAGAATGGACAA-3'
GAPDH	Forward	5'-CCACCCATGGCAAATTCCATGGCA-3'
	Reverse	5'-TCTAGACGGCAGGTCAGGTCCACC-3'

Table II.1: Primers used for RT-PCR for MMPs and the house keeping control gene GAPDH, supplied by Invitrogen Life Technologies.

Primer set	Annealing temperature (°C)	Number of cycles
MMP-2	57	32
MMP-3	52	32
MMP-9	52	35
MMP-10	52	35
MMP-12	52	35
GAPDH	55	35

Table II.2: RT-PCR conditions used for MMPs and the house keeping control gene

II.3.3.6 Agarose gel electrophoresis to analyse PCR products

PCR products were separated through a 1% v/w agarose/Tris-Acetate EDTA (TAE) gel containing 0.01% ethidium bromide. Prior to loading samples into the gel, 10% loading dye (30% glycerol, 0.25% bromophenol blue) was added to each reaction tube to allow sample visualisation. Quickload 1kb DNA Ladder (New England Biolabs) was loaded into the gel, allowing for later determination of PCR product sizes. Electrophoresis was carried out in 1 x TAE buffer at 100 V for 1 h to separate PCR products. cDNA in the gel was visualised under a UV light using a UV-transilluminator and digital gel images saved.

II.3.4 Western Blotting of MMP-10 expression

II.3.4.1 Sample preparation

II.3.4.1.1 Extraction of protein from cells

Cells were grown to subconfluency in 75 cm^2 flasks. The culture medium was transferred into sterile 15 ml centrifuge tube, for later extraction of protein from the medium. Ice cold lysis buffer (50 mM Tris-HCl pH 7.5, 1 mM EDTA, 1 mM EGTA, 1 mM Na$_3$VO$_4$, 10 mM β-glycerol phosphate, 50 mM NaF, 5 mM Na$_3$PO$_4$, 0.27 M sucrose and 1% TritonX-100) was applied directly onto the cell monolayer and incubated at 4°C for 15 minutes to allow for lysis of the cells and release of cytoplasmic proteins. The resulting extract was collected, centrifuged at 10,000 rpm, 4°C for 10 minutes and stored at -20°C until use.

II.3.4.1.2 Extraction of protein from cell culture medium

Media protein extraction was performed using Vivaspin-2 Protein Concentrator Spin Columns (GE Healthcare, Buckinghamshire, UK). The concentrator was filled

up to 2 ml and centrifuged at 4000 x *g* for 10 minutes. The concentrated protein collected in the concentrator cap was transferred into microcentrifuge tubes and stored at -20°C until use.

II.3.4.2 Polyacrylamide gel electrophoresis

Proteins were separated through 10% polyacrylamide SDS gels. Each lane was loaded with a relevant amount of sample (representing 30 μg of protein from cell lysates) diluted in lysis buffer and 2 x sample buffer (65.7 mM Tris-HCl (pH 6.8), 2% SDS, 10% glycerol, 0.01% bromophenol blue, 2% β-mercaptoethanol) to make final 30 μl volume. Samples were denatured at 95°C for 5 minutes and incubated on ice prior to loading. Gels were immersed in electrophoresis running buffer (25 mM Tris, 190 mM glycine, 0.1% SDS) and the samples loaded into the gel. In addition, one lane was loaded with Full Range Rainbow Marker (Amersham Biosciences) to allow for later protein mass determination. Electrophoresis was run at 50 V until samples reached the edge of stacking gel, followed by 150 V until the marker relevant to the size of protein of interest was located in the middle of the separating gel.

II.3.4.3 Protein transfer to polyvinyl membrane

Protein was transferred from the acrylamide gel to Hybond-P membrane (Amersham) using a VWR transfer kit immersed in transfer buffer (20 mM Tris, 150 mM glycine, 20% methanol). The transfer tank was placed in an ice bath and the transfer run for 2 h at 300 mA.

II.3.4.4 Antibody incubations

Blots were incubated in 5% non-fat milk in TBS-Tween buffer (10 mM Tris, 150 mM NaCl (pH 8.5), 0.1% Tween 20) for 90 minutes at room temperature to block

non-specific antibody binding. Antibodies were diluted to their final concentration (Table II.3) in 1% non-fat milk in 0.1% TBS-Tween and incubated overnight at 4°C with agitation. Excess antibody was removed by washing the blot thrice for 15 minutes in 0.1% TBS-Tween. The blot was incubated with the appropriate horseradish peroxidase conjugated secondary antibody at a 1:2000 dilution in 1% non-fat milk in TBS-Tween, for 60 minutes at room temperature. Blots were rinsed for a further 3 times for 5 minutes in TBS-Tween to remove excess secondary antibody.

Antibody	Supplier	Final concentration	Secondary antibody
Ab-5 (Rabbit polyclonal)	Neomarkers, Fremont, CA	0.3 µg/ml (1:3000 dilution)	Goat anti-rabbit
Clone 5E4 (monoclonal)	Novocastra, Newcastle, UK	1 µg/ml (1:1000 dilution)	Rabbit anti-mouse

Table II.3: Optimised western blotting conditions for MMP primary antibodies. This represents a subset of antibodies tested in these studies.

II.3.4.5   Visualisation of antibody binding

Antibody binding was detected chemiluminescently using ECL substrate (125 mM Luminol, 45 mM p-Coumaric acid, 1 mM Tris-HCl (pH 8.5), 15% H_2O_2). Blots were exposed to ECL substrate for 3 minutes in the dark at room temperature, excess reagent was blotted from the surface and the blot wrapped in Saran Wrap. Each blot was exposed for an appropriate time (between 10 s and 3 minutes) and the staining intensity determined using a Biorad Chemidoc Imaging System.

II.3.5 Immunohistochemistry

Immunohistochemical (IHC) images and raw data of MMP expression in tumour sections were kindly provided by the Human Protein Atlas.[218-220] The complete IHC staining scores provided by the Human Protein Atlas were analysed further to assess the level of MMP expression in a panel of human glioblastoma tissues relative to normal brain tissues. All IHC staining in the Human Protein Atlas project was performed using a standard protocol as described.[218-220]

II.3.5.5 Scoring of immunohistochemical staining of clinical samples

Sections of clinical tissue samples were examined using a light microscope (Leica biosystems, CA, USA).[218-220] Immunoreactivity was scored according to both its intensity and its distribution throughout the tissue observed within the field of view. The level of staining intensity was scored as follows: Score 0: no staining (no protein expression or below detectable levels); Score 1: low staining (low protein expression); Score 2: moderate intense staining (moderate protein expression); Score 3: high or strong intense staining (high protein expression); Score 4: very high intense staining (very high protein expression). Similarly, the extent of the staining thoughout the field of view was scored as follows: Score 1: represented ≤10% positively stained cells (low distribution of protein expression); Score 2: 11-40% positively stained cells (low to moderate distribution of protein expression); Score 3: 41-70% positively stained cells (moderate to very common distribution); Score 4: 71-100% positively stained cells (very common to ubiquitous distribution). The samples were assessed from dataset of five individual patients for each tissue type tested.

II.3.6 Assay of MMP activity

i)   Determination of MMP-selective proteolytic activity

Recombinant human MMP proteins (MMP-2, MMP-3, MMP-9 and MMP-10) (R&D Systems, UK) were assayed for their ability to hydrolyse the stromelysin-selective fluorogenic substrate M-2110 (Mca-Arg-Pro-Lys-Pro-Val-Glu-Nva-Trp-Arg-Lys(Dnp)-NH$_2$) and gelatinase-selective fluorogenic substrate M-2055 (Dnp-Pro-β-cyclohexyl-Ala-Gly-Cys(Me)-His-Ala-Lys(N-Me-Abz)-NH$_2$) (Bachem, Switzerland). The stock solution of MMP proteins were prepared by dilution in MMP activity buffer (100 mM Tris-HCl pH 7.6, 10 mM CaCl$_2$, 100 mM NaCl, 0.16% v/v Brij-35), to a concentration of 20 ng/µl. The assay was performed in a 96-well plate by reacting 200 ng recombinant protein and 1 µM substrate in 100 µl MMP activity buffer. Using a fluorescent spectrophotometer (Varioskan Flash, Thermo Fisher scientific), continuous fluorescence was measured (excitation wavelength, λ_{ex} = 325 nm and emission wavelength, λ_{em} = 393 nm with M-2110 substrate; and λ_{ex} = 365 nm and λ_{em} = 450 nm with M-2055 substrate) at 37°C following a 200 minute incubation.

ii)   Determination of MMP activity in human tumour cell lines

Similarly, MMP activity was defined as the ability of the protein extract, from tumour cell media, to hydrolyse the fluorescent MMP subfamily selective substrates: M-2110 and M-2055. Briefly, the reactions (100 µl) contained protein extract from cell media representing 1 x 10^5 cells (10 µl) and 1 µM fluorogenic substrate in MMP activity buffer. Continuous fluorometric assay was performed in 96-well plate at 37°C using fluorescent spectrophotometer.

A negative reaction blank was included by omission of recombinant MMP/media protein extract. For each sample, the relative activity was calculated as the fluorescence obtained from the sample minus that obtained from the reaction blank following the 200 minute incubation. Activity was expressed as change in fluorescence per minute per ng of protein (or 1×10^5 cells). The reliability and reproducibility of the assay were determined using three independent studies.

I.4   Results

II.4.1   Expression of MMP mRNA in human tumour cell lines

II.4.1.1   Optimisation of RT-PCR evaluation of MMPs

To assess the gene expression of the MMP subfamily in cell lines, primer pairs were optimised in order to identify an appropriate annealing temperature, elongation time and number of PCR cycles to yield optimum reaction products. A panel of four human tumour cell lines were screened for gene expression of MMP using semi-quantitative RT-PCR. The amount of cDNA used in each PCR reaction was optimised using a range of cDNA concentrations, with 5 ng being identified as optimal (Figure II.1). Primer concentrations were optimised in the same way (2.5 µM-12.5 µM). Addition of each primer at a concentration of 25 nM per reaction (for MMPs and GAPDH) resulted in adequate PCR products and this was chosen as optimal concentration for future studies (Figure II.2).

II.4.1.2   Expression of MMPs in human tumour cell lines determined by RT-PCR

A range of human tumour cell lines including glioma grade-IV (U87-MG), glioma grade-II (1321N1), lung (H460) and breast (MCF7); and a normal brain cell line (SVG-P12) were screened for MMP (MMP-2, MMP-3, MMP-9, MMP-10 and MMP-12) gene expression based primarily on studies of Nuttall *et al.*[173] The lack of gene product in control lanes (without reverse transcriptase, RT-) for each well indicated that there was no genomic DNA contamination of samples (Figure II.3).

The H460 and MCF7 cell lines were used as positive/negative controls for MMP gene expression based on studies of Atkinson *et al.*[203] All the human cell lines demonstrated a differential expression of the MMPs evaluated. The U87-MG and

1321N1 cell lines expressed all studied MMPs, supporting their use as relevant tumour models in prospective studies. Whereas SVG-P12 cell line showed low/negligible expression of MMP-10 (Figures II.3, II.4 and II.5).
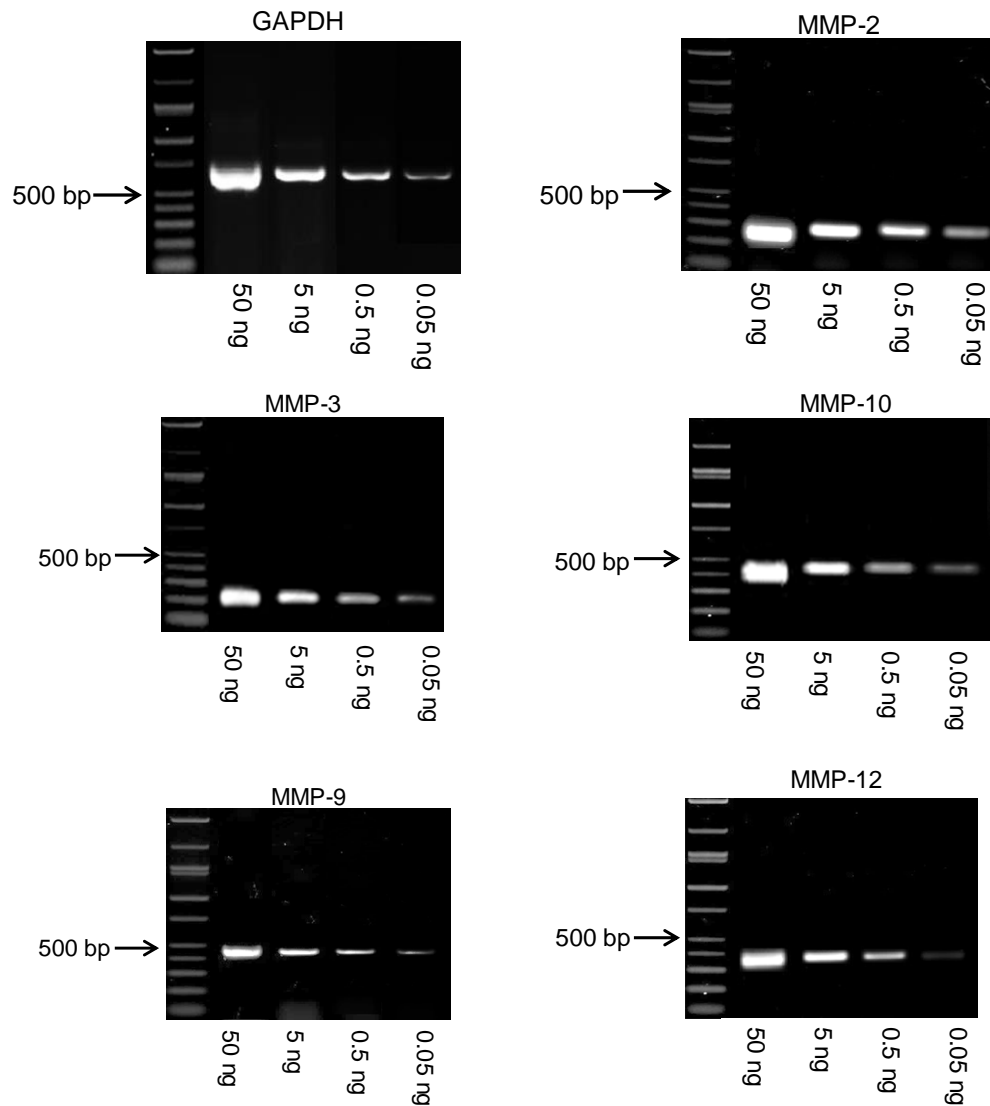
Figure II.1: Identification of optimal cDNA concentration for RT-PCR analysis. Optimum cDNA concentration identified as 5 ng U87-MG cDNA per reaction for GAPDH and MMPs.
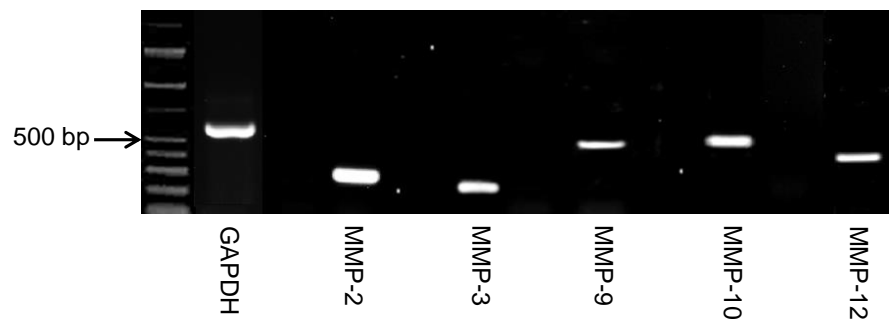
Figure II.2: Detection of MMPs by RT-PCR. Product sizes; GAPDH, 561 bp; MMP-2, 253 bp; MMP-3, 205 bp; MMP-9, 455 bp; MMP-10, 471 bp; MMP-12, 392 bp.
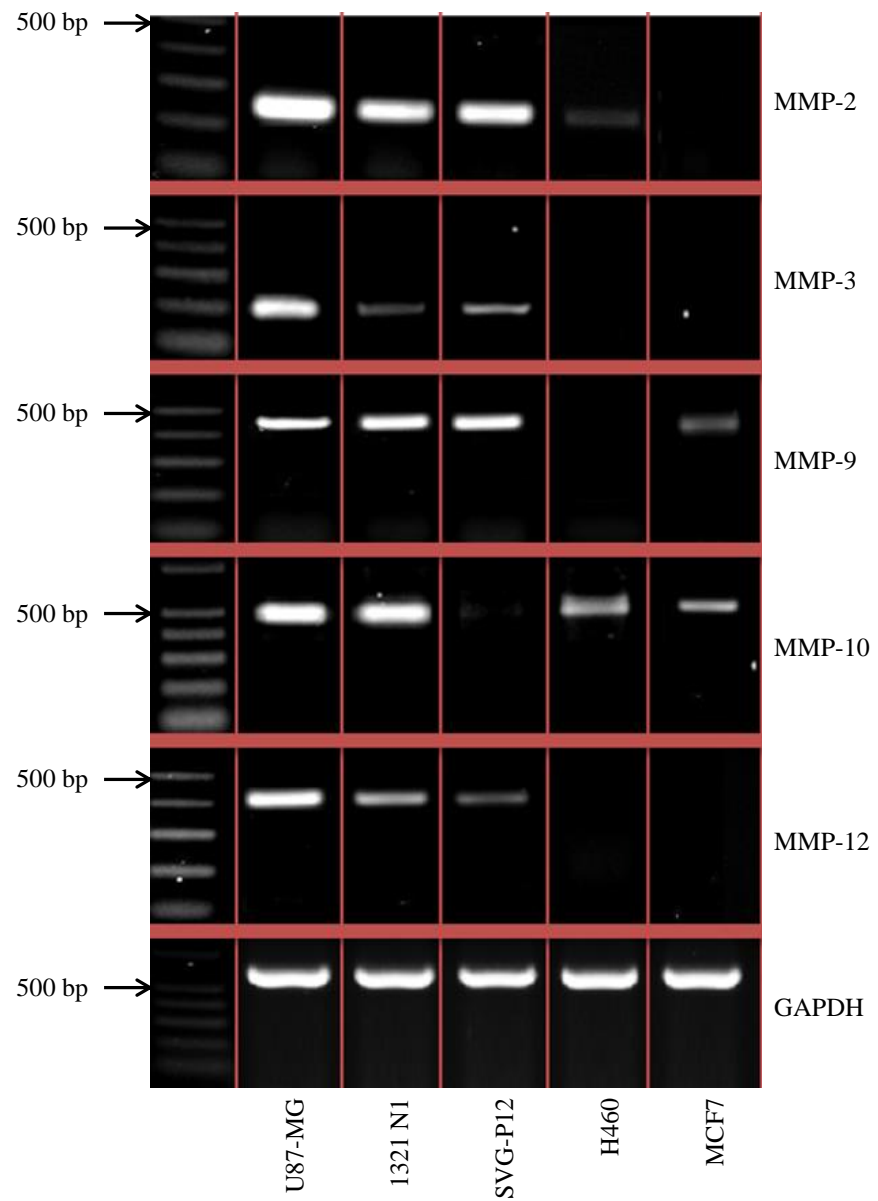
Figure II.3: RT-PCR analysis of the MMPs in human tumour cell lines and a normal glial cell line, demonstrating varied expression of MMPs
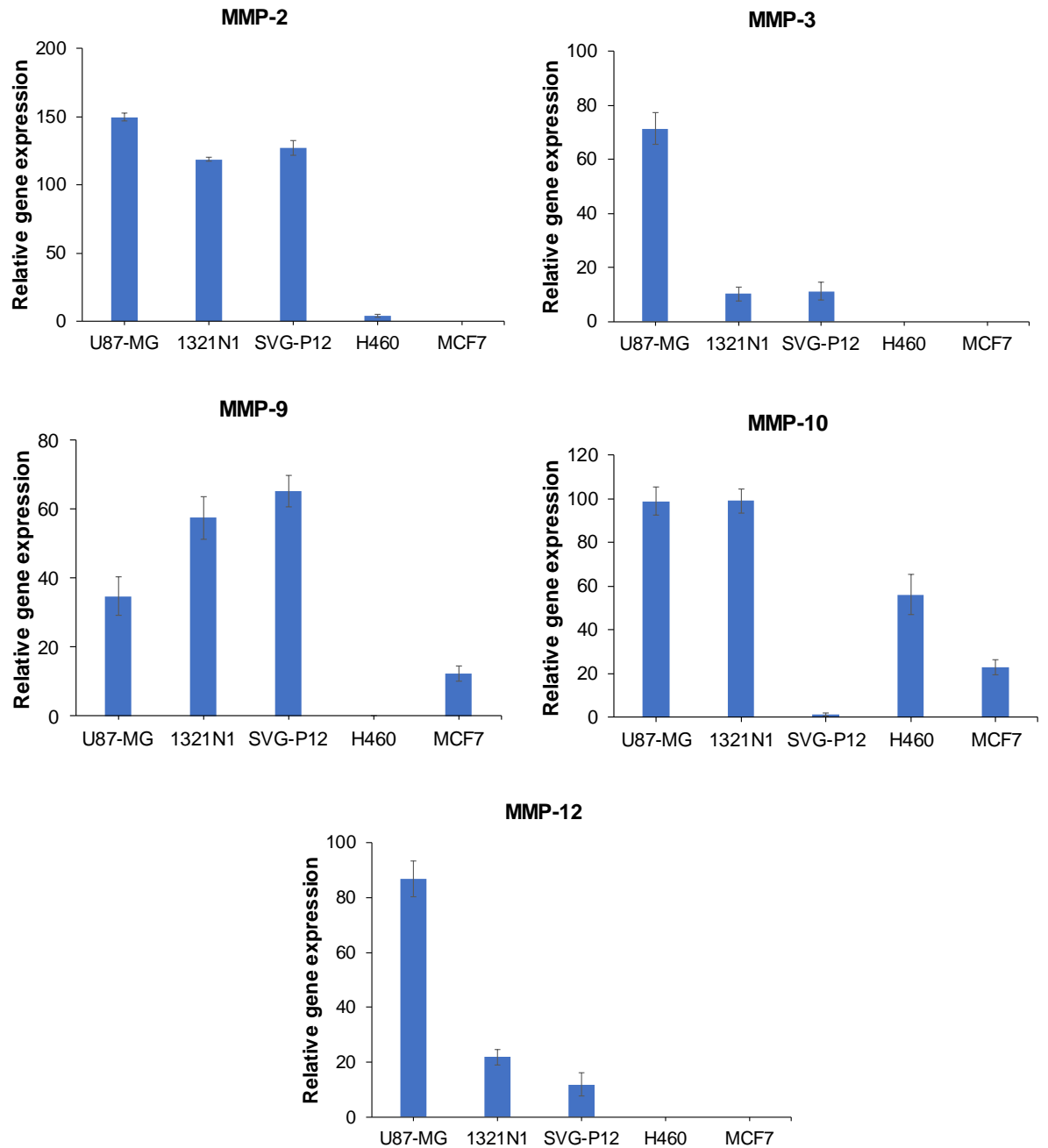
Figure II.4: Quantitative densitometry of the relative gene MMPs detected by RT-PCR. Human cell lines; U87-MG (glioma grade-IV), 1321N1 (glioma grade-II), SVG-P12 (normal glial) and H460 (NSCLC) and MCF7 (breast cancer). The values of gene quantified are after normalisation to GAPDH and therefore gene specific, thus precluding comparison of expression between genes.

	Relative gene expression				
Cell line	MMP-2	MMP-3	MMP-9	MMP-10	MMP-12
U87-MG	+++	+++	++	+++	+++
1321N1	+++	+	+++	+++	+
SVG-P12	+++	+	+++	+/-	+
H460	+	-	-	++	-
MCF7	-	-	+	+	-

Key: | - | Negative | + | Low | ++ | Moderate | +++ | High expression

Figure II.5: Relative abundance of human MMP gene expression in human tumour and normal glial cell lines as analysed by RT-PCR and quantified by densitometry. The expression grade is representative of the genes quantified after normalisation to GAPDH.

II.5.1 Optimisation of MMP-10 protein in human preclinical cell lines by western blotting

Western blotting was employed to assess the protein expression of MMPs in the preclinical tumour model panel. Human MMP-10 Ab-5 polyclonal (Neomarkers) and 5E4 monoclonal (Novocastra) antibodies were evaluated for the determination of MMP-10 protein by western blotting. These antibodies have previously been shown to be specific for MMP-10, detecting both active and pro forms of the enzyme by Western blot analysis.[155] H460 cell line was used a positive control for MMP-10 detection based on literature.[155]

Differential bands were detected indicating different specificities of the two antibodies (Figure II.6). Ab-5 and Clone 5E4 produced bands of approximately the correct size for pro- and active MMP-10; 57 kDa and 44 kDa respectively, with Ab-5 being more specific for active MMP-10 and 5E4 demonstrating specificity for pro-MMP-10 (Figure II.6). The two antibodies were successful in this study in demonstrating differential expression of MMP-10 between the positive sample (H460), glioma cell models (U87-MG and 1321N1) and normal glial cells (SVG-P12) (Figure II.6).

II.5.2 MMP-10 protein expression in human preclinical glioma cell lines

Expression of MMP-10 protein was evaluated in human cell lines by western blotting. MMP-10 expression was probed using Ab-5 and Clone 5E4 anti-MMP-10 antibodies, to differentially detect active and pro MMP-10, respectively. Cells grown in monolayers were assayed for western blot analysis of MMP-10 expression at 48 h and 96 h post cell seeding. The tumour cell lines demonstrated

a time-dependent increase in expression of active form of MMP-10, whereas normal glial cells demonstrated an unchanged and low/negligible expression pattern (Figures II.6 and II.7). Active MMP-10 protein detected in all the cell lines demonstrated differential varying level of expression; in agreement with gene expression data obtained using RT-PCR (Figure II.8).
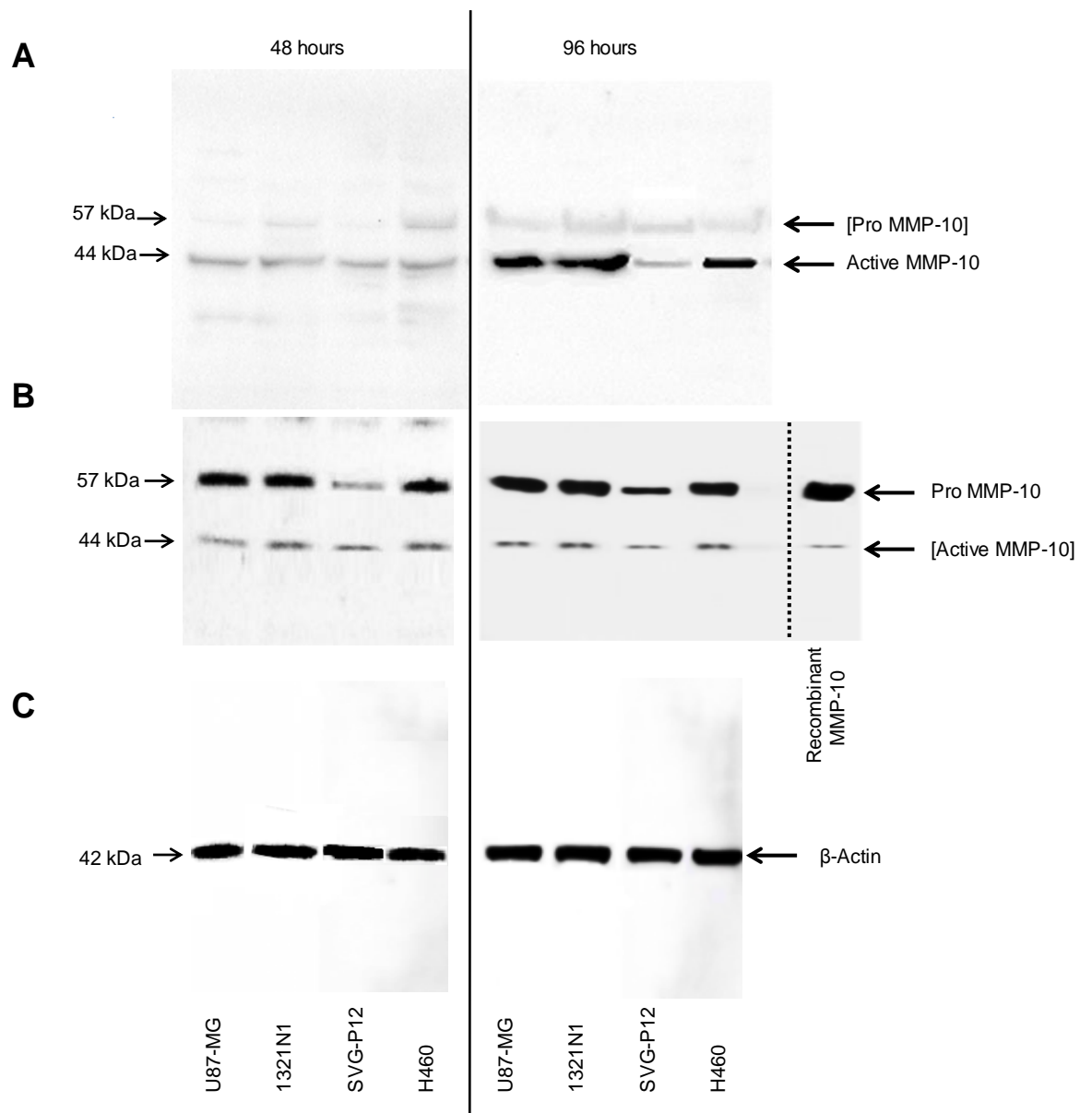
Figure II.6: Western blotting of human cell lines for MMP-10 at 48 h and 96 h post-seeding. (A) Ab-5 anti-MMP-10 polyclonal antibody detected active MMP-10 protein. **(B)** 5E4 NCL-MMP-10 monoclonal antibody detected pro-MMP-10 protein in the cell lysates. **(C)** Equal loading of protein sample in each well was confirmed by β-Actin protein expression.
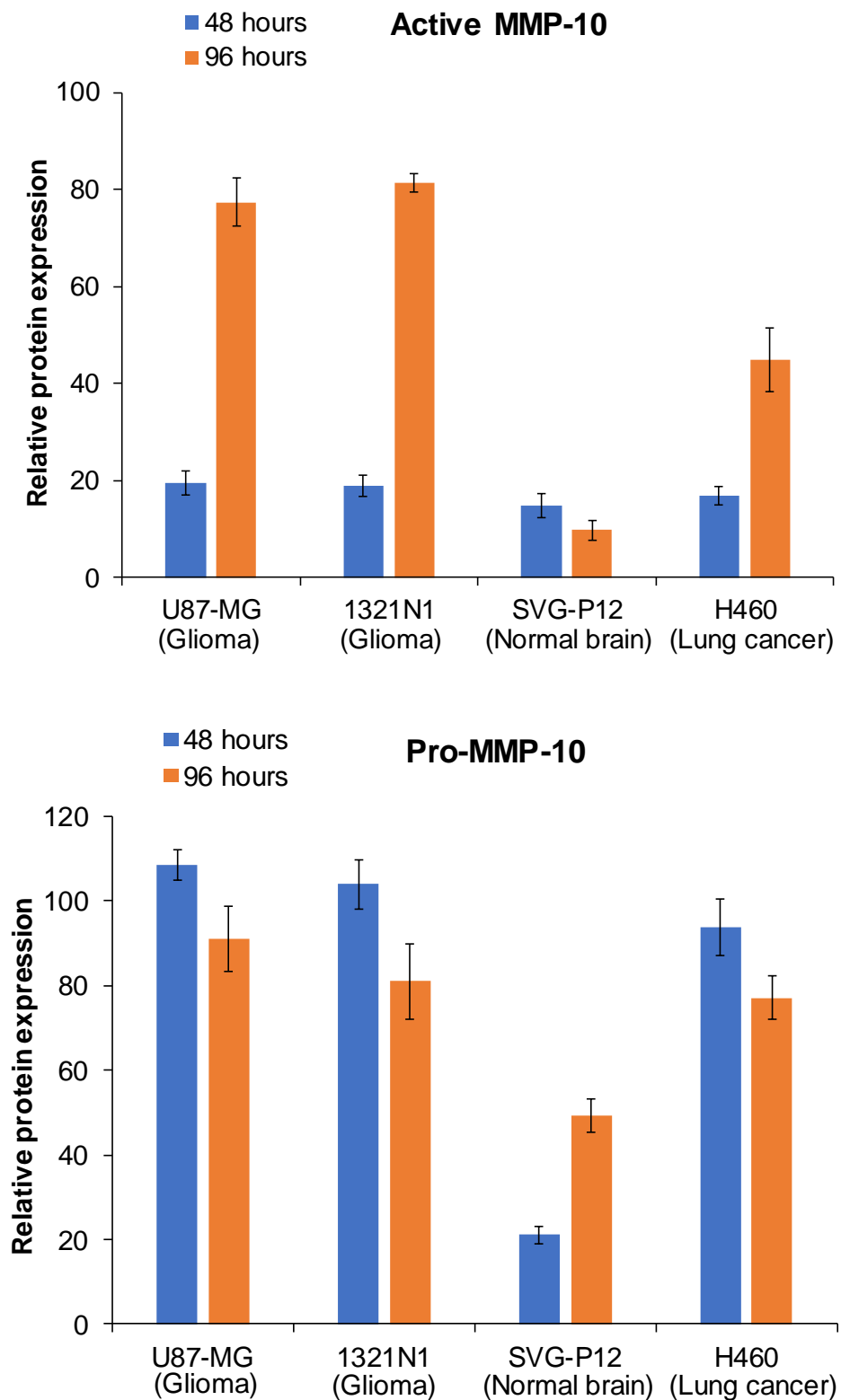
Figure II.7: Quantitative densitometry of the protein expressions of active and pro MMP-10 in human tumour and normal glial cell lines at 48 h and 96 h post-seeding. The values of protein quantified are after normalisation to β-Actin for each cell line at specific time point.

A

MMP-10 gene

B

Active MMP-10 protein

C

R² = 0.9962
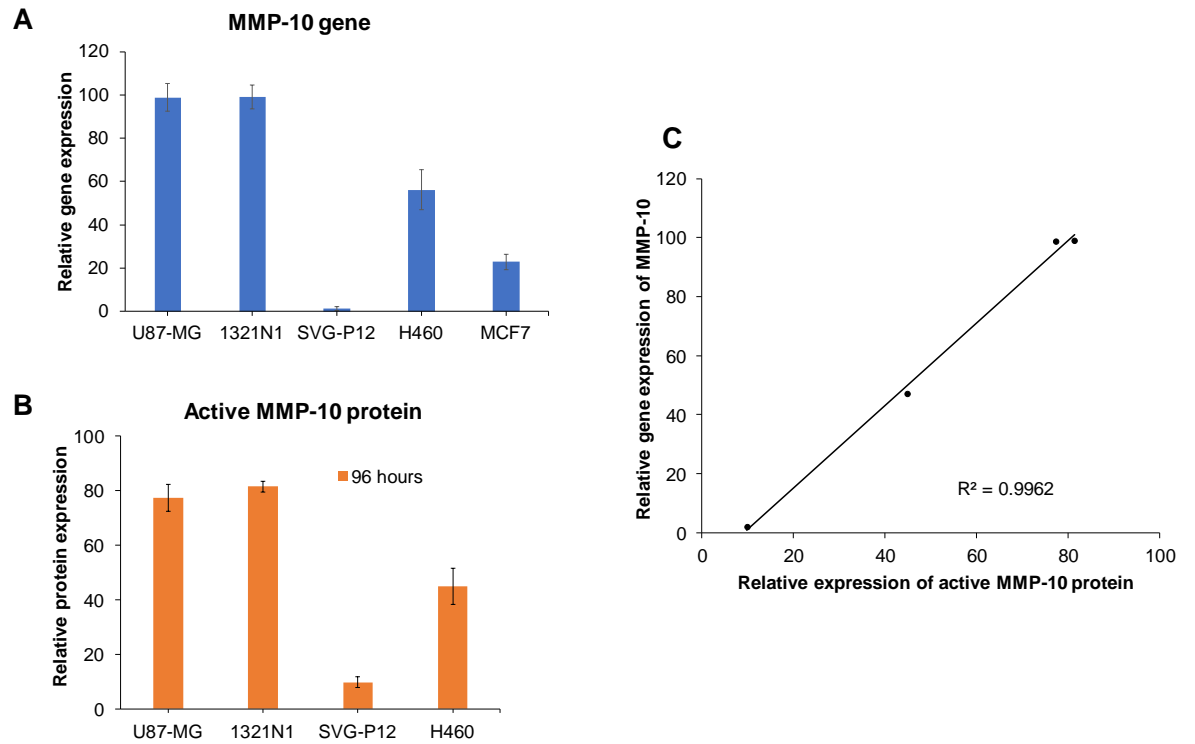
Figure II.8: Relationship between MMP-10 gene expression and active protein expression in human tumour and normal glial cell lines. (A) MMP-10 relative gene expression, normalised to GAPDH, **(B)** Active MMP-10 relative protein expression, normalised to β-Actin, **(C)** Correlation between MMP-10 protein and gene expression, R^2=0.9962. Results demonstrated a good correlation between gene expression and protein expression of MMP-10.

II.6 Expression of MMPs in clinical tumour specimens, by immunohistochemistry

The glioma samples demonstrate a very high expression of MMP-2, high expression of MMP-3 and; moderate expression of MMP-9 (Figures II.9, II.10 and II.11). However, MMP-2, MMP-3 and MMP-9 are also expressed at moderate levels in normal brain samples (Figures II.9, II.10 and II.11). In contrast, strong positive staining of MMP-10 was detected in the glioma tissues with expression throughout the whole specimen relative to low/negligible staining in normal brain tissues (Figure II.12). More specifically, in the normal brain tissues; cerebral cortex, hippocampus and cerebellum from glial and neuronal origin demonstrate low expression of MMP-10. In contrast, expression of MMP-10 in glioma tissues is very high (Figure II.12). The staining pattern observed in the panel of glioma and normal brain tissues correlate well with the MMP-10 expression as determined by western blotting or RT-PCR (Figures II.4, II.8 and II.12).

MMP-2

High grade glioma

Low grade glioma

Cerebral cortex

Hippocampus

Cerebellum

Key: Low | Moderate | High | Very high expression

Figure II.9: Immunohistochemical detection of MMP-2 in glioma and normal brain tissues; demonstrating overexpression in clinical glioma specimens and moderate expression in histologically normal brain tissues. Classification of expression levels was determined from the IHC staining score of each tumour as either very high (score of 4), high (score of 3), moderate (score of 2), low (score of 1) or negative (score of 0) MMP-2 expression. (**Image credit**: Human Protein Atlas)

MMP-3

High grade glioma   Low grade glioma

Cerebral cortex   Hippocampus   Cerebellum

Key: Low   Moderate   High   Very high expression

Figure II.10: Immunohistochemical detection of MMP-3 in glioma and normal brain tissues; demonstrating overexpression in clinical glioma specimens and moderate expression in histologically normal brain tissues. Classification of expression levels was determined from the IHC staining score of each tumour as either very high (score of 4), high (score of 3), moderate (score of 2), low (score of 1) or negative (score of 0) MMP-3 expression. (**Image credit**: Human Protein Atlas)
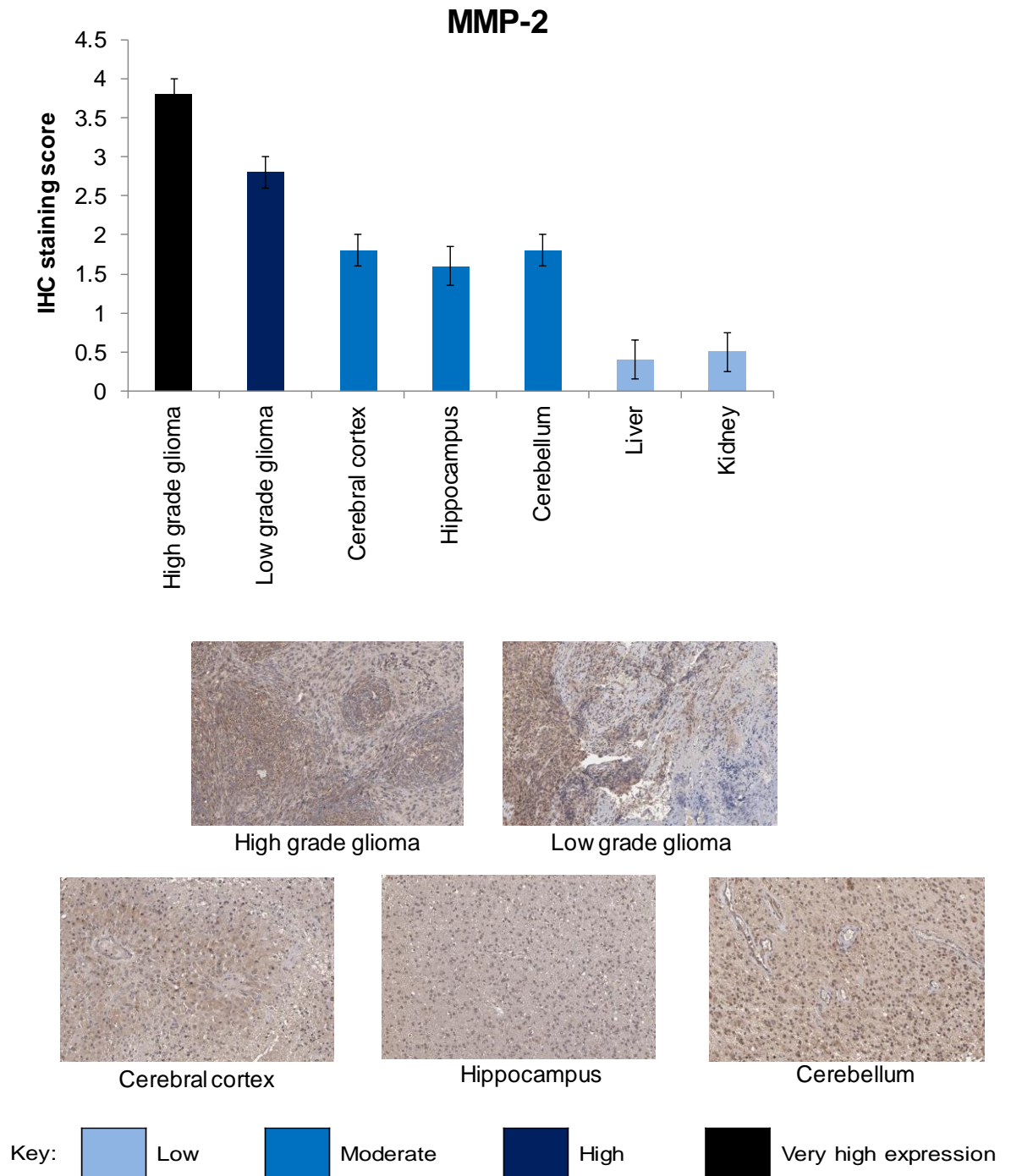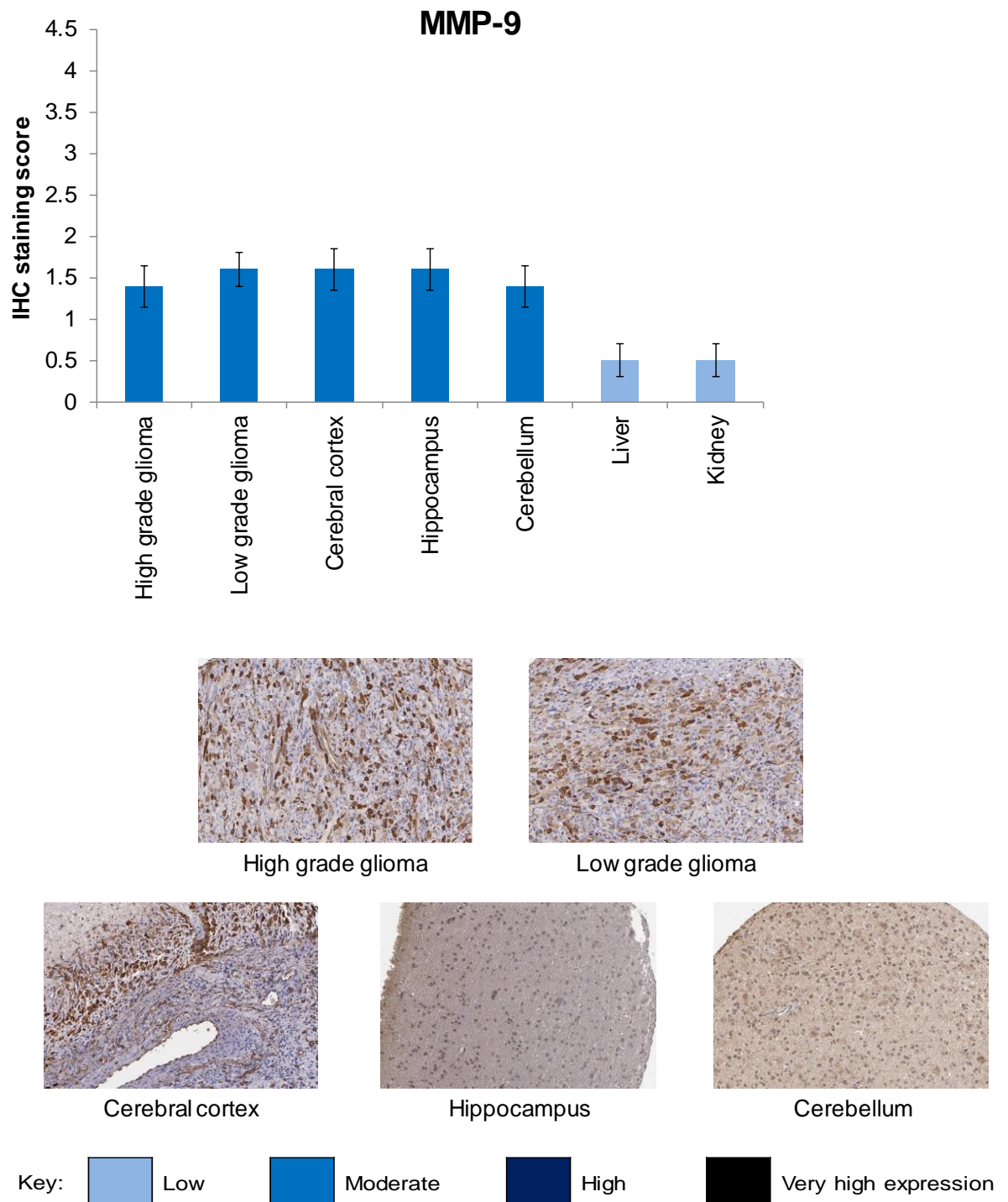
Figure II.11: Immunohistochemical detection of MMP-9 in glioma and normal brain tissues; demonstrating moderate expression in both clinical glioma specimens and histologically normal brain tissues. Classification of expression levels was determined from the IHC staining score of each tumour as either very high (score of 4), high (score of 3), moderate (score of 2), low (score of 1) or negative (score of 0) MMP-3 expression. (**Image credit**: Human Protein Atlas)

MMP-10

Figure II.12: Immunohistochemical detection of MMP-10 in glioma and normal brain tissues. Representative images of Clone 5E4 NCL antibody. MMP-10 is overexpressed in clinical tumour specimens relative to low expression in histologically normal tissues. Classification of expression levels was determined from the IHC staining score of each tumour as either very high (score of 4), high (score of 3), moderate (score of 2), low (score of 1) or negative (score of 0) MMP-3 expression. (**Image credit**: Human Protein Atlas)
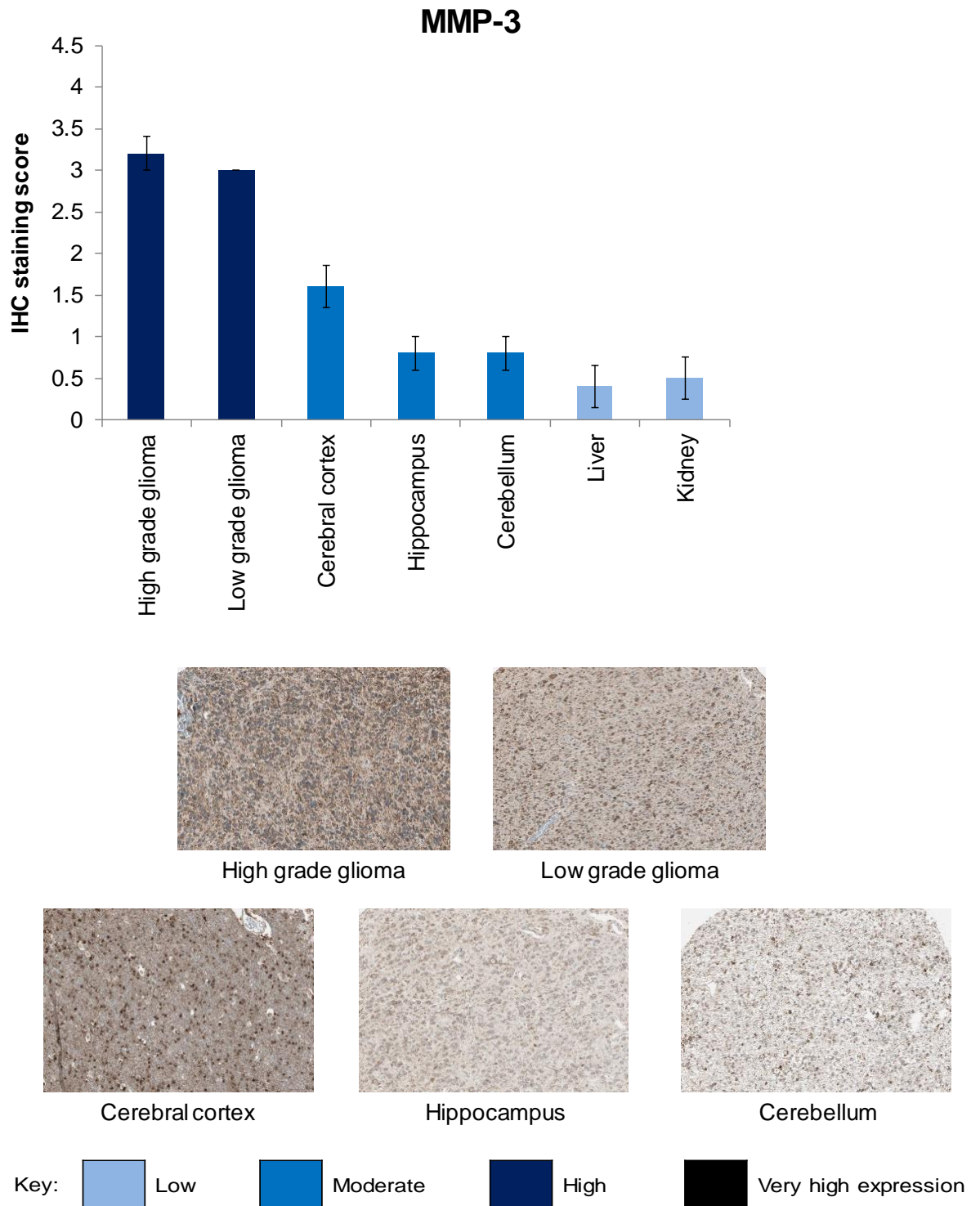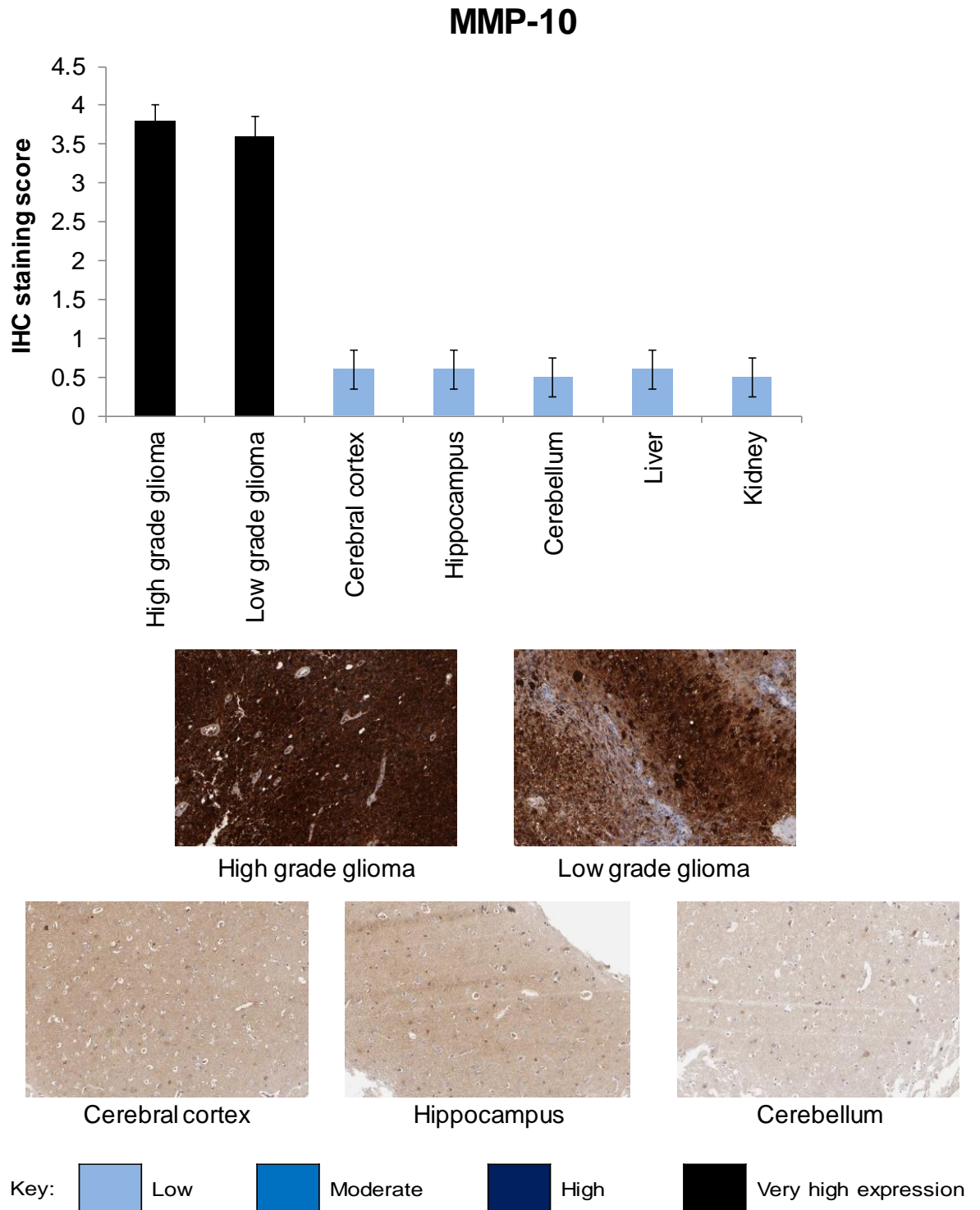
II.7 Measurement of MMP activity: Fluorometric enzyme assay

II.7.1 Determination of MMP-selective proteolytic activity

In order to assess levels of functional MMPs, a continuous fluorometric assay was used and optimised using recombinant MMPs. For initial optimisation, the activity of recombinant MMPs was measured for their ability to hydrolyse MMP-subfamily selective fluorescently labelled substrates, M-2055 and M-2110 (Bachem, Switzerland). A time dependent increase in absorbance was observed at all concentrations of substrate (ranging from 50 µM to 500 nM) with 1 µM being chosen as the optimum concentration for testing MMP activity. M-2110, stromelysin-selective substrate, was preferentially cleaved by stromelysins (MMP-3 and MMP-10) with very slow hydrolysis by MMP-9 and negligible activity with MMP-2 (Figure II.13).[221] Conversely, M-2055, a gelatinase-selective substrate, was efficiently hydrolysed by gelatinases over stromelysins (Figure II.13).[222] The activity of recombinant MMPs with selective substrates and the initial rates of reaction demonstrated a correlation with the available literature, thus verifying the utility of these substrates for further assessment of MMPs in tumour cell models.

II.7.2 Differential levels of active MMP sub-families in culture media of human tumour cell lines

Using the stromelysin-selective substrate, M-2110, the MMP-10 expressing cell lines, U87-MG, 1321N1 and H460, produced high MMP activity levels compared to SVG-P12 cell line, which possess low levels of MMP-10 protein (Figure II.14). The active MMP levels, demonstrated against M-2110, observed in the cell lines

correlated to gene and protein expression of these MMPs (Figures II.4, II.8 and II.15).

With the gelatinase-selective substrate, M-2055, the MMP-2 and MMP-9 expressing glioma (U87-GM and 1321N1) and normal glial (SVG-P12) cell lines demonstrated high MMP activity levels. The H460 and MCF7 reference cell lines possess low or negative levels of gelatinases (Figure II.14). The MMP activities in these cell lines showed a good correlation to that detected by RT-PCR. (Figure II.4, II.8 and II.15).

M-2110 substrate (MMP-10/-3 selective)

M-2055 substrate (MMP-2/-9 selective)
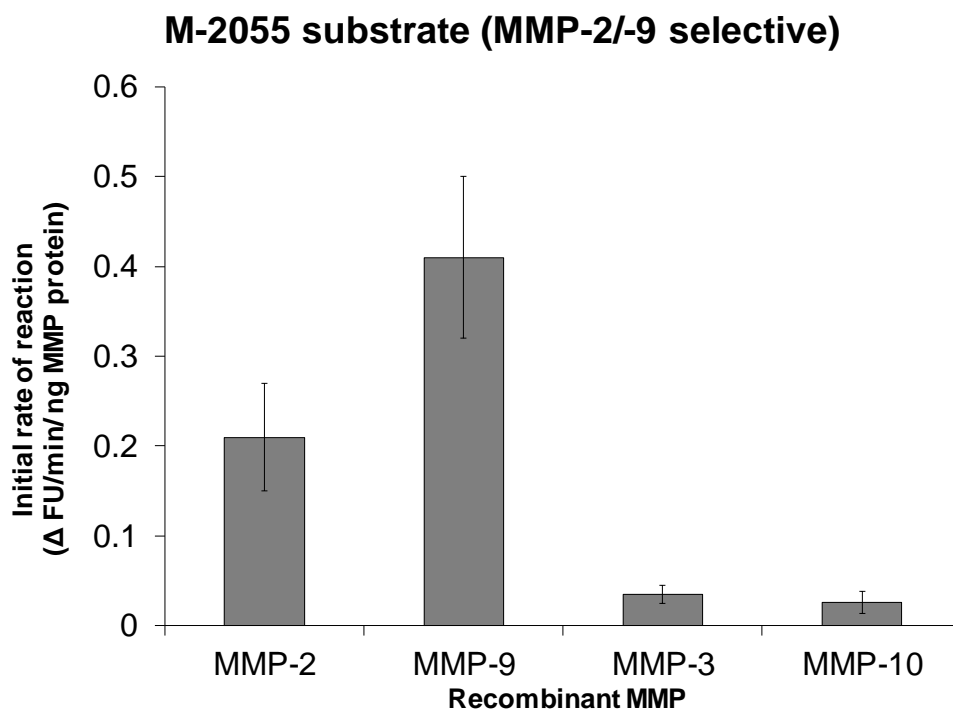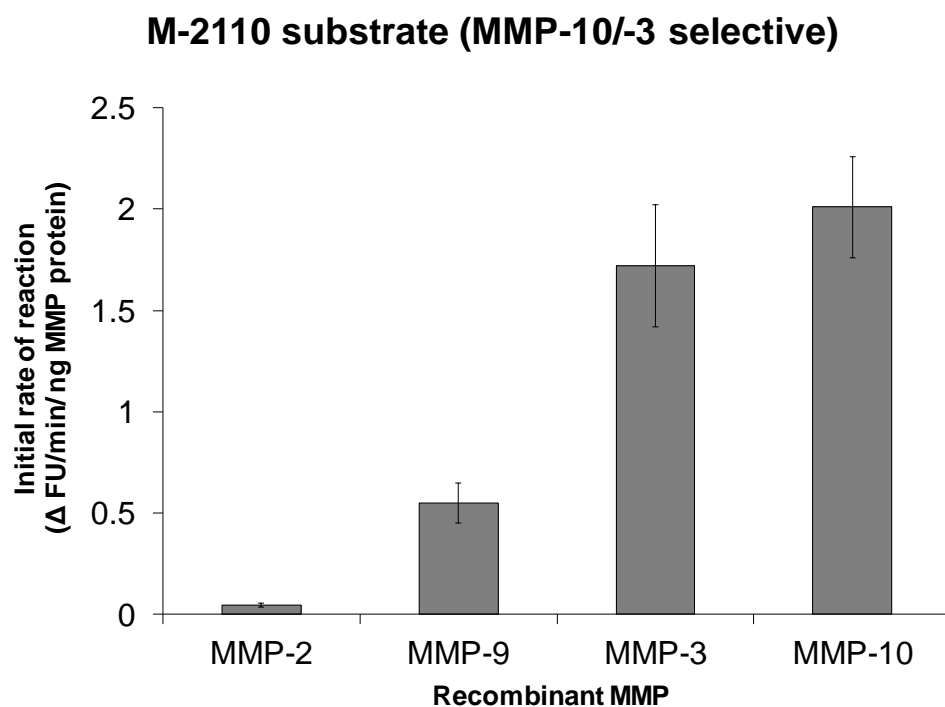
Figure II.13: Continuous fluorometric assay of MMPs with M-2110 (Mca-Arg-Pro-Lys-Pro-Val-Glu-Nva-trp-Arg-Lys(Dnp)-NH$_2$) and M-2055 (Dnp-Pro-β-cyclohexyl-Ala-Gly-Cys(Me)-His-Ala-Lys(N-Me-Abz)-NH$_2$) substrates. Assay was performed at 37°C by reacting 1µM substrate and 200 ng of MMPs in 100 µl solution of assay buffer. Fluorescence was read with λ_{ex} = 325 nm and λ_{em} = 393 nm for M-2110; and λ_{ex} = 365 nm and λ_{em} = 450 nm for M-2055.
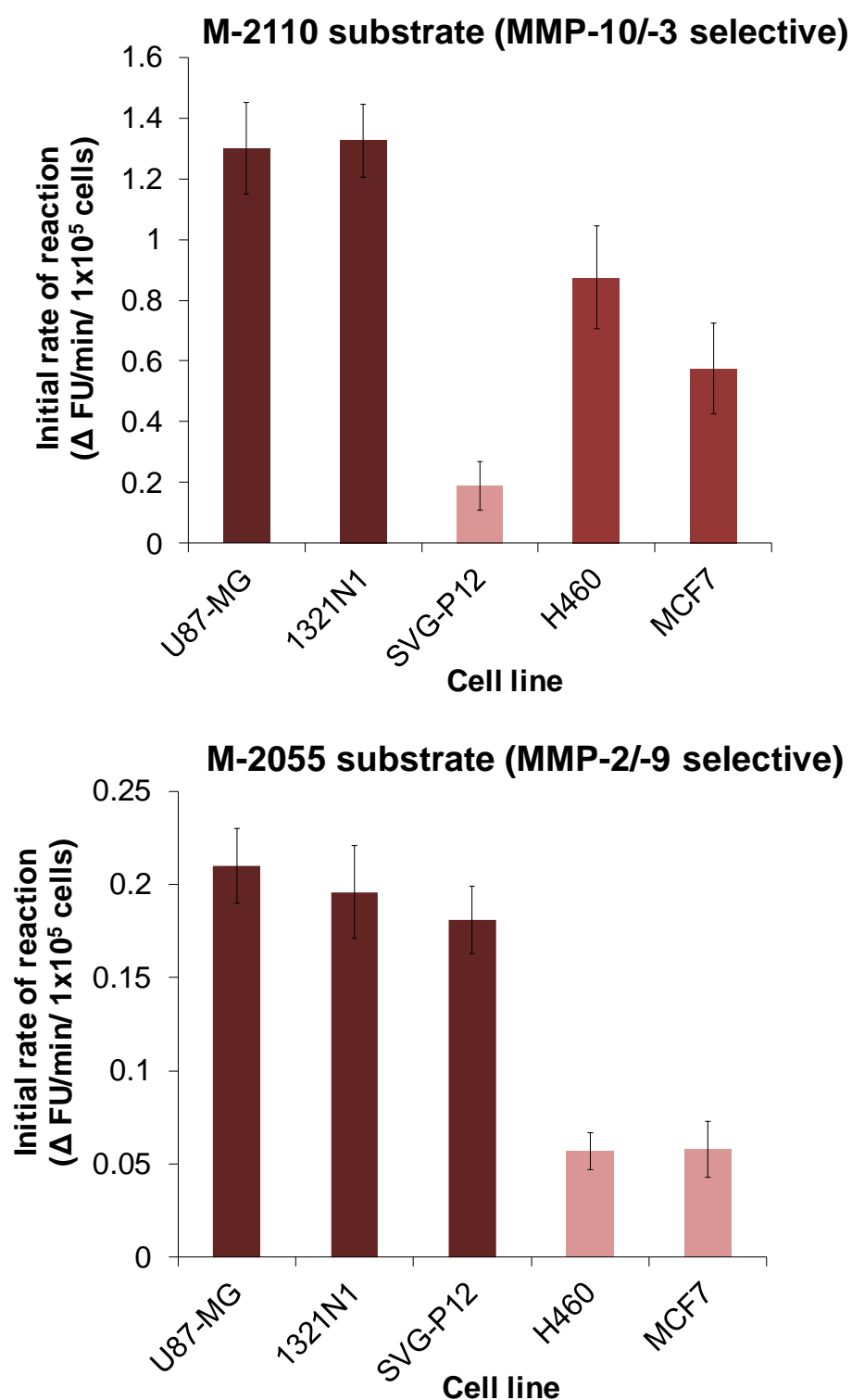
Figure II.14: Continuous fluorometric assay for determination of active MMPs in human preclinical cell models, measured with M-2110 and M-2055 substrates. Assay was performed at 37°C by reacting 1μM substrate and culture media protein extracts (representing 1×10^5 cells) in 100 μl solution of assay buffer.

A

B

Cell line	Relative gene expression				Activity against substrates	
	MMP-2	MMP-3	MMP-9	MMP-10	M-2110 (MMP-10/-3 selective)	M-2055 (MMP-2/-9 selective)
U87-MG	+++	+++	++	+++		
1321N1	+++	+	+++	+++		
SVG-P12	+++	+	+++	+/-		

C

	U87-MG	1321N1	SVG-P12
MMP-10 gene expression	+++	+++	+/-
Active MMP-10 protein expression	+++	+++	+
Enzyme activity against stromelysin-selective substrate	+++	+++	+
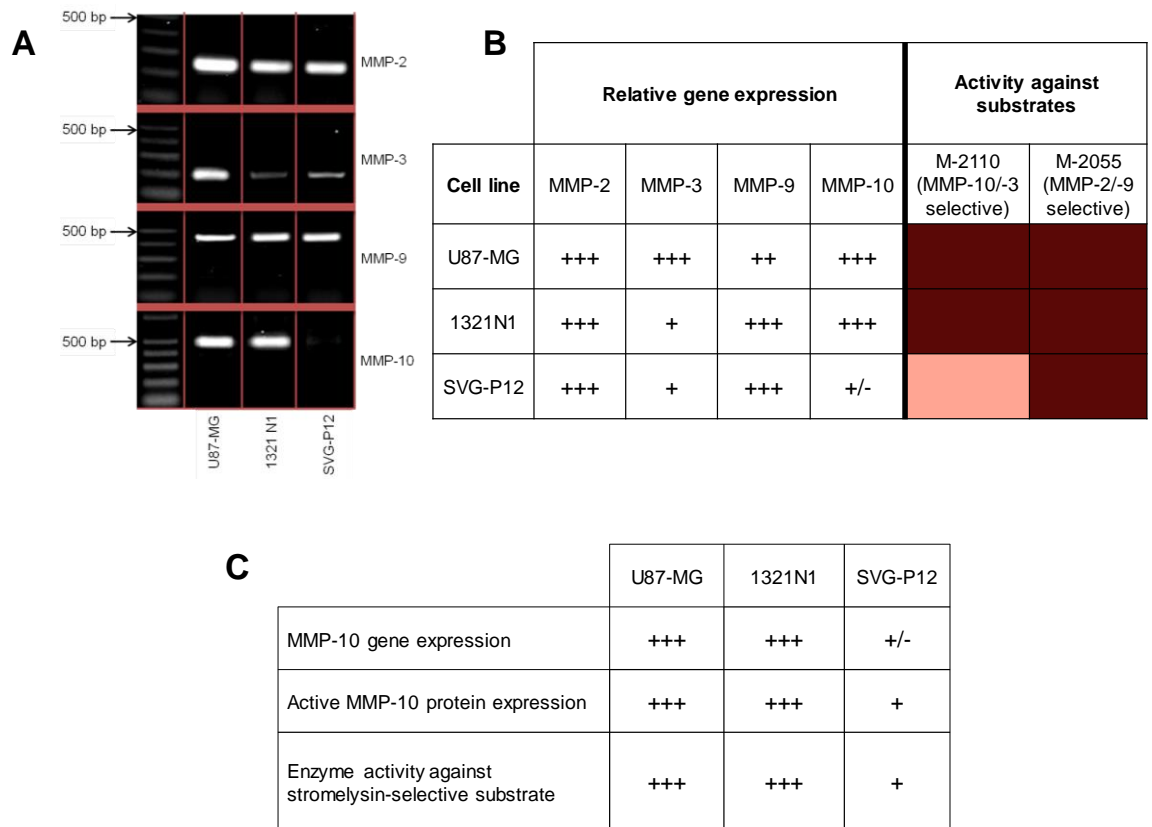
Figure II.15: Relationship between MMP expression and active MMP levels in human glioma and normal glial cell lines. (A) RT-PCR analysis demonstrating varied expression of MMPs in preclinical cell lines. **(B)** Relationship between MMP activity levels and gene expression. Activity of MMPs demonstrated by the ability of human cell media protein to cleave stromelysin-selective (M-2110) and gelatinase-selective (M-2055) substrates. **(C)** Expression and activity profile of MMP-10 in human glioma and normal brain cell lines demonstrating strong correlation between gene, protein and active proteolytic levels.

1.8   Discussion

The strong correlation between RT-PCR, western blotting and fluorogenic substrate cleavage assay to demonstrate overexpression of MMP-10 in tumour cell lines relative to normal glial cell line, suggests a predominant role of MMP-10 in the growth and development of tumour in glioma. The immunohistochemical overexpression of MMP-10 in clinical samples of human glioma relative to normal brain also established the viability of MMP-10 as a target for therapeutic intervention in human glioblastoma.

Overexpression of MMP-10 has been shown in several malignancies including oral carcinoma, head and neck squamous cell carcinoma (HNSCC), skin cancer, oesophageal carcinoma and non-small cell lung carcinoma (NSCLC).[155, 223-226] However, the expression of MMP-10 protein in human glioblastoma has not been previously reported. To our knowledge, the present study is the first to address the overexpression and elevated proteolytic activity of MMP-10 in preclinical models of human glioma relative to normal glial cells. MMP-10 expression was significantly higher in the analysed glioblastoma tumour tissues compared to histologically normal brain tissues.

In this study we demonstrated that MMP-10 expression is concomitantly increased with glioma cell proliferation relative to the low MMP-10 expression maintained at basal level in normal glial cells *in vitro*. The human glioma cells demonstrating a higher expression of MMP-10 also showed a greater ability to cleave the stromelysin-selective fluorogenic substrate. In contrast, normal glial cells demonstrating low expression of MMP-10 showed no significant increase in fluorescence. This result confirmed the clear differential of MMP-10 proteolytic activity between normal glial and glioma cells. Indeed, the overexpression of

MMP-10 in a large population of tumour cells and tissues were positively correlated with tumour size, suggesting the importance of MMP-10 function in tumour growth and expansion.[227, 228] In fact, MMP-10 expression is elevated in NSCLC tissues with NSCLC patients whose tumours showed high MMP-10 proteolytic activity exhibited significantly worse survival than those whose tumours express low MMP-10.[155, 229]

Glioblastoma is a fatal malignant primary brain tumour and contains self-renewing, tumorigenic cancer stem cells (CSCs) that contribute to tumour initiation and therapeutic resistance.[230] CSCs are defined by their ability to clonally expand, differentiate into tumour cells and initiate tumours. The ECM is an essential non-cellular component of the adult stem cell niche.[230, 231] In malignancy, increased ECM stiffness can be a physical barrier for chemotherapeutics and thus protect CSCs from therapeutic agents.[230] MMPs can degrade components of ECM in tumours, releasing cytokines, growth factors and other molecules from the cell surface.[230] Unlike many MMPs that are implicated in tumour invasion and metastasis, it was recently demonstrated that MMP-10 overexpression can promote tumour initiation and growth through maintenance of CSCs.[231-233] The involvement of MMP-10 is suggested to be involved in early stages of tumour formation and invasion. MMP-10 overexpression in CSC-enriched cultures of mouse lung adenocarcinoma has been linked to enhanced tumour growth and clonal expansion *in vitro*, and tumour initiation *in vivo*.[231-233] Inhibition of MMP-10 expression leads to a significant decrease in CSC related gene expression.[232] Interestingly, the U87-MG and 1321N1 cells are enriched in CD133$^+$/Notch4$^+$ cell population, the two markers implicated in both human CSCs from various tumour types, including glioblastoma.[234] Notch inhibition blocks the proliferation and

tumour initiating activity of human lung CSCs.[235] Likewise, Inhibition of Notch signalling blocks the ability of glioblastoma-derived CSCs to propagate tumours and depletes CD133^{+} stem-like cells in neurospheres.[234, 236] The enhanced expression of MMP-10/Notch is required for tumour invasion of human NSCLC cells *in vitro* and primary oncosphere-derived lung tumours.[232] More specific to this study, MMP-10 expression is also elevated in these CSC-like U87-MG and 1321N1 glioma cells, suggesting that MMP-10 may also function in the maintenance of glioma stem cells. Inhibition of MMP-10 leads to significant reduction in tumour migration and blocks the growth and metastatic behaviour.[232] Therefore MMP-10^{+}/Notch[+] may be useful markers of glioma stem cell species. CSCs also enhances the expression of Wnt genes, that are significantly overexpressed in U87-MG cells and implicated in glioma progression and aggressiveness.[237] Interestingly, MMP-10 knockdown inhibited the invasion promoted by Wnt overexpression in HNSCC.[228] In support of these findings, MMP-10 could be a potential marker for predicting the tumour migration and invasion in glioblastoma.

Analysis of expression profiling data on preclinical glioma cells revealed a significant correlation between MMP-10 expression and proteolytic activity. H460 (NSCLC) reference cell line has been demonstrated to possess high expression and proteolytic activity MMP-10, which was confirmed in this study.[155] The expression and proteolytic activity of MMP-10 is elevated in human NSCLC and unlike the majority of MMPs, MMP-10 was suggested to play a central role in tumour growth and development rather than invasion and metastasis.[155] In this study similar associations were observed between MMP-10 expression and proteolytic activity of human glioma cells. Thus, MMP-10 may play a widespread

role in the glioma malignancy. MMP-10 is an upstream regulator of the MMP activation cascade demonstrated by its ability to cleave several proMMPs such as MMP-1, MMP-7, MMP-8, MMP-9 and MMP-13.[238, 239] This broad activity could be suggestive of glioma tumour initiator role of MMP-10 in the MMP cascade.

The excessive proteolytic processing by various MMPs via cleavage of substrates or interacting proteins have pivotal roles in the regulation of myriad of biological pathways and is described as an initial step in the degradation of ECM components in numerous pathological processes such as tumour growth, angiogenesis, invasion and metastasis. In this study, MMP-10 was proteolytically active in glioma cells relative to normal glial cells. However, glioma and normal glial cells demonstrating a higher expression of gelatinases (MMP-2 and MMP-9), also showed greater ability to cleave the gelatinase-selective fluorogenic substrate. This observation also correlated with the expression of gelatinases in brain tumour and normal brain samples. It is proposed that moderate to high proteolytic activity of MMPs in normal tissues are not necessarily tumour specific but may be indicative of physiological processess, such as maintanance of the ECM.[240] Importantly for this study however, validation of specific MMP as a drug target is important for the efficient functioning of drug targeting systems such as prodrugs. Though MMP-2 and MMP-9 have been implicated in glioblastoma progression and invasion, the proteolytic function of MMPs in glioma vs normal brain has never been elucidated. The observation that gelatinases are proteolytically active in normal brain cells suggests their role as anti-targets in glioma. These MMPs have been implicated as targets in one disease and counter or anti-targets in another.[194] The proteolytic activity of MMPs is essential for efficient cleavage of substrates, peptide linkers or prodrugs and targeting by

inhibitors.[205] It is therefore vital to realise the the clinical implication of the MMP systems in glioblastoma so that specific MMPs that are overactive in the tumour microenvironment relative to surrounding normal tissues, can be selectively targeted by choosing specific linkers, selective substrates or peptide-prodrugs. Taken together with the observation that MMP-10 is overexpressed in glioma samples analysed and is active in glioma cell lines, this further supports MMP-10 as a potential glioma tumour initiator and a clinically viable target for therapeutic intervention of glioblastoma.

Since MMP-10 is involved in tumour initiation and growth, it is directly secreted by tumours and CSCs, and its inhibition leads to reduction in metastasis and invasion; it is therefore reasonable to postulate that inhibitors or selective peptide prodrugs with specificity against overactive MMPs, such as MMP-10, may be a better approach for the treatment of glioblastoma.

In conclusion, this study shows the increased expression and activity of MMP-10 in human glioma tumours, suggesting MMP-10 is a potential drug target for therapeutic intervention of glioblastoma. This observation led to the development of *in silico* model to rationalise the functional similarity and substrate cleavage preferences between the members of MMP subfamily, to facilitate progress towards the development of MMP-10 selective anticancer prodrugs.

Chapter 3: Rationalised drug design approaches through identification of proteolytic selectivity of MMPs *via* molecular modelling

III.1 Introduction

A requirement for success in prodrug approaches is MMP selectivity through incorporation of MMP-subtype unique peptide sequence. Rational drug discovery approaches can fine-tune the selectivity of peptide substrates and inhibitors. Visualising and quantifying binding preferences and motifs can provide valuable insight into the structural determinants of substrate selectivity and enable MMP-targeted drug development.[134, 241]

III.1.1 Rational drug discovery

Therapeutic drugs are essential for the prevention and treatment of diseases such as cancer, to restore the normal functioning of the human body when it goes wrong. The process of drug discovery is challenging, time consuming, expensive and relies on trial-and-error approach for testing of chemical compounds on cultured cells or animals to match the desired effects of treatment. To overcome these challenges, several multidisciplinary stages are required for successful drug discovery and these form the basis of rational drug design. Rational drug discovery begins with the identification and characterisation of a biological macromolecule implicated in disease pathology i.e. finding a target.[242]

Once a target is identified, the most fundamental goal in rational drug design is to predict whether a given drug molecule will bind to the target and if so how strongly,

with minimal cross selectivity with other biomolecules. This can be achieved in two broadly categorised ways:[243-246]

A. Ligand-based approach relies on the knowledge of small molecules and their binding potencies to the target of interest. A spatial understanding within the binding pocket is built up by rational systematic changes to small molecule backbones. Thus though trial and error, using such approaches as matched pair analysis, a structure activity relationship can be built without molecular level knowledge of the target protein.[247, 248] However, accurate knowledge of the receptor or protein structure is unknown and 3D-quantitative structure activity relationships (3D QSAR) using pharmacophore modelling is routinely used instead, to predict the activity of new analogues (Figure III.1).[247, 248] A pharmacophore is defined as a molecular framework that carries the essential features responsible for a drug's biological activity.[246] QSAR is a mathematical model that relates to biological or chemical activity of a drug. In the absence of a target protein the 3D pharmacophore and QSAR models would predict the key amino acid positions within the active site of the target protein, based on the activity of known ligands. However, without the accurate knowledge of the target protein, the prediction results may be prone to error.[249]

B. Structure-based approach relies on the knowledge of the three dimensional (3D) structure of the drug target bound to its natural ligand or a drug which is determined either by X-ray crystallography or by NMR. Once the ligand bound 3D structure is known, a virtual screening or computational technique is used to identify new drug ligands for a given receptor. The obtained 3D structure further enables the researchers to identify its binding site, the so called active site.[250] The concept of this approach is to predict the binding affinity and selectivity of new

drug candidates for the drug target through knowledge of its 3D conformation. The identification of new ligands for a given receptor is achieved in a step-wise manner: determination of 3D structure of the drug target and identification of its binding site through *in silico* study, docking of minimum energy conformers of known drug ligands into the target to highlight key binding sites, rational design of novel drugs through the exploitation of the binding site and; experimentally validate the *in silico* prediction (Figure III.2).[250]
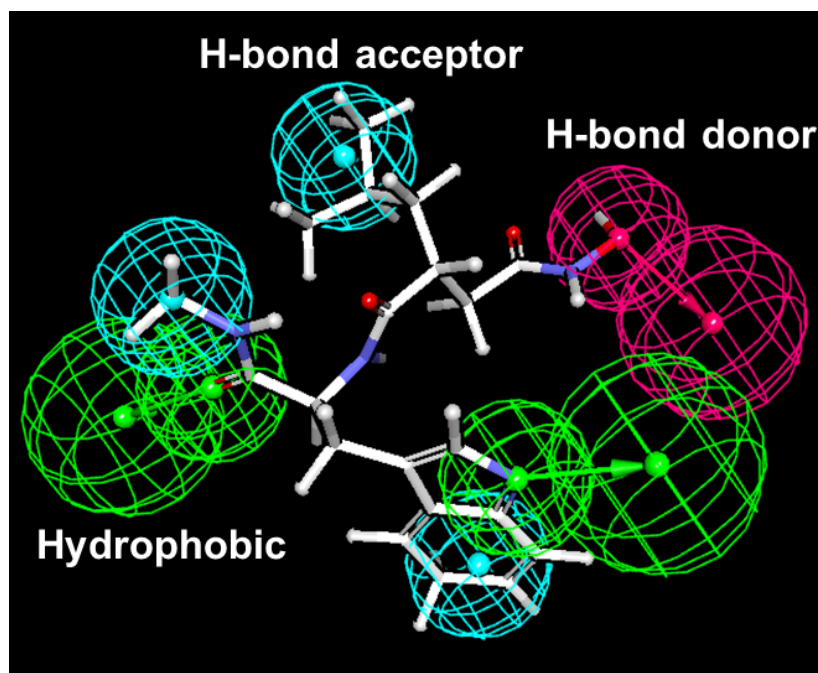
Figure III.1: Pharmacophore query for molecular binding recognition of MMP inhibitor (Ilomastat). The features represent recognition motifs such as hydrogen bond acceptors (cyan) or donors (pink), and hydrophobic groups (green). The radius of the sphere determines the strictness of the geometric constraint. For features where the correct orientation of the interaction is important such as hydrogen bonds and the aromatic plane, the vector indications are added to the structure. Pharmacophore modelling is useful for predicting of interaction of known ligand with a theoretical or similar receptor structure.
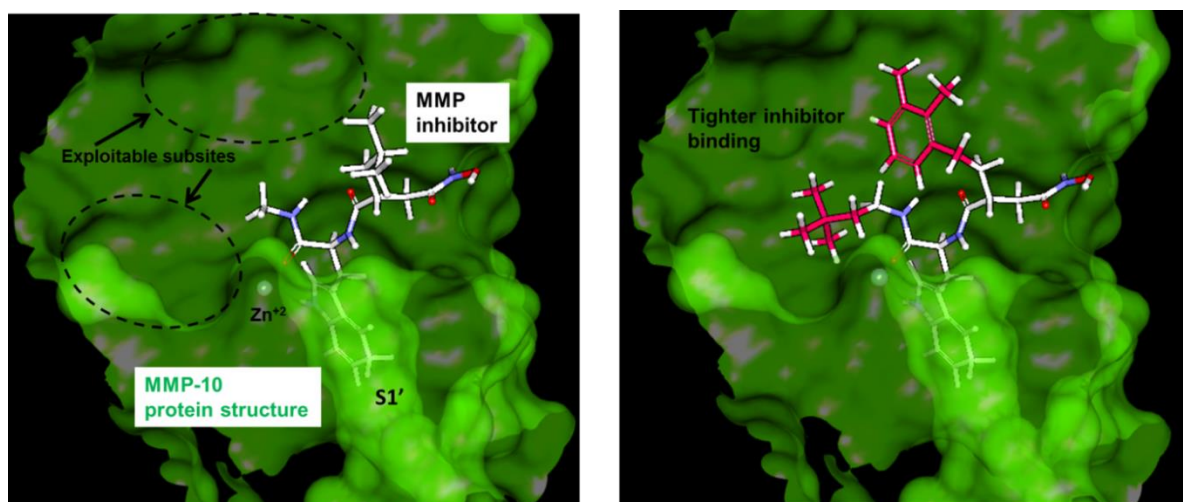

Figure III.2: A structure-based drug design approach uses the 3D structure of the drug bound (e.g. MMP inhibitor, Ilomastat) to a target protein (e.g. MMP-10 protein) as a direct means for visualising protein-ligand interactions. The ligand bound receptor allows for determination of chemical modifications that can improve drug potency and selectivity.

III.1.2 X-Ray crystallography

X-Ray crystallography is the most reliable and preferred technique for structural determination of biological macromolecules and proteins. The availability of protein structure can provide a more detailed understanding on structure-based drug design, elucidation of enzyme mechanisms and site-directed mutagenesis and improving specificity of protein-ligand interactions.[251]

The aim of X-Ray crystallography is to obtain a three dimensional atomic and molecular structure from a crystal. A purified protein sample at high concentration is crystallised and exposed to an X-Ray beam. The resulting pattern of diffraction spots are then processed to yield information about the symmetry of crystal packing and size of the repeating unit that constitute the crystal. The intensity of the diffraction spots are used to calculate the map of electron density. The resulting molecular structure is then refined to adopt a thermodynamically favoured conformation and to fit the map more accurately.[251] The following methodologies briefly describe the process from protein crystallisation to model building:

III.1.2.1 Protein crystallisation

Successful protein crystallography is achieved when a reliable protein source is available, along with high quality and homogenous yields are achieved from purification and concentration protocol. The growth of protein crystals is the rate limiting and a complex step in most protein crystallographic work. The principle of protein crystallisation is to take a high concentration solution of the protein sample and cause it to come out of solution.[251, 252] For the purpose of analysing the catalytic binding sites of the protein and drug design, a synthetic/endogenous

inhibitor or a ligand bound protein is also prepared and purified prior to undertaking the crystallisation experiment.[251, 253] Crystal growth is dependent upon factors such as the concentration of the protein concentration, buffer, the choice of precipitant and its concentration, its pH, temperature and the crystallisation technique. Crystal screen packages (commercially available) consisting of solutions varying widely in buffer, precipitant, pH and salt are often used at this stage.[251, 253] The experiments can be set up using techniques like hanging drop vapour diffusion, sitting drop vapour diffusion and dialysis, commonly at both 4°C and room temperature.[251, 254] Under correct conditions crystals will grow. At this stage it is more usual to see showers of microcrystals or a few tiny crystals, indicating that the crystal subunits possess sufficient intrinsic structural symmetry to make crystallisation achievable and also encourages the researcher to proceed for diffraction analysis of the crystals.[254, 255] For the purpose of diffraction analysis, protein crystals should be a minimum of 0.1 mm in length, to provide sufficient exposure of crystal lattice to the X-Ray beam.[251, 256]

III.1.2.2 Optical setup and diffraction analysis

The X-Rays are generated from electrons striking a copper anode or from accelerating electrons in a synchrotron storage ring. The X-Rays must be focused into a beam and then collimated with sets of adjustable slits to 0.1-0.3 mm diameter.[251, 256] The crystal is mounted in this beam and adjusted to a device called goniometer head. For cryogenic data collection, a cold liquid nitrogen gas stream is used to keep the crystal at 100K throughout the experiment.[251, 257] Before the exposure, the distance from the crystal to the detector is adjusted to allow for collection of diffraction spots up to maximum of 1.5-3.0 Å resolution. A collimator produces focused X-Rays on to the crystal to produce diffraction

pattern, detected on the X-Ray detector. The diffraction data is analysed by confirming the diffraction to sufficient resolution to make structure determination to inter-atomic detail possible. Usually, diffraction spots beyond 3 Å are required with carbon-carbon bond of approximately 1.5 Å and the resolution of 3 Å is sufficient to detect the amino acid side chains in the electron density map.[251, 257]

III.1.2.3   Data processing

There are many software packages available with well-established algorithms to overcome the mathematical complexity involved in processing of diffraction data. The first step involves the accurate determination of the crystal structure and of the unit cell dimensions in the space. The next step of the data processing is the measurement of the intensities of the diffraction spots. In theory, the larger the volume of the protein crystal the stronger the diffraction, so larger proteins are preferred to fully determine all atom positions.[251]

III.1.2.4   Model building and refinement

The quality of the electron density map can be refined by the geometrical operation that connects the non-crystallographic symmetry (NCS) subunits.[251, 258] This is further confirmed by comparing the observed structure factors with the calculated ones and the difference is expressed as the percentage of correlation factor known as the R-factor.[251, 258, 259] Model building involves the use of a computer graphics program to display the electron density map and with the alignment of protein sequence, the insertion of each amino acid residue. The model of a molecule's structure that has been built is then published and deposited in a crystallographic database; such as the Protein Data Bank (PDB) (for protein structures). PDB files can be downloaded from the RSCB PDB

software such as Discovery Studio and PyMOL.[251, 260]

III.1.3 Molecular dynamics and force field

Further refinement of the molecular structure of the protein is carried out by computational modelling programs to minimise the energy conformation of the protein. In the field of computational chemistry, energy minimisation or geometry optimisation is the process of aligning the collection of atoms arranged in space where the net interatomic force on each atom is close to zero.[261] This can be achieved by utilising a computer simulation method called molecular mechanics (MM) or molecular dynamics (MD). MD is used to estimate the strength of the intermolecular interaction between the small molecule and its receptor or drug target. These methods further enable the researcher to rationally predict and modify the conformation of the small molecule docked into the receptor. During the course of simulation, MD uses a combination of the mathematical parameters and functions commonly referred to as a force field. A force field is defined as a mathematical expression designating the dependence of the energy of the system on the coordinates of its particles.[261-263] A Force field consists of a set of parameters used to calculate the interatomic potential energy of a system, U (r_1, r_2,....,r_N) (Where 'r' represents the interatomic distance between molecules). These parameters are typically obtained either from the beginning or semi-practical molecular mechanical calculations or by aligning to experimental data such as X-Ray and electron diffraction, Raman spectroscopy and NMR. Molecules are described as a series of atoms held together by simple elastic forces and the

force field simulation replaces the true of potential of the molecules with a simplified model effective in the region being simulated. Ideally it is sufficiently detailed to reproduce the molecular geometry and selected properties of the system studied, but must be simple enough to be evaluated quickly.

Many force fields are available in the literature, designed for different simulation purposes and having different degrees of complexity. A force field is generally represented by the following equation (1):[261-264]

$$U = \sum_{bonds} \frac{1}{2} K_b \ (r - r_0)^2 + \sum_{angles} \frac{1}{2} K_a \ (\theta - \theta_0)^2 + \sum_{torsions} \frac{V_n}{2} \left[1 + \cos(n\phi - \delta)\right] \quad (1)$$

$$+ \sum_{improper} V_{imp} + \sum_{LJ} 4\epsilon_{ij} \left(\frac{\sigma_{ij}^{12}}{r_{ij}^{12}} - \frac{\sigma_{ij}^{6}}{r_{ij}^{6}}\right) + \sum_{elec} \frac{q_i q_j}{r_{ij}}$$

Where the first four terms refer to intermolecular or local contributions to the total energy (angle bending, bond stretching, improper torsions and dihedral), and the last two terms describe the Van der Waals interactions (by application of 12-6 Lennard-Jones potential) and the Coulombic interactions.[261-263]

Widely used biomolecular protein force fields are CHARMM (Chemistry at Harvard Macromolecular Mechanics), AMBER (Assisted Model Building with Energy Refinement), GROMOS (Groningen Molecular Simulation), MMFF (Merck Molecular Force Field) and CFF (Consistent Force Field). These force fields were developed by different academic research groups, the associated parameters have been peer reviewed and made publicly available.[264-267] By default, when a force field is applied *in silico*, attempts are made to ensure that the molecule simulates correctly by performing the following steps:

1. Add hydrogens appropriate for the selected force field.
2. Evaluate and assign partial charges to the system.

3. Determine atom types by applying forcefield-specific typing rules or by using residue templates.

4. Identify missing forcefield types and assign the correct mathematical parameters for that force field.[264-267]

III.2   Aims and objectives

In this chapter, a reiterative approach using *in silico* proteolytic docking coupled to *in vitro* biochemical assessment have been applied to characterise the MMP catalytic site domains responsible for specific binding with known selective substrate residues. The rationale for this study is to examine the differences between the active site of MMPs docked with selective substrates and prodrugs; and create a robust approach which could be exploited for development of MMP-activated diagnostic probes and therapeutics. The availability of 3-D crystal structures of MMPs allowed us to critically examine the differences existing between the catalytic domains of two closely related MMP subfamilies, the gelatinases: MMP-2 (PDB ID: 1QIB[268]) and MMP-9 (PDB ID: 1GKC[269]); and the stromelysins: MMP-3 (PDB ID: 1CIZ[270]) and MMP-10 (PDB ID: 1Q3A[271]). This allowed rational characterisation of the substrate cleavage site for a particular MMP and its selective substrate.   The commercially available (Bachem, Switzerland) MMP-cleavable fluorogenic substrates were used: M-2055[222] and M-2110[221], reportedly to be selectively hydrolysed by gelatinases and stromelysins respectively. M-2055 is hydrolysed efficiently by MMP-9 at the Gly-Cys(Me) scissile bond and less efficiently by MMP-2 and stromelysins, whereas M-2110 is hydrolysed efficiently by stromelysins at the Glu-Nva scissile bond and less efficiently by MMP-9. The specific cleavage site of M-2055 by stromelysins and M-

2110 by MMP-9 are yet to be determined. In order to rationally characterise these cleavage sites an *in silico* model was developed utilising 3-D flexible docking, identifying P1-P1' substrate subsites chelating the Zn^{+2} ions in the active site of gelatinases and stromelysins; and subsequently analysing the intermolecular atomic distances and associated binding energies. To experimentally validate the computation study LC-MS was carried out to determine the product of MMP-mediated cleavage of these substrates.

Specific objectives include:

1. To optimise *in silico* molecular dynamics model by complete energy minimisations using the appropriate forcefields supported by the Discovery Studio Client, Accelrys.

2. To develop *in silico* models of MMPs based on the reported crystal structures and define the catalytic domains of the disease relevant proteases.

3. To validate the models through flexible-ligand docking of MMP-selective substrates and highlight key catalytic binding determinants.

4. To identify the cleavage site on substrates based on Zn^{+2} ion interaction and calculate total binding energy of the docked models.

5. To experimentally validate the predictability of the *in silico* model for development of MMP-selective therapeutics.

III.3   Materials and methods

III.3.1 3D-Molecular modelling

All molecular modelling and calculations were performed using the BIOVIA Discovery Studio 4.0 molecular modelling package, developed by Accelrys. The X-ray crystal structure of proteins MMP-2 (PDB ID: 1QIB), MMP-3 (PDB ID: 1CIZ), MMP-9 (PDB ID: 1GKC) and MMP-10 (PDB ID: 1Q3A) were acquired from the Protein Data Bank (PDB) and were prepared by omitting the ligands associated with the co-crystal structure. Substrate ligand structures were prepared in the Discovery studio in MOL format.

Preparation of proteins: The protein structure (receptor) was acquired from the Protein Data Bank, the ligand was deleted and the protein structure was prepared for 'flexible docking'. The 'Prepare Protein' protocol ensured the MMP protein was ready for input into future calculations, performing tasks such as cleaning the protein, optimising side-chain conformations, for those residues with inserted atoms and protonating the structure at the specified pH range (6.8 – 7.2 pH). After preparation, the receptor binding sites were identified from the receptor cavities (those cavities created on the removal of the original X-ray structure ligand). PDB files often have active sites defined using the SITE records. When a PDB file is imported, groups are created for each SITE. This tool highlights each site with a transparent red sphere which enables a check against the original co-crystal X-ray structure.

Preparation of ligands: The new ligand structures were built and CHARMM (Chemistry at Harvard Macromolecular Mechanics) forcefield minimisation (using 100,000 minimisation cycles) was applied until the final energy state of the molecule was near to zero kcal/mol. Following minimisation, the ligands were

prepared for 'flexible docking'. The Prepare Ligand protocol helps to prepare ligands for input into other protocols, performing tasks such as removing duplicates, enumerating isomers and tautomers, and generating 3-D conformations. The minimum energy conformation was selected and used as the input for future calculations. Discovery Studio has a maximum allowable ligand size, so once minimised the peptide conformation was locked and the protecting groups along with the drug molecule (doxorubicin) were removed. This left the conformationally constrained peptide chain for docking.

Once the protein and ligand structures were prepared and receptor binding sites identified, the docking was initialised using 'flexible receptor-ligand docking' tool. In this method the substrate ligands were docked into the active site clefts of MMPs via the DS flexible docking tool, wherein the protein structure was selected as the 'receptor molecule' and the substrate structures as the 'ligand molecule'. This protocol allows for some flexibility in receptor cavities during docking of low energy ligand conformations. The amino acid side-chains of specified binding site are allowed to move during docking. This allows receptors to adapt to different ligands in an induced-fit model. The protocol uses a combination of components from other protocols to perform docking, and utilises CHARMM based methods to sample side-chain and ligand conformations. The Flexible Docking protocol performs the following steps:

1. Generation of protein conformations

2. Rigid docking of low energy ligand conformers to protein

3. Flexible docking. A final simulated annealing and energy minimisation of each ligand pose is performed using CDOCKER algorithm.

This procedure is automated within the Discovery Studio package and undertakes the process described by Koska and co-workers, which is outlined below.

Adapted from J. Chem. Inf. Model., Vol. 48, No. 10, **2008**
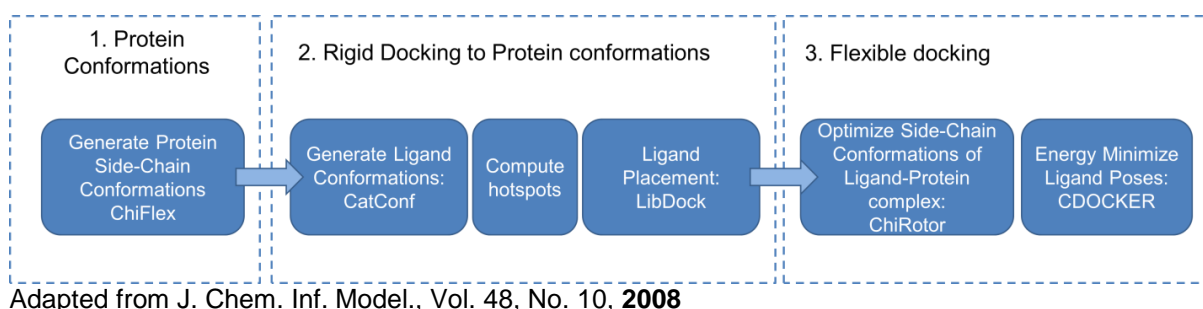
Once completed for the respective substrates, docking results were analysed using Discovery Studio by viewing the ligand interactions hydrophobic receptor surfaces and the location of zinc ion in the receptor with respect to the ligand. This enabled the determination of any coordination of water molecules within the active site, interaction of active site residues with the ligand and the interatomic distances. The binding free energies between a receptor and a ligand were also calculated using the CHARMM implicit solvation models. The binding energy was calculated using the following equation:

Energy binding = Energy complex – Energy ligand - Energy receptor (in kcal/mol)

III.3.2 Liquid Chromatography-Mass spectrometry (LCMS) detection of substrates

LC conditions: High-purity HPLC-grade solvents (Sigma-Aldrich), analytical grade chemicals (Sigma-Aldrich) and triple distilled water were used throughout. Reverse-phase chromatographic separation of substrates was performed using an Acquity UPLC comprising a BEH C18 1.7 µm column (2.1 mm x 100 mm) (Waters, UK). Mobile phases were as follows: Mobile Phase A consisted of 90% HPLC

grade water, 10% HPLC grade MeCN and 0.1% HCO2H. Mobile phase B consisted of 40% HPLC grade water, 60% MeCN and 0.1% HCO_2H.

<u>MS conditions</u>: A Micromass ZMD single quadrupole electrospray MS was used in positive mode (Micromass, Manchester, UK) and MassLynx software was used to identify substrates and anticipated metabolites. MS source parameters were optimised to: desolvation gas 375 L/hr, cone gas 33 L/hr, capillary 2.9 kV, sample cone 16 V, extraction cone 5 V, fR lens 0.1 V, source block temperature 150°C and desolvation temperature 200°C. Parent compounds and metabolites were detected as singularly charged ions using selected ion readings (SIR).

### III.3.3 Cleavage of substrates by recombinant MMPs

Recombinant human MMP proteins (MMP-2, MMP-3, MMP-9 and MMP-10; R&D Systems, UK) were assayed for their ability to cleave fluorogenic substrates, M-2055 (Dnp-Pro-Cha-Gly-Cys(Me)-His-Ala-Lys(N-Me-Abz)-amide) and M-2110 (Mca-Arg-Pro-Lys-Pro-Val-Glu-Nva-Trp-Arg-Lys(Dnp)-NH_2). Reactions (100 µL) contained 20 ng recombinant protein and 10 mM substrates in MMP activity buffer (100 mM Tris-HCl pH 7.6, 10 mM $CaCl_2$, 100 mM NaCl, 0.16% v/v Brij-35), and incubated at 37°C for 12 h. At T_{12}, The sample was removed and diluted 1:3 with MeCN to precipitate proteins. The sample was then centrifuged at 10,000 x *g* for 3 minutes and supernatant assayed for substrate cleavage by LCMS.

III.4 Results

III.4.1 Optimisation of force fields for *in silico* modelling

A collection of well-known classes of force fields supported by the Discovery Studio Client allowed for rationalised optimisation and selection of the appropriate force field for *in silico* drug discovery studies. The peptide fragment of the MMP-cleavable substrate, M-2055 (Dnp-Pro-β-cyclohexyl-Ala-Gly-Cys(Me)-His-Ala-Lys(N-Me-Abz)-NH$_2$), is presented as an example demonstrating the energy minimisation characteristics acquired in the presence of different force fields. (Figure III.3). Firstly, the substrate was prepared for simulation by selection and application of a force field using the 'forcefield tool'. When the process was finished and ready for simulation, the substrate was exposed to complete energy minimisation using the selected force fields until the final minimised energy state was close to zero. The substrate was able to minimise to the lowest energy state with CHARMM (Chemistry at HARvard and Macromolecular Mechanics) force field (0.55 kcal/mol). Whereas, the complete energy minimisation was not possible with MMFF (Merck Molecular Force Field) and CFF (Consistent Force Field) force fields (102.3 and 87.3 kcal/mol) (Figure III.3). The protein folding characteristics of the substrate further elucidated these energy states. The CHARMM, MMFF and CFF force field molecules attained α-helix conformation, near-straight chain and loop conformations, respectively; suggesting the differences in flexibility attained by the molecules and their minimised energies. With different energy minimisation capabilities of the force fields, the resulting structural conformations and the previously mentioned inherent energetic properties ascertained that CHARMM force field is a suitable force field for further *in silico* studies involved in this project.
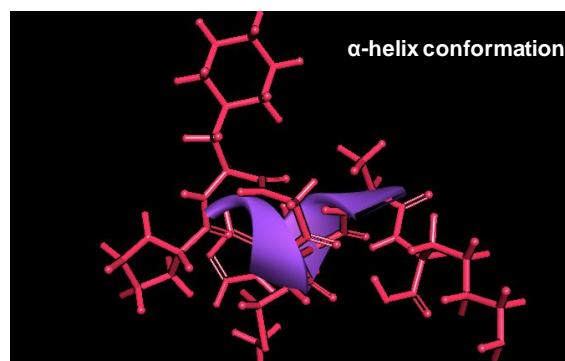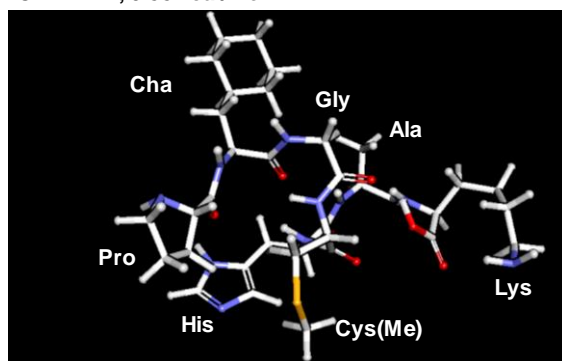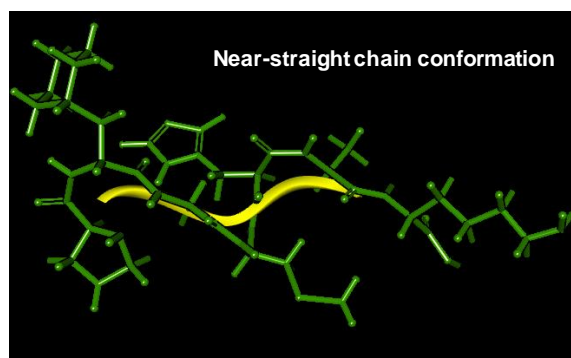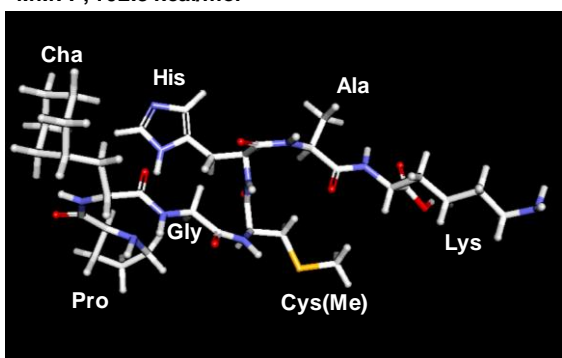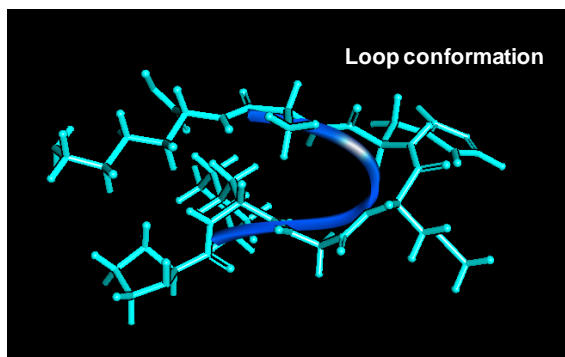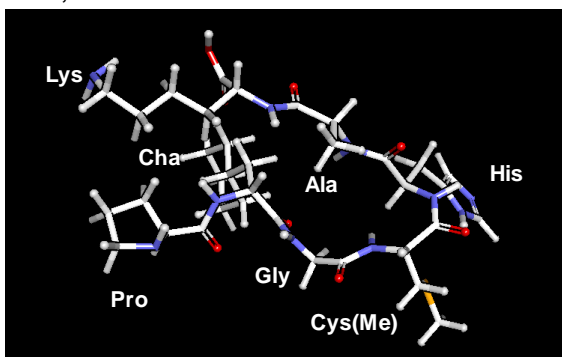
Figure III.3: Energy minimisation simulation of M-2055 substrate with different force fields. Representative images of M-2055 peptide sequence minimised with CHARMM, MMFF and CFF force fields. The substrate residues are labelled and represented as white sticks. The respective structural conformations of CHARMM is shown as pink (sticks) and purple (folding); MMFF as green (sticks) and yellow (folding); and CFF as cyan (sticks) and blue (folding).

III.4.2 Description of MMP structures

The catalytic domain of MMPs consists of five β-sheet strands and three α-helixes. The catalytic centre comprises of a catalytic zinc ion coordinated by three histidine residues and a glutamic acid. The N-terminal part of the molecule is rich in secondary structures with amphiphilic Helix αβ separating the β-strands of the twisted β-sheet. The Helix αβ provides two of the histidine residues, which bind the catalytic zinc ion, and the third being provided by the wide loop connecting the Helix αβ and the specificity loop. The specificity loop (S1' subsite) within the catalytic site of MMPs shows the largest structural differences, this can be visualised in Figures III.4 and III.5.

III.4.2.1 Comparison between the MMP binding sites

The overall folding of the gelatinases and stromelysins resemble those of other MMPs, which is expected based on their structural similarity. The cavity of S1' pockets in MMPs are well-suited to accommodate a wide-range of hydrophobic residues, with the main functional difference between MMP subtypes lying in this region (Figure III.4 and III.5).

Although highly similar (75% structural similarity), the two gelatinase residues are different at the catalytic centre. In MMP-9, residues 421 – 423 form the wall of the binding pocket and the specificity loop is formed by the residues 424 – 430. Arg424 is present at the bottom of S1' pocket and closes off the end of the pocket. Arg424 is therefore responsible for making the pocket cavity smaller in MMP-9 than MMP2 (Figure III.4). Due to this difference, the S1' pocket of MMP-9 can host only smaller hydrophobic groups. Whereas in MMP-2, the external wall of the S1' pocket is largely formed by Thr227 – Phe232 specificity residues. These specificity

determinants can potentially be exploited for rational design of MMP-selective substrates/conjugates (Figure III.4).

Figure III.4: Overall 3D-structures of MMP-2 (PDB ID: 1QIB- represented as pink ribbons) and MMP-9 (PDB ID: 1GKC- represented as cyan ribbons). Helix αβ and specificity loops are shown in MMP-2 and MMP-9 respectively. Zinc and calcium ions in both MMPs are shown in purple and green respectively. Close-up view of the specificity loops in MMP-2 and MMP-9 (lower images) represents the difference between their S1' pocket size and depth. Specificity loops also show the different amino acid residues responsible for the difference between their S1' pockets sizes.

With the highest structural similarity (89%) between the stromelysins (MMP-3 and MMP-10),[271] the catalytic residues are also very similar with slight differences (Figure III.5). The specificity loop is larger in stromelysins compared to the gelatinases. The external wall of MMP-3 and MMP-10 specificity pockets are comprised of residues His224 – Phe232 and Asn240 – Phe248. This is the only region between the two MMPs where relatively large variability in amino acids can be observed in one stretch. In MMP-3, Leu226 is present at the bottom of the pocket and closes off the end of the pocket. The side chain of Phe232 is facing the wall of the pocket which is further responsible for the narrowing of the pocket. Therefore the S1' pocket of MMP-3 is long and narrow. In MMP-10, Phe242 and Thr243 are present at the bottom of the pocket but the residue side chains are facing away from the pocket making the pocket slightly longer than MMP-3. Compared to Phe232 in MMP-3, Phe248 in MMP-10 is facing away from the wall of the pocket, which is further responsible for the widening of the pocket. Therefore, the S1' pocket of MMP-10 if larger and wider compared to MMP-3 (Figure III.5). These binding characteristics of MMPs can potentially be considered as determinants for rationalising the substrate binding and examining binding subsites to enable progress towards developing MMP-selective therapeutics.
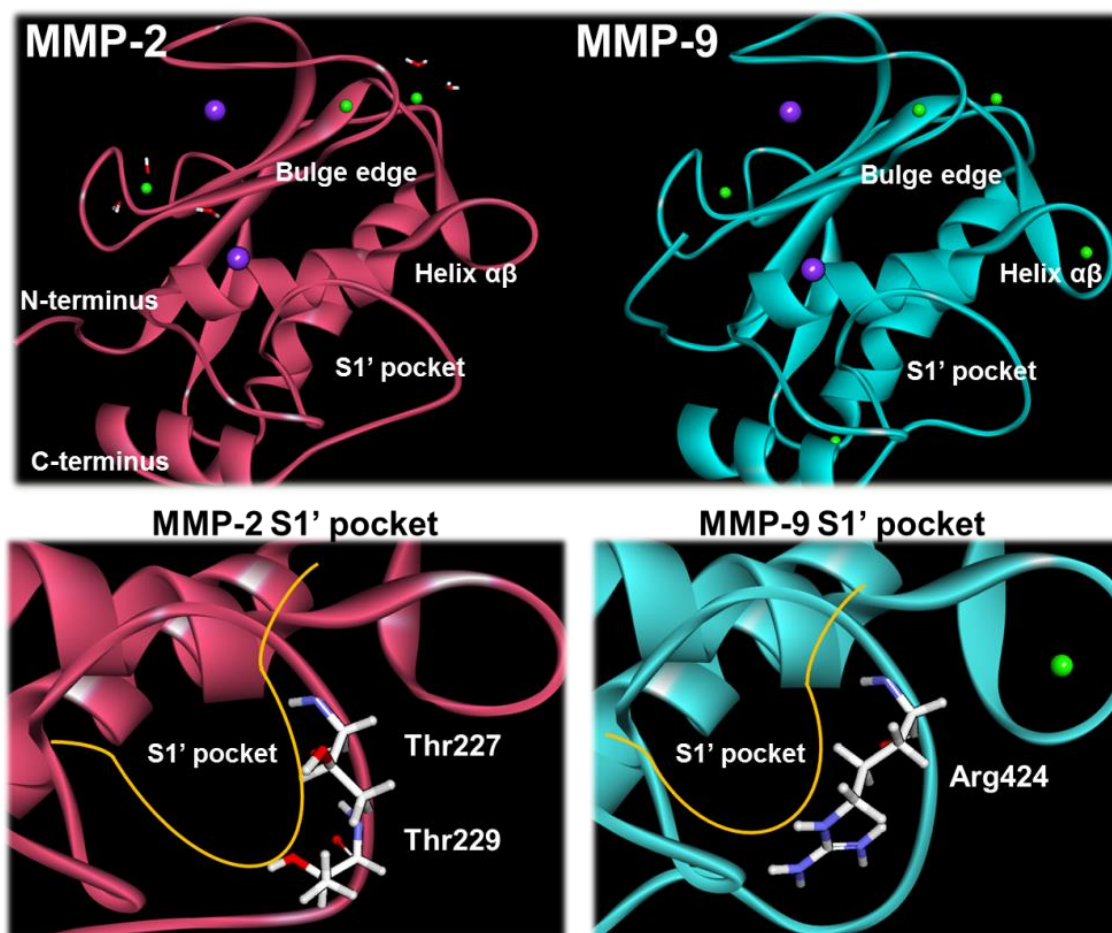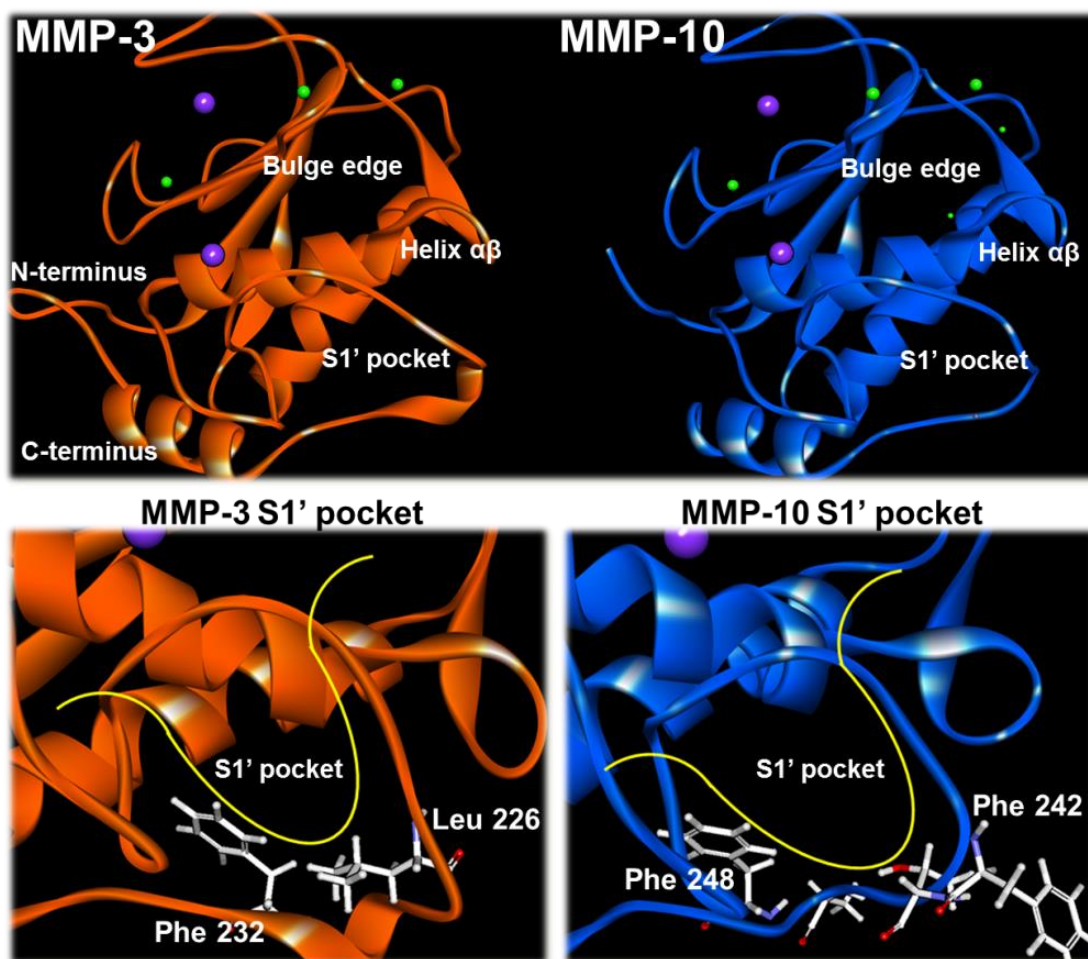
Figure III.5 Overall 3D-structures of MMP-3 (PDB ID: 1CIZ- represented as orange ribbons) and MMP-10 (PDB ID: 1Q3A- represented as blue ribbons). Helix αβ and specificity loops are shown in MMP-3 and MMP-10 respectively. Zinc and calcium ions in both MMPs are shown in purple and green respectively. Close-up view of the specificity loops in MMP-3 and MMP-10 (lower images) represents the difference between their S1' pocket size and depth. Specificity loops also show the different amino acid residues responsible for the difference between their S1' pockets sizes.

To probe the selective binding of potential substrates, the peptide sequences of the non-specific gelatinase substrate (M-2055) and stromelysin substrate (M-2110) were input into BIOVIA Discovery Studio 4.0, minimised with respect to their geometry and then docked into the MMPs. Before undertaking this computational work, attempts at crystallisation of substrates were undertaken in order to determine the X-Ray crystal structure. Crystallisation experiments failed to yield suitable crystals for structure determination, therefore the optimised CHARMM minimised geometries of the substrates were employed throughout this study.

III.4.3 Flexible-ligand docking of substrate M-2055 and MMPs

M-2055 is a fluorogenic substrate (Dnp-Pro-Cha-Gly-Cys(Me)-His-Ala-Lys(N-Me-Abz)-amide) known to be efficiently cleaved by interstitial collagenase (MMP-1) and gelatinase-2 (MMP-9).[222] Both enzymes cleave this substrate at the Gly-Cys(Me) bond, liberating a cleavage product with a fluorescent signal suitable for determining enzymatic activity. The gelatinase-1 and Stromelysin subfamilies also cleave this substrate at a relatively slower rate compared to MMP-9, however the cleavage sites are unknown. In order to determine the proteolytic cleavage and rationalise the binding selectivity, *in silico* flexible-ligand docking was applied using the substrate peptide residues and X-Ray crystal structures of gelatinases (MMP-2 PDB ID: 1QIB[268] and MMP-9 PDB ID: 1GKC[269]) and stromelysins (MMP-3 PDB ID: 1CIZ[270] and MMP-10 PDB ID: 1Q3A[271]).

In both MMP-2 and MMP-9, the zinc ion interacts with the carboxylic acid between Gly and Cys(Me) bond, the known cleavage site according to Bickett *et al.*[222] MMP-9 is able to bind tightly with the substrate residues compared to MMP-2, as determined by differences in their interatomic zinc distances and overall binding energies. The substrate bound MMP-complexes provided crucial insights into the

differences in their subsites as S1 and S3 subsites in MMP-2 demonstrated affinity to accommodate longer side-chains than MMP-9. The charged nature of the S2 subsite (presence of His205) in MMP-2 lends affinity for acidic residues, whereas this feature is not observed in MMP-9.

In the MMP-9 structure, the carboxylic acid between Gly and Cys(Me) chelates the zinc ion (2.1 Å) and is involved in a strong H-bond to the carboxylate O of Glu402. The zinc ion is further coordinated by three Histidine residues namely His 401, His 405 and His 411 present in Helix αβ segment of the protein. Only the P1' amino acid is involved in strong H-bonds with Arg424 (2.2 Å), which creates the wall-forming segment. Arg424 closes off the end of the S1' pocket and forms a more enclosed pocket. The strong binding of Arg424 with the P1' residue is an important determinant of the specificity pocket. Remaining substrate residues are involved in strong interactions with the bulge-edge segment molecules (Gly186 to His190) with interatomic distances ranging from 2.5 to 3.1 Å. The docked complex of M-2055 and MMP-9 has an overall binding energy of 706 kcal/mol (Figure III.6).

Consideration of the interaction of M-2055 with the active site of MMP-2 shows a marked reduction in affinity in energetic terms, the predicted interaction seven times weaker than the M-2055 and MMP-9 complex (binding energy of 101 kcal/mol). Gly forms the P1 subsite and Cys(Me) forms the P1' subsite and the presence of a zinc ion, chelated by the carboxylic acid between P1-P1' residues (3.8 Å), further confirms this. The P1' residue, although favourable for the MMP-2 specificity pocket, is not involved in any significant interaction with MMP-2 residues. The remaining substrate residues have weak H-bond interactions with wall-forming and bulge-edge segments of MMP-2 with interatomic distances

ranging from 3.1 to 5.1 Å. This is expected as M-2055 residues are oriented away from further MMP-2 binding pockets (Figure III.6).

When considering the interaction of M-2055 with the active sites of MMP-3 and MMP-10 the binding affinity was nine times weaker than the M-2055 and MMP-9-complex (binding energy of 77 kcal/mol for MMP-10 and 79 kcal/mol for MMP-3). In the case of both stromelysins, proline forms the P1 subsite and β-cyclohexyl-Alanine forms the P1' subsite. The presence of the zinc ion, chelated by the carboxylic acid between P1-P1' residues (3.8 Å), further confirms this. The P1' residue, although favourable for the stromelysin, specificity pocket is not involved in any significant interaction with MMP-10 residues. The remaining substrate residues have weak H-bond interactions with wall-forming and bulge-edge segments of stromelysins with interatomic distances ranging from 2.8 to 5.0 Å. The M-2055 residues are oriented further away from stromelysin binding pockets where it occupies the S1, S1' and S2' subsites (Figure III.7).

Figure III.6: (*Left*) Stereo view of the docked complexes of M-2055 substrate (white sticks) and the catalytic domain of human MMP-2 (PDB ID: 1GKC) and MMP-9 (PDB ID: 1GKC). Catalytic and structural zinc ions are shown as purple spheres. Active-site cleft residues (the αβ-helix loop and the specificity loop) are shown in green. (*Right*) Schematic representation of M-2055: active site binding interaction in human MMP-2 and MMP-9. MMP-2 and MMP-9 enzyme binding pockets are shown in red and green respectively. Substrate chemical structure and its scissile bond is shown in black. The zinc ion coordinated by histidine is indicated in blue.
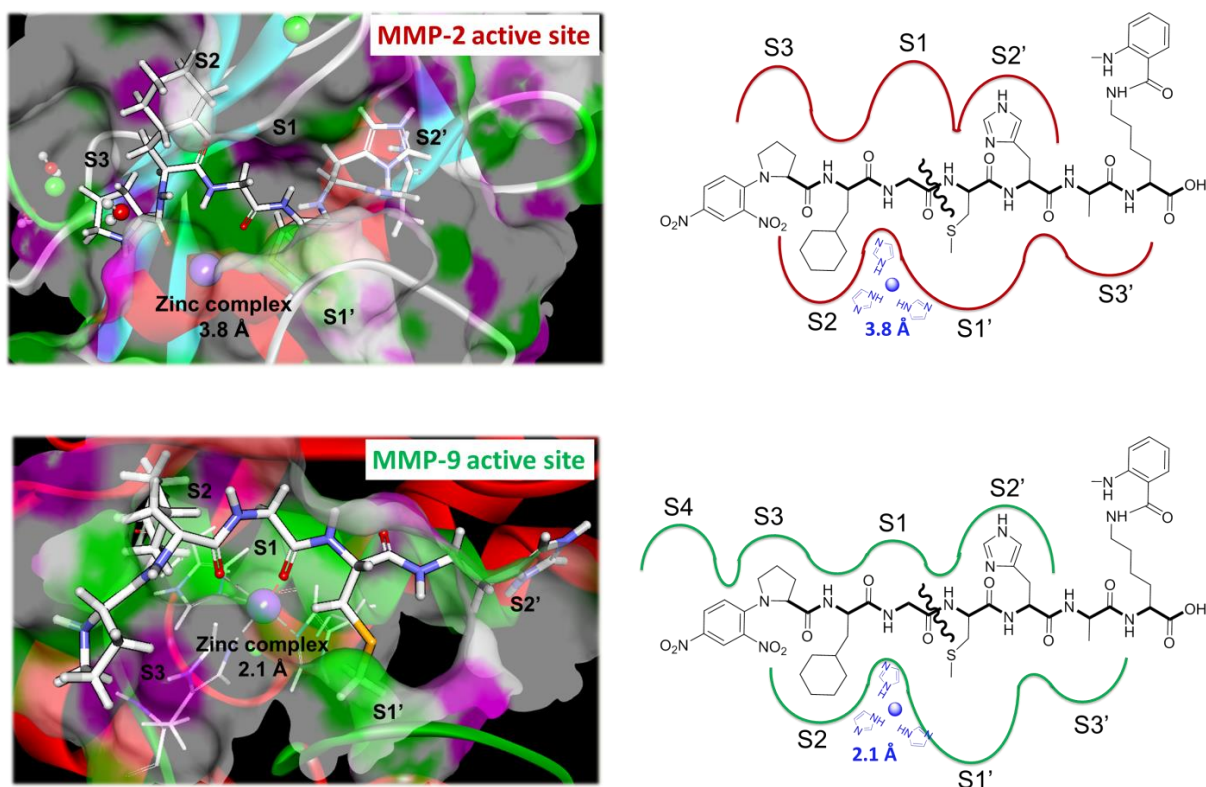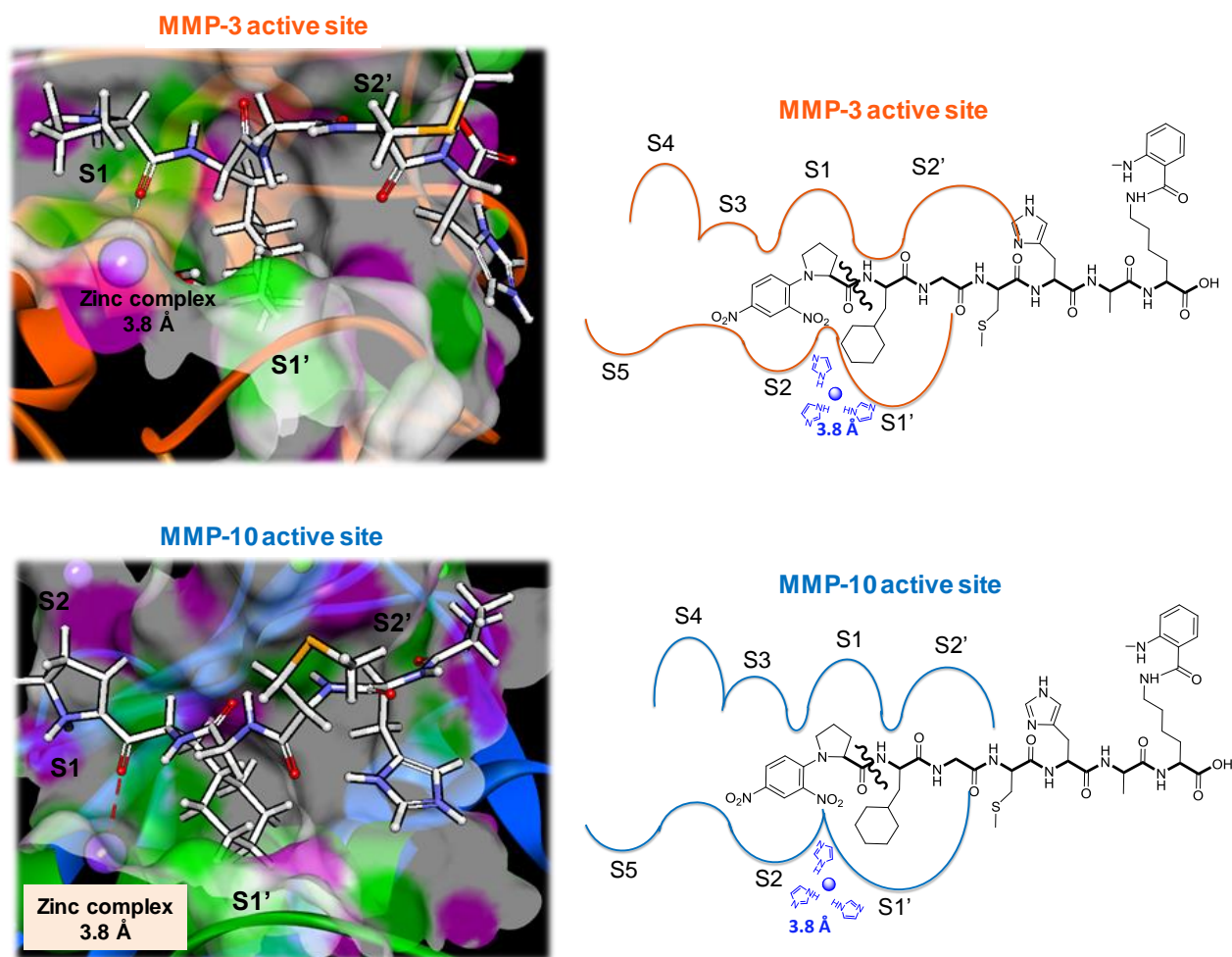
Figure III.7 (*Left*) Stereo view of the docked complexes of M-2055 substrate (white sticks) and the catalytic domain of human MMP-3 (PDB ID: 1CIZ) and MMP-10 (PDB ID: 1Q3A). Catalytic and structural zinc ions are shown as purple spheres. Active-site cleft residues (the αβ-helix loop and the specificity loop) of MMP-3 and MMP-10 are shown in orange and blue respectively. (*Right*) Schematic representation of M-2055: active site binding interaction in human MMP-3 and MMP-10. MMP-3 and MMP-10 enzyme binding pockets are shown in orange and blue respectively. Substrate chemical structure and its scissile bond is shown in black. The zinc ion coordinated by histidine is indicated in blue.

III.4.4 Experimental validation of M-2055 and MMP binding

To experimentally validate the predictability of this model, and confirm the *in vitro* cleavage position of M-2055, hydrolysis of the substrate by recombinant MMPs was assessed over a 12 h period. The resultant products were assessed by LCMS using a reverse phase gradient system to separate the substrate (M-2055) and proteolytic products. The identification of these species was confirmed by retention time and mass spectrometry (MS) data. M-2055 demonstrated a retention time (t_R) of 2.8 minutes (Figure III.8) and rapid cleavage by MMP-9 at Gly-Cys(Me) bond was confirmed by LCMS, two peaks corresponding to Dnp-Pro-β-Cyclohexyl-Ala-Gly at t_R of 2.3 minutes ($^m/_z$ 491.5Da, [M+H]$^+$) and Cys(Me)-His-Ala-Lys(*N*-Me-Abz)-NH$_2$ at t_R of 2.47 minutes ($^m/_z$ 604.7Da, [M+H]$^+$) (Figures III.9 and III.10). Slow hydrolysis of M-2055 by MMP-2 (compared to MMP 9) at Gly-Cys(Me) bond was confirmed by two peaks at t_R 2.3 minutes and t_R of 2.47 minutes. MMP-2 cleavage experiments displayed a parent peak of M-2055, detected at t_R 2.8 minutes ($^m/_z$ 1077.5Da, [M+H]$^+$) (Figures III.9 and III.11, suggesting that MMP-2 metabolised M-2055 at a slower rate than MMP-9 (Section II.7.1, Figure II.13).
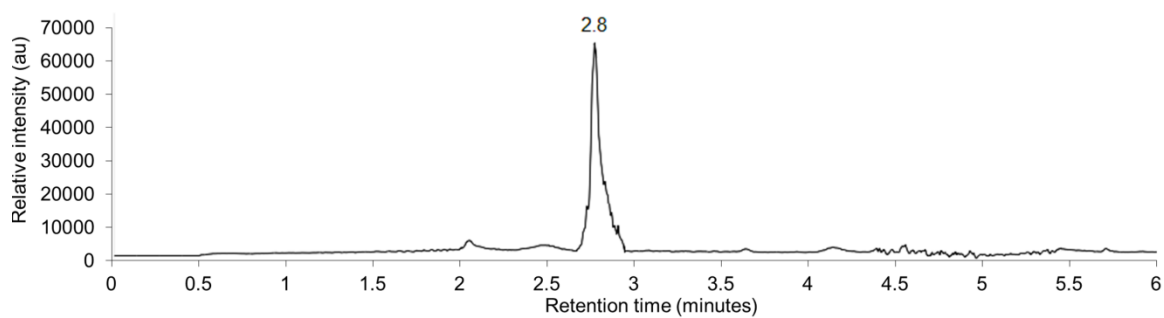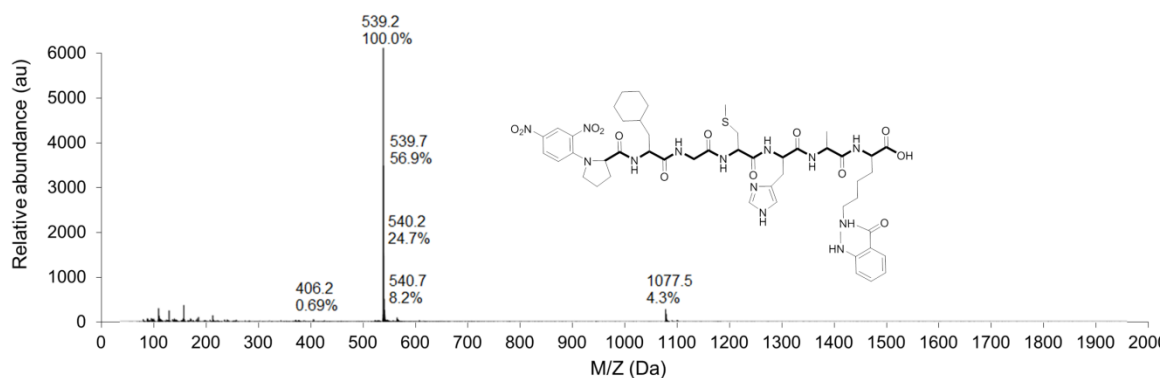
Figure III.8: Detection of M-2055 at retention time (tR) of 2.8 minutes ($^m/_z$ 1077.5Da, [M+H]$^+$), confirmed by LC-MS
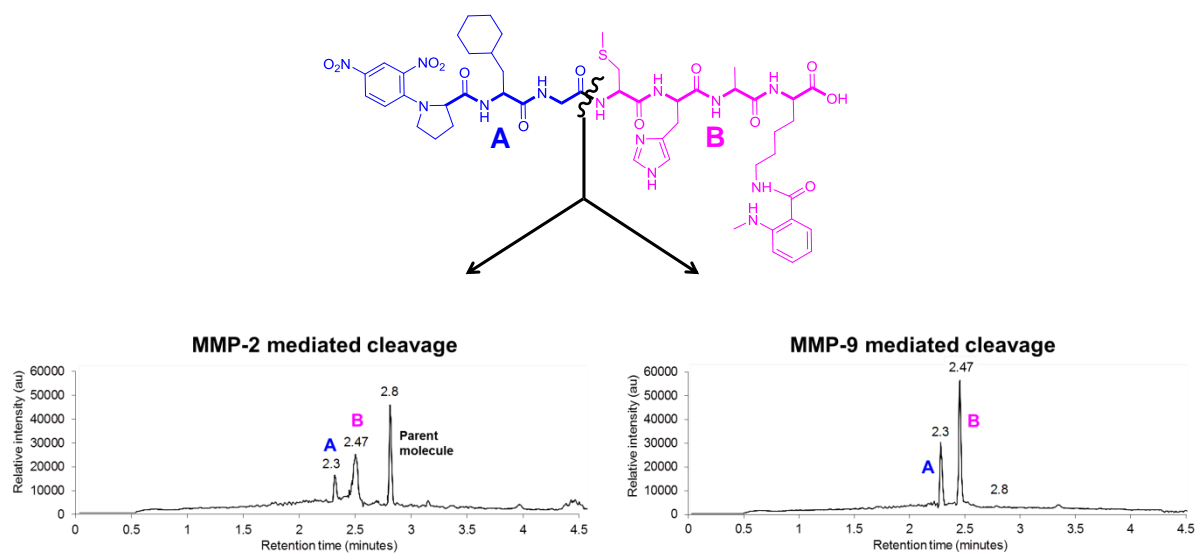
Figure III.9. Schematic representation of the cleavage of M-2055 substrate by recombinant MMP-2 and MMP-9 enzymes at Gly-Cys(Me) bond.

Figure III.10: Cleavage of substrate M-2055 by recombinant MMP-9, detected by LCMS: (A) LC of MMP-9 mediated cleaved metabolites, (t_R 2.3 and 2.47 minutes); (B) MS identification of Dnp half of cleaved substrate (Dnp-Pro-β-Cyclohexyl-Ala-Gly), t_R 2.3 minutes ($^m/_z$ 491.5Da, [M+H]$^+$); (C) MS identification of Abz half of cleaved substrate (Cys(Me)-His-Ala-Lys(*N*-Me-Abz)-NH$_2$) t_R 2.47 minutes ($^m/_z$ 604.7Da, [M+H]$^+$).

Figure III.11: Cleavage of substrate M-2055 by recombinant MMP-2, detected by LCMS: (A) LC of MMP-2 mediated cleaved metabolites, (tR 2.3 and 2.47 minutes); (B) MS identification of Dnp half of cleaved substrate (Dnp-Pro-β-Cyclohexyl-Ala-Gly), tR 2.3 minutes ($^m/_z$ 491.5Da, [M+H]$^+$); (C) MS identification of Abz half of cleaved substrate (Cys(Me)-His-Ala-Lys(N-Me-Abz)-NH$_2$) tR of 2.47 minutes ($^m/_z$ 604.7Da, [M+H]$^+$).

Whereas, the cleavage of M-2055 by MMP-3 and MMP-10 at the Pro – β-Cyclohexyl-Ala bond was confirmed by the production of two peaks of cleaved metabolites corresponding to Dnp-Pro at t_R 1.75 minutes ($^m/_z$ 282.2Da, [M+H]$^+$) and; β-Cyclohexyl-Ala-Gly-Cys(Me)-His-Ala-Lys(N-Me-Abz)-NH$_2$ at t_R 2.68 minutes ($^m/_z$ 815.4 Da, [M+H]$^+$) (Figures III.12, III.13 and III.14). As expected, with MMP-3 and MMP-10 cleavage, a parent peak of M-2055 was also detected at Rt of 2.8 minutes ($^m/_z$ 1077.5Da, [M+H]$^+$) suggesting that MMP-3 and MMP-10 metabolised M-2055 at a slower rate than MMP-9. This *in vitro* assessment successfully supports the validity of the predicted *in silico* model of M-2055 substrate and MMP interactions (Figures III.6 and III.7).
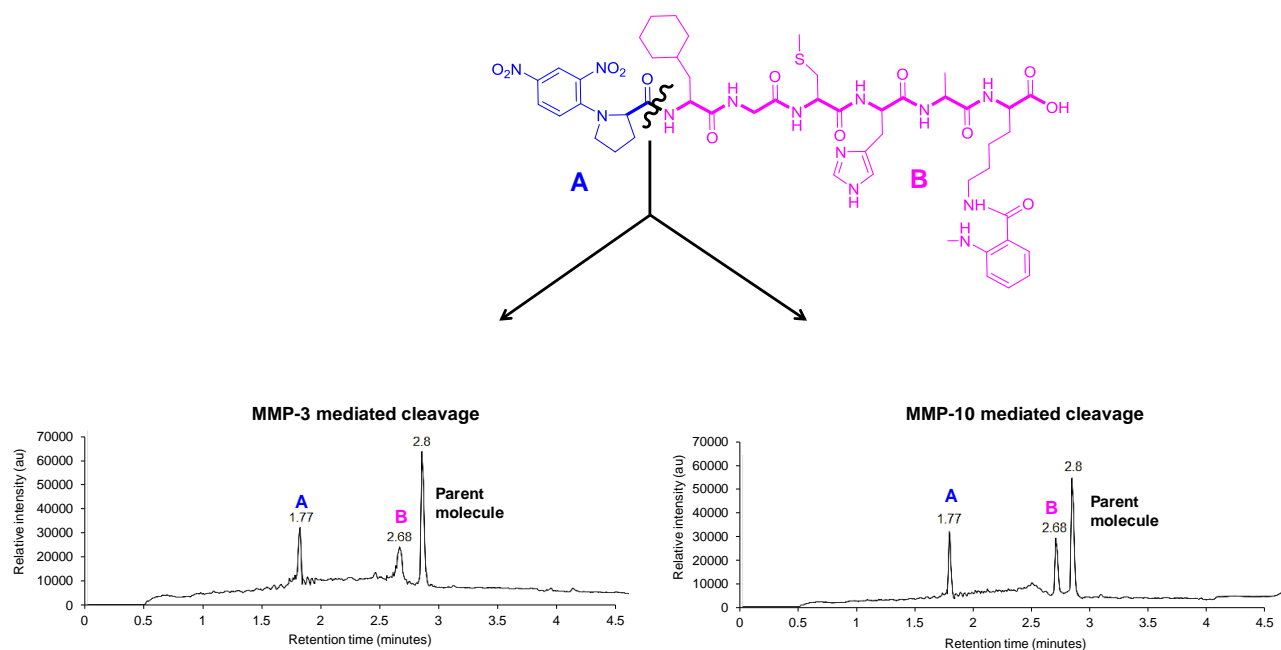
Figure III.12: Schematic representation of the cleavage of M-2055 substrate by recombinant MMP-3 and MMP-10 enzymes at Pro- β-Cyclohexyl-Ala bond.
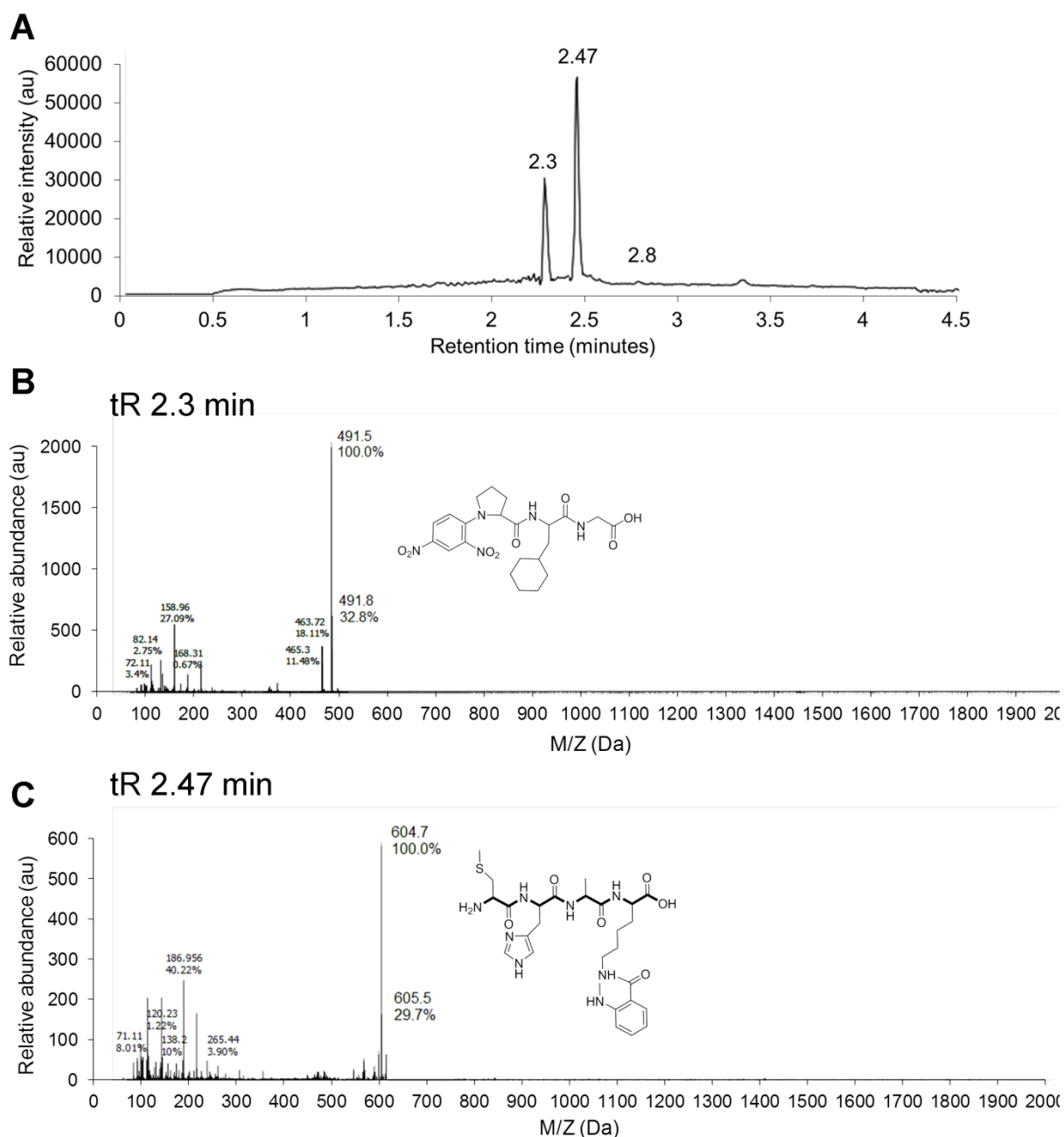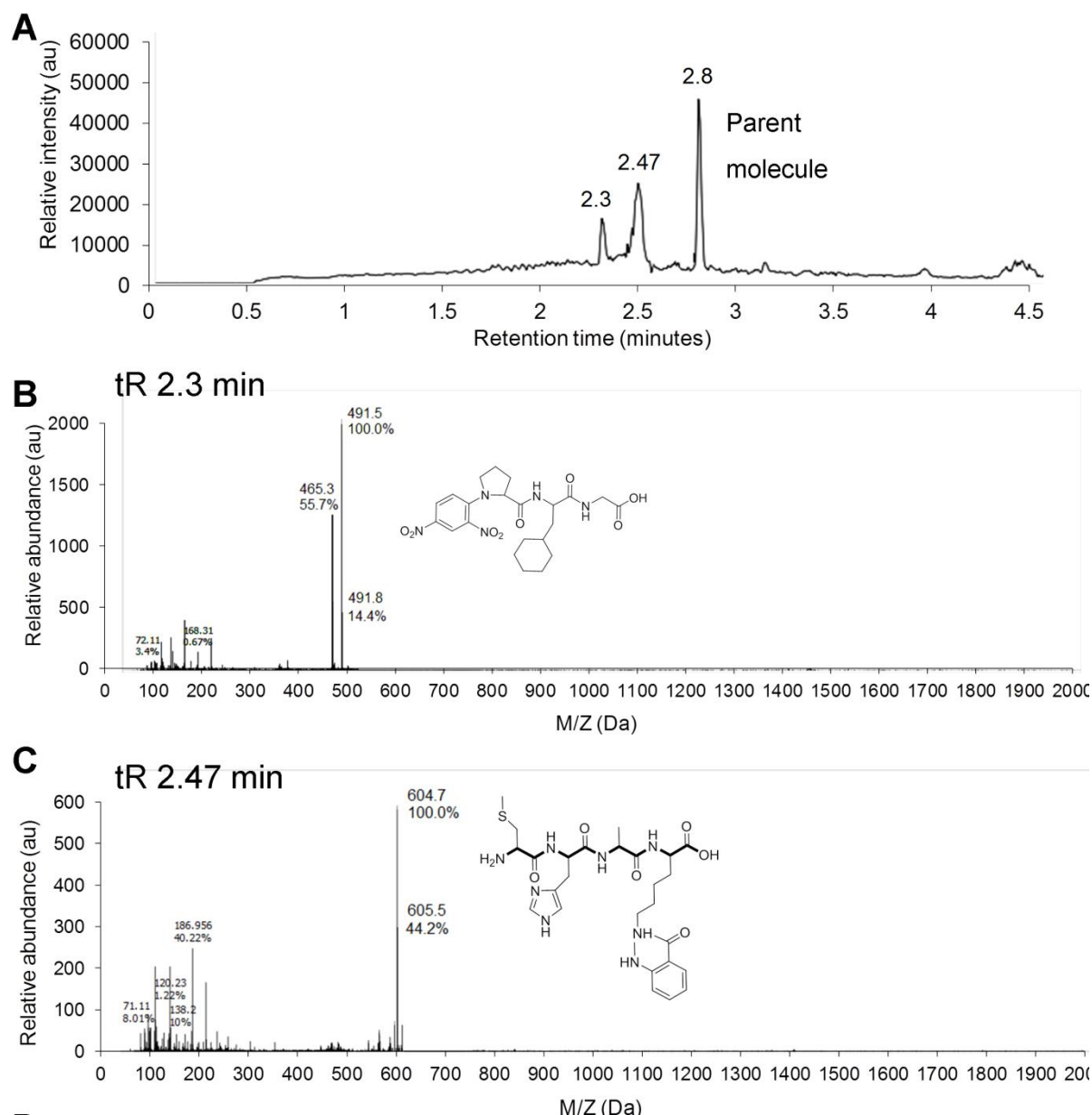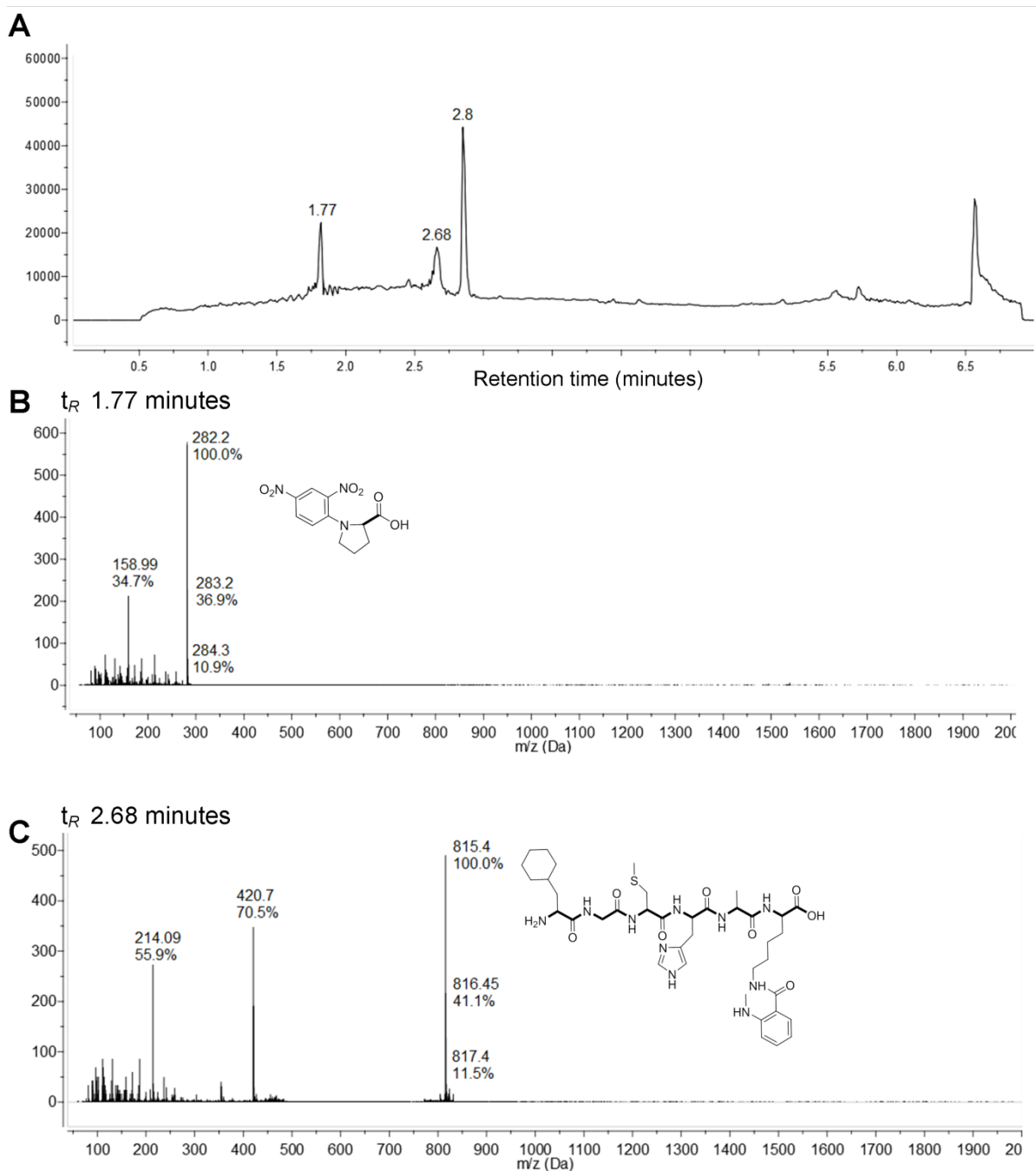
Figure III.13: Cleavage of substrate M-2055 by recombinant MMP-3, detected by LCMS: (A) LC of MMP-3 mediated cleaved metabolites, (t_R 1.77 and 2.68 minutes); (B) MS identification of Dnp half of cleaved substrate (Dnp-Pro), t_R 1.77 minutes ($^m/_z$ 282.2 Da, [M+H]$^+$); (C) MS identification of Abz half of cleaved substrate (β-Cyclohexyl-Ala-Gly-Cys(Me)-His-Ala-Lys(*N*-Me-Abz)-NH$_2$) t_R 2.68 minutes ($^m/_z$ 815.4 Da, [M+H]$^+$).
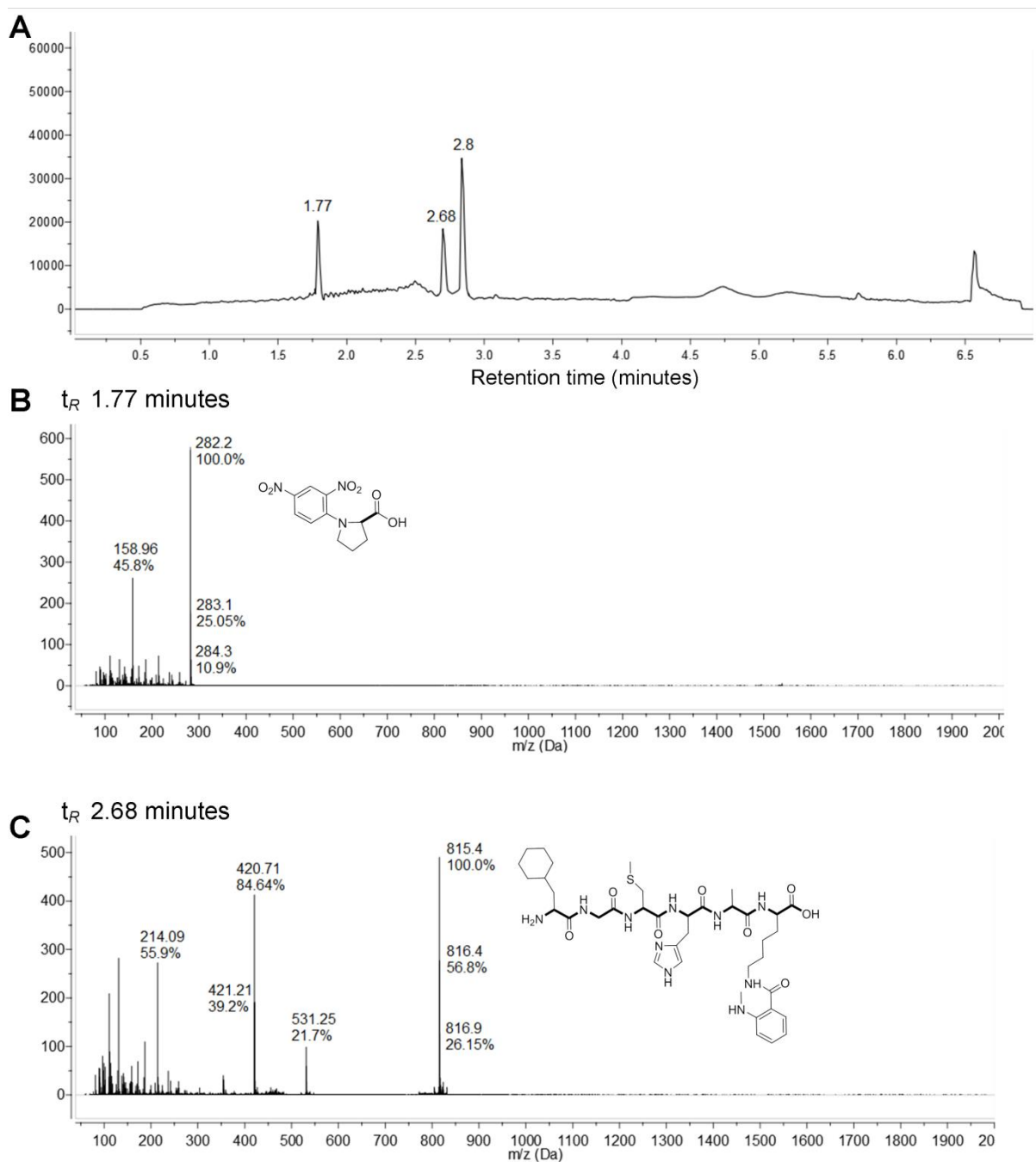
Figure III.14: Cleavage of substrate M-2055 by recombinant MMP-10, detected by LCMS: (A) LC of MMP-10 mediated cleaved metabolites, (t_R 1.77 and 2.68 minutes); (B) MS identification of Dnp half of cleaved substrate (Dnp-Pro), t_R 1.77 minutes ($^m/_z$ 282.2 Da, [M+H]$^+$); (C) MS identification of Abz half of cleaved substrate (β-Cyclohexyl-Ala-Gly-Cys(Me)-His-Ala-Lys(N-Me-Abz)-NH$_2$) t_R 2.68 minutes ($^m/_z$ 815.4 Da, [M+H]$^+$).

III.4.5 Flexible-ligand docking of substrate M-2110 and MMPs

When considering the interaction between M-2110 and stromelysins (the selective substrate for this MMP subfamily)[221] individually, it was observed that zinc ion coordinates strongly with the carboxylate between the Glu- Nva (Norvaline) bond, the known cleavage site according to Nagase *et al.*[221] The interatomic zinc distance in MMP-3 is 1.9 Å and that in mmp-10 is 2.1 Å. The Glu forms the P1 subsite and makes significant contributions to the substrate binding energy. The Nva side chain of the P1' subsite is inserted into the S1' pocket of both stromelysins, and is further coordinated by the wall-forming segment residues (at distances of 2.1 to 2.3 Å). The side chains of Leu223 and Leu229 in MMP-3 and; the side chains of Phe212, Leu213, Leu234 and Phe248 in MMP-10 make the hydrophobic cluster at the bottom of the pocket. The complete binding energies of M-2110 – MMP-3 and M-2110 – MMP-10 docked complexes are 591 kcal/mol and 522 kcal/mol, respectively (Figure III.15).

Whereas, the interaction between M-2110 and MMP-9 is nearly five times weaker (binding energy = 102 kcal/mol) than the M-2110 and MMP-10 complex. In this case, the carboxylic acid between proline-valine, which forms the P1-P1' subsite, chelates the zinc ion (3.6 Å) and it is also involved in a weak polar interaction with the carboxylate O of Glu402. Arg424 possesses a weak interaction (4 Å) with P1' residue, that is inserted into the enclosed S1' pocket. The remaining substrate residues have weak binding interactions (3.5 to 4.1 Å) with the bulge-edge segment molecules. On the other hand, the docking of M-2110 and MMP-2 revealed negative binding energy. Although proline-valine formed the P1-P1' subsite, the catalytic zinc of MMP-2 was unable to interact with the peptide residues of M-2110 (Figure III.16.
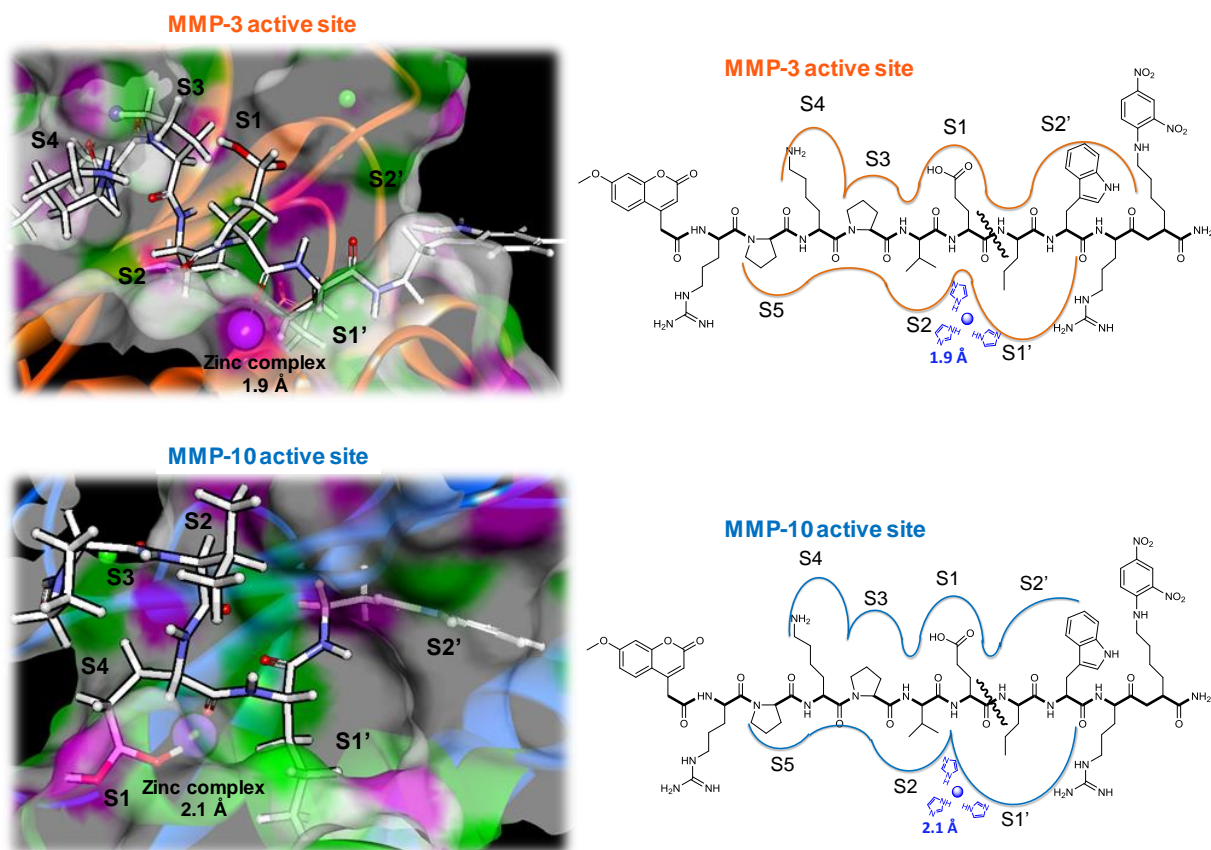
Figure III.15: (*Left*) Stereo view of the docked complexes of M-2110 substrate (white sticks) and the catalytic domain of human MMP-3 (PDB ID: 1CIZ) and MMP-10 (PDB ID: 1Q3A). Catalytic and structural zinc ions are shown as purple spheres. Active-site cleft residues (the αβ-helix loop and the specificity loop) of MMP-3 and MMP-10 are shown in orange and blue respectively. (*Right*) Schematic representation of M-2110: active site binding interaction in human MMP-3 and MMP-10. MMP-3 and MMP-10 enzyme binding pockets are shown in orange and blue respectively. Substrate chemical structure and its scissile bond is shown in black. The zinc ion coordinated by histidine is indicated in blue.

Figure III.16 (*Left*) Stereo view of the docked complexes of M-2110 substrate (white sticks) and the catalytic domain of human MMP-2 (PDB ID: 1GKC) and MMP-9 (PDB ID: 1GKC). Catalytic and structural zinc ions are shown as purple spheres. Active-site cleft residues (the αβ-helix loop and the specificity loop) of MMP-2 and MMP-9 are shown in pink and cyan respectively. (*Right*) Schematic representation of M-2110: active site binding interaction in human MMP-2 and MMP-9. MMP-2 and MMP-9 enzyme binding pockets are shown in red and green respectively. Substrate chemical structure and its scissile bond is shown in black. The zinc ion coordinated by histidine is indicated in blue.

138

III.4.6 Experimental validation of M-2110 and MMP binding

In vitro biochemical assessment further validated the predictability of this model and confirmed the cleavage of positions of M-2110 by respective MMPs. The hydrolysis of the substrate by recombinant MMPs was assessed over 12 h period and the resultant products were assessed by LCMS using a reverse phase gradient system to separate the substrate and proteolytic products. The identification of these species was confirmed by retention time and mass spectrometry (MS) data. M-2110 was detected at t_R 4.15 minutes (Figure III.17). The rapid cleavage by stromelysins at the Glu-Nva bond was confirmed by two peaks corresponding to Mca-Arg-Pro-Lys-Pro-Val-Glu at tR of 2.8 minutes ($^m/_z$ 940.5Da, $[M+H]^+$) and Nva-Trp-Arg-Lys(Dnp)-NH$_2$ at tR of 2.5 minutes ($^m/_z$ 751.4 Da, $[M+H]^+$) (Figures III.18, III.19 and III.20).

Figure III.17: Detection of M-2055 at t_R 4.152 minutes ($^m/_z$ 1673.8 Da, [M+H]$^+$), confirmed by LC-MS
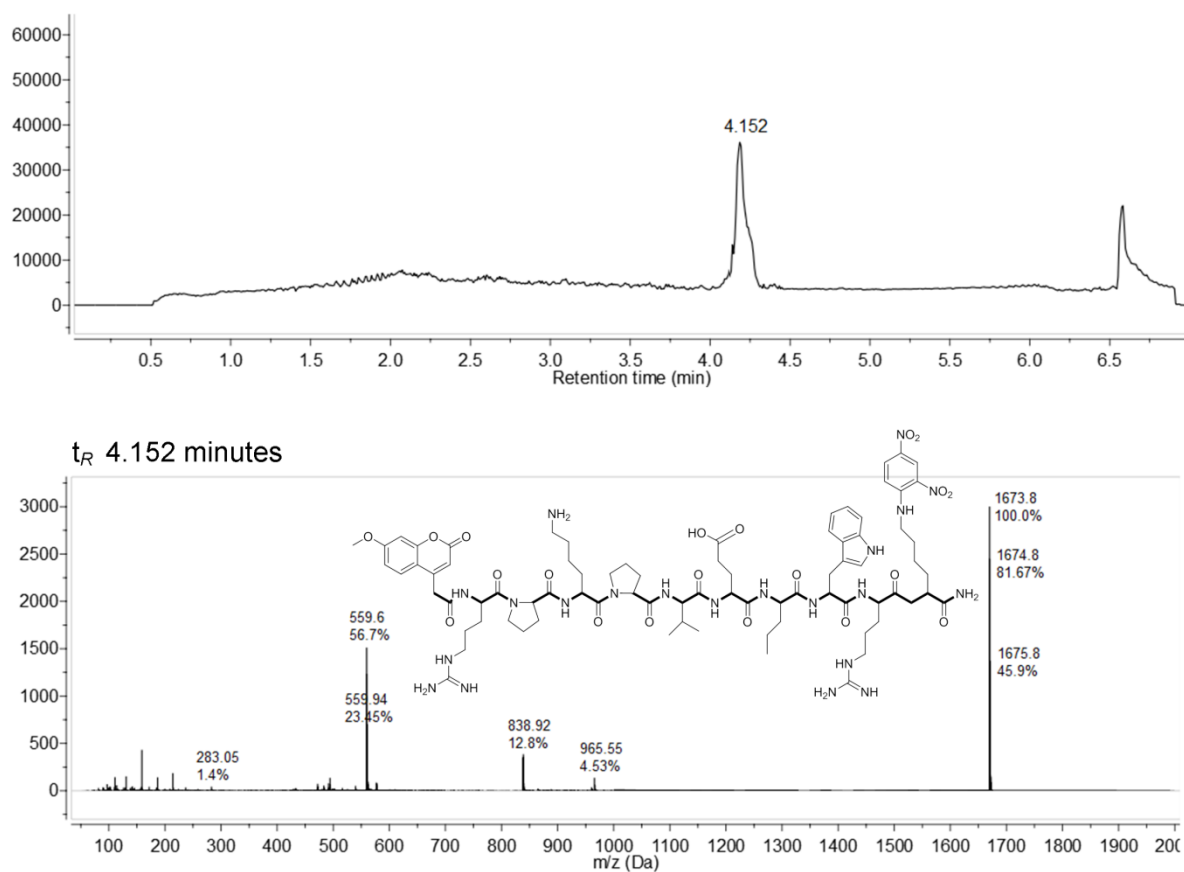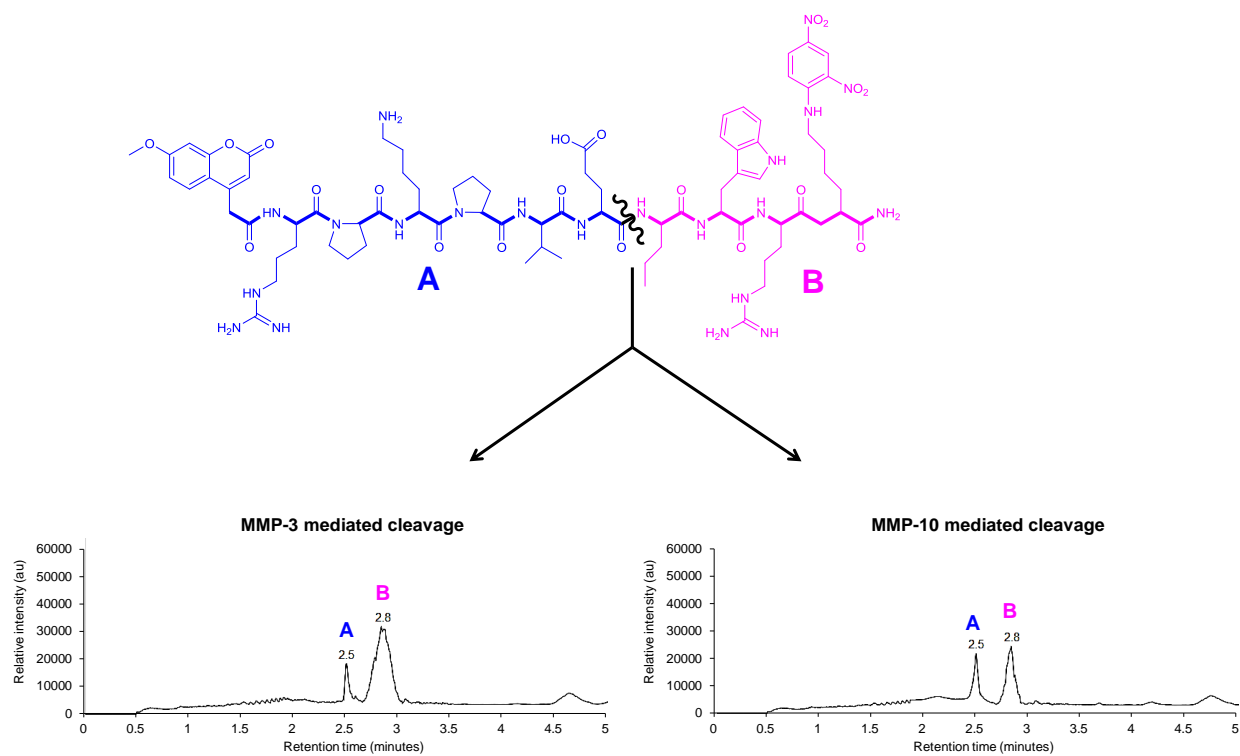
Figure III.18. Schematic representation of the cleavage of M-2110 substrate by recombinant MMP-3 and MMP-10 enzymes at Glu-Nva bond.

Figure III.19: Cleavage of substrate M-2110 by recombinant MMP-3, detected by LCMS: (A) LC of MMP-3 mediated cleaved metabolites, (t_R 2.5 and 2.8 minutes); (B) MS identification of Dnp half of cleaved substrate (Nva-Trp-Arg-Lys(Dnp)-NH$_2$), t_R 2.5 minutes ($^m/_z$ 751.4 Da, [M+H]$^+$); (C) MS identification of Mca half of cleaved substrate (Mca-Arg-Pro-Lys-Pro-Val-Glu) t_R 2.8 minutes ($^m/_z$ 940.5 Da, [M+H]$^+$).
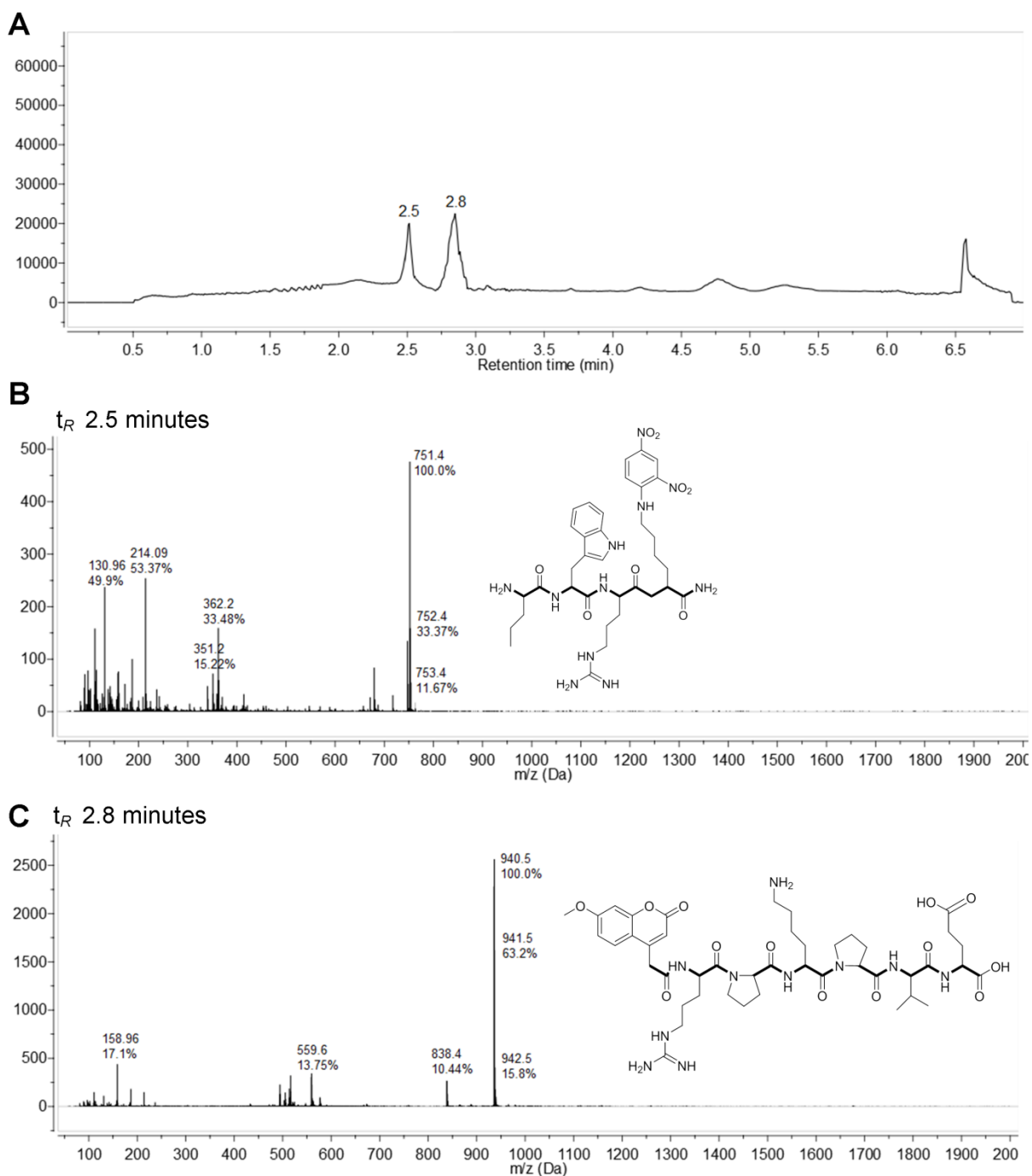
Figure III.20: Cleavage of substrate M-2110 by recombinant MMP-10, detected by LCMS: (A) LC of MMP-10 mediated cleaved metabolites, (t_R 2.5 and 2.8 minutes); (B) MS identification of Dnp half of cleaved substrate (Nva-Trp-Arg-Lys(Dnp)-NH$_2$), t_R 2.5 minutes ($^m/_z$ 751.4 Da, [M+H]$^+$); (C) MS identification of Mca half of cleaved substrate (Mca-Arg-Pro-Lys-Pro-Val-Glu) t_R 2.8 minutes ($^m/_z$ 940.5 Da, [M+H]$^+$).

Whereas, the slow hydrolysis of M-2110 by MMP-9 at the Pro-Val bond was confirmed by two peaks corresponding to Mca-Arg-Pro-Lys-Pro t_R 2.4 minutes ($^m/_z$ 712.4 Da, [M+H]$^+$) and Val-Glu-Nva-Trp-Arg-Lys(Dnp)-NH$_2$ t_R 2.87 minutes ($^m/_z$ 977.5 Da, [M+H]$^+$) (Figures III.21 and III.22). As expected, with MMP-9 cleavage, a parent peak of M-2110 was also detected at t_R 4.15 minutes ($^m/_z$ 1674.8 Da, [M+H]$^+$), suggesting that MMP-9 metabolised M-2110 at a slower rate than stromelysins (Figures III.19 and III.20). The differential cleavage of M-2110 by stromelysins and MMP-9 occurred exactly at the predicted subsites (Figures III.16). Furthermore, MMP-2 did not display any experimental cleavage of M-2110, reflecting the negative or weak *in silico* binding of MMP-2 and M-2110 (Figure III.21).
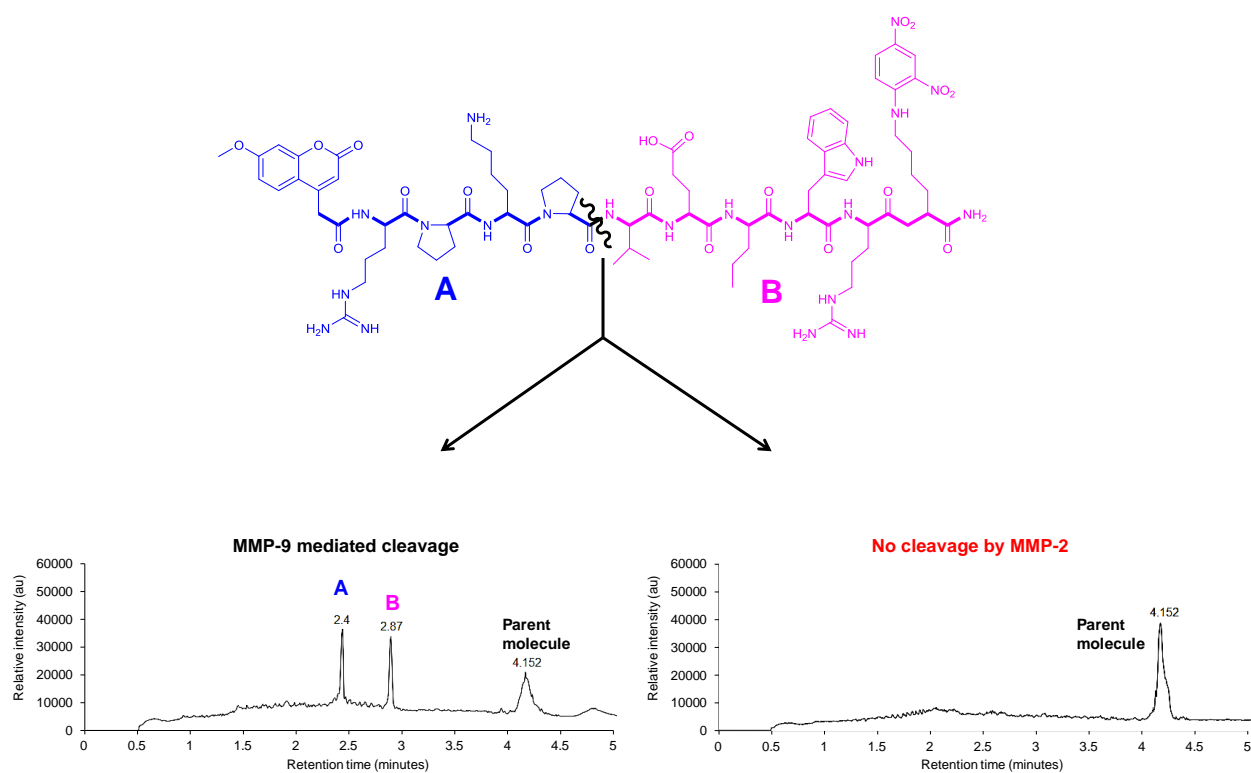
Figure III.21 Schematic representation of the cleavage of M-2110 substrate by recombinant MMP-9 at Pro-Val bond, whereas no cleavage was detected with recombinant MMP-2.
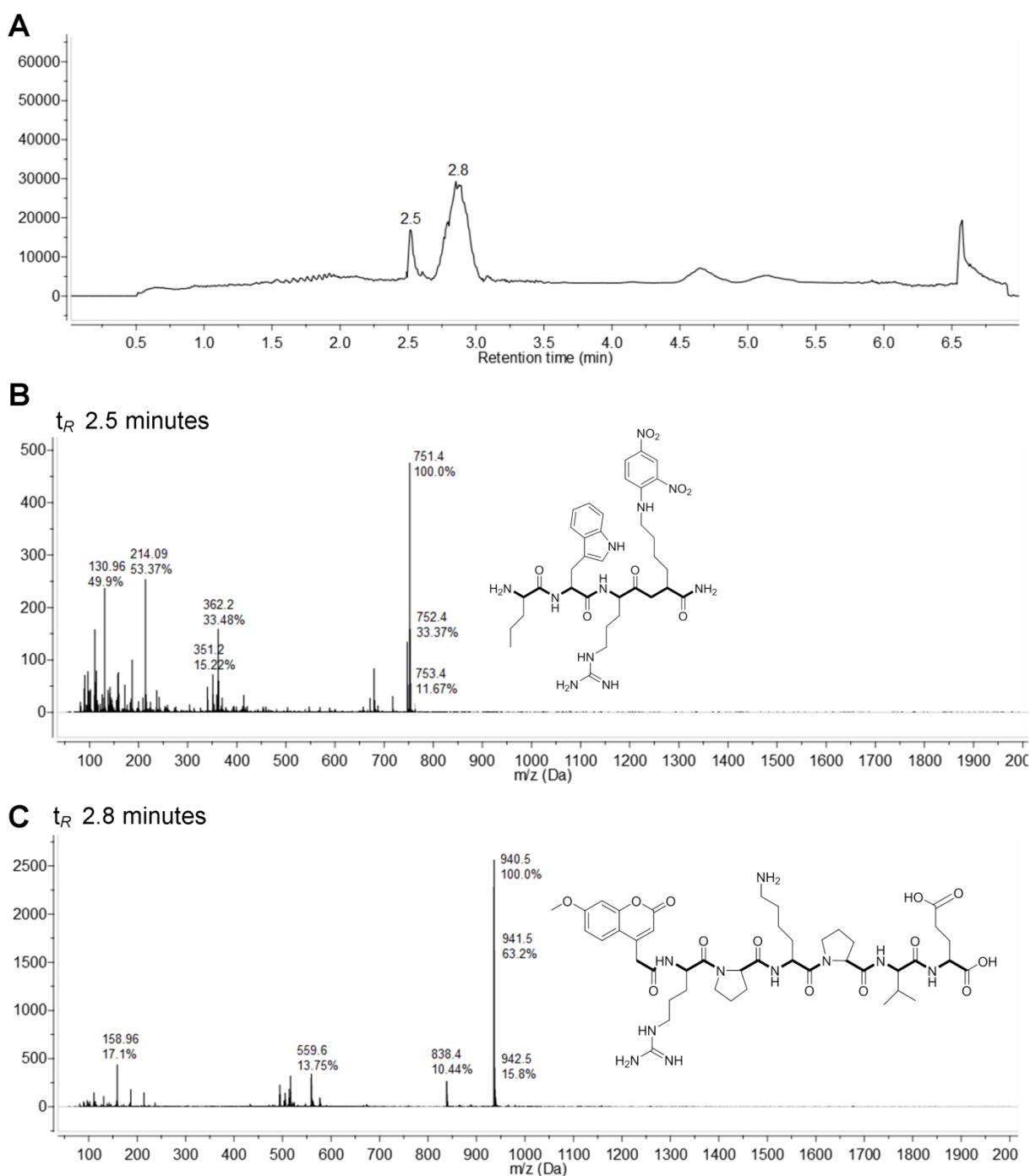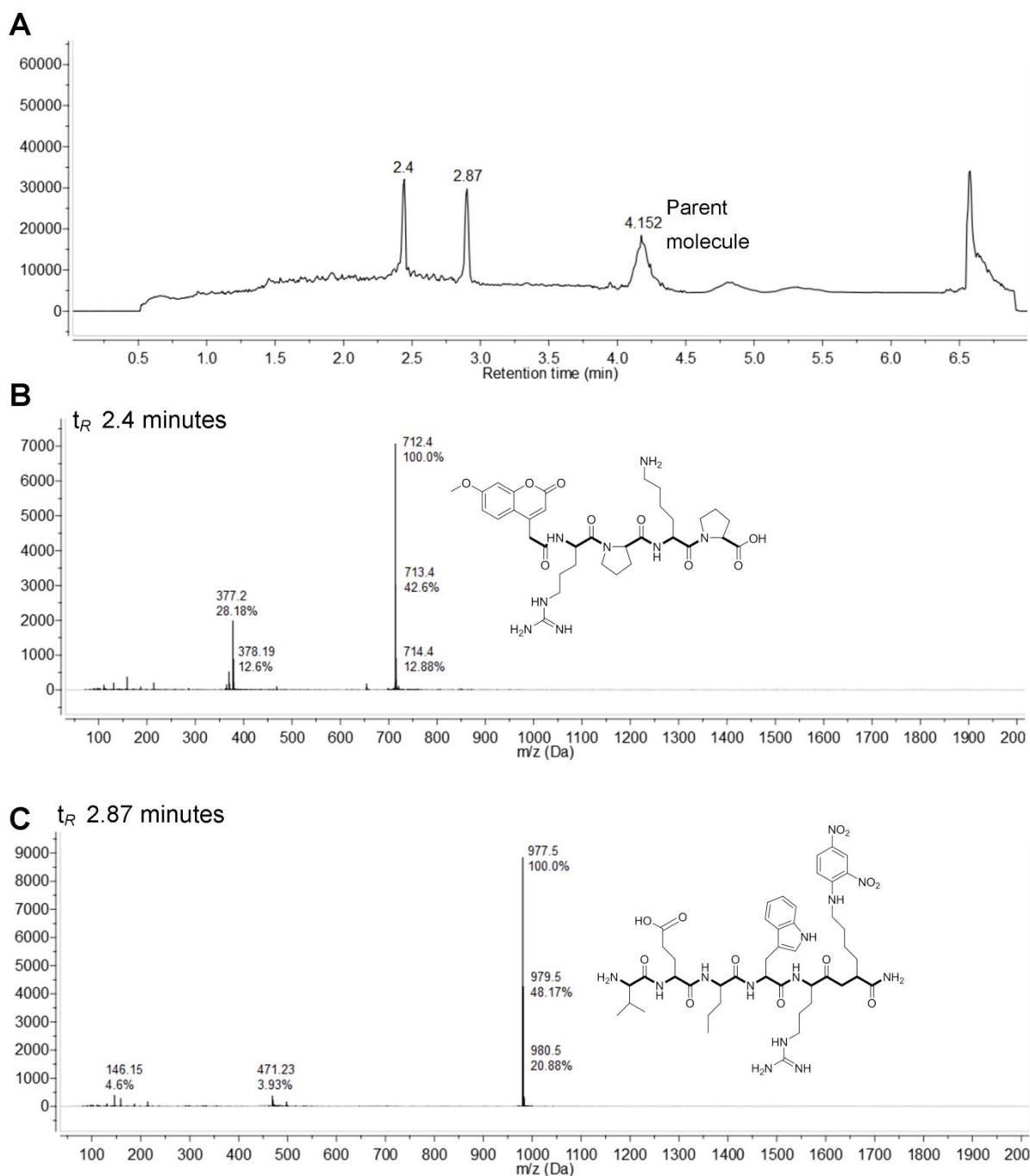
Figure III.22: Cleavage of substrate M-2110 by recombinant MMP-9, detected by LCMS: (A) LC of MMP-9 mediated cleaved metabolites, (t_R 2.4 and 2.87 minutes); (B) MS identification of Mcs half of cleaved substrate (Mca-Arg-Pro-Lys-Pro), t_R 2.4 minutes ($^m/_z$ 712.4 Da, [M+H]$^+$); (C) MS identification of Mca half of cleaved substrate (Val-Glu Nva-Trp-Arg-Lys(Dnp)-NH$_2$) t_R 2.87 minutes ($^m/_z$ 977.5 Da, [M+H]$^+$).

III.5 Discussion

Difficulties in identifying substrate preferences within MMP subfamilies are a major hindrance for progressive design and development of therapeutics exploiting specific MMPs. A major requirement for prodrug or theranostic approaches is MMP-selectivity through incorporation of MMP subtype unique peptide sequences and subsequent disease-selective activation. Thus, determination of the optimum peptide sequence to enable biochemical activity through selective cleavage by the targeted MMP, in conjunction with pharmacological stability of the un-activated molecule, is crucial for the design and development of disease-selective probes and therapeutics.[204, 205] This chapter was aimed at rationalising the functional similarity and substrate cleavage preferences between the members of the MMP subfamily. The utilisation of *in silico* proteolytic docking of MMP-selective substrates within the active site of MMPs, coupled to *in vitro* biochemical assessment provided a robust tool for identifying MMP-subtype specific substrates and progress towards subsequent development of MMP-selective therapeutic approaches.

The molecular dynamics suite, Discovery Studio, was utilised for *in silico* studies. This application supports authentic and comprehensive molecular dynamics simulations tools for multidisciplinary research. Molecular dynamics simulations can help in the study of protein folding and stability, molecular recognition, conformational changes and developing new ligands selective to the protein of interest. In order to successfully utilise MD simulations, its mathematical parameters, collectively termed as force field, were first assigned and optimised to the input molecule. The availability of widely used force fields such as CHARMM, MMFF and CFF within this application allowed for systematic selection of suitable

force field for simulation studies.[272] The aim of force field optimisation study was to select a correct force field for complete energy minimisation that can be applied for structure-based drug design approaches. The *in silico* evidence is presented, showing the application of various force fields for complete energy minimisation of MMP-selective substrate, M-2055. CHARMM demonstrated complete energy minimisation of the substrate and the molecule acquired a flexible α-helix conformation. The complete energy minimisation of the substrate structure was not observed with MMFF and CFF force fields. The final energy of the molecule with MMFF and CFF force fields were relatively higher and the molecule demonstrated rigid conformations compared to CHARMM. Therefore, CHARMM was chosen as the suitable force field for energy minimisation and conformation studies. CHARMM minimised geometries of substrates were employed throughout this study for validation of the *in silico* flexible-ligand docking model. These force fields have unique parameters to support the simulation of many organic molecules. For instance, class-I force fields such as CHARMM has the broadest coverage for organic molecules amongst all the forcefields available in this application. CHARMM has a large collection of general parameters for majority of organic molecules, including non-standard nucleic acid bases, non-standard amino acids, and co-factors; and even has optimised parameters for proteins and nucleic acids. It has parameter coverage for all the physiologically relevant ions and is able to assess the missing parameters based on the local chemical environment of the atom. The CHARMM force field can be used for simulations with different solvent models, including explicit solvents and generalised implicit solvent models. It also has adequate accuracy for energy minimisation of small

molecules; and studying protein-ligand and protein-protein interactions, a feature that is not observed in class-II forcefields such as MMFF and CFF.[273, 274]

Class-II force fields such as CFF and MMFF are general purpose force fields with good parameter coverage for many organic molecules. CFF has additional cross terms in its potential energy function, compared to class-I force fields. MMFF is derived from *ab initio* calculations and experimental data. It was designed to be a transferable force field for pharmaceutical compounds that accurately treats conformational energetics and non-bonded interactions. The two force fields have wide coverage for all organic molecules, allowing for a large number of compounds to be tested for database screening in drug design.[273, 274]

While they are highly successful with general organic molecules, class-II force fields are considered to be less accurate for protein simulations in explicit solvent models when compared with CHARMM. To remedy this deficiency, structural restraints are applied on protein molecules when simulating protein-ligand complexes. They have not been adequately tested or validated for working with implicit protein models and cannot be run with simulations in parallel mode. CFF and MMFF force fields do not possess adequate accuracy for studying protein-ligand and protein-protein interaction when compared to CHARMM.[272-274]

The next step in this study was to review how the 3D-structure of MMPs can be used as a guide to rationalise functional similarity between MMP catalytic domains. The 3D-strutures of closely related MMP sub-families: Gelatinases (MMP-2 and MMP-9) and Stromelysins (MMP-3 and MMP-10) and their flexible docked complexes with MMP-substrates, provided valuable insights into the structural determinants of substrate selectivity of a particular MMP. According to literature, M-2110 is hydrolysed rapidly by Stromelysins and very slowly by MMP-

9; whereas M-2055 is hydrolysed rapidly by MMP-9 and very slowly by Gelatinase B (MMP-2) and Stromelysins. The cleavage pattern reported in the literature[222] and observed via 3-D molecular docking (current study), demonstrated that MMP-9 strongly interacts with M-2055 at the Gly-Cys(Me) bond, and the present study confirmed this finding. However, the cleavage of this substrate by MMP-2 and Stromelysins is unknown. Based on 3-D molecular modelling and the respective zinc-chelation sites, it was predicted that MMP-2 interacts with the substrate at Gly-Cys(Me) bond and Stromelysins interacts at Pro-β-cyclohexyl-Ala bond. This prediction data was experimentally confirmed by incubating M-2055 substrate with recombinant MMPs and analysing the cleaved metabolites via LCMS.

The cleavage of M-2110 reported in the literature[221] and observed in our 3-D molecular modelling indicated that stromelysins strongly interact with M-2110 at the Glu-Nva bond, which was confirmed by the *in vitro* cleavage assay. Again, as for the non-selective use of M-2110, the cleavage pattern of this substrate by MMP-9 is unknown/unreported. Based on 3-D molecular modelling and the respective zinc-chelation sites, it was predicted that MMP-9 interacts with the substrate at the Pro-Val bond. This prediction was also experimentally confirmed highlighting that a suitable predictive model has been created for the determination of substrate cleavage sites by these MMPs.

Most members of the MMP family share a similar catalytic domain constituted by about 170 residues. The domain contains a catalytic zinc ion and a chelated histidine complex, which is responsible for the peptide hydrolysis reaction. MMP catalytic sites share a marked sequence similarity, where the percentage of similar residues ranges from 33% (between MMP-21 and MMP-23) to 86% (between

MMP-3 and MMP-10).[271] The successful validation of the *in silico* proteolytic docking coupled to *in vitro* biochemical assessment provided significant knowledge about the subtle differences in substrate binding efficiencies between the closely related MMP subfamilies studied.
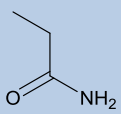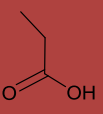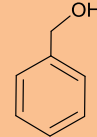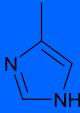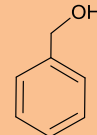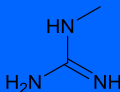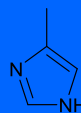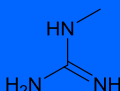
The key observed differences between the binding affinity of MMP-2 and MMP-9 with M-2055 are (Figure III.23):

In MMP-2 the S1 subsite is located near the bulge-edge segment and; the S2 and S3 subsites are located in the helix αβ segment. In MMP-9, the S1 and S3 subsites are located in the helix αβ segment and the S2 subsite is located near the bulge-edge segment. Furthermore, the S1 and S3 subsites in MMP-2 have deeper cavity than MMP-9, suggesting that MMP-2 can accommodate longer side chains then MMP-9. The presence of small chain Ala165 residue in MMP-2 S1 subsite accounts for bigger hydrophobic pocket, whereas Glu402 residue in MMP-9 causes the S1 pocket to become shallow in comparison. Similarly, the presence of Gly204 in MMP-2 at S3 subsite accounts for a large neutrally charged pocket. On the contrary, Asp410 present at the bottom of the S3 subsite in MMP-9 accounts for a small pocket. It was also observed that both these MMPs consisted of large S2 pockets with a difference in polarity. His205 in MMP-2 αβ-Helix loop makes the S2 pocket charged in nature and could potentially accommodate acidic residues. Whereas, the presence of Phe192 residue in MMP-9 account for a hydrophobic S2 pocket.

The key observed differences between the binding affinity of MMP-3 and MMP-10 with M-2110 are (Figure III.23):

In spite of identical substrate selectivity of MMP-3 and MMP-10, there were subtle but significant binding differences between the two. As previously detailed, the S1' pocket of MMP-10 is wider in comparison to MMP-3. The difference in S2 and S3 pockets may hold the key in rationalising the substrate selectivity between the two stromelysins. Ser179 and Leu180 are present on either sides of the S2 pocket in MMP-10, suggesting that it can accommodate both hydrophobic and hydrophilic residues. Whereas, the presence of Ile203 in MMP-3 makes the S2 pocket hydrophobic in nature. Similarly, the presence of Ala229 and His227 on either side of the S3 pocket of MMP-10 suggests that it can accept both polar and non-polar residues. On the other hand, the S3 pocket of MMP-3 contains His166 and is smaller in comparison to MMP-10.

Using the X-ray structure of MMPs published on the RSCB Protein Data Bank *in silico* model was developed which described the binding of selective MMP substrates into the active sites gelatinases and stromelysins. This showed the binding mode of M-2055 and M-2110 in both MMP families, with the modelling results confirmed by in-vitro cleavage studies. This study demonstrated that it is possible to accurately predict the substrate binding within these systems without a substrate 'small molecule' crystal structure to guide molecular binding conformation. In conclusion, such a strategy would be applicable, and valuable, in the development of prodrug approaches to selectively target tumours with MMP overexpression.

	P4	P3	P2	P1	P1'	P2'	P3'
MMP-2							
MMP-9							
MMP-3							
MMP-10							

Non-polar residues

Polar residues

Acidic residues (-vely charged)

Basic residues (+vely charged)

Special amino acids

Figure III.23: Rationalised differences between the substrate residues binding preferences of the studied MMPs. To indicate the type of residues preferred, amino acid side chains are suggested as examples.

Chapter 4: Design, synthesis and preclinical screening of MMP-targeted prodrugs

One of the most significant problems with standard chemotherapeutic agents is their lack of selectivity for tumour tissue. Targeted cancer therapies offer the potential of reduced side effects along with benefits of prolonging drug exposure to cancerous tissues, enabling improved tumour response and survival rates. Harnessing the elevated enzymatic activity of MMPs within the tumour microenvironment to selectively convert a non-toxic prodrug into a potent chemotherapeutic agent is one such approach with significant therapeutic scope.[200, 203-205] Chapter 3 demonstrates the feasibility of utilising *in silico* approaches coupled to *in vitro* biochemical assessment for rationalising the differences in catalytic domain of MMPs and validating the 3D-docking model, thus enabling progress towards development of MMP-targeted prodrugs. Whilst linking a peptide sequence to a number of cytotoxic agents renders them inactive, the most crucial and challenging step in the design of prodrugs is determining an amino acid sequence which allows for selective cleavage only by the MMPs, or indeed, specific members of the MMP family.[205] This chapter aims to build on previous computational modelling studies, exploiting the binding site preferences between MMPs and rationally design peptide prodrugs selectively activated by specific MMP subfamily members.

IV.1   Identification of MMP-selective peptide sequences

Determining the *in vivo* substrate degradome of proteases is a challenging task but, one that has made significant progress in the last few years. Protease degradome account for 1.7% of the human genome and is essential for dynamic

regulation of virtually every biological process, suggesting the elucidation of protease substrates is essential.[194, 275] There are a number of approaches which have been employed to identify *in vivo* and *in vitro* protease substrates and cleavage subsites, an area which is collectively known as 'protease degradomics'.[275, 276] Such techniques include the application of large series of synthetic peptides based on natural substrates, phage display libraries, activity-based probes and mixture-based libraries.[277]

If the protease substrate is defined as …P3-P2-P1~P1'-P2'-P3'… where P is any specific amino acid, cleavage of the substrate (by a protease) occurs between P1 and P1' amino acids (Figure IV.1).
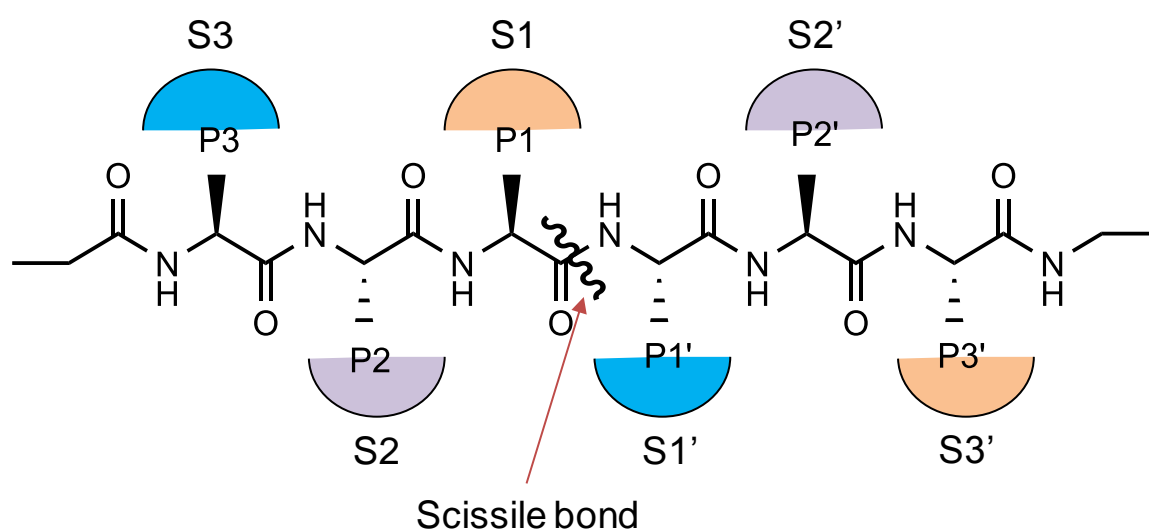
Figure IV.1: Protease binding sites (P) directly contact the substrate binding sites (S) of the substrate. The S-sites nomenclature is concordant with the P sites. S*n* sites are amino terminal to the scissile bond, and the S*n*' sites are carboxy-terminal to the scissile bond.

Utilising a mixture-based peptide library and recombinant MMPs to identify MMP cleavage motifs, a MMP cleavable substrate sequence was identified containing a Pro at P3 position, small residues particularly Ser at P1 position and hydrophobic

amino acids such as Leu/Met at P1' position.[278] This study also identified for the first time the binding preference of MMPs for substrate residues outside of the P1-P1' cleavage subsite.[278] Although a number of cleavage motifs have been identified that are common to all MMPs, certain differences have also been observed that can distinguish the substrate specificity of MMPs. The difference in substrate recognition by MMP-3 and MMP-7 was found to depend heavily on the type of amino acids at the P2 and P1' positions. While both enzymes favoured Pro at P3 position, the substitution of Leu for Met at P1' resulted in a modest increase in MMP-3 activity but decreased MMP-7 activity by eightfold. The substitution of Leu for Phe at P2 resulted in a threefold decrease in MMP-3 activity but increased MMP-7 activity by threefold.[279] Collagen-sequence based synthetic peptides have also been used to provide a number of important insights into the differences and similarities in subsite requirement among MMPs. This study observed that aliphatic side chains at P1' position provided good substrates for all MMPs. The catalytic efficiency of MMPs is dependent upon the length of the peptide substrate. For example, MMP-3 preferred extended peptide for enhanced catalytic activity compared to a peptide containing only three residues or two residues in the P' subsite.[279, 280]

P2' position also showed marked influence in specificity. The study of crystal structures of MMPs with peptide inhibitors indicated that the side chain at the P2' site points away from the enzyme surface and bulky side chains such as Leu is preferred compared to Ala. Substitution of the P1 position for Gly also produced reasonable substrates for certain MMPs. Ala was found to be well tolerated by collagenases, stromelysins and gelatinases. Glu at this position was well tolerated by MMP-3 and MMP-8. Val substitution made the peptide a poor substrate for

most of the MMPs except MMP-3. Bulky aliphatic chains were not favoured by MMP-2 and MMP-9 at P1 position.[281-283]

MMP-3 (Stromelysin-1) and MMP-10 (Stromelysin-2) share a marked sequence similarity and substrate specificity. The crystal structure of MMP-3 bound to endogenous inhibitors has been studied more extensively to reveal the structural basis of MMP-TIMP interaction. MMP-10 has been less thoroughly characterised but, with 86% amino acid residue identity to MMP-3 throughout the catalytic domain and with similar macromolecular substrates, has been predicted to possess similar biochemical properties and substrate cleavage specificities.[134, 271] Substrate recognition by stromelysin was proposed to depend heavily on the P1, P2 and P1' residues. MMP-3 was found to selectively cleave fluorogenic substrate containing charged residues at P1 position and hydrophobic residues at P2 position. The P1' position in MMP-3 was able to tolerate aliphatic chains rather than bulky aromatic residues.[221] Selective modification of the binding subsites increased the substrates selectivity for stromelysin family, over MMP-1, MMP-2 and MMP-9. Multiplexed iTRAQ-based Terminal Amine Isotopic Labelling of Substrates (TAILS) have also been employed to refine the substrate specificity of MMP-10. This study revealed for the first time the preference of MMP-10 for glutamic acid at P1 position on the substrates.[284] However, this substrate was also cleaved by MMP-3, the closest homologue of MMP-10, but lacked selectivity for MMP-9. This preference reinforced the suggestion that MMP-10, similar to MMP-3, preferred substrates with charged residues at P1, the basis for several commercial stromelysin-selective substrates.[221, 284] However, since MMP-10 has been mostly neglected in the quest for new peptide substrates, it remains to be elucidated if

there are any specific differences in the binding subsites and amino acid preferences compared to MMP-3 and gelatinases.

IV.2   MMP-10 targeted therapeutics

Although MMP-10 is closely related to MMP-3 with respect to structure and substrate specificity, differences in activity and cellular distribution exist, suggesting distinct roles of MMP-3 and MMP-10.[155] Unlike several other MMPs that are localised predominantly in tumour stroma, the tumour cells themselves overexpress MMP-10.[155] Overexpression of MMP-10 has been validated in several human tumours of epithelial origin including, head and neck, oesophageal and oral squamous cell carcinoma (SCC) and non-small cell lung carcinoma (NSCLC). MMP-10 has also been found to possess distinct roles (compared to MMP-3) in cancers, including lung cancer, lymphoma, and head and neck cancer.[155, 223-225, 227-229, 232] As demonstrated in Chapter-2, the overexpression and elevated proteolytic activity of MMP-10 in human glioblastoma samples and cell lines relative to normal brain tissues, suggests MMP-10 as a potential therapeutic target for selective drug activation. As outlined in sections I.13 and I.14 (Chapter 1), a number of studies relating to the targeting of MMPs only assessed the feasibility of targeting gelatinases and MT-MMPs with peptide prodrugs. The peptide sequences of stromelysin selective fluorogenic substrates (M2110) however, are unlikely to represent MMP-10 selective sequence since it also has broad selectivity by other MMPs including MMP-3 and MMP-9. Cleavage of the linker by other MMPs expressed in non-diseased tissues would lead to non-specific release of drug causing systemic side effects.[205] Several studies have shown that most peptide prodrugs are cleaved by multiple MMPs, which may not be important but when a target and anti-target both cleave a particular sequence, the MMP-

selective drug activation system will fail. Thus, it is apparent that the MMPs, particularly stromelysin subfamily, are underutilised targets for anticancer drug delivery.

IV.3 Aims and objectives

The overall aim was to develop prodrugs of doxorubicin and the analogues of colchicine (azademethlycolchicine) to be preferentially cleaved by MMP-10. Chapter 2 demonstrates the overexpression of MMP-10 in high grade glioma relative to histologically normal brain tissue, indicating that this enzyme is a potential drug target. Since MMP-10 participates in angiogenesis and is proteolytically expressed by tumour tissue, targeting prodrugs to MMP-10 should allow for activation of the agent selectively in the tumour microenvironment. MMP subfamily activated peptide-prodrugs were rationally designed and synthesised by coupling MMP-cleavable peptides to antitumour agents, to selectively target doxorubicin (Dox) and azademethylcolchicine to tumour tissue.

Specific objectives include:

1. To exploit the substrate binding selectivity between closely related MMPs

2. To rationally design prodrugs selectively activated by specific MMPs over a close family homologue i.e. MMP-2 and MMP-10 but not by MMP-9 and MMP-3.

3. To assess specificity of prodrug cytotoxicity utilising MMP positive and negative preclinical tumour models.

4. To assess metabolism of prodrugs in tissues such as human tumour, mouse liver, mouse kidney and blood plasma *ex vivo*.

5. To rationally design prodrugs cleaved selectively by MMP-10 relative to other MMP family members, MMP-2, MMP-9 and MMP-3.

IV.4   Materials and methods

IV.4.1   Synthesis of MMP-targeted peptide conjugates

Custom designed peptide sequences with Cbz (Benzyloxycarbonyl) as the chemical endcap were purchased from Bachem (Bubendorf, Switzerland)/ synthesised using solid phase strategy. Activation of the pre-loaded 2-chlorotrityl resin was carried out in a fritted polypropylene reaction chamber. 0.1 mmol of resin was weighed into the reaction chamber and 2 ml of dry DCM added. The reaction vessel was shaken for 45 minutes. After this time, DCM removed and the resin washed further with DCM. Single couplings were carried out using 5 equivalents of peptide (compared to resin), 5 equivalents of benzotriazol-1-yloxytripyrrolidinophosphonium hexafluorophosphate (PyBOP®), 10 equivalents of N,N-Diisopropylethylamine (DIPEA) and 2 mL of DMF under agitation for 45 minutes. Double peptide couplings were carried out - 2 x 45 minute couplings for each residue addition, the reaction drained after each coupling and fresh reagents added. After each set of coupling reactions, the reaction solution was drained and resin washed with 5 portions of 2 mL DMF. Removal of the Fmoc group was carried out using 5 mL of a solution of 20% piperidine in DMF for 5 under agitation. Piperidine solution was drained and fresh solution added for a further 10 minutes under agitation. Piperidine solution was drained and the resin rinsed using 5 portions of 2 mL DMF. Peptide-resin was treated with a solution of 20% hexafluoroisopropanol in DCM for 1 h. The resin was removed by filtration and the solvent removed from the filtrate under reduced pressure before precipitation using diethyl ether and decanting of the liquid (followed by subsequent ether washes). The resulting solid peptide (with free COOH-terminus) was dissolved in deionized water and acetonitrile mix and lyophilized. Purification of peptides was

carried out using Perking Elmer HPLC. Samples were injected into a column and a gradient of 0-100% solvent B (solvent A= 95% H_2O, 5% MeCN, 0.01% TFA, solvent B = 95% MeCN, 5%H_2O, 0.01% TFA) over 95 minutes with a flow rate of 2.0 ml/min. Doxorubicin/azademethylcolchicine was conjugated to the peptide C-terminus as follows: Doxorubicin.HCl or azademethylcolchicine (0.0012 g, 0.002 mol, 1 equiv.), peptide (0.0022 g, 0.002 mol, 1 equiv.), PyBOP® (0.0015 g, 0.003 mol, 1.3 equiv.), and hydroxybenzotriazole hydrate (0.0073 g, 0.0054 mol, 2.6 equiv.) were added together under nitrogen in anhydrous DMF (2 mL). DIPEA (8 equiv., 0.016 mol) was added and the reaction mixture was stirred overnight in the absence of light. Solvent was removed *in vacuo* and the mixture triturated with cold Et_2O (5 mL) to precipitate the crude peptide which was then obtained through centrifugation to obtain the crude solid peptide conjugate. The product was then purified using a C18 column and reverse phase HPLC (H_2O/MeCN) gradient system using mass spectrometry as confirmation of molecular mass to give a pale red doxorubicin peptide conjugate (0.0021 g, 70% yield) or pale yellow azademethylcolchicine peptide conjugate (0.0015 g, 50% yield).

Cbz-E(*O^tBu*)PLGS(OBn)Y(*O^tBu*)L-COOH + Doxorubicin

1) Conjugation
PyBOP, HOBt
————————————→   **Cbz-E(*O^tBu*)PLGS(OBn)Y(*O^tBu*)L-Doxorubicin**
DMF DIPEA

2) Deprotection
————————————→   **Cbz-EPLGS(OBn)YL-Doxorubicin**
25% TFA in DCM   **(Crude)**

3) Purification
————————————→   **Cbz-EPLGS(OBn)YL-Doxorubicin**
                                    (Purified, 70% yield)
Mobile phase A: 90:10 H$_2$O:MeCN
Mobile phase B: 40:60 H$_2$O:MeCN
And 0.1% HCO$_2$H
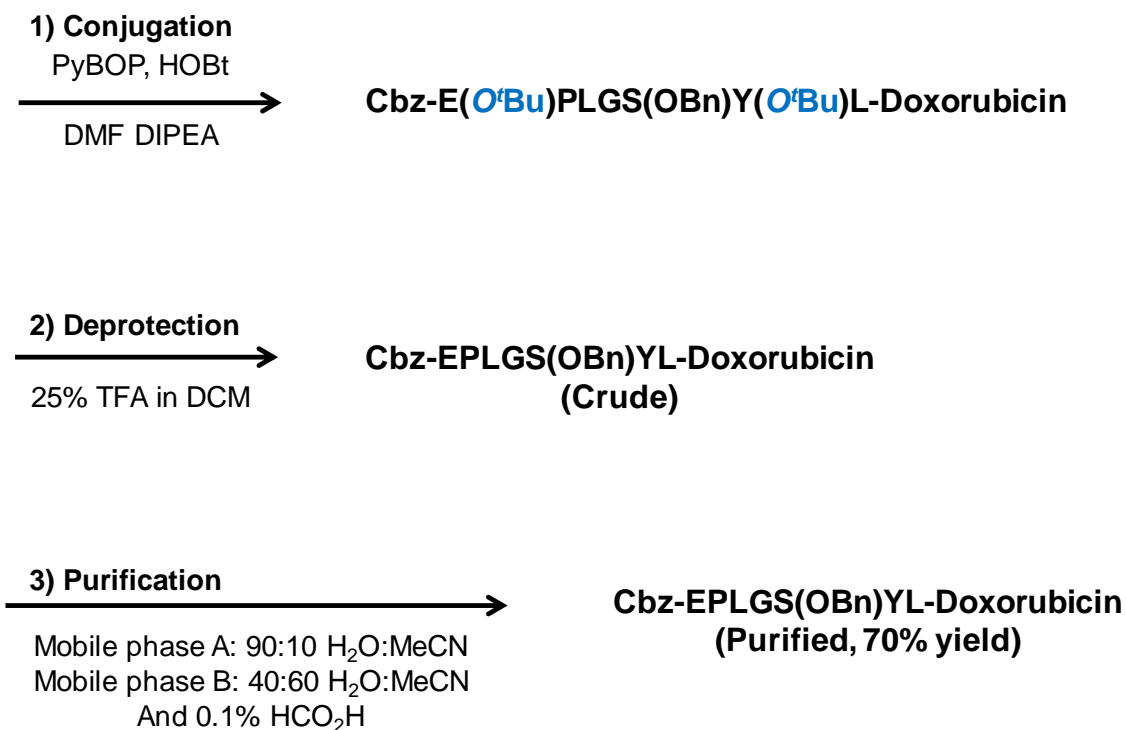
Figure IV.2: Synthetic scheme for peptide-doxorubicin conjugates

IV.4.2 Development of azademethylcolchicine

Colchicine was dissolved in 25% ammonioa solution (BDH) and stirred overnight at room temperature. Thin layer chromatography (TLC) was used to monitor the reaction and the product, azademethylcolchicine (Figure IV.3).
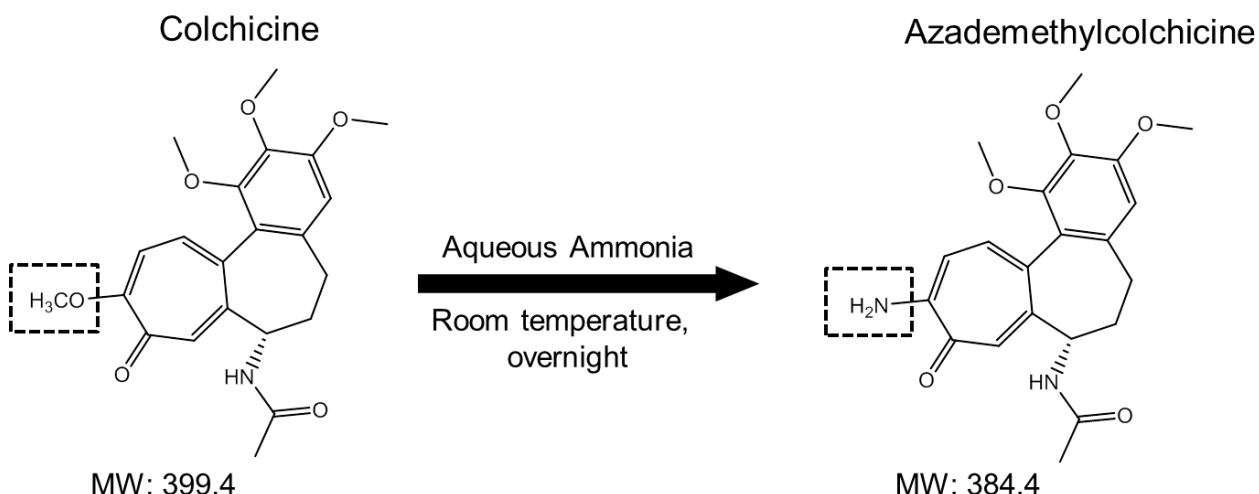
Figure IV.3: Reaction of colchicine with ammonia to yield azademethylcolchicine

IV.4.3 Thin Layer Chromatorgraphy (TLC)

TLC was used to monitor the conversion of colchicine into azademethycolchicine. Aluminium siilca TLC sheets (silica gel 60, f_{254}) (Merck, Darmstadt, Germany) were used as the solid phase whilst dichloromethane, methanol and NH_2 were used in a 10:1:0.1 ratio to form the mobile phase. TLC plates were spotted with reaction products approximately 1cm from the bottom of the plate and the plate placed into the mobile phase. After the mobile phase had migrated towards the top of the plate by capillary action, the plate was removed and the products viewed under a UV light. The migration of each product was dependent upon the polarity of the substance (i.e. the partition coefficient between stationary and mobile phases).

TLC was used to track both the disappearance of starting material and the appearance of product during synthesis.

IV.4.4 Liquid Chromatography-Mass spectrometry detection of peptide prodrugs

LC conditions: High-purity HPLC-grade solvents (Sigma-Aldrich), analytical grade chemicals (Sigma-Aldrich) and triple distilled water were used throughout. Reverse-phase chromatographic separation of substrates was performed using an Acquity UPLC comprising a BEH C18 1.7 µm column (2.1 mm x 100 mm) (Waters, UK). Mobile phases were as follows: Mobile Phase A consisted of 90% HPLC grade water, 10% HPLC grade MeCN and 0.1% HCO_2H. Mobile phase B consisted of 40% HPLC grade water, 60% MeCN and 0.1% HCO_2H.

MS conditions: A Micromass ZMD single quadrupole electrospray MS was used in positive mode (Micromass, Manchester, UK) and MassLynx software was used to identify substrates and anticipated metabolites. MS source parameters were optimised to: desolvation gas 375 L/hr, cone gas 33 L/hr, capillary 2.9 kV, sample cone 16 V, extraction cone 5 V, fR lens 0.1 V, source block temperature 150°C and desolvation temperature 200°C. Parent compounds and metabolites were detected as singularly charged ions using selected ion readings (SIR).

IV.4.5 Cleavage of prodrugs by recombinant MMPs

Recombinant human MMP proteins (MMP-2, MMP-3, MMP-9 and MMP-10; R&D Systems, UK) were assayed for their ability to cleave peptide-prodrug conjugates. Reactions (100 µL) contained 20 ng recombinant protein and 10 µM prodrug in MMP activity buffer (100 mM Tris-HCl pH 7.6, 10 mM $CaCl_2$, 100 mM NaCl, 0.16% v/v Brij-35), and incubated at 37˚C for 12 h. At T_{12}, The sample was removed and

diluted 1:3 with MeCN to precipitate proteins. The sample was then centrifuged at 10,000 x *g* for 3 minutes and supernatant assayed for substrate cleavage by LCMS.

IV.4.6 Metabolism of prodrugs in tissues *ex vivo*

Female Balb/c immunodeficient nude mice (Harlan Blackthorne) were housed in an air-conditioned room with regular alternating cycles of light and darkness. The animal model received Harlan diet and water as required. The facilities have been approved by the Home Office and meet all current regulations and standards of the United Kingdom. The mice were used between the ages of 6-8 weeks in accordance with institutional guidelines. All procedures were performed under a United Kingdom Home Office Project Licence, UKCCCR guidelines. Mice were subcutaneously implanted with 2-3 mm^3 fragments of HT1080 tumour xenografts. Resultant tumours were removed, snap-frozen in liquid nitrogen and stored at -70°C. Xenograft tissues (tumour, liver and kidney) were homogenized in MMP activity buffer and resultant supernatants collected by centrifugation. Supernatants, equivalent to 100 mg tissue/mL, were assayed for their ability to activate the prodrugs. Reaction aliquots were removed over a 60 min period of incubation at 37 °C, proteins were precipitated using MeCN and the metabolites analysed by LCMS.

IV.4.7 Determination of cellular viability

IV.4.7.1   MTT assay

Cell viability was measured using the MTT assay. Cells seeded on 96-well plates, which had been incubated with varying concentrations of compound for a specific time frame, were treated with 3-(4,5-Dimethylthiazol-2-yl)-2,5-diphenyltetrazolium

Bromide (MTT) (500 µg/well) (method adapted from Mosmann, 1983). Plates were incubated at 37°C for 4 h, allowing mitochondrial dehydrogenase in viable cells to metabolise MTT and produce purple crystals of formazan. Media was removed and 150 µL of DMSO added to each well to solubilize the formazan and produce a uniform colour in each well. The plate was then analysed using a plate reader (GO Multiskan, Thermo Life Sciences) measuring absorbance at 550 nm where the absorbance reading and the viable number, is directly proportional to the level of the formazan product created.

IV.4.7.2   Growth curve analysis

In order to observe the growth characteristics of the U87-MG, 1321N1 and SVG12 cell lines, in which the cytotoxicity of peptide conjugates was to be assessed, growth curve analysis for each cell line was conducted in 96-well plates. Varying cell densities of each cell line were seeded (250, 500, 1000, 2000 and 4000 cells per well) and monitored for 10 days to show cell growth kinetics. On each day, the increase in cell number for each cell density was calculated using the MTT assay. The data obtained was used to produce cell growth curves for each cell line for a number of seeding densities. For both U87-MG and SVG-P12 cell lines, 1000 cells per well and for 1321N1 cell lines, 500 cells per well were chosen as the seeding densities during cytotoxicity assays as cells would be in the exponential phase of their growth cycle for the duration of the assay.

IV.4.7.3   Assessment of compound cytotoxicity

Cells were seeded in 96-well plates at the respective chosen seeding densities in a total volume of 200 µL culture medium and allowed to adhere to the plate overnight. Following a 24 h incubation, media was removed and fresh media

added containing specific concentration of the compound of choice (Doxorubicin prodrug, azademethylcolchicine prodrug, doxorubicin alone or azademethylcolchicine alone, dissolved in DMSO) over a selected concentration range for a specific time period. For doxorubicin prodrugs and doxorubicin alone, concentrations ranged from 100 µM to 10 pM produced by serial dilutions whilst for azademethylcolchicine prodrugs and azademethylcolchicine alone, concentrations ranged from 100 µM to 1 pM. Control lanes included a DMSO control containing the same concentration of DMSO as the highest drug concentration (0.1% DMSO), one lane containing no drug treatment and one lane containing no cells. For each compound, plates were set up for drug exposures of 48 h and 96 h. After incubation, viable cell number was calculated using the MTT assay.

IV.5 Results

IV.5.1 Flexible-ligand docking of "Standard prodrug" and MMPs

Following successful validation of the *in silico* model for the peptide substrates (Chapter 3) a known pan-MMP-targeted peptide conjugated doxorubicin prodrug was evaluated as a basis for further drug design. This prodrug is known to be cleaved by MMP-2, 9 and 14,[207, 285] presenting an excellent model for further modification.

When considering the *in silico* interaction of the peptide fragment of the 'Albright prodrug' with MMP-2 and MMP-9, the zinc ions are chelated by the carboxylate between Gly-Ser(*O*-Benzyl) bond at interatomic distances of 2.6 Å and 2.8 Å respectively (the known cleavage site). The peptide aligns tightly into the active site of the MMPs as determined by their interatomic zinc distances and binding energies (555 kcal/mol and 492 kcal/mol) in MMP-2 and MMP-9 respectively (Figure IV.4).

The *in silico* interaction of Albright prodrug sequence with MMP-3 and MMP-10 shows the chelation of zinc ions by the carboxylate between Ser(*O*-Benzyl)-Tyr bond (3.4 Å and 3.6 Å respectively), the unknown cleavage site by stromelysins. The interaction of the peptide in the active site of MMP-3 and MMP-10 is nearly eight times weaker (70 kcal/mol and 66 kcal/mol) than gelatinases. The P1 and P1' residues align tightly into the S1 and S1' subsite of stromelysins (2.2 Å), whereas other residues demonstrated weaker binding (3.8 Å), resulting in decreased overall binding (Figure IV.5).
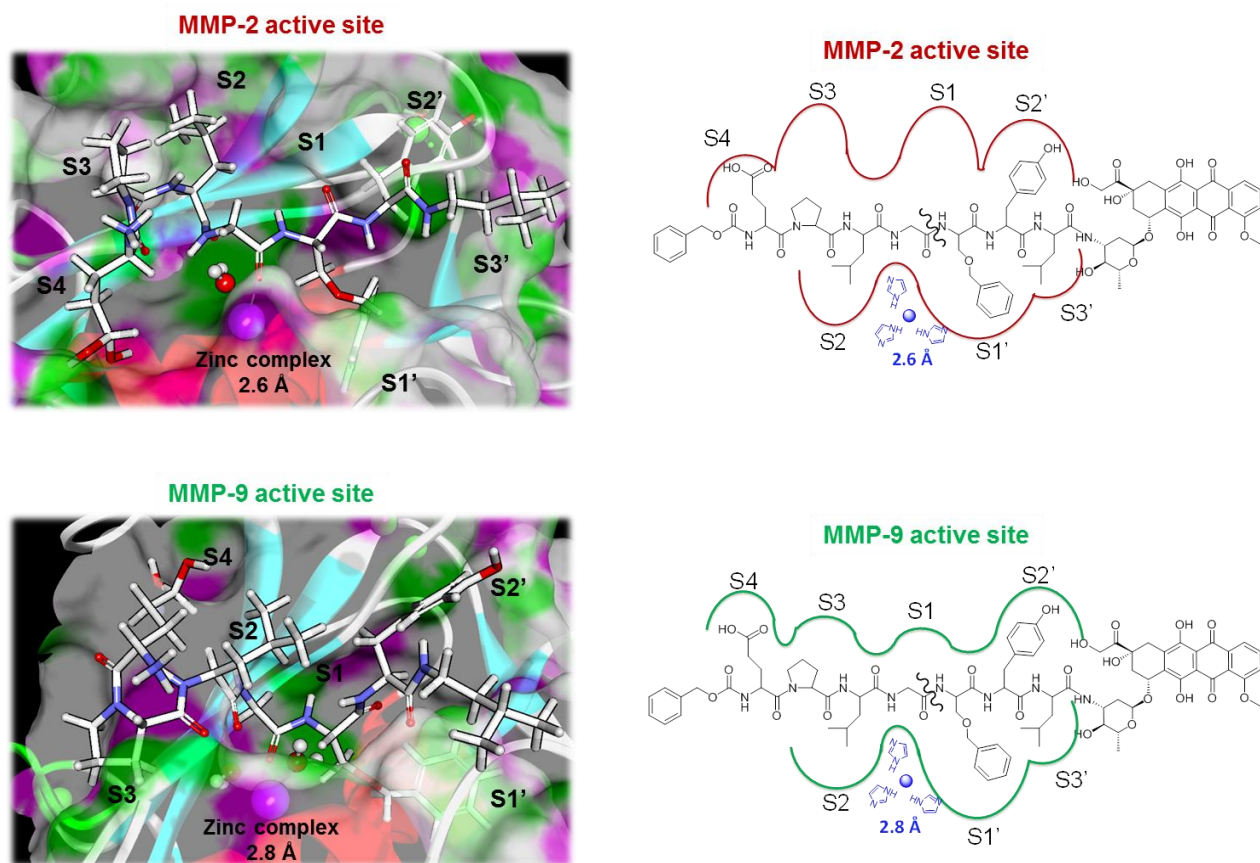
Figure IV.4: (*Left*) Stereo view of the docked complexes of 'Albright prodrug' (white sticks) and the catalytic domain of human MMP-2 (PDB ID: 1GKC) and MMP-9 (PDB ID: 1GKC). Catalytic and structural zinc ions are shown as purple spheres. Active-site cleft residues (the αβ-helix loop and the specificity loop) are represented by ribbons. (*Right*) Schematic representation of 'Albright prodrug': active site binding interaction in human MMP-2 and MMP-9. MMP-2 and MMP-9 enzyme binding pockets are shown in red and green respectively. Substrate chemical structure and its scissile bond is shown in black. The zinc ion coordinated by histidine is indicated in blue.
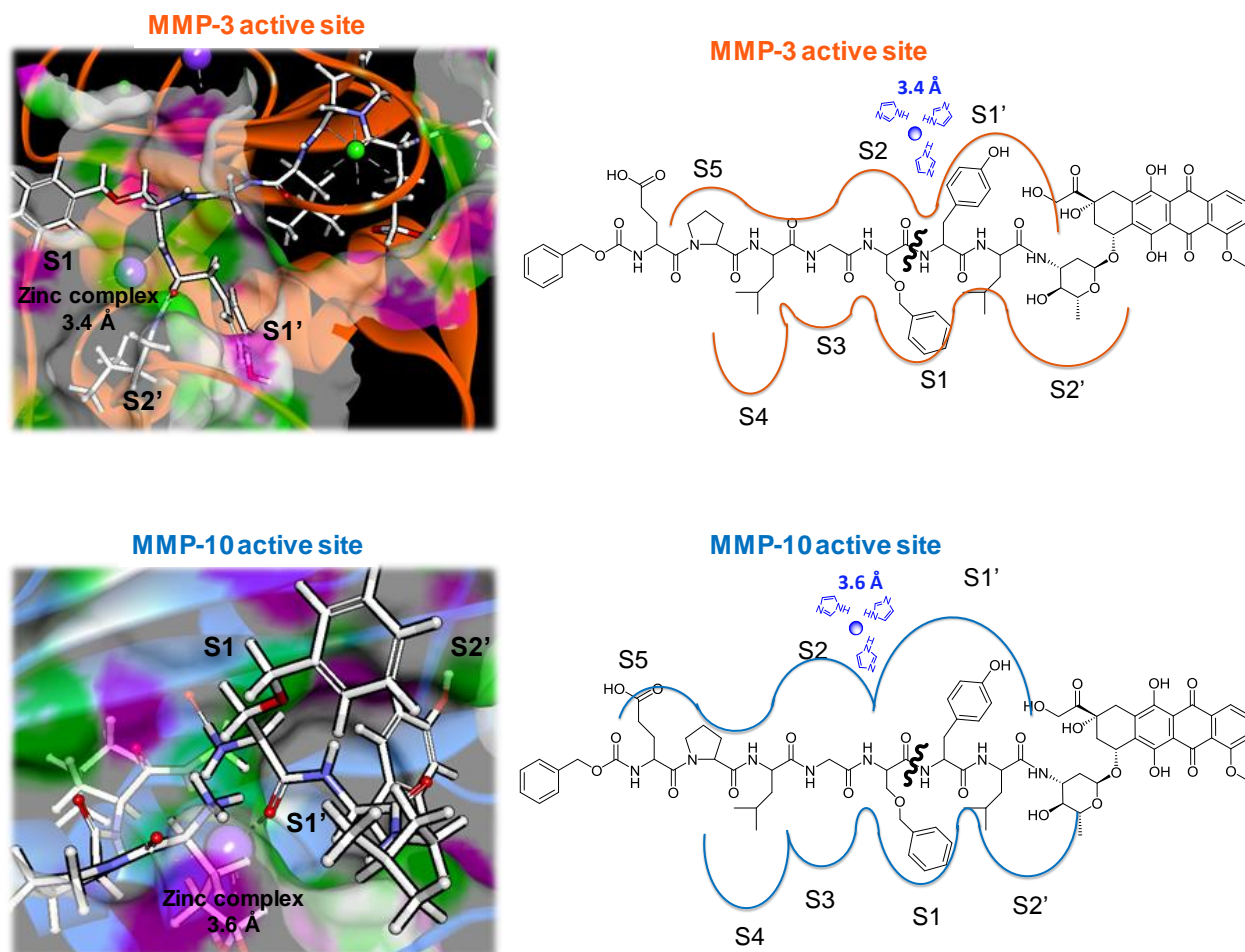
Figure IV.5: (*Left*) Stereo view of the docked complexes of 'Albright prodrug' (white sticks) and the catalytic domain of human MMP-3 (PDB ID: 1CIZ) and MMP-10 (PDB ID: 1Q3A). Catalytic and structural zinc ions are shown as purple spheres. Active-site cleft residues (the αβ-helix loop and the specificity loop) of MMP-3 and MMP-10 are shown in orange and blue respectively. (*Right*) Schematic representation of Albright prodrug: active site binding interaction in human MMP-3 and MMP-10. MMP-3 and MMP-10 enzyme binding pockets are shown in orange and blue respectively. Substrate chemical structure and its scissile bond is shown in black. The zinc ion coordinated by histidine is indicated in blue.

IV.5.2 Development of MMP-targeted "Standard prodrug"

To experimentally validate the predictability of *in silico* model, the 'Albright prodrug' was synthesised in order to endcap the peptide sequence. The peptide sequence of prodrugs was conjugated between Dox warhead and a Cbz (Benzyloxycarbonyl) non-polar endcap protecting group, and purified as described in materials and methods (Section IV.4.1) (Figures IV.6 and IV.7).

Cbz-E(*O*^tBu)PLGS(OBn)Y(*O*^tBu)L-COOH + Doxorubicin

1) Conjugation
PyBOP, HOBt

DMF DIPEA
→

Cbz-E(*O*^tBu)PLGS(OBn)Y(*O*^tBu)L-Doxorubicin

2) Deprotection

25% TFA in DCM
→

**Cbz-EPLGS(OBn)YL-Doxorubicin
(Crude)**

3) Purification

Mobile phase A: 90:10 H_2O:MeCN
Mobile phase B: 40:60 H_2O:MeCN
And 0.1% HCO_2H
→

**Cbz-EPLGS(OBn)YL-Doxorubicin
(Purified, 70% yield)**
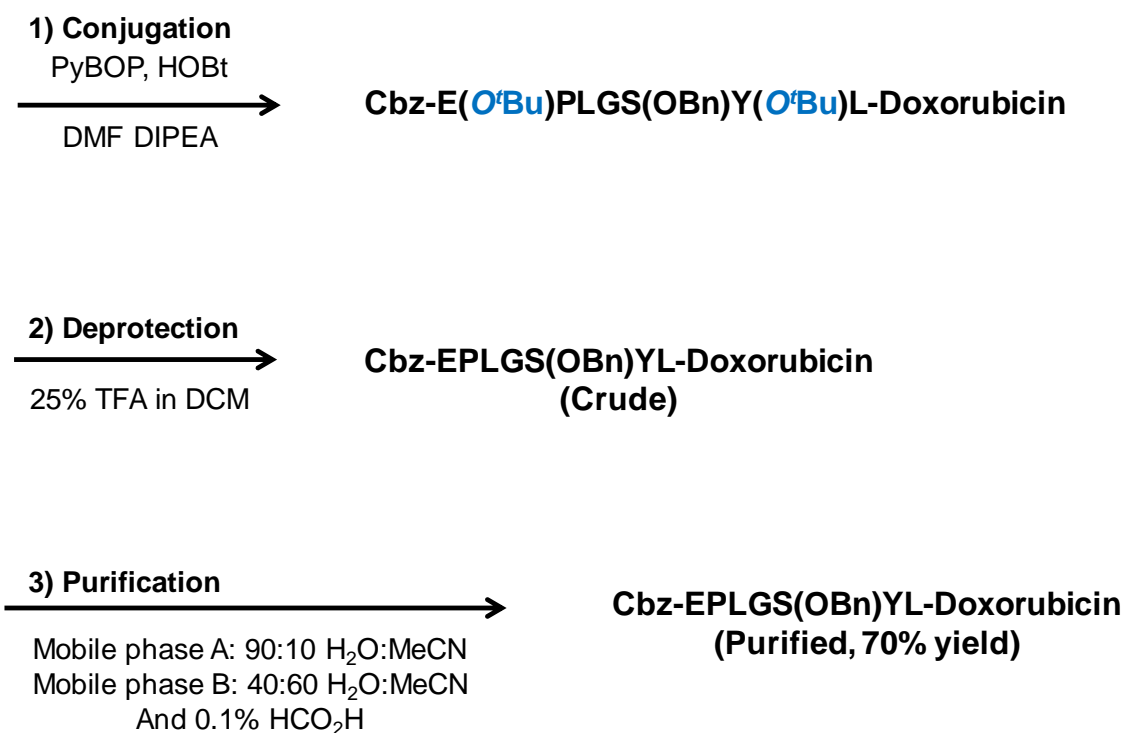
Figure IV.6: Synthetic scheme for peptide-doxorubicin conjugates
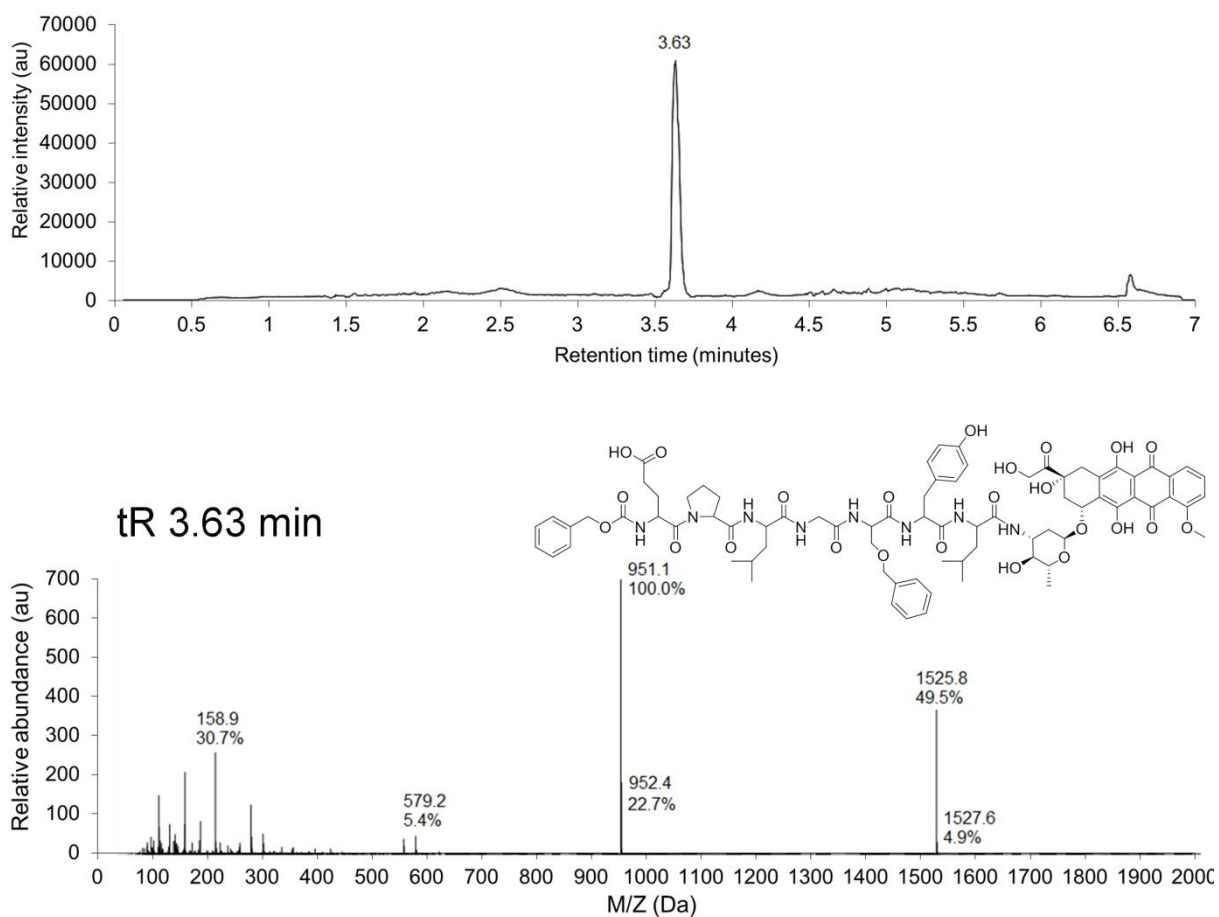
Figure IV.7: Detection of MMP-targeted prodrug (reference compound at retention time (tR) of 3.63 minutes ($^m/_z$ 1525.8 Da, [M+H]$^+$), confirmed by LC-MS

IV.5.3   Analysis of "Albright prodrug" cleavage by recombinant MMPs

To confirm the *in vitro* cleavage site and validate the *in silico* prediction, lysis was performed with recombinant MMP-2 and MMP-9 in the presence of the 'Albright prodrug' and results analysed by LC-MS (reverse phase) over a 12 h period. The 'Albright prodrug' (Cbz-Glu-Pro-Leu-Gly-Ser(O-Benzyl)-Tyr-Leu-Doxorubicin), was identified (t_R) 3.63 minutes ($^m/_z$ 1525.8 Da, [M+H]$^+$, Figure IV.7) and cleavage of by both MMP-2 and MMP-9 at Gly-Ser(O-Benzyl) bond was confirmed by LCMS, Cbz-Glu-Pro-Leu-Gly at t_R 2.87 minutes ($^m/_z$ 547.2 Da, [M+H]$^+$) and Ser(O-Benzyl)-Tyr-Leu-Doxorubicin at t_R 3.23 minutes ($^m/_z$ 997.4, [M+H]$^+$). (Figures IV.8, IV.9 and IV.10).
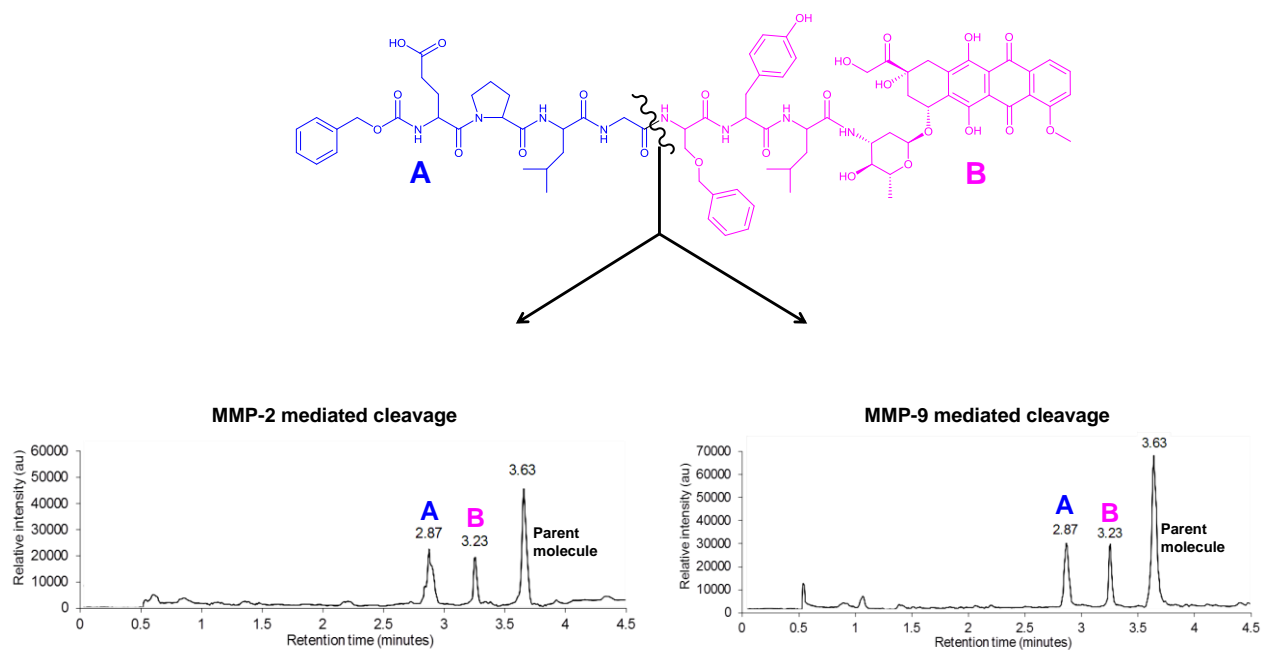
Figure IV.8: Schematic representation of the cleavage of Albright prodrug by recombinant MMP-2 and MMP-9 enzymes at Gly-Ser(OBenzyl) bond.
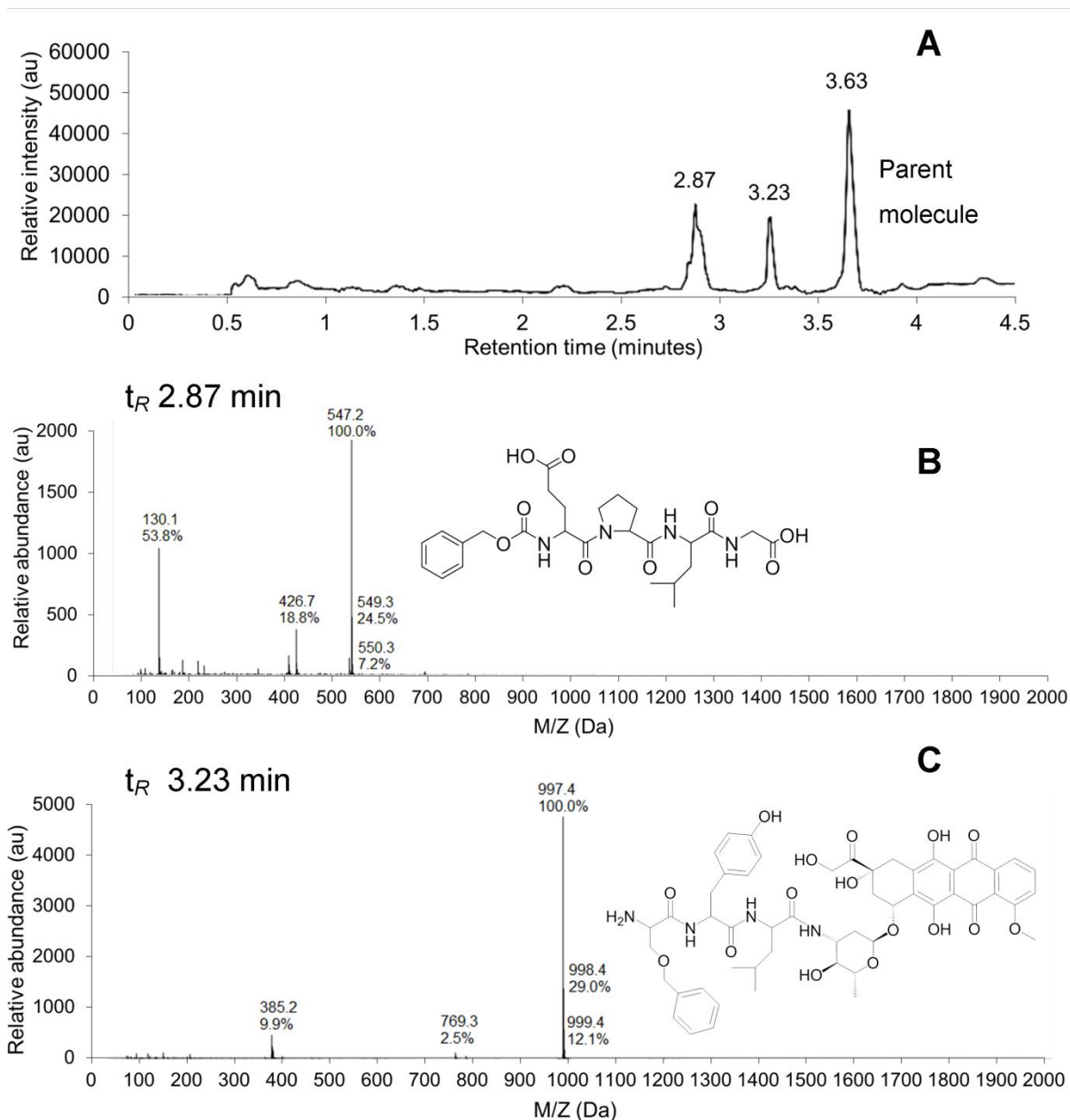
Figure IV.9: Cleavage of MMP-targeted prodrug (Albright prodrug) by recombinant MMP-2, detected by LCMS: (A) LC of MMP-2 mediated cleaved metabolites, (t_R 2.87 and 3.23 minutes); (B) MS identification of Cbz-Glu-Pro-Leu-Gly, t_R 2.87 minutes ($^m/_z$ 547.2 Da, [M+H]$^+$); (C) MS identification of Ser(OBn)-Tyr-Leu-Doxorubicin t_R of 3.23 minutes ($^m/_z$ 997.4 Da, [M+H]$^+$).
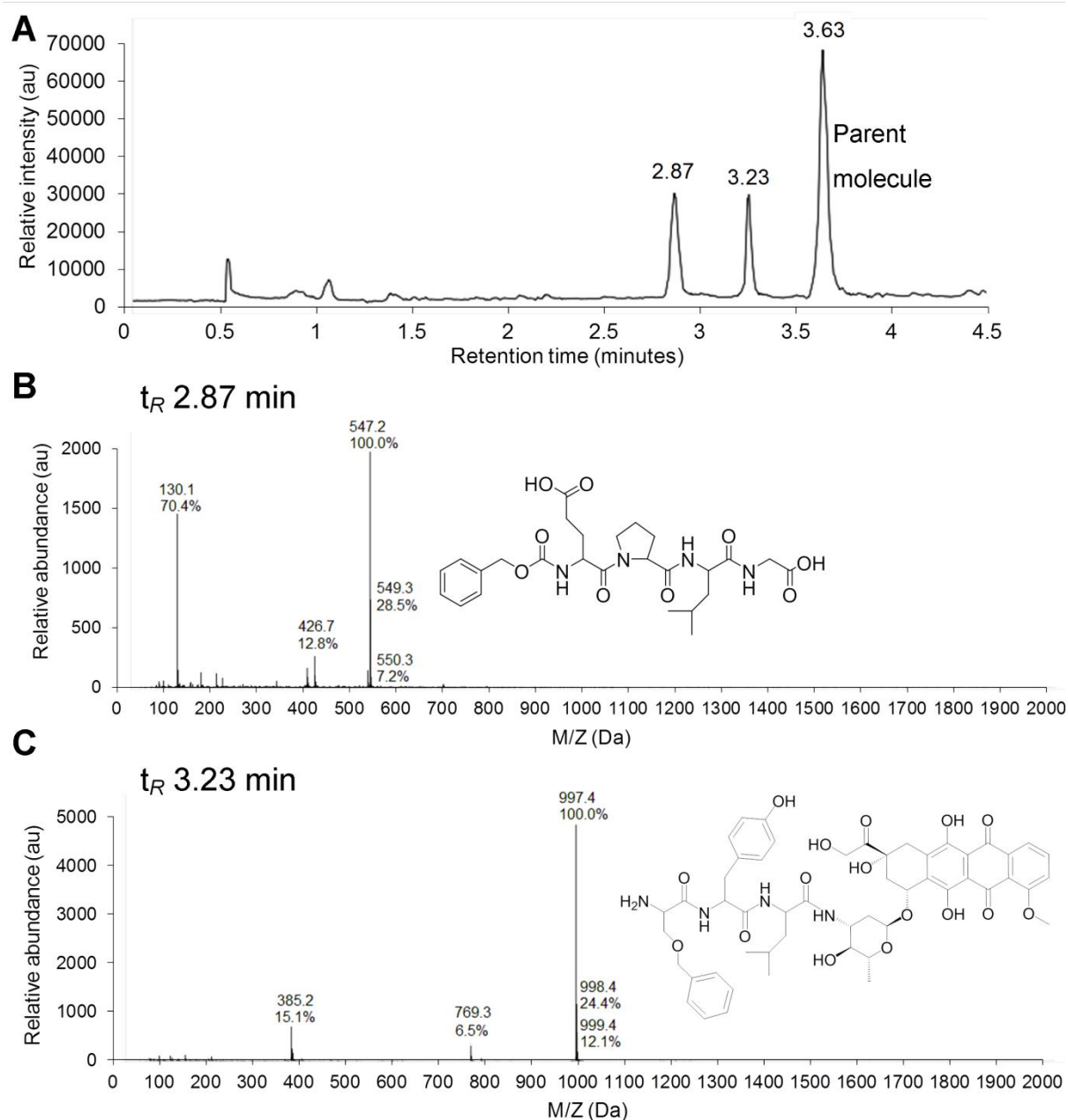
Figure IV.10: Cleavage of MMP-targeted prodrug (Albright prodrug) by recombinant MMP-9, detected by LCMS: (A) LC of MMP-2 mediated cleaved metabolites, (t_R 2.87 and 3.23 minutes); (B) MS identification of Cbz-Glu-Pro-L9u-Gly, t_R 2.87 minutes ($^m/_z$ 547.2 Da, [M+H]$^+$); (C) MS identification of Ser(OBn)-Tyr-Leu-Doxorubicin t_R of 3.23 minutes ($^m/_z$ 997.4 Da, [M+H]$^+$).

IV.5.4 Rationalised design of MMP-subtype selective peptide conjugates (MJ02)

To discriminate MMP-2 over MMP-9 subtype modification of the 'Albright prodrug' was explored through incorporating the following modifications: Aromatic residues in S1 subsite; acidic side-chain in S2 subsite and a polar side-chain at the S3 subsite and small non-polar residues were included at the S1' subsite to create MJ02 (Figure IV.11).

The flexible docking of MJ02 sequence within the active site of MMP-2 demonstrated the interaction of catalytic zinc at the carboxylate between Homophenylalanine (Hof)-Leu bond (1.9 Å), indicating the predicted cleavage site. Residues of MMP-2 tightly bind with MJ02 as demonstrated by strong interactions with the bulge-edge segment molecules (Gly162 to His166) and the wall-forming segment molecules (Tyr223 to Thr229) with interatomic distances ranging from 1.8 to 2.8 Å and has a predicted binding energy of 805 kcal/mol. In MMP-9 the predicted zinc interaction is not detectable and the binding energy is negative (-107 kcal/mol) suggesting the modified peptide residues should give selectivity for MMP-2 over MMP-9 (Figure IV.12).
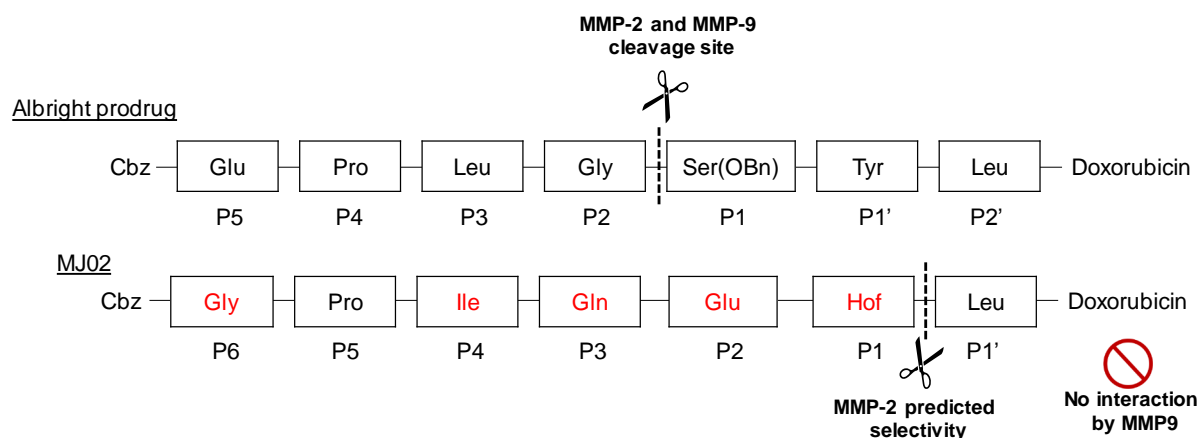
Figure IV.11: Modified 'Albright prodrug' residues to form MJ02, highlighting the modified amino acid sequence and predicted MMP-2 selectivity
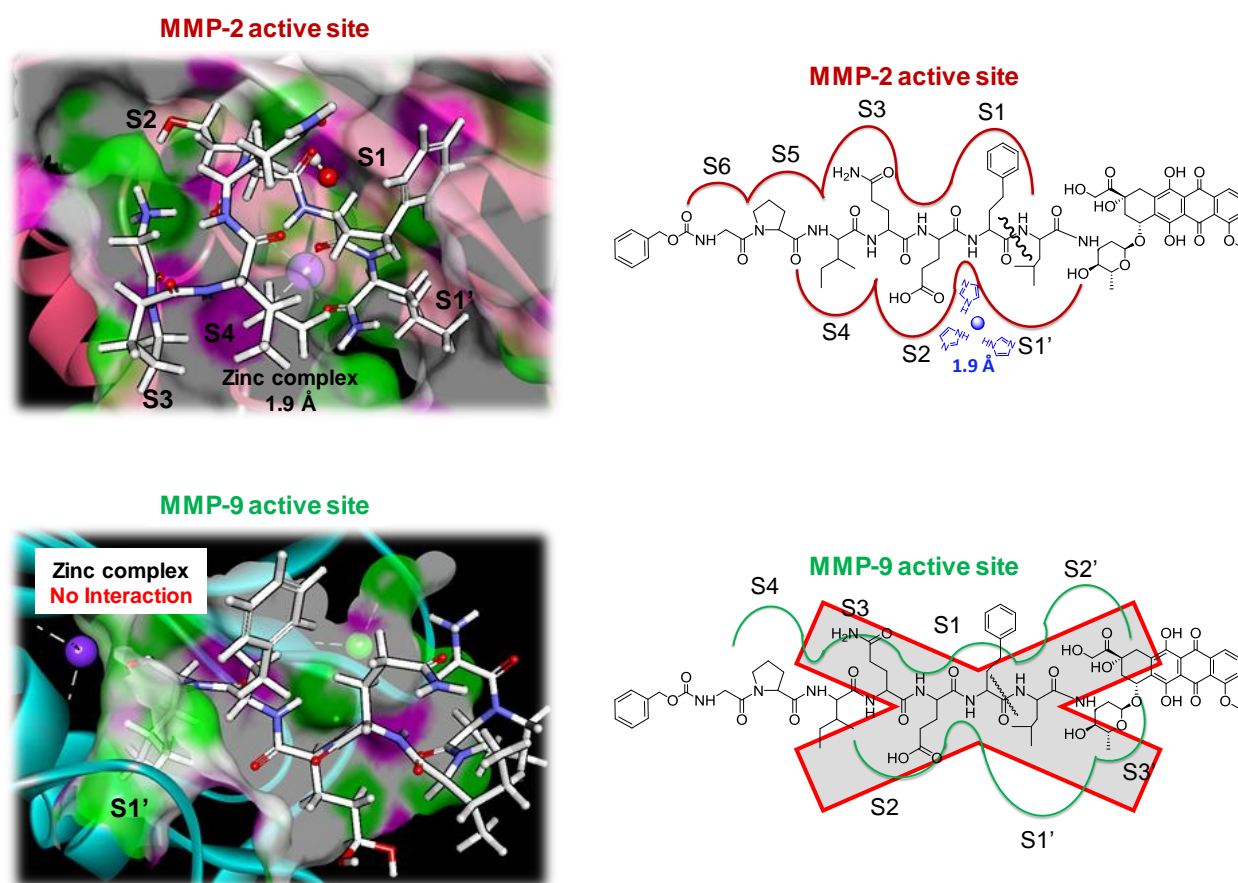
Figure IV.12: (Left) Stereo view of docked complexes of MJ02 (white sticks), catalytic domain of human MMP-2 (PDB ID: 1GKC) (Red) and MMP-9 (PDB ID: 1GKC) (Green). Catalytic and structural zinc ions are shown as purple spheres and active-site cleft residues (αβ-helix loop and the specificity loop) are shown as green. (Right) Schematic representation of MJ02: active site binding interaction in MMP-2 and MMP-9, are shown in red and green respectively. MJ02 chemical structure and its scissile bond is shown in black and zinc ion coordinated by histidine is indicated in blue.

Considering the catalytic differences between the stromelysins, the rational design of a peptide conjugate selective for MMP-10 over MMP-3 was achieved by incorporating residues to fit S1, S2, S3, S5 and S1' pockets of MMP-10 which differ in size and polar affinity compared MMP-3. The following modifications were incorporated: charged residues in S1 subsite – acidic residues preferred by Stromelysins;[284] polar side-chain in S2 subsite; non-polar side-chains in S3 subsite; simple side-chain residues in S5 subsite and aromatic residues in S1' subsite (Figure IV.13).

The predicted interaction between MJ02 and MMP-10 demonstrated strong chelation of zinc ion with the carboxylate between Glu-Hof bond (2.1 Å), indicating a predicted cleavage site with binding energy of 780 kcal/mol. In MMP-3 the zinc interaction is not detectable and the predicted binding energy is negative (-88 kcal/mol) suggesting the modified peptide residues should give selectivity for MMP-10 over MMP-3 (Figures IV.14).
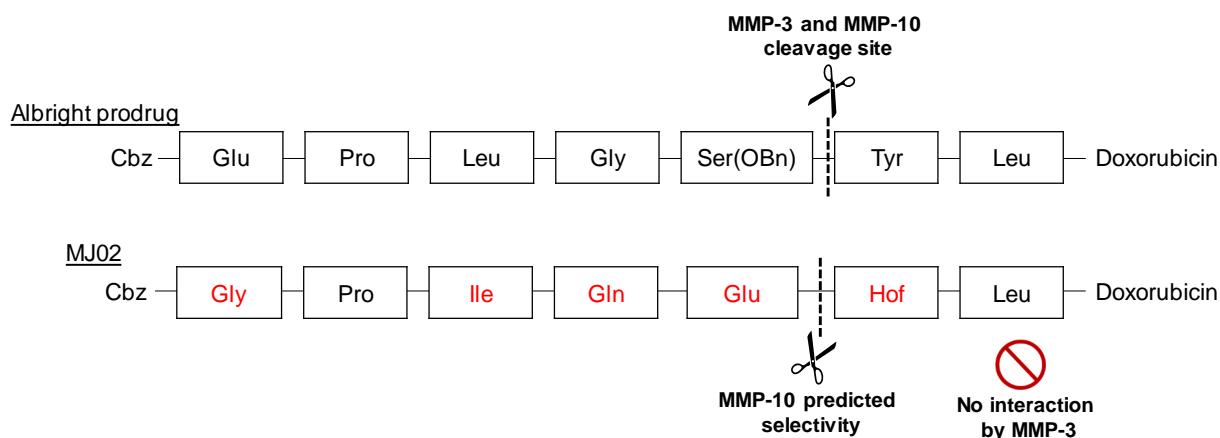
Figure IV.13: Modified 'Albright prodrug' residues to form MJ02, highlighting the modified amino acid sequence and predicted MMP-10 selectivity
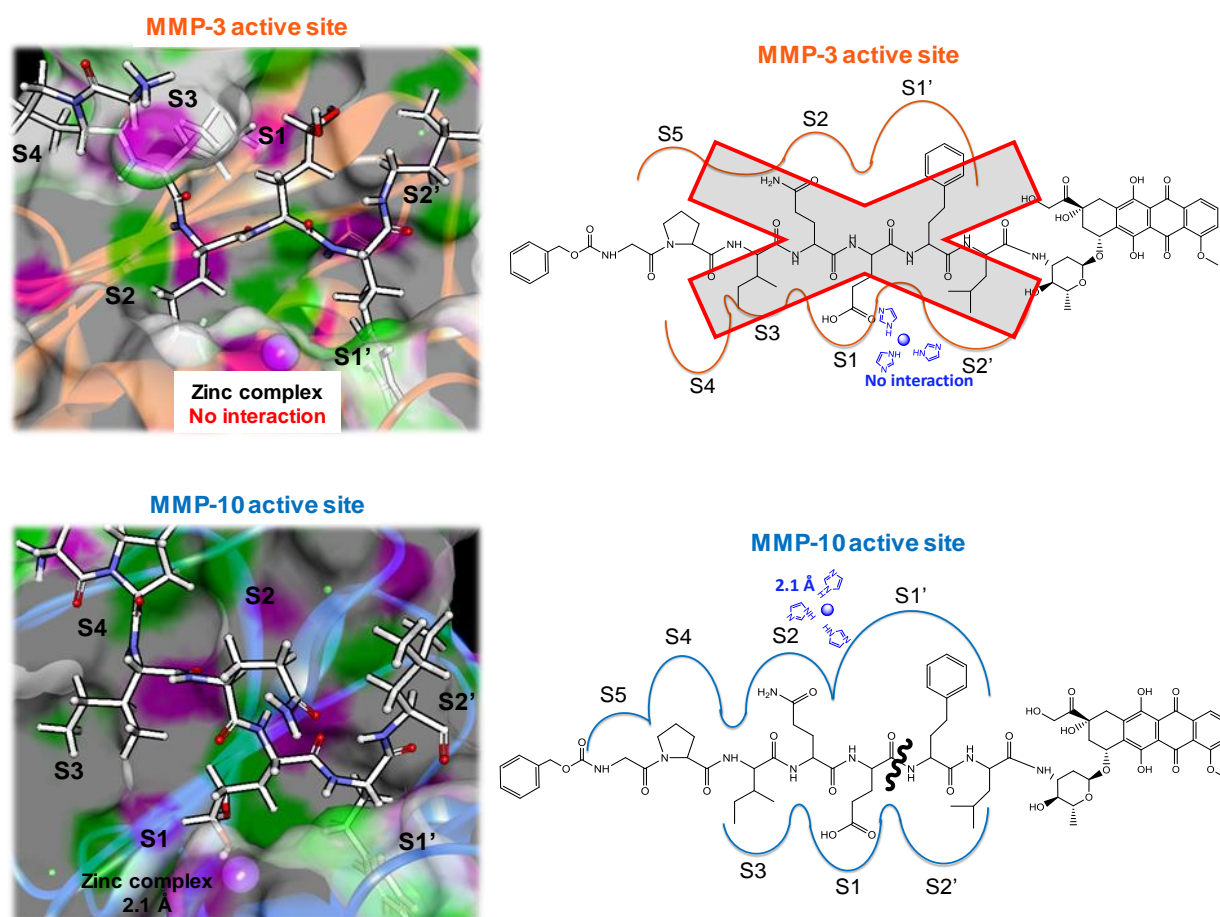
Figure IV.14: (Left) Stereo view of docked complexes of MJ02 (white sticks), catalytic domain of human MMP-3 (PDB ID: 1CIZ) (Orange) and MMP-10 (PDB ID: 1Q3A) (Blue). Catalytic and structural zinc ions are shown as purple spheres and active-site cleft residues (αβ-helix loop and the specificity loop) are shown as orange and blue. (Right) Schematic representation of MJ02: active site binding interaction in MMP-3 and MMP-10, are shown in orange and blue respectively. MJ02 chemical structure and its scissile bond is shown in black and zinc ion coordinated by histidine is indicated in blue.

IV.5.5 Development of MMP-subtype selective doxorubicin prodrug (MJ02)

To experimentally validate the *in silico* prediction that MJ02 is selectively interacted by MMP-2 and MMP-10, the prodrug was synthesised in-house in order to endcap the peptide sequence. The peptide sequence of MJ02 was nested between doxorubicin warhead and a Cbz (benzyloxycarbonyl) non-polar endcapping group, as described in materials and methods (Section IV.4.1). MJ02 was synthesised, containing the amino acids sequence Gly-Pro-Ile-Gln-Glu-Hof-Leu which has doxorubicin at the C-terminus of the peptide and Cbz group at the N-terminus (Figure IV.15).

Side-chain protected peptide sequence

Doxorubicin

Cbz - NH-Gly- Pro- Ile- Gln(Boc)- Glu(tBu)- Homophenylalanine- Leu-OH

+

A. Conjugation
Peptide:Doxorubicin (1:1 mol equiv) + HoBT (2.7 mol equiv)
+ PyBOP (1.35 mol equiv) + DIPEA (8 mol equiv);
dissolved in DMF (1 mL if 10 mg of peptide is reacted)

Stirred in dark overnight

Doxorubicin conjugated peptide with side chain protecting groups

Cbz - NH-Gly- Pro- Ile- Gln(Boc)- Glu(tBu)- Homophenylalanine- Leu-OH -Doxorubicin

B. Deprotection
Side-chain protecting groups were deprotected with
50% TFA in DCM; reaction stirred for 2 - 2.5 hours

minus Boc, tBu

C. Purification
Mobile phase A: 90:10 H_2O: MeCN
Mobile phase B: 40:60 H_2O: MeCN
And 0.1% HCO_2H

MJ02 Final product: Doxorubicin conjugated peptide

Cbz - NH-Gly- Pro- Ile- Gln- Glu- Homophenylalanine- Leu-OH -Doxorubicin

Chemical Formula: $C_{74}H_{93}N_9O_{23}$
Molecular Weight: 1476.6

Figure IV.15: Synthesis route of MMP targeted doxorubicin prodrug (MJ02)

IV.5.6 Analytical detection of MJ02

Using the LCMS methods described in section IV.4.4, MJ02 was detected by mass spectrometry as a confirmation of molecular mass. Preparative-HPLC gradient system (H₂O/MeCN) with a C18 column was used to purify MJ02, after side chain deprotection, at t_R 3.58 minutes ($^m/_z$ 1476.65 Da, [M]$^+$), to give a pale red solid (65% yield).
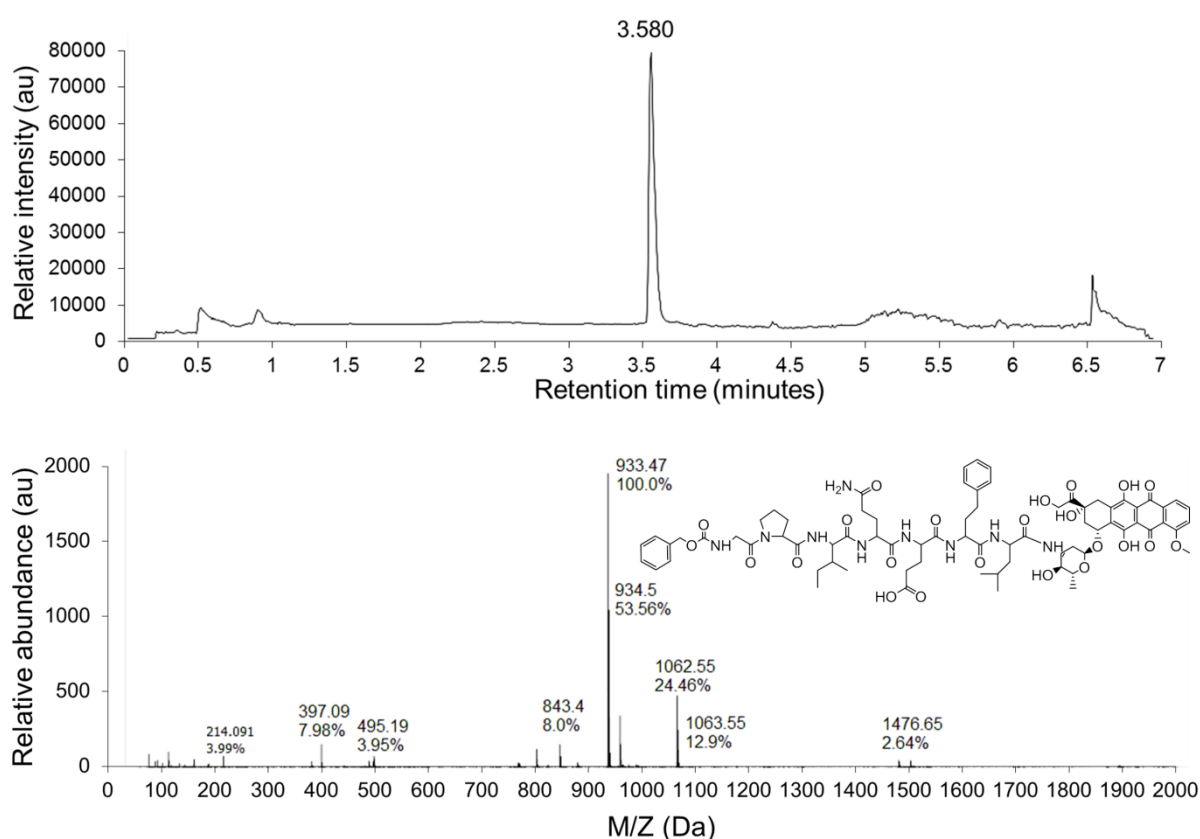
Figure IV.16: LCMS detection of purified MJ02. Preparative-HPLC purified MJ02 detection at t_R 3.580 minutes ($^m/_z$ 1476.6 Da, [M]$^+$).

IV.5.7   Analysis of MJ02 cleavage by recombinant MMP-2 and MMP-10

As the pan-MMP prodrug, Albright prodrug, demonstrated cleavage by both gelatinases and stromelysins, the hydrolysis of MJ02 by appropriate recombinant enzymes was investigated over a 12 h period and analysed by LCMS. From the predicted modelling earlier MJ02 should be more selectively cleaved by MMP-2 and MMP-10 over MMP-9 and MMP-3 relative to 'Albright prodrug' (Figures IV.11, IV.12, IV.13 and IV.14). Reverse phase LC-MS identified MJ02 at t_R 3.58 minutes ($^m/_z$ 1476.6 Da, [M]$^+$) (Figure IV.16), which was preferentially cleaved by MMP-2 at Hof-Leu to give Leu-Doxorubicin t_R 2.078 minutes ($^m/_z$ 657.2 Da, [M+H]$^+$) and Cbz-Gly-Pro-Ile-Gln-Glu-Hof t_R of 2.826 minutes ($^m/_z$ 821.4 Da, [M+H]$^+$) (Figures IV.17, IV.18, IV.19 and IV.20). MJ02 was also cleaved by MMP-10 at Glu-Hof bond to give Cbz-Gly-Pro-Ile-Gln-Glu t_R 2.621 minutes ($^m/_z$ 661.26 Da, [M+H]$^+$) and Hof-Leu-Doxorubicin t_R of 2.996 minutes ($^m/_z$ 816.66 Da, [M+H]$^+$) (Figures IV.21, IV.22, IV.23 and IV.24). Conversely MMP-9 and MMP-3 did not cleave MJ02 in the same timeframe, indicating that MJ02 is MMP-2 and MMP-10 selective, supporting the *in silico* prediction (Figure IV.25). Using M-2055 and M-2110, as control substrates to verify enzyme activity, MMP-9 and MMP-3 displayed no cleavage of MJ02 over 12 h period, whilst control substrates were efficiently cleaved (Figure II.13).

CBZ - Gly-Pro-Ile-Gln-Glu-Homophe-Leu - Doxorubicin

MMP-2
mediated cleavage

CBZ – Gly-Pro-Ile-Gln-Glu-Homophe

Leu - Doxorubicin
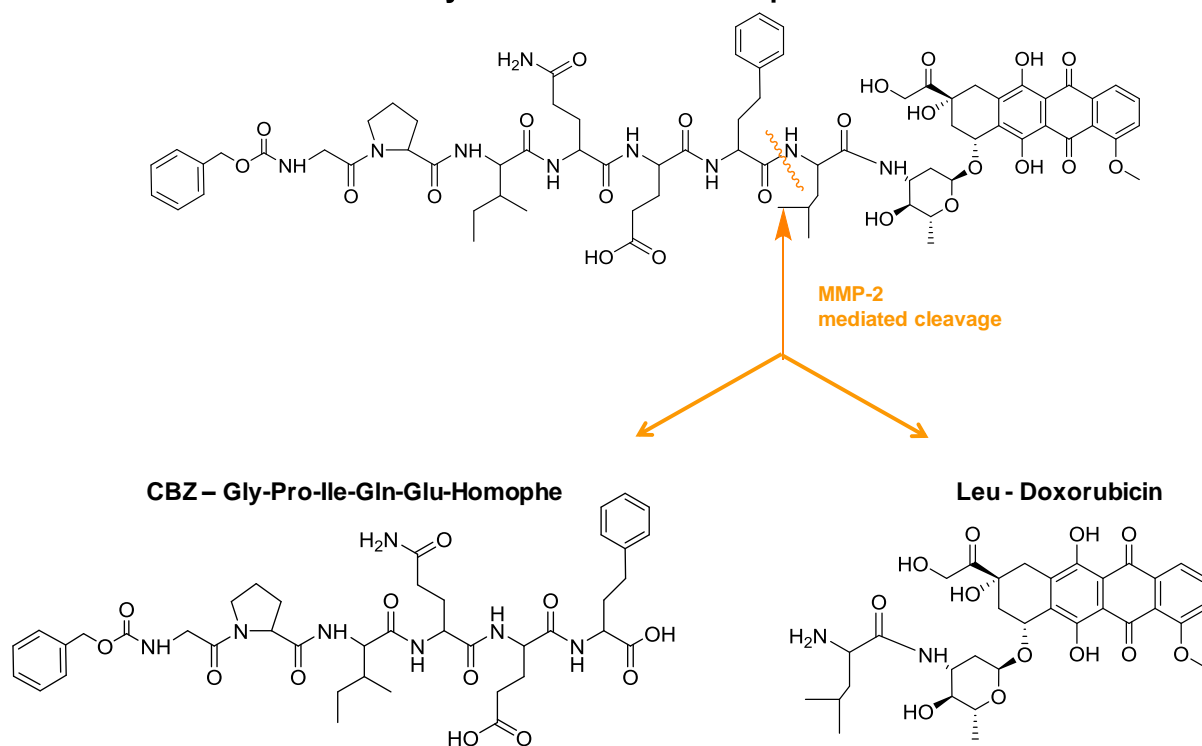
Figure IV.17: Schematic representation of the cleavage of MJ02 by recombinant MMP-2. Indicating cleavage of MJ02 at the Hof-Leu bond
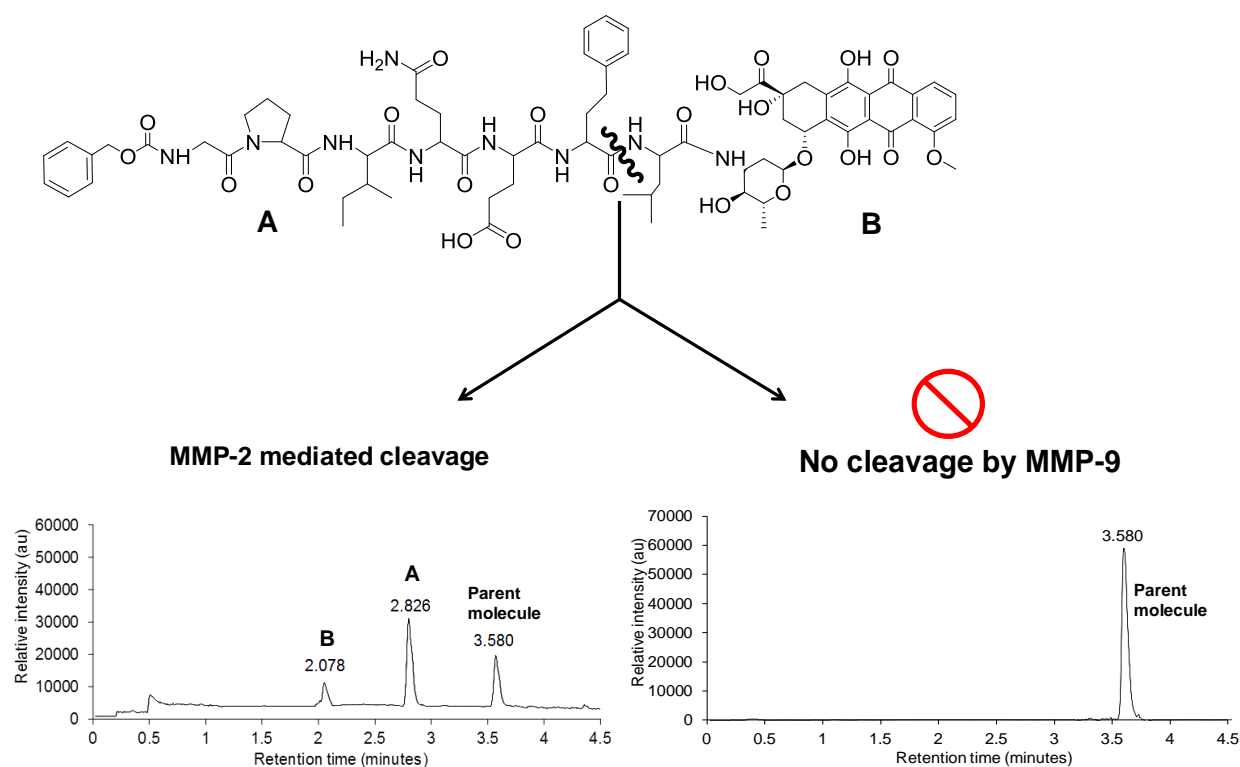
Figure IV.18: Schematic representation of the cleavage of MJ02 by MMP-2 but not by MMP-9, indicating MMP-2 mediated cleavage at the predicted subsite.
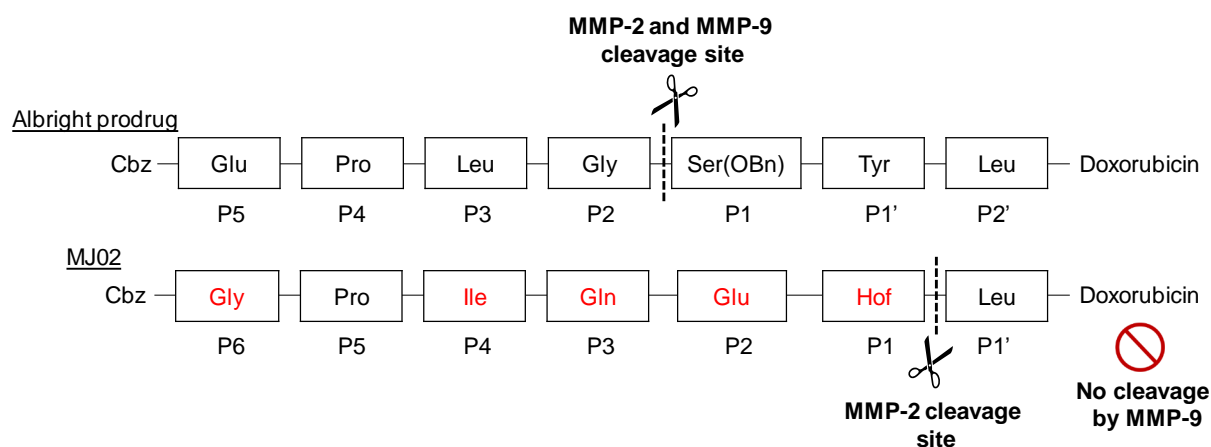
Figure IV.19: Representation of *in vitro* cleavage of MJ02 by MMP-2 over MMP-9
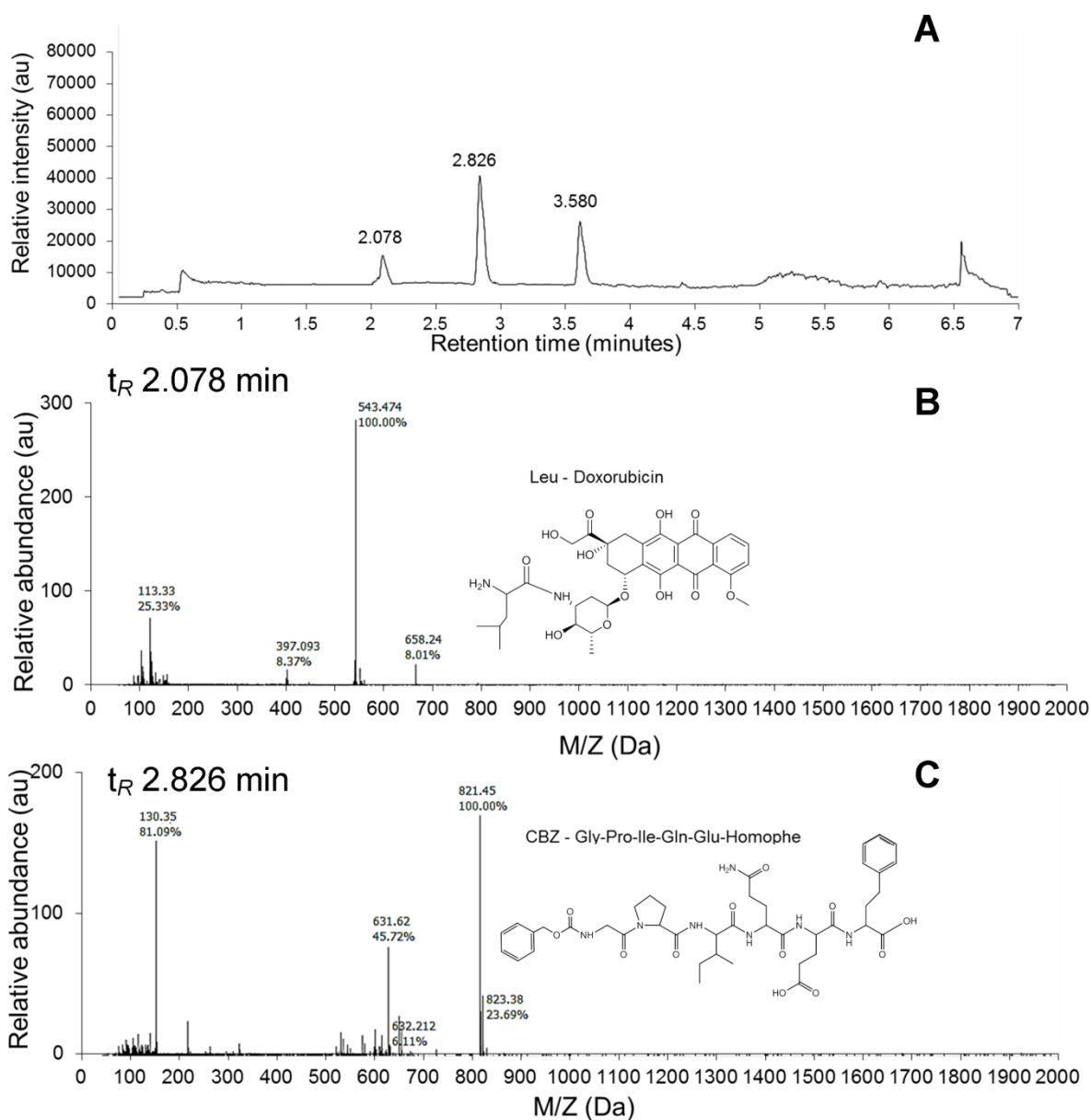
Figure IV.20: Cleavage of MJ02 by recombinant MMP-2, detected by LCMS: (A) LC of MMP-2 mediated cleaved metabolites, (t_R 2.078 and 2.826 minutes); (B) MS identification of doxorubicin half of the prodrug, t_R 2.078 minutes ($^m/_z$ 658.2 Da, [M+H]$^+$); (C) MS identification of Cbz half of the prodrug, t_R 2.826 minutes ($^m/_z$ 821.4 Da, [M+H]$^+$).

CBZ - Gly-Pro-Ile-Gln-Glu-Homophe-Leu - Doxorubicin

MMP-10 mediated cleavage

CBZ - Gly-Pro-Ile-Gln-Glu

Homophe-Leu - Doxorubicin
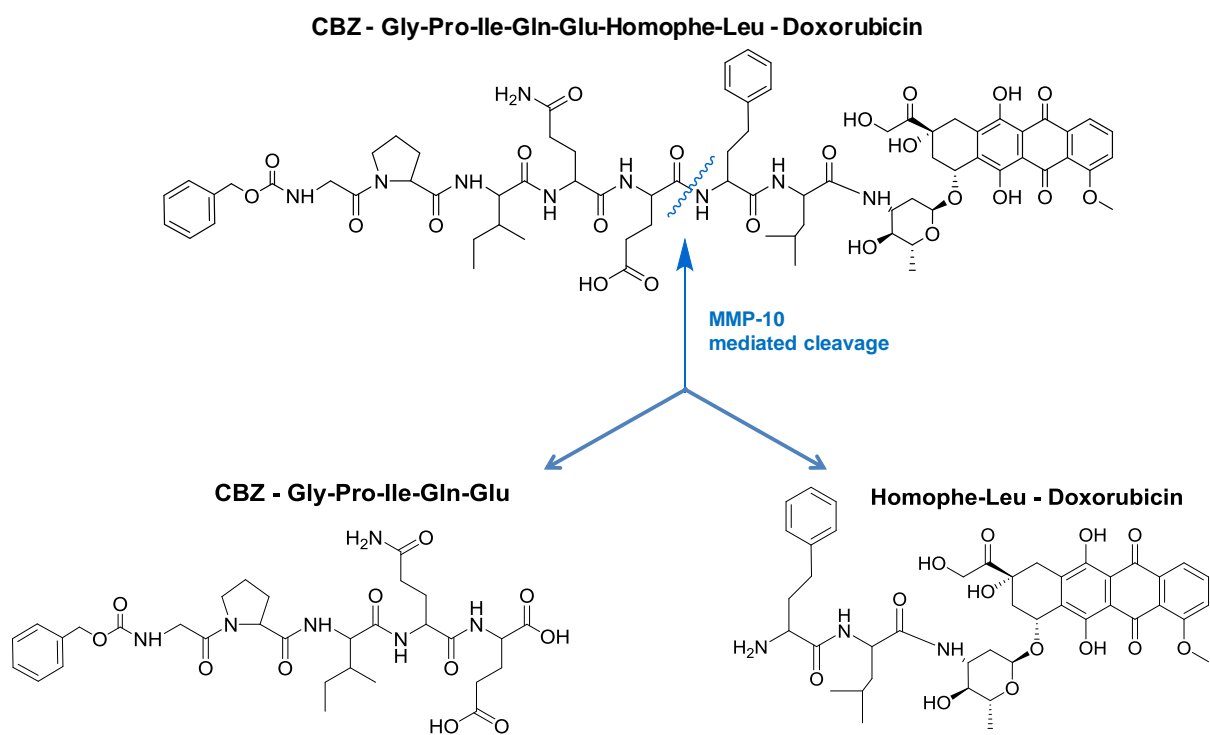
Figure IV.21: Schematic representation of the cleavage of MJ02 by recombinant MMP-10. Indicating cleavage of MJ02 at the Glu-Homophe bond
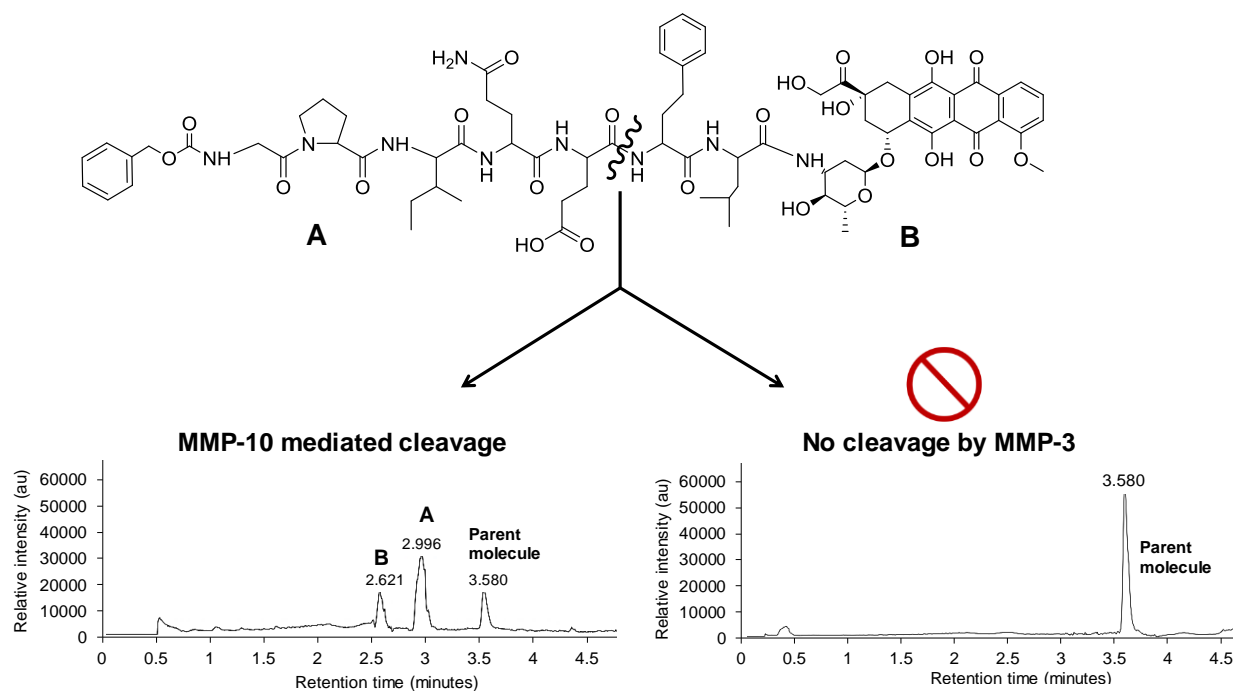
Figure IV.22: Schematic representation of the cleavage of MJ02 by MMP-10 but not by MMP-3, indicating MMP-10 mediated cleavage at the predicted subsite.
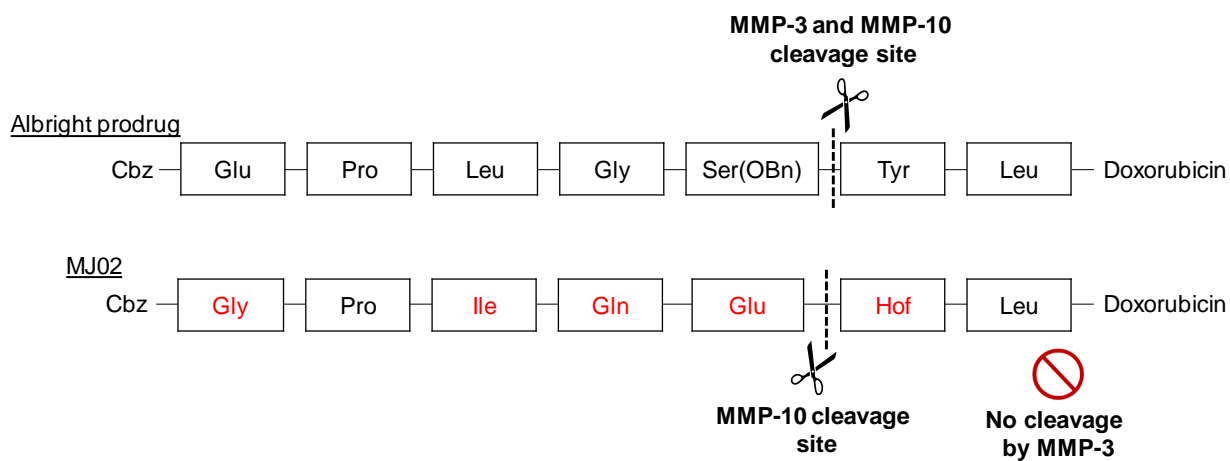
Figure IV.23: Representation of *in vitro* cleavage of MJ02 by MMP-10 over MMP-3
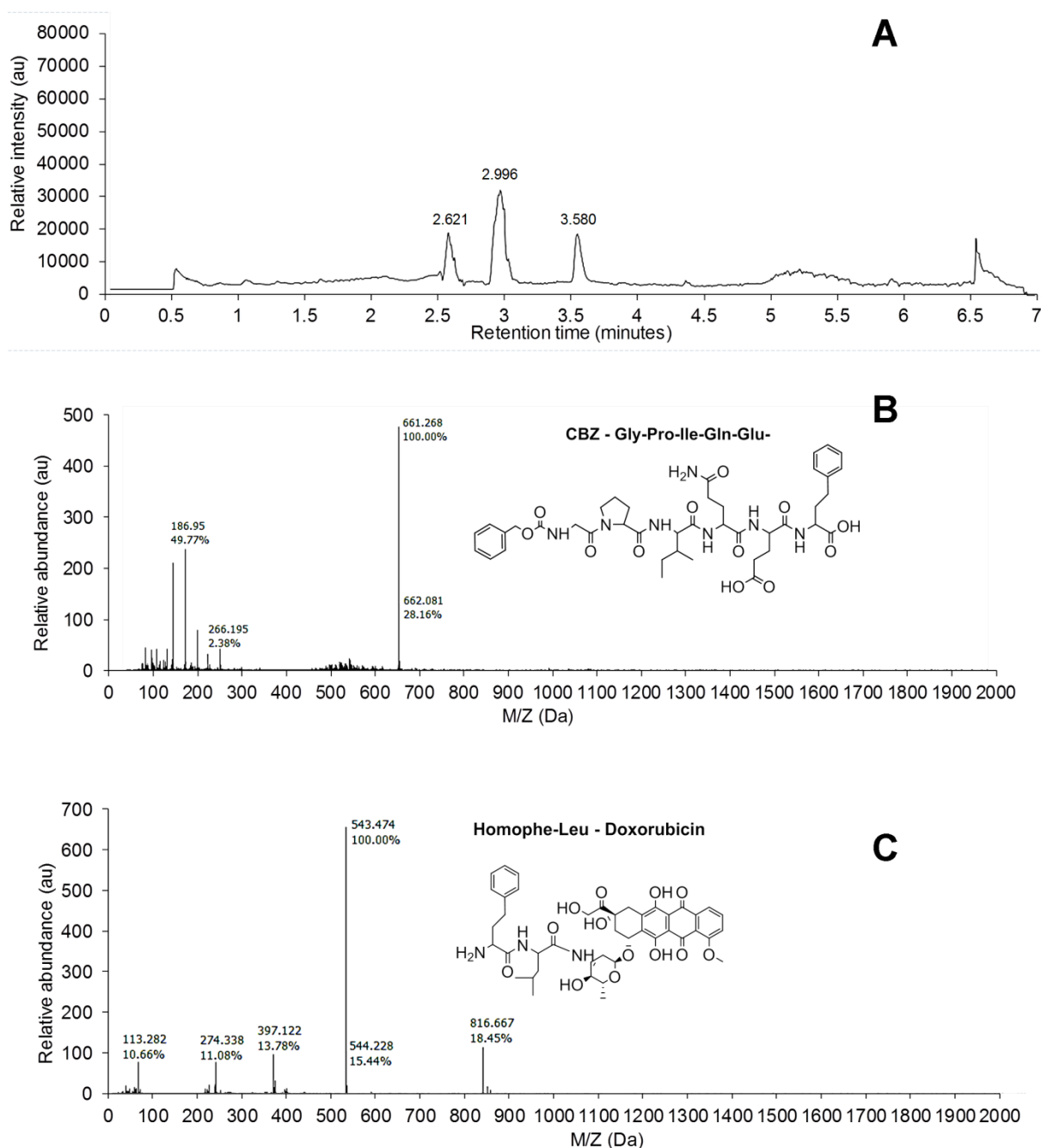
Figure IV.24: Determination of MMP-10 cleavage site in MJ02. Recombinant MMP-10 cleavage of MJ02 at the Glu-Homophe bond, as determined by LCMS analysis. **A,** HPLC trace of MJ02 metabolism following 12h incubation with recombinant MMP-10 at 37°C, showing MJ02 (t_R of 3.580 minutes) and cleaved metabolites, t_R 2.996 and 2.621 minutes; **B,** MS detection of metabolite as $^m/_z$ 661.2 Da [M+H]$^+$ corresponding to CBZ-Gly-Pro-Ile-Gln-Glu; **C,** MS detection of metabolite as $^m/_z$ 816.6 Da [M+H]$^+$corresponding to Homophe-Leu-Doxorubicin; confirming cleavage at the Glu-Homophe bond.
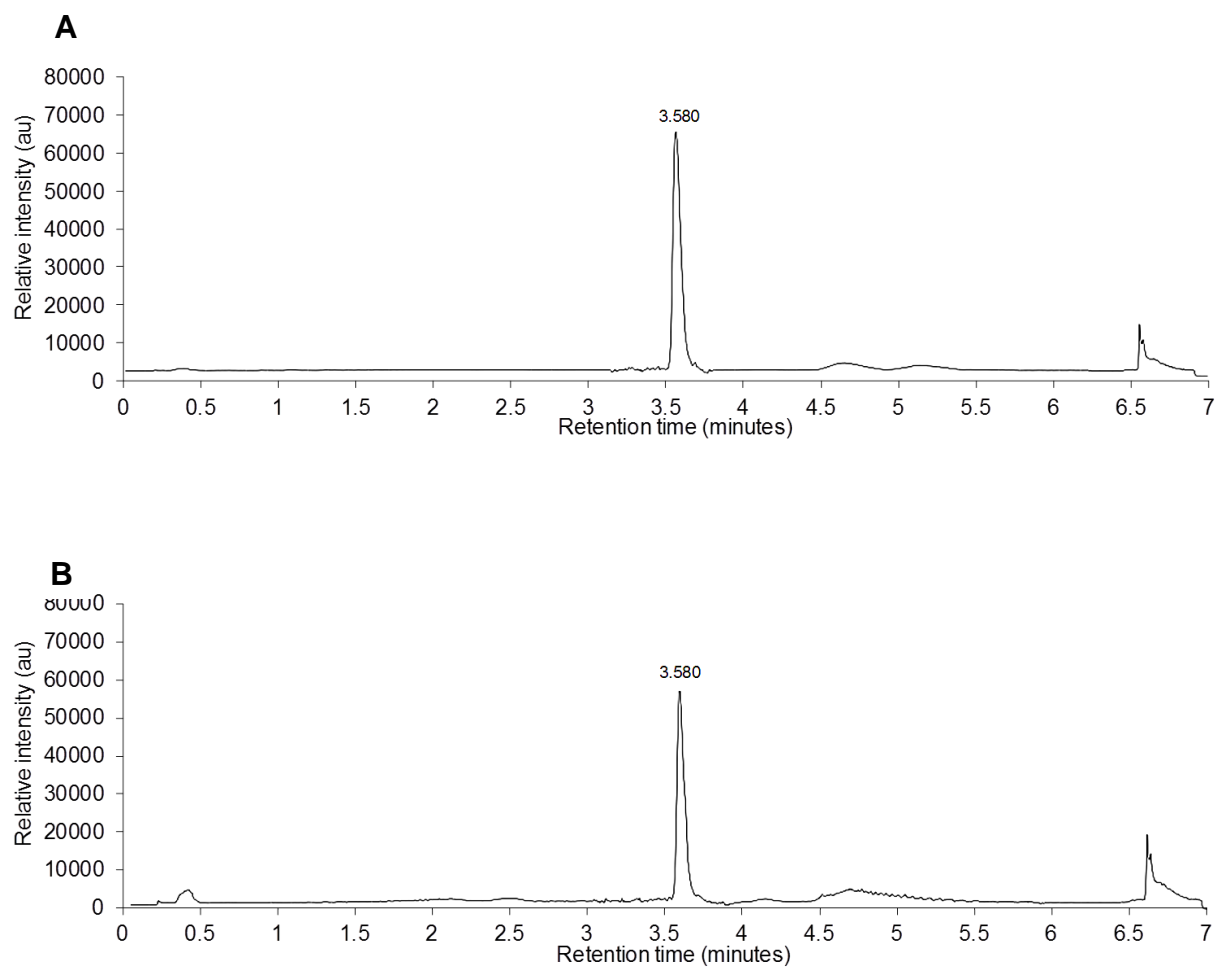
Figure IV.25: A and B represents HPLC traces of MMP-9 and MMP-3 mediated activity on MJ02, respectively. These graphs demonstrate that both MMP-9 and MMP-3 displayed no cleavage of MJ02 over 12 h incubation period. Whilst MJ02 was cleaved by MMP-10 and MMP-2, MMP-9&3 were unable to cleave this prodrug.

IV.5.8 Stability of MJ02 in MMP positive and MMP negative cell lines

Using semi-quantitative RT-PCR and western blotting (Figures II.3, II.4, II.6, II.7 and II.8), U87-MG was determined as a high MMP-10 expressing cell line and therefore was selected as a positive control for the metabolism of MJ02. SVG-P12 was selected as a negative control model since this cell line demonstrated low/negligible expression of MMP-10 (Figures II.3, II.4, II.6, II.7 and II.8). SVG-P12, despite being negative for MMP-10, does express MMP-2 (Figures II.3, II.4, II.6, II.7 and II.8). These cell lines grown in monolayer were assayed for their ability to metabolise MJ02 and were analysed after 24 h, 48 h and 96 h drug exposures, determined by LCMS. As Figure IV.26 demonstrates, MJ02 was rapidly metabolised by U87-MG ($t_{1/2}$ = 40 h) with a significantly slower metabolism observed by SVG-P12 ($t_{1/2}$ = 89 h). In both cell lines, the metabolism of MJ02 resulted in production of the chemotherapeutic agent, Leu-Dox. The involvement of MMPs was assessed by determining the degree of MJ02 metabolism by U87-MG cells in the presence of pan-MMP inhibitor Ilomastat (GM6001) and a MMP-10 selective inhibitor JJH-III-012A (developed by Dr Jonathan Harburn for a parallel project), at non-potent concentrations of 1 µM and 500 nM, respectively. Ilomastat resulted in a significant decrease in metabolism of MJ02 by U87-MG ($t_{1/2}$ = >96 h). In contrast, MJ02 displayed relatively faster metabolism in the presence of MMP-10 selective inhibitor ($t_{1/2}$ = 96 h) (inhibiting 50% of MMP-10 enzyme at 1 nM, based on fluorometric enzyme assay studies). It is interesting to note that there is a significant differential between metabolism by U87-MG alone and in the presence of MMP-10 inhibitor, suggesting the involvement of MMP-10 rapidly metabolising MJ02 in MMP-positive cells. Since MJ02 is selectively activated by both MMP-2 and MMP-10 (Figures IV.18, IV.20, IV.22 and IV.24), the differential metabolism of

MJ02 in the presence of MMP-10 inhibitor (compared to Ilomastat) could suggest a selective metabolism by MMP-2, which remains uninhibited at the treated dose (Figure IV.26).

IV.5.9 MJ02 stability in tumour tissue *ex vivo*

Following the demonstration of selective metabolism in human tumour cell lines, metabolism of MJ02 by HT1080 human tumour xenograft, mouse blood plasma and homogenised murine liver and kidney tissues was assessed. Rapid metabolism of MJ02 was observed in the MMP expressing HT1080 xenograft homogenate ($t_{1/2}$ = 9.8 minutes). In comparison, MJ02 was relatively stable in plasma ($t_{1/2}$ >> 90 minutes), murine liver ($t_{1/2} \geq$ 17 minutes) and murine kidney ($t_{1/2}$ = $\geq$ 38.1 minutes) (Figure IV.27). Metabolism of MJ02 in HT1080 homogenates resulted in rapid production of the chemotherapeutic agent, doxorubicin.

Differential metabolism of MJ02 by U87-MG and SVG-P12 cell lines

- U87-MG
- SVG-P12
- Media

t½ = > 96h

t½ = 89h

t½ = 40h

% MJ02 remaining

Time (hours)

Differential metabolism of MJ02 by U87-MG in the presence of Ilomastat (GM6001)

- U87-MG
- U87-MG + GM6001
- Media + GM6001

t½ = > 96h

t½ = > 96h

t½ = 40h

% MJ02 remaining

Time (hours)

Differential metabolism of MJ02 by U87-MG in the presence of MMP-10 selective inhibitor

- U87-MG
- U87-MG + MMP-10 inhibitor
- Media + MMP-10 inhibitor

t½ = > 96h

t½ = 96h

t½ = 40h

% MJ02 remaining

Time (hours)

Selectivity of MMP-10 inhibitor

MMPs	IC_{50} values
MMP-2	> 100 µM
MMP-9	> 100 µM
MMP-3	80 ± 10 nM
MMP-10	1 ± 0.8 nM

Figure IV.26: Differential metabolism of MJ02 by U87-MG (high MMP expressing) and SVG-P12 (low MMP expressing) cell lines. Cells in monolayer were assayed for their ability to metabolise MJ02 over 24 h, 48 h and 96 h time points, as detected by LCMS. Metabolism of MJ02 by cell lines representing 1 x 10^4 cells, demonstrated rapid metabolism by U87-MG relative to SVG-P12. In contrast, MJ02 demonstrated a decreased metabolism by U87-MG in the presence of pan-MMP inhibitor (Ilomastat, GM6001) and MMP-10 selective inhibitor. Metabolism values are representative of average from two independent experiments. Each value of inhibition study represents the mean ± SE of three independent experiments.
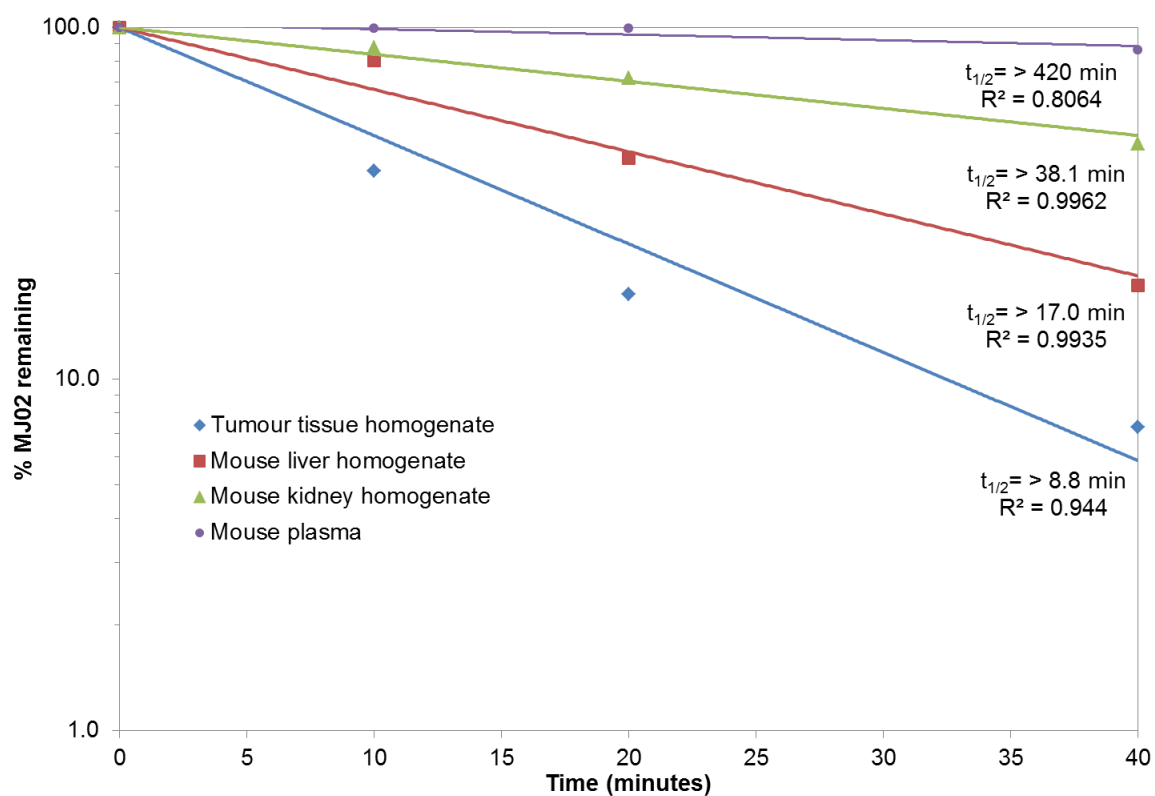
Figure IV.27: Metabolism of MJ02 by HT1080 tumour relative to mouse liver and mouse kidney. Metabolites expressed as concentration of MJ02 remaining.

IV.5.10 *In vitro* cytotoxicity of Doxorubicin and MJ02

The response of these human glioma cell lines (U87-MG and 1321N1) and normal glial (SVG-P12) cell line to Dox and MJ02 was investigated using the MTT assay. Responses of cell lines to Dox and MJ02 were analysed after 96 h exposures (Figure IV.28).

All the cell lines were sensitive to Dox following 96 h exposure, whereas, as predicted, malignant human glioma cells (U87-MG and 1321N1) expressing MMP-10, were able to metabolise the prodrug efficiently and, thus, has a significantly lower IC_{50} for MJ02 compared to SVG-P12 (MMP-10 negative) at 96 h exposures. The differential cytotoxicity between doxorubicin and MJ02 against glioma models supports the requirement of MJ02 to be activated prior to inducing its effects. Furthermore, MJ02 remained inactive in the presence of a pan-MMP inhibitor (GM6001; Ilomastat), demonstrating MMP-selective chemotherapeutic action of this prodrug. Whereas, in the presence of MMP-10 selective inhibitor, MJ02 demonstrated a 20-fold weaker cytotoxicity against U87-MG suggesting MMP-10 selective chemotherapeutic action of MJ02 (Figure IV.26).

Figure IV.28: Chemosensitivity of U87-MG, 1321N1 and SVG-P12 to Doxorubicin and MJ02. Assessed using MTT assay following 96 h drug exposure. Cell survival is represented as relative to solvent control and demonstrates sensitivity of U87-MG and 1321N1 cell lines to both Doxorubicin and MJ02 whilst SVG-P12 is sensitive only to Doxorubicin. Potency of compounds is reported as IC_{50} values (the concentration of drug required to reduce cell viability by 50% relative to control).

IV.5.11 Development of MMP-subtype selective azademethylcolchicine prodrug (MJ03)

The doxorubicin prodrug, MJ02, demonstrated selective activation by MMP-2 and MMP-10, over MMP-3 and MMP-9. The *in silico* docking system of MJ02 was rationalised based on the CHARMM minimised geometry of peptide sequence conjugated with doxorubicin. In order to identify whether the selectivity of peptide sequence would change in the presence of different chemotherapeutic drugs, we endeavoured to take advantage of a colchicine derivative, azademethylcolchicine, and its established antitumour activity.[203] The peptide sequence of MJ02 conjugated with a different warhead, azademethylcolchicine, was minimised *in silico* and docked into the active site of respective MMPs. MJ03, similar to MJ02, demonstrated strong and selective interaction with the active sites of MMP-2 and MMP-10 suggesting that the prodrug of azademethylcolchicine (derived from MJ02) should still provide selectivity for MMP-2 and MMP-10.

To experimentally validate the *in silico* prediction that MJ03 is selectively interacted by MMP-2 and MMP-10, over MMP-3 and MMP-9, the prodrug was synthesised in-house in order to endcap the peptide sequence. The peptide sequence of MJ03 was conjugated between azademethylcolchicine warhead (Section IV.4.2) and a Cbz non-polar endcapping group, as described in materials and methods (Section IV.4.1). MJ03 was synthesised, containing the amino acids sequence Gly-Pro-Ile-Gln-Glu-Hof-Leu which has azademethylcolchicine at the C-terminus of the peptide and Cbz group at the N-terminus (Figure IV.29).

Side-chain protected peptide sequence

Azademethylcolchicine

Cbz - NH-Gly- Pro- Ile- Gln(Boc)- Glu(tBu)- Homophenylalanine- Leu-OH

+

A. Conjugation
Peptide:Azademethylcolchicine (1:1 mol equiv) +
HoBT (2.7 mol equiv) + PyBOP (1.35 mol equiv)
+ DIPEA (8 mol equiv); dissolved in DMF
(1 mL if 10 mg of peptide is reacted)

Stirred in dark overnight

Azademethylcolchicine conjugated peptide with side chain protecting groups

Cbz - NH-Gly- Pro- Ile- Gln(Boc)- Glu(tBu)- Homophenylalanine- Leu-OH -Azademethylcolchicine

B. Deprotection
Side-chain protecting groups were deprotected with
50% TFA in DCM; reaction stirred for 2 - 2.5 hours

minus Boc, tBu

C. Purification
Mobile phase A: 90:10 H_2O: MeCN
Mobile phase B: 40:60 H_2O: MeCN
And 0.1% HCO_2H

MJ03 Final product: Azademethylcolchicine conjugated peptide

Cbz - NH-Gly- Pro- Ile- Gln- Glu- Homophenylalanine- Leu-OH -Azademethylcolchicine

Chemical Formula: $C_{68}H_{88}N_{10}O_{17}$
Molecular Weight: 1317.5

Figure IV.29: Synthesis route of MMP-targeted Azademethylcolchicine prodrug (MJ03)

200

IV.5.12   Analytical detection of MJ03

Using the LCMS methods described in section IV.4.4, MJ03 was detected by mass spectrometry as a confirmation of molecular mass. Preparative-HPLC (reverse phase) used to purify MJ03, t_R 3.68 minutes ($^m/_z$ 1317.6 Da, $[M]^+$) (Figure IV.30), to give a pale yellow solid (55% yield).
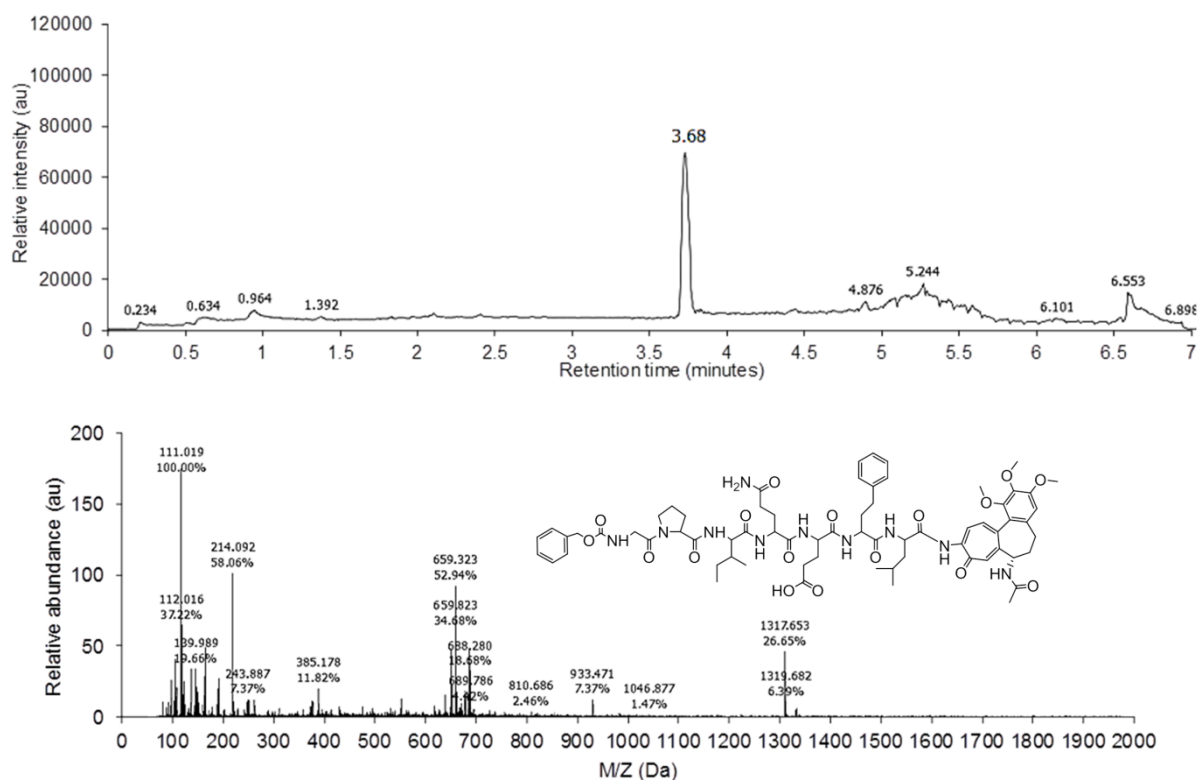
Figure IV.30: LCMS detection of purified MJ03. Preparative-HPLC system was used to purify MJ03 t_R 3.68 minutes ($^m/_z$ 1317.6 Da, $[M]^+$).

CBZ - Gly-Pro-Ile-Gln-Glu-Homophe-Leu - MB2

MMP-2
mediated cleavage

CBZ - Gly-Pro-Ile-Gln-Glu-Homophe-

Leu – MB2
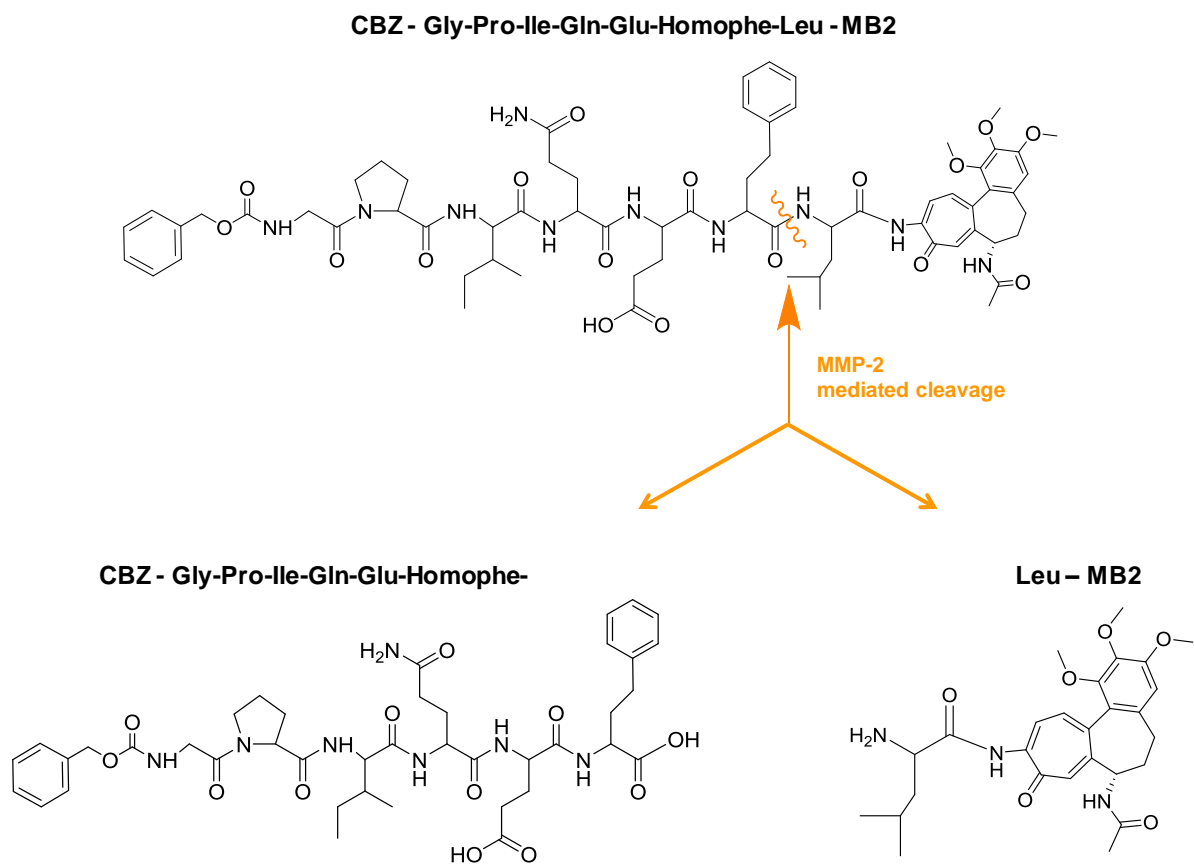
Figure IV.31: Schematic representation of the cleavage of MJ03 by recombinant MMP-2. Indicating cleavage of MJ03 at the Homophe-Leu bond
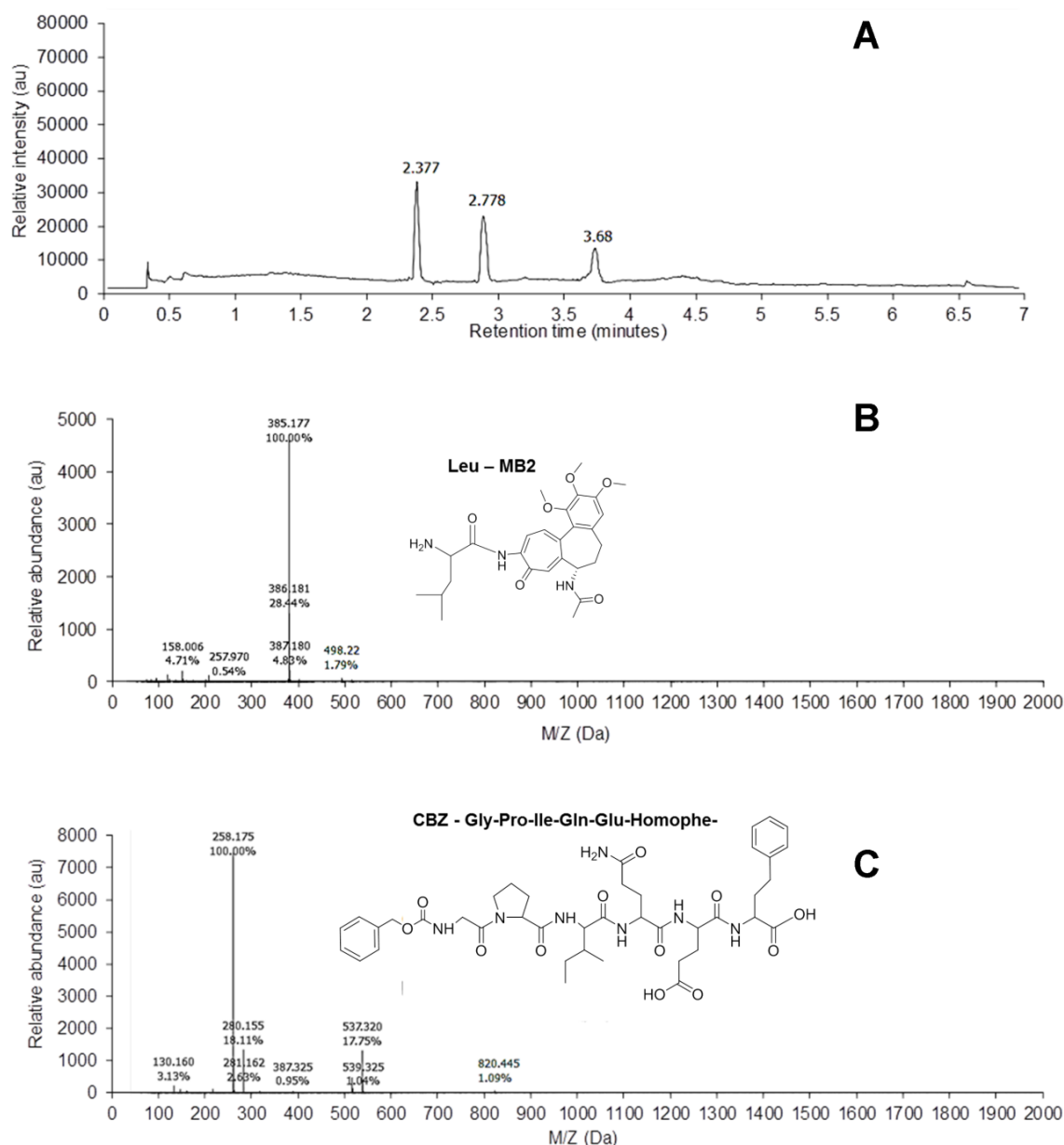
Figure IV.32: Determination of MMP-2 cleavage site in MJ03. Recombinant MMP-2 cleavage of MJ03 at the Homophe-Leu bond, as determined by LCMS analysis. **A,** HPLC trace of MJ03 metabolism following 12 h incubation with recombinant MMP-2 at 37°C, showing MJ03 (t_R of 3.68 minutes) and cleaved metabolites, t_R 2.377 and 2.778 minutes; **B,** MS detection of metabolite as $^m/_z$ 498.22 Da [M]$^+$ corresponding to Leu-MB2; **C,** MS detection of metabolite as $^m/_z$ 820.4 Da [M]$^+$ corresponding to CBZ-Gly-Pro-Ile-Gln-Glu-Homophe; confirming cleavage at the Homophe-Leu bond.

CBZ - Gly-Pro-Ile-Gln-Glu-Homophe-Leu - MB2

MMP-10 mediated cleavage

CBZ - Gly-Pro-Ile-Gln-Glu

Homophe-Leu - MB2
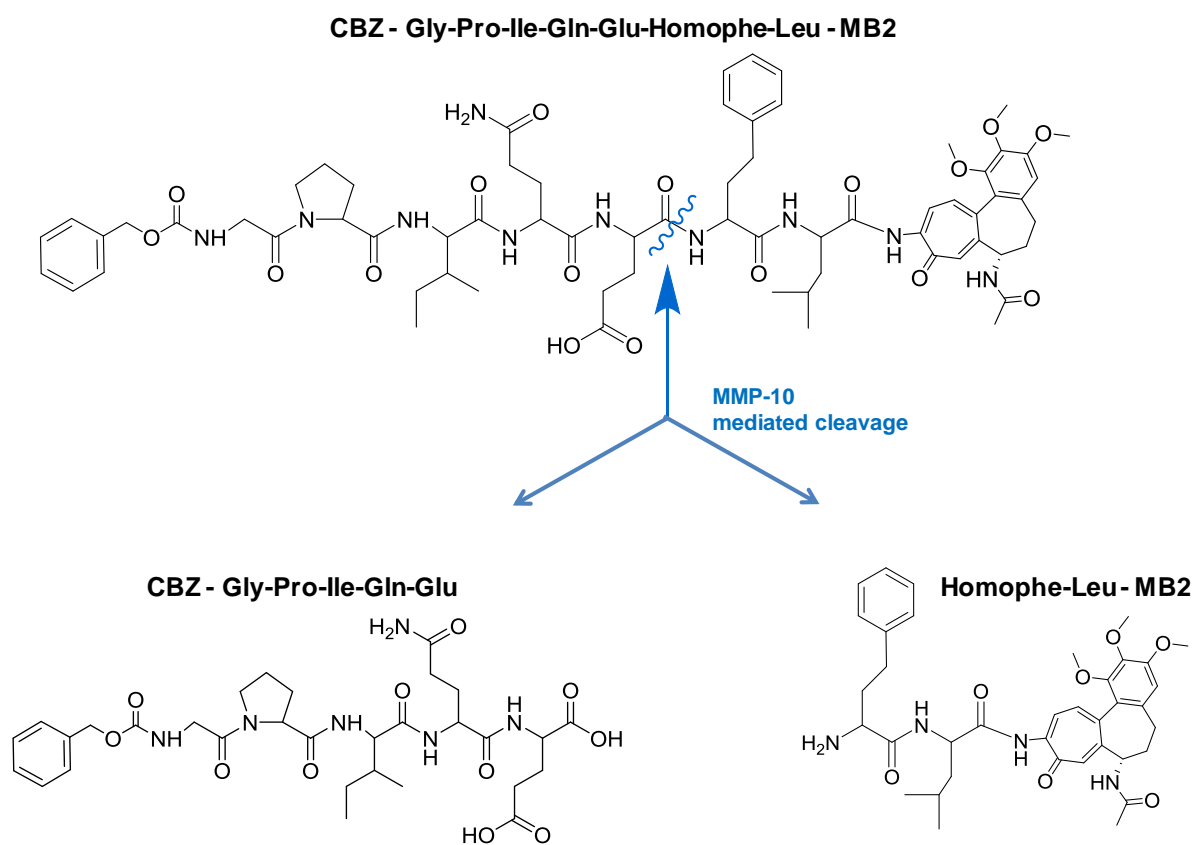
Figure IV.33: Schematic representation of the cleavage of MJ03 by recombinant MMP-10. Indicating cleavage of MJ03 at the Glu-Homophe bond
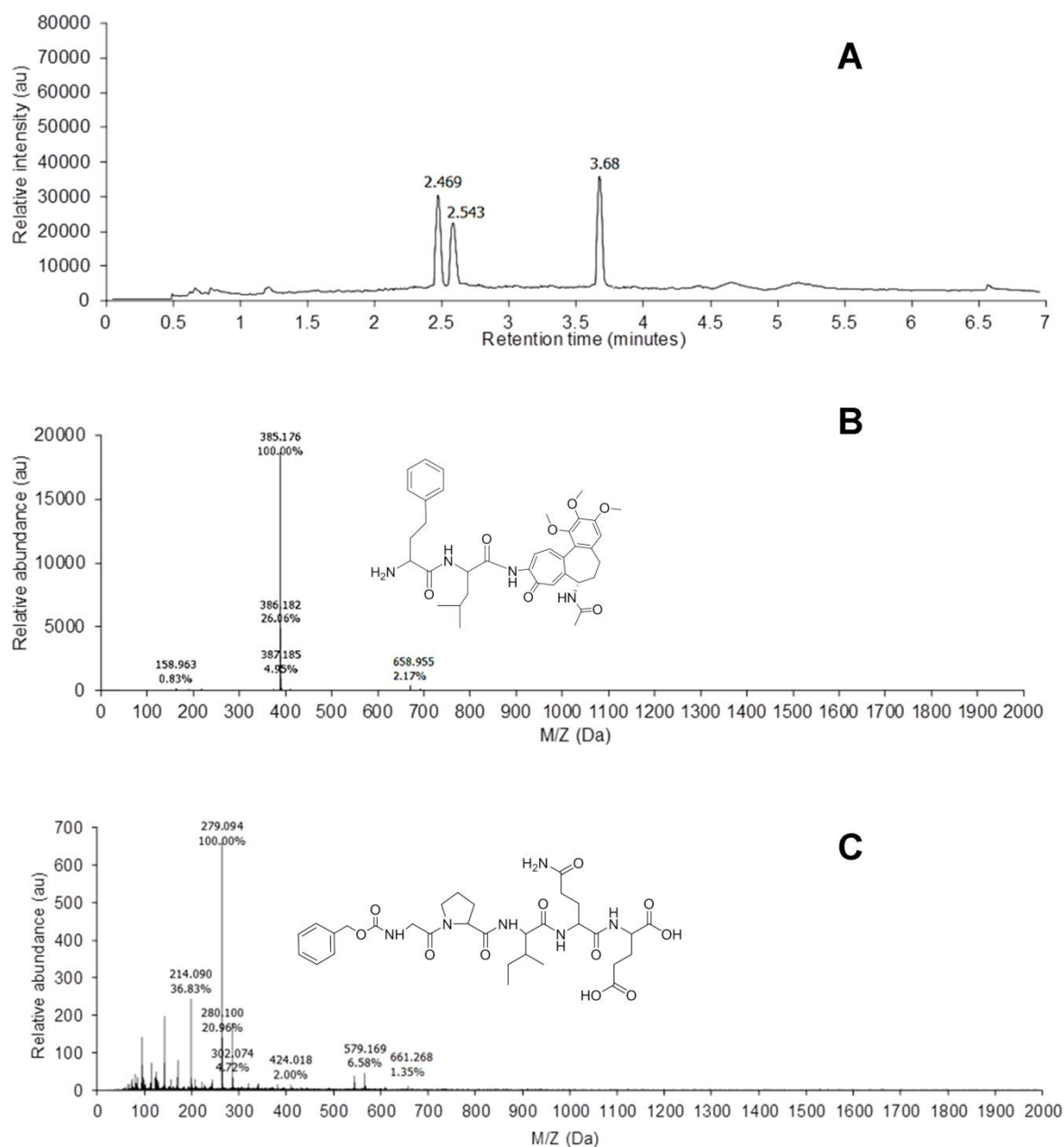
Figure IV.34: Determination of MMP-10 cleavage site in MJ03. Recombinant MMP-10 cleavage of MJ03 at the Glu-Homophe bond, as determined by LCMS analysis. **A,** HPLC trace of MJ03 metabolism following 12 h incubation with recombinant MMP-10 at 37°C, showing MJ03 t_R 3.68 minutes and cleaved metabolites, Rt 2.469 and 2.543 minutes; **B,** t_R 2.469 minutes, MS detection of metabolite ($^m/_z$ 658.9 Da, [M]$^+$) corresponding to Homophe-Leu-MB2; **C,** t_R 2.543 minutes, MS detection of metabolite ($^m/_z$ 661.2 Da, [M]$^+$) corresponding to CBZ-Gly-Pro-Ile-Gln-Glu; confirming cleavage at the Glu-Homophe bond.
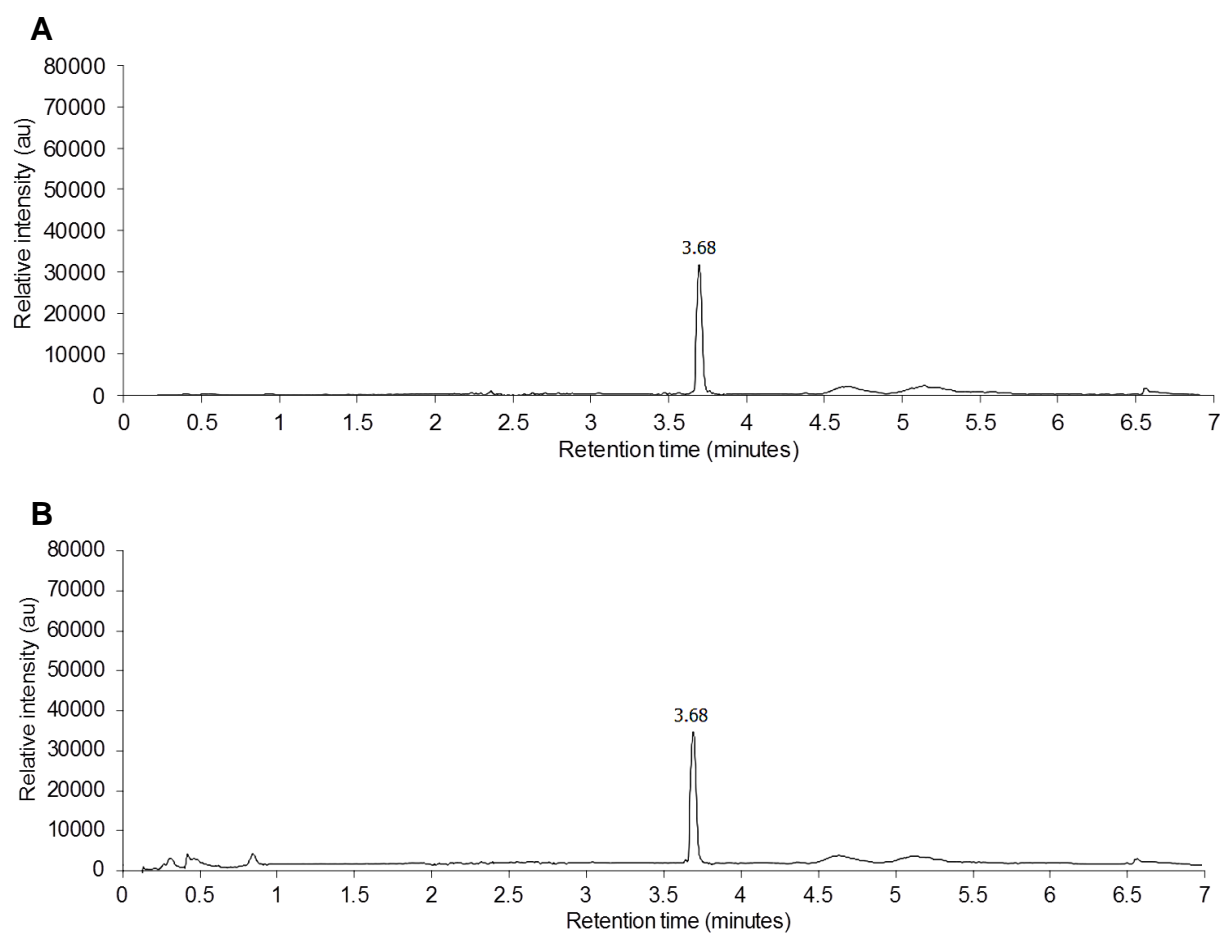
Figure IV.35: A and B represents HPLC traces of MMP-9 and MMP-3 mediated activity on MJ03, respectively. These graphs demonstrate that both MMP-9 and MMP-3 displayed no cleavage of MJ02 over 12 h incubation period.

IV.5.13 Stability of MJ03 in MMP positive and MMP negative cell lines

Similar to the stability studies of MJ02 (Section IV.5.7), the selectivity of MJ03 was also tested in the two cell models i.e. U87-MG (MMP-positive) and SVG-P12 (MMP-negative) cells. These cell lines grown in monolayer were assayed for their ability to metabolise MJ03 and were analysed after 24 h, 48 h and 96 h drug exposures, determined by LCMS. As Figure IV.36 demonstrates, MJ03 was rapidly metabolised by U87-MG (t½ = 38 h) with a significantly slower metabolism observed by SVG-P12 (t½ = 86 h). In both cell lines, the metabolism of MJ03 resulted in production of the chemotherapeutic agent, azademethylcolchicine. The involvement of MMPs was assessed by determining the degree of MJ03 metabolism by U87-MG cells in the presence of pan-MMP inhibitor Ilomastat (GM6001) and the MMP-10 selective inhibitor JJH-III-012A (developed by Dr Jonathan Harburn for a parallel project), at non-potent concentrations of 1 µM and 500 nM, respectively. Ilomastat resulted in a significant decrease in metabolism of MJ03 by U87-MG (t½ = >96 h). In contrast, MJ03 displayed relatively faster metabolism in the presence of MMP-10 selective inhibitor (t½ = 71 h) (inhibiting 50% of MMP-10 enzyme at 1nM). It is interesting to note that there is a significant differential between the metabolism by U87-MG alone and the one in the presence of MMP-10 inhibitor, suggesting the involvement of MMP-10 enzyme to rapidly metabolise MJ03 in MMP-positive cells. Since MJ03 is selectively activated by both MMP-2 and MMP-10 (Figures IV.32 and IV.34), the differential metabolism of MJ03 in the presence of MMP-10 inhibitor (compared to Ilomastat) could suggest a selective metabolism by MMP-2 (Figure IV.36), which remains uninhibited at the treated dose.
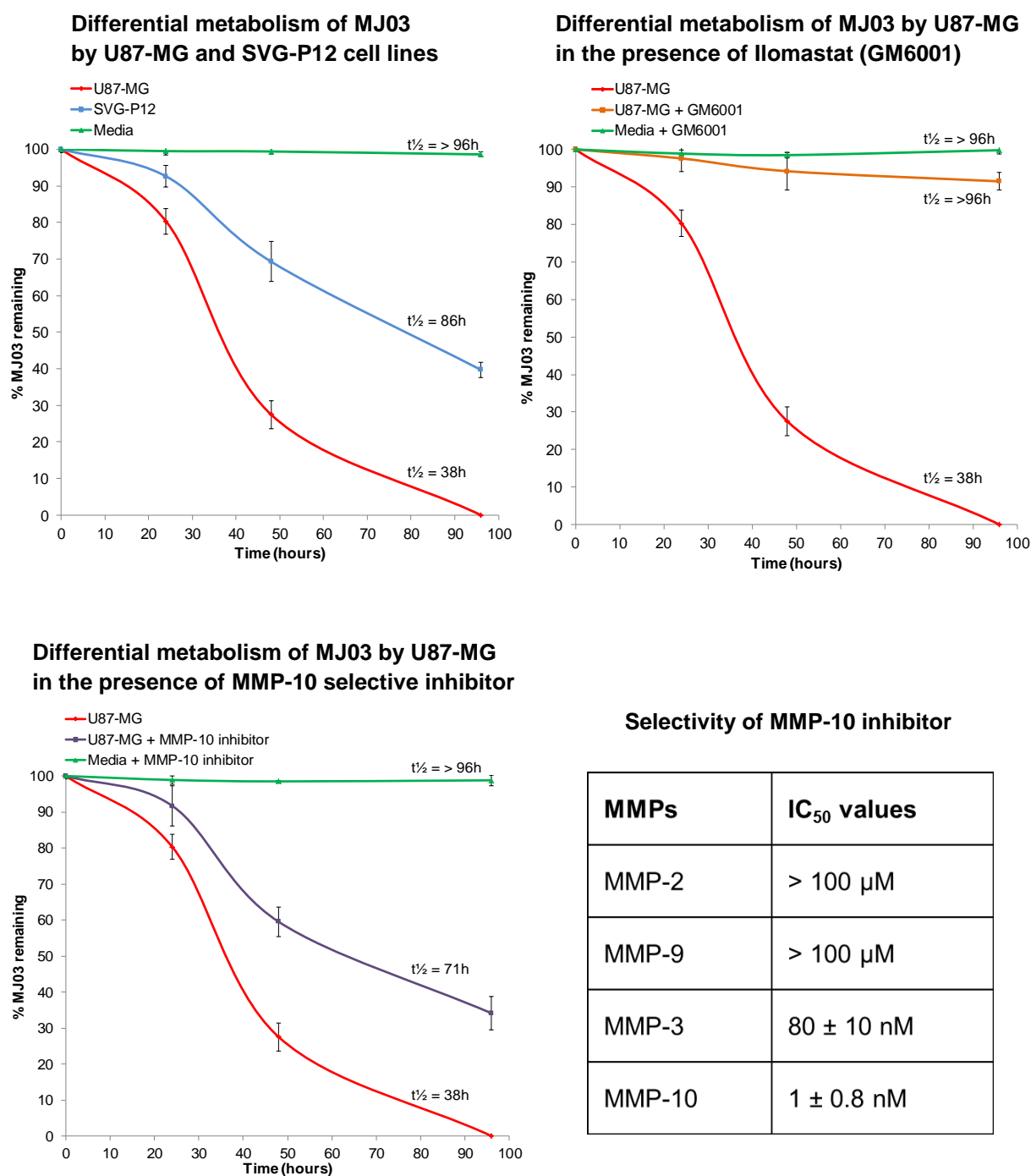
Figure IV.36: Differential metabolism of MJ03 by U87-MG (high MMP expressing) and SVG-P12 (low MMP expressing) cell lines. Cells in monolayer were assayed for their ability to metabolise MJ03 over 24 h, 48 h and 96 h time points, as detected by LCMS. Metabolism of MJ03 by cell lines representing 1×10^4 cells, demonstrated rapid metabolism by U87-MG relative to SVG-P12. In contrast, MJ03 demonstrated a decreased metabolism by U87-MG in the presence of pan-MMP inhibitor (Ilomastat, GM6001) and MMP-10 selective inhibitor (JJH-III-012A). Metabolism values are representative of average from two independent experiments. Each value of inhibition study represents the mean ± SE of three independent experiments.

IV.5.14   *In vitro* cytotoxicity of Azademethylcolchicine and MJ03

The response of these human glioma (U87-MG and 1321N1) and normal glial (SVG-P12) cell lines to azademethylcolchicine and MJ03 was investigated using the MTT assay. Responses of the cell lines to azademethylcolchicine and MJ03 were analysed after 96 h exposures (Figure IV.37).

All the cell lines were sensitive to azademethylcolchicine following 96 hexposure, whereas, as predicted, malignant human glioma cells (U87-MG and 1321N1) expressing MMP-10, were able to metabolise the prodrug efficiently and thus has a significantly lower IC_{50} for MJ03 compared to SVG-P12 (MMP-10 negative) at 96 h exposures. The differential cytotoxicity between azademethylcolchicine and MJ03 against glioma models supports the requirement of MJ03 to be activated prior to inducing its effects. Furthermore, MJ03 remained inactive in the presence of a pan-MMP inhibitor (GM6001; Ilomastat), demonstrating MMP-selective chemotherapeutic action of this prodrug (Figure IV.37). Whereas, in the presence of MMP-10 selective inhibitor (Figure IV.37), MJ03 demonstrated a 30-fold weaker cytotoxicity against U87-MG suggesting MMP-10 selective chemotherapeutic action of MJ03.
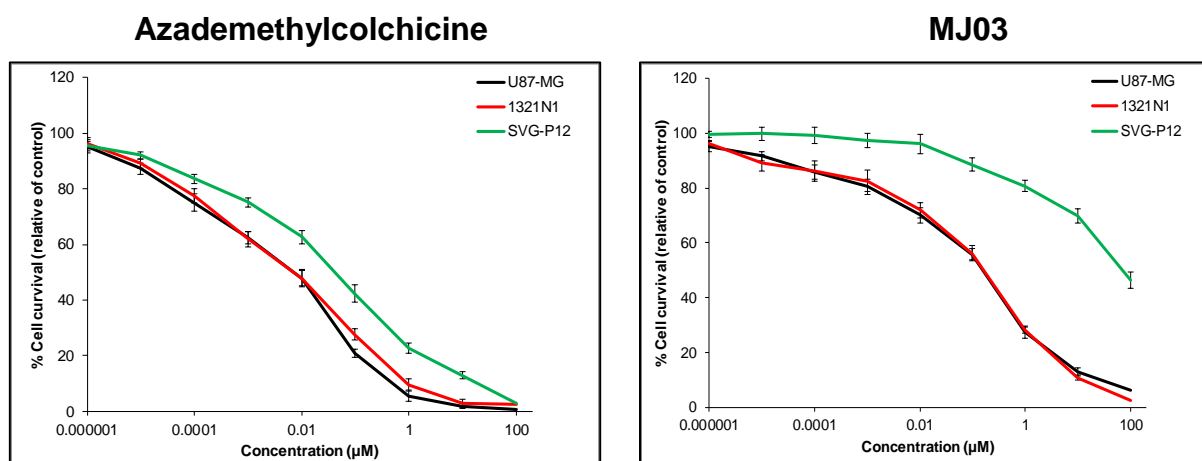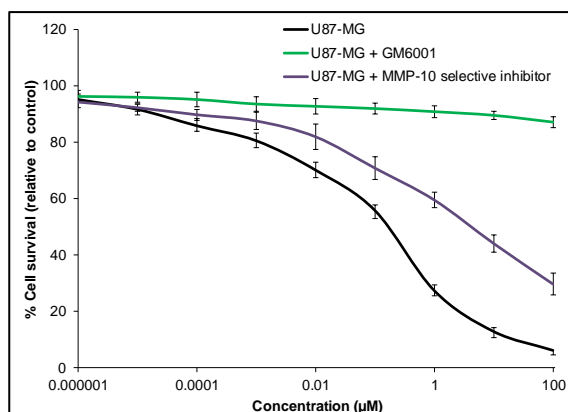
Azademethylcolchicine

MJ03

MJ03 in the presence of MMP inhibitors

IC$_{50}$ value of compounds

	Compound	U87-MG IC$_{50}$ (µM)	1321N1 IC$_{50}$ (µM)	SVG-P12 IC$_{50}$ (µM)
96 hours	Azademethyl -colchicine	0.01 ± 0.005	0.01 ± 0.007	0.05 ± 0.025
	MJ03	0.25 ± 0.1	0.3 ± 0.25	80 ± 5.2

Compound	U87-MG IC$_{50}$ (µM)
MJ03	0.25 ± 0.1
MJ03 + GM6001	> 100
MJ03 + JJH-III-012A	8 ± 1.3

Figure IV.37: Chemosensitivity of U87-MG, 1321N1 and SVG-P12 to MB2 and MJ03.
Assessed using MTT assay following 96 h drug exposure. Cell survival is represented as relative to solvent control and demonstrates sensitivity of U87-MG and 1321N1 cell lines to both MB2 and MJ03 whilst SVG-P12 is sensitive only to MB2. Potency of compounds is reported as IC$_{50}$ values (the concentration of drug required to reduce cell viability by 50% relative to control).

IV.5.15 Rationalised design of MMP-10 selective peptide conjugates (MJ04)

Following the success of *in silico* model for rationalised development of MMP-subtype selective prodrugs of doxorubicin (MJ02) and azademethylcolchicine (MJ03), we further attempted to modify the peptide sequence in an effort to make the prodrugs more specific for MMP-10, and to eliminate or reduce metabolism by its close family homologues i.e. MMP-3 and gelatinases. MJ04 was designed based on the MMP-docked models of M-2110 substrate.[221] M-2110 substrate is a stromelysin-selective substrate and has been shown to be rapidly cleaved by both MMP-3 and MMP-10. The *in silico* models of M-2110 substrate (Chapter 3; Figures III.15 and III.18) demonstrated effective catalytic binding with the active sites of MMP-3 and MMP-10, and thus provided a suitable model to rationally exploit the differences in stromelysin binding sites. MJ04 sequence consisted of the following modifications: branched non-polar residues in S2 subsite; basic residues in S1' subsite and branched non-polar residues in S2' subsite (Figure IV.38).
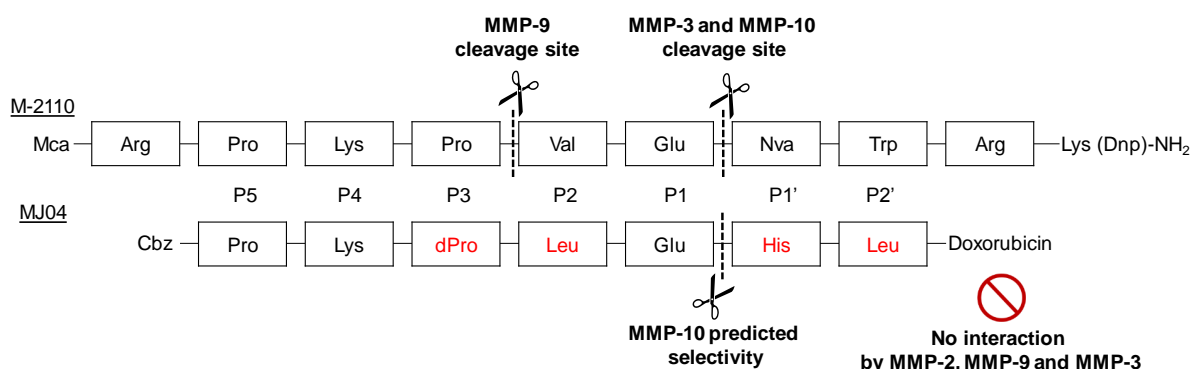
Figure IV.38: Modification of M-2110 peptide residues to achieve MMP-10 selectivity over MMP-3 and gelatinases, indicating predicted selectivity of MMP-10 at Glu-His bond

IV.5.16 Flexible-ligand docking of MJ04 and MMPs

The *in silico* interaction between MJ04 peptide sequence and MMP-10 demonstrated the strong chelation of zinc ion with the carboxylate between Glu-His bond (1.5 Å), indicating the predicted cleavage site (Figure IV.39). The zinc interaction here is stronger than the MJ02 and MMP-10 docked complex (2.1 Å, section IV.5.3). The ligand interactions with the binding residues of MMP-10 were similar to the interactions observed with MJ02 (Section IV.5.3). The Glu at P1 position is strongly coordinated by Ala181 and His182 of the bulge-edge segment (1.4 Å). The Leu inserted into the S2 pocket is able to interact with Leu180 residue and the D-Pro at P3 position is strongly coordinated by Ala183 in MMP-10 (2.1 Å). The side-chain of His is inserted into the S1' pocket; and is further interacted by Glu218 (2.0 Å), wall-forming segments (2.2 Å to 2.4 Å) and the hydrophobic cluster of Phe and Leu at the bottom of the pocket (1.8 Å). The docked complex of MJ04 and MMP-10 has an overall binding energy of 1012 kcal/mol (Figure IV.39).

However, the docked complexes of MMP-2, MMP-3 and MMP-9 demonstrated weak catalytic interaction with MJ04. The zinc interactions were not detectable and the predicted binding energies of MJ04 were -212 kcal/mol, -77 kcal/mol and -176 kcal/mol, with MMP-2, MMP-9 and MMP-3, respectively. The prediction model of MJ04 and MMPs suggests that the peptide residues should give selectivity for MMP-10 over MMP-3 and gelatinases (Figure IV.40).
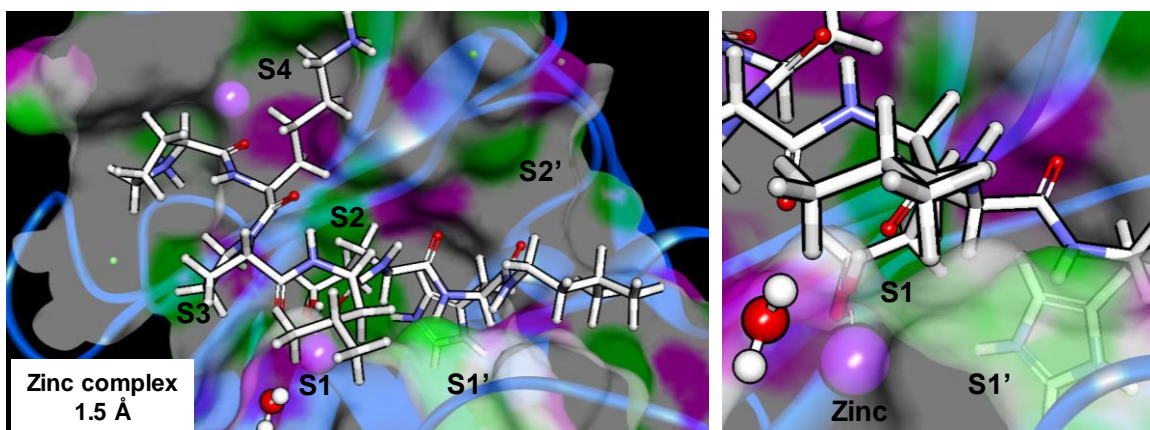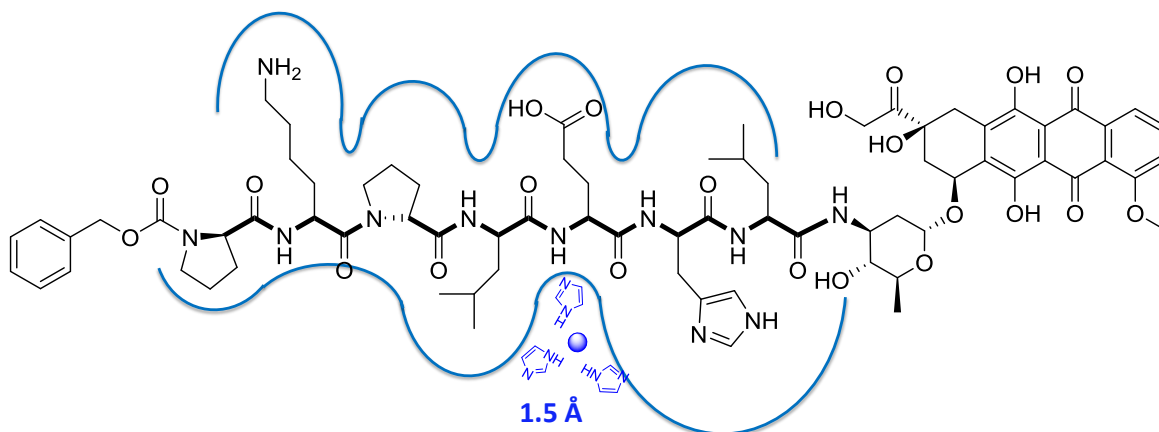
Figure IV.39: (Above) Stereo view of docked complexes of MJ04 (white sticks) and catalytic domain of human MMP-10 (PDB ID: 1Q3A) (Blue). Catalytic and structural zinc ions are shown as purple spheres and active-site cleft residues (αβ-helix loop and the specificity loop) are shown as blue. (Below) Schematic representation of MJ04: active site binding interaction in MMP-10, are shown in blue, respectively. MJ04 chemical structure and its scissile bond is shown in black and zinc ion coordinated by histidine is indicated in blue.
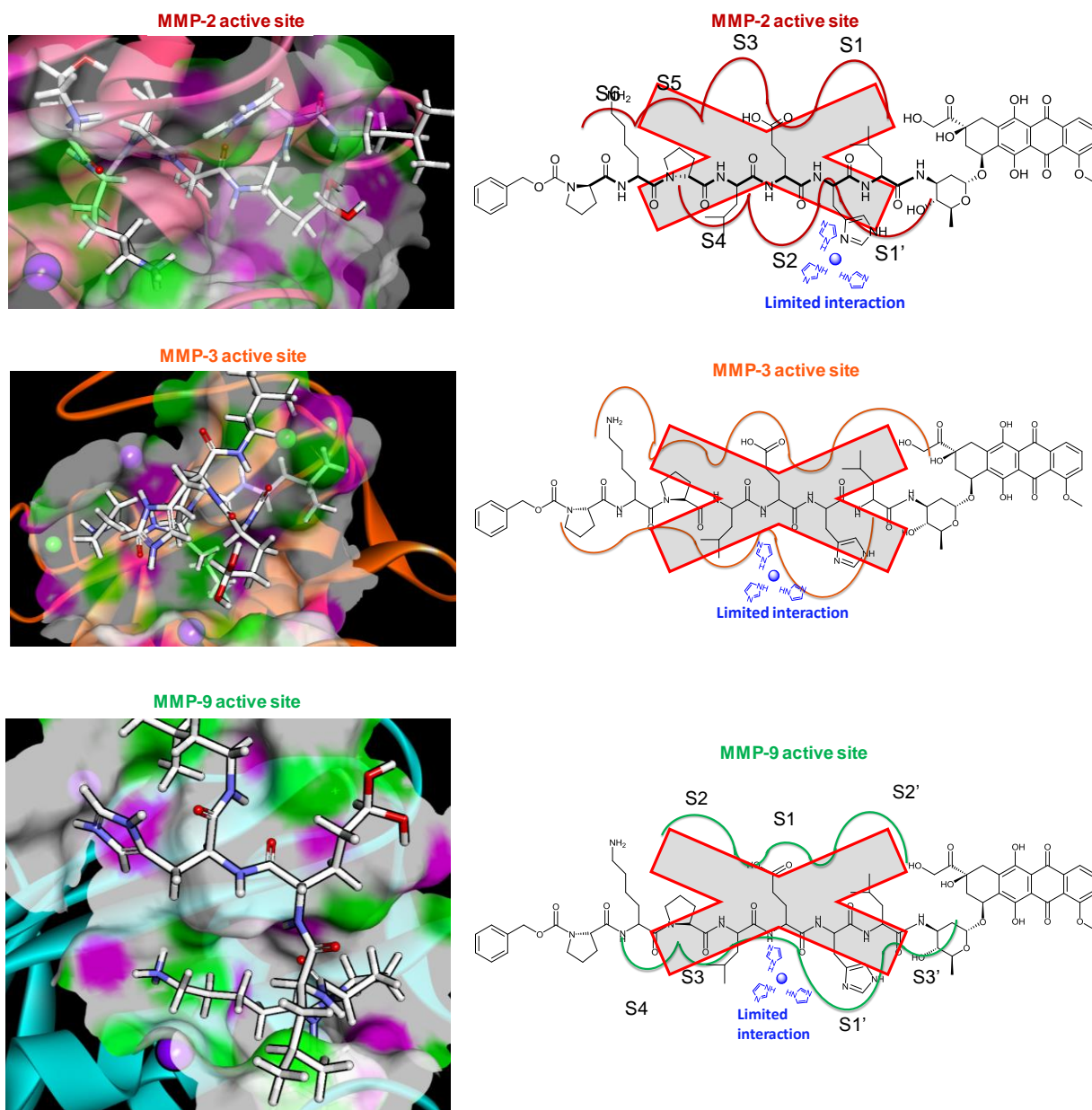
Figure IV.40: (Left) Stereo view of docked complexes of MJ04 (white sticks) within catalytic domain of human MMP-2 (PDB ID: 1QIB) (Pink), MMP-3 (PDB ID: 1CIZ) (Orange), MMP-9 (PDB ID: 1GKC) (Cyan). (Right) Schematic representation of MJ04 and its active site binding interactions in MMP-2, MMP-3 and MMP-9. MJ04 demonstrates negligible chemical interaction with MMP-3 and gelatinases (MMP-2 and MMP-9), relative to strong interaction with MMP-10

IV.5.17 Development of MMP-subtype selective doxorubicin prodrug (MJ04)

To experimentally validate the *in silico* prediction that MJ04 is selectively interacted by MMP-10, the prodrug was synthesised in-house in order to endcap the peptide sequence. The peptide sequence of MJ04 was conjugated between doxorubicin warhead and a Cbz (benzyloxycarbonyl) non-polar endcapping group, as described in materials and methods (Section IV.4.1). MJ04 was synthesised, containing the amino acids sequence Pro-Lys-DPro-Leu-Glu-His-Leu which has doxorubicin at the C-terminus of the peptide and Cbz group at the N-terminus (Section IV.4.1).

IV.5.18 Analytical detection of MJ04

Using the LCMS methods described in section IV.4.4, MJ04 (Figure IV.41) was detected by mass spectrometry as a confirmation of molecular mass. Preparative-HPLC gradient system (H_2O/MeCN) with a C18 column was used to purify MJ04 at retention time (tR) of 4.10 minutes ($^m/_z$ 1491.7 Da, $[M]^+$) (Figure IV.42), to give a pale red solid (60% yield).
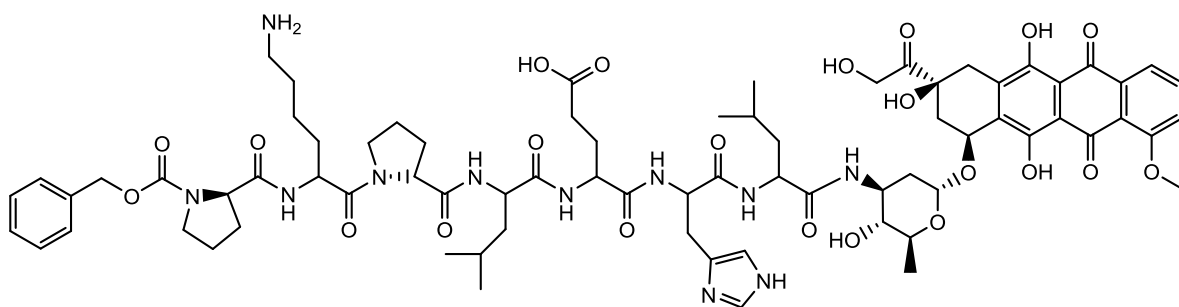
Chemical Formula: $C_{74}H_{97}N_{11}O_{22}$
Molecular Weight: 1492.6

Figure IV.41: Chemical structure of MMP-10 targeted doxorubicin prodrug.
Sequence: Cbz – Pro-Lys- D-Pro -Leu-Glu-His-Leu – Doxorubicin
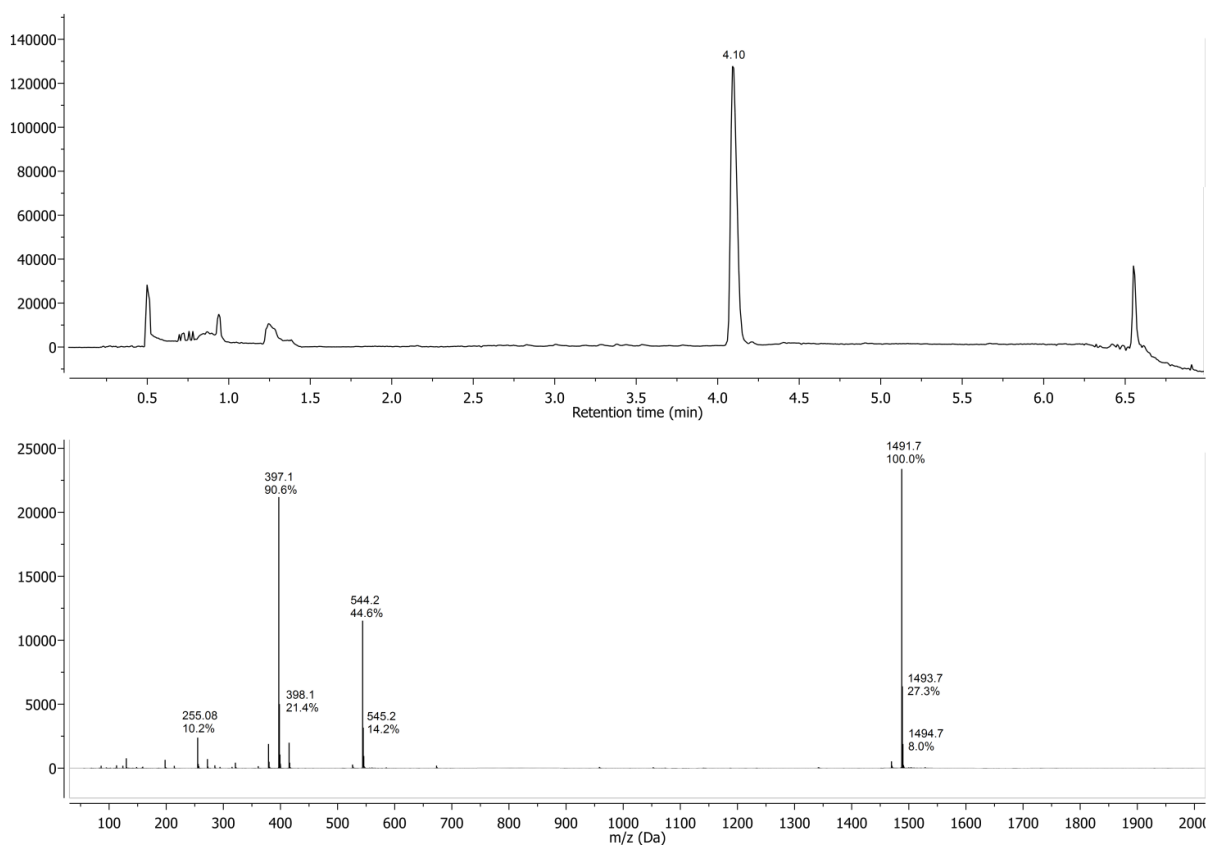
Figure IV.42: LCMS detection of purified MJ04. Preparative-HPLC purified MJ04 detection at t_R 4.10 minutes ($^m/_z$ 1491.7 Da, $[M]^+$).

IV.5.19 Analysis of MJ04 cleavage by recombinant MMP-10

Rationalised computational-aided development of MJ02 (prodrug of doxorubicin) and MJ03 (prodrug of azademethylcolchicine) prodrugs demonstrated cleavage by both MMP-2 and MMP-10, over MMP-3 and MMP-9. It was predicted *in silico* that by rationalised alteration of M-2110 substrate amino acid sequence, MJ04 should be more selectively cleaved by MMP-10 over its close family homologue MMP-3 and gelatinases; relative to 'Albright prodrug', MJ02 and MJ03. To experimentally validate the predictability of the *in silico* model, and confirm the *in vitro* cleavage position of MJ04, hydrolysis of the prodrug by appropriate recombinant MMPs were investigated over a 12 h period and analysed by LCMS. As figures IV.43 and IV.44 show, MMP-10 cleaved MJ04 at the Glu-His bond, as predicted. Reverse phase HPLC identified MJ04 at t_R 4.10 minutes (Figure IV.42). MJ04 was preferentially cleaved by MMP-10 at the Glu-His bond and two peaks identified; corresponding to Cbz-Pro-Lys-DPro-Leu-Glu at t_R 2.85 minutes ($^m/_z$ 716.4 Da, [M+H]$^+$) and Cbz-Gly-Pro-Ile-Gln-Glu-Hof at t_R 3.07 minutes ($^m/_z$ 793.3 Da, [M+H]$^+$) (Figure IV.44). Conversely MMP-2, MMP-3 and MMP-9 did not cleave MJ04 in the same timeframe, indicating that MJ04 is MMP-10 selective, thus, supporting the *in silico* prediction (Figure IV.45).

CBZ – Pro-Lys-ᴅPro-Leu-Glu-His-Leu-Doxorubicin

MMP-10 mediated cleavage

CBZ – Pro-Lys-ᴅPro-Leu-Glu-

His-Leu - Doxorubicin
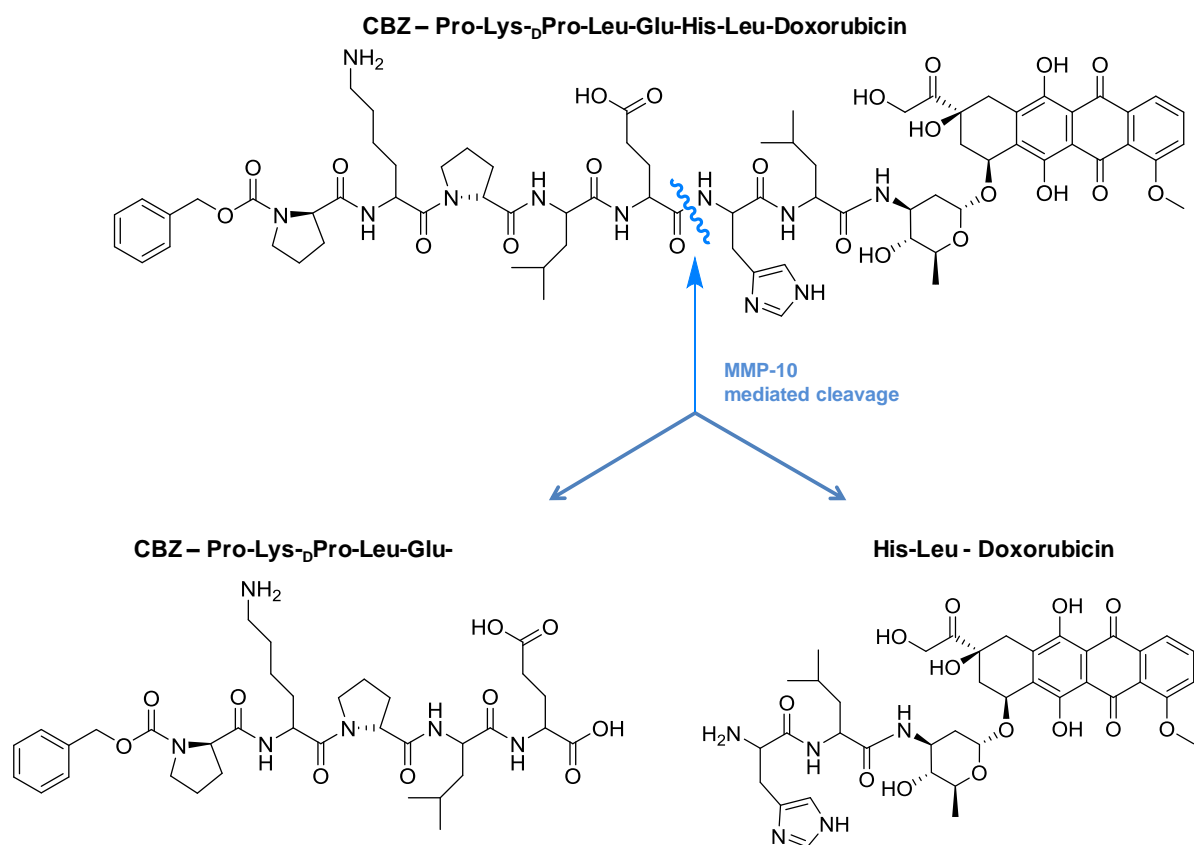
Figure IV.43: Schematic representation of the cleavage of MJ04 by recombinant MMP-10. Indicating cleavage of MJ04 at the Glu-His bond.
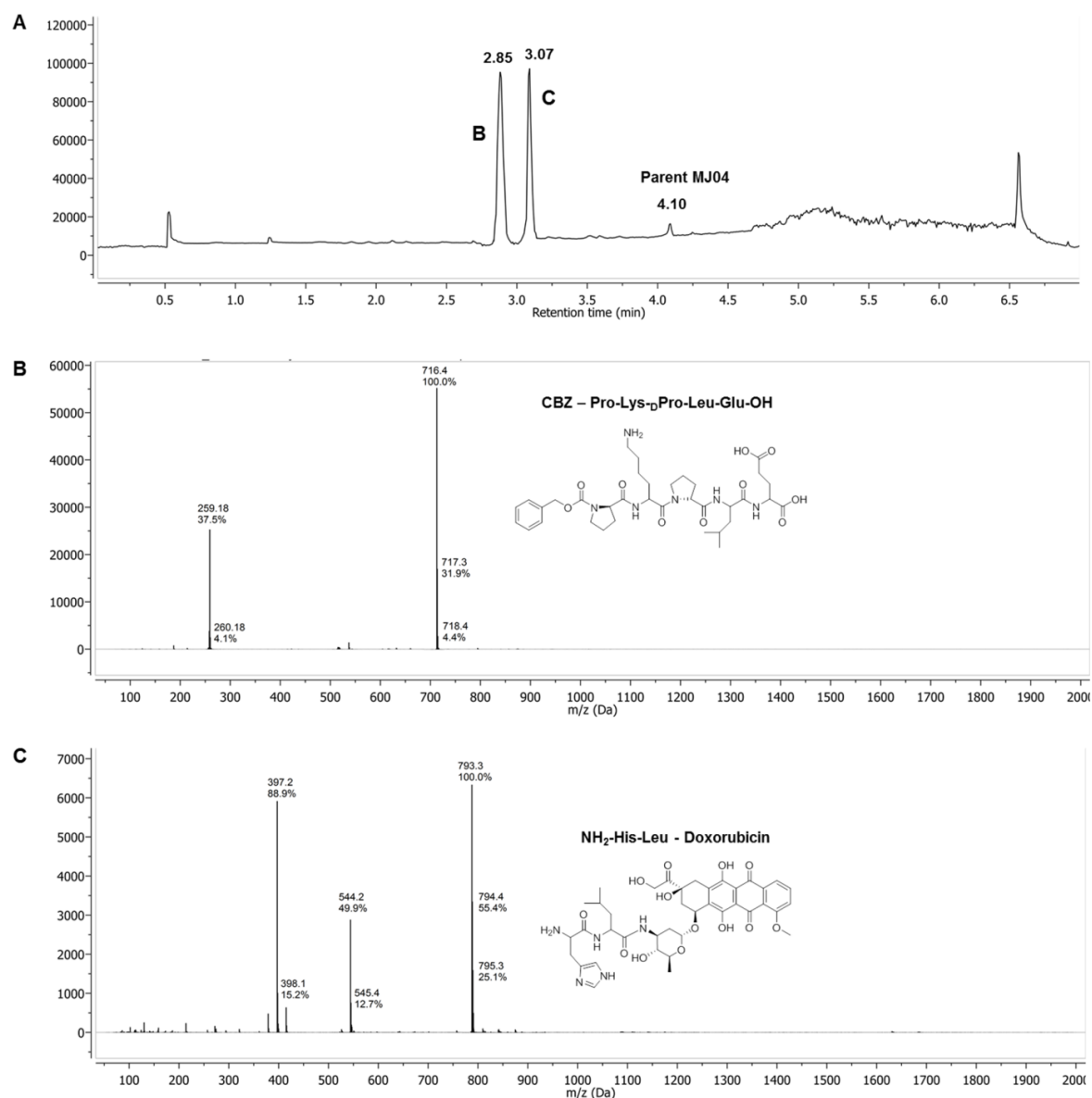
Figure IV.44: Determination of MMP-10 cleavage site in MJ04. Recombinant MMP-10 cleavage of MJ04 at the Glu-His bond, as determined by LCMS analysis. **A,** HPLC trace of MJ04 metabolism following 12 h incubation with recombinant MMP-10 at 37°C, showing MJ04 (t_R of 4.10 minutes) and cleaved metabolites, t_R 2.85 and 3.07 minutes; **B,** MS detection of metabolite as $^m/_z$ 716.4 Da [M+H]$^+$ corresponding to Cbz-Pro-Lys- D-Pro -Leu-Glu; **C,** MS detection of metabolite as $^m/_z$ 793.3 Da [M+H]$^+$, corresponding to His-Leu-Doxorubicin; confirming cleavage at the Glu-His bond.
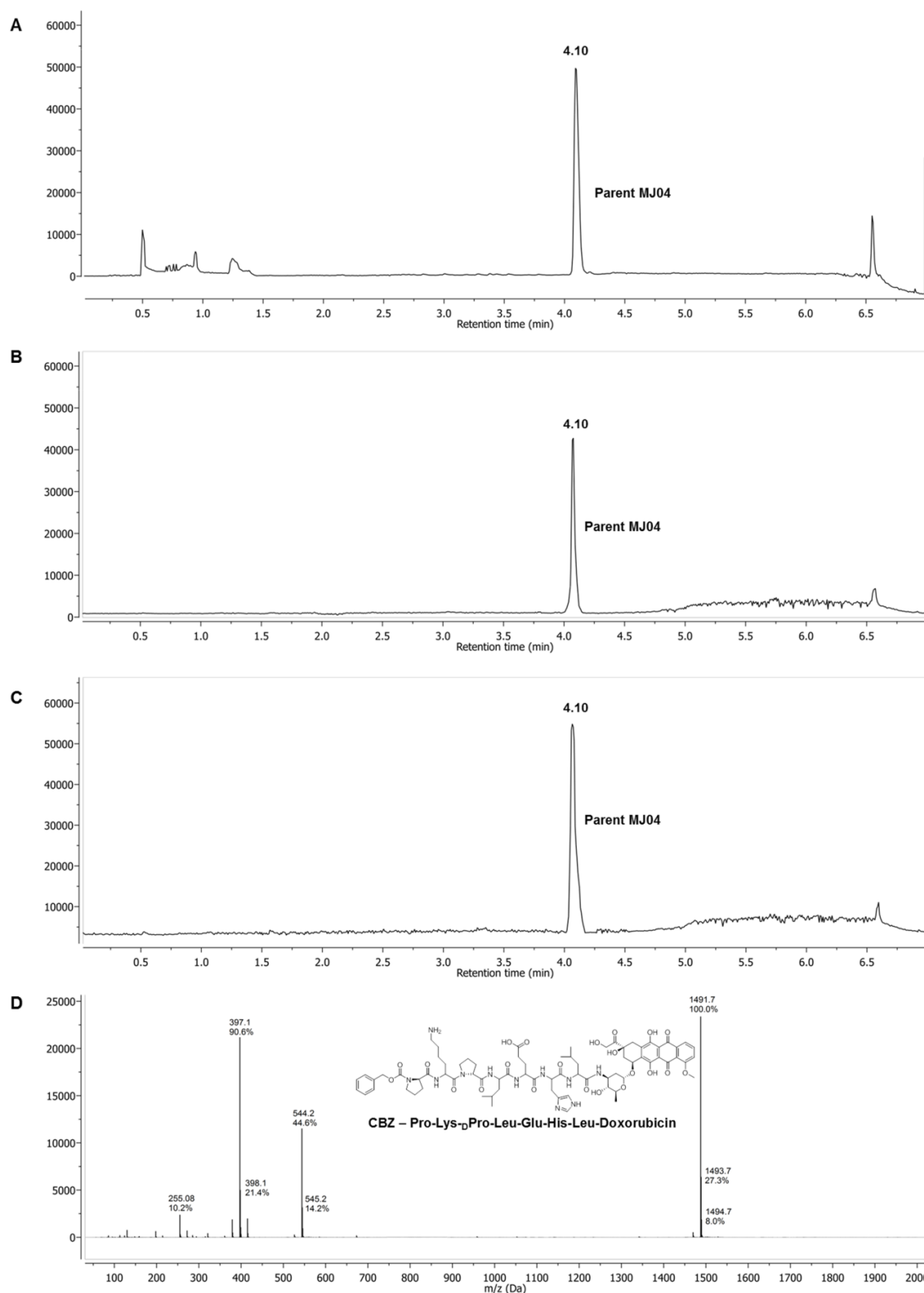
Figure IV.45: MJ04 did not demonstrate cleavage by recombinant MMP-2, MMP-3 and MMP-9. A, B and C represents HPLC traces of MMP-2, MMP-3 and MMP-9 mediated activity on MJ04, respectively. The MS confirmation of non-cleaved MJ04 (parent, $^m/_z$ 1491.7 Da [M]⁻) is shown in graph D. These graphs demonstrate that whilst MJ04 was cleaved by MMP-10; MMPs -2, -3 and -9 were unable to cleave this prodrug over 12 h incubation period.

IV.5.20 Stability of MJ04 in MMP positive and MMP negative cell lines

Similar to the stability of MJ02 and MJ03 described in sections IV.5.7 and IV.5.12, the selective metabolism of MJ04 was tested in two cell models i.e. U87-MG and SVG-P12 cell lines. These cell lines grown in monolayer were assayed for their ability to metabolise MJ04 and were analysed after 24 h, 48 h and 96 h drug exposures, determined by LCMS. As figure IV.46 demonstrates, MJ04 was rapidly metabolised by U87-MG (t½ = 40 h) with a significantly slower metabolism observed by SVG-P12 (t½ = >96 h). The exposure of MJ04 in MMP-10 negative cell line, SVG-P12, resulted in significantly decreased metabolism of the prodrug compared to MJ02 (t½ = 89 h) and MJ03 (t½ = 86 h) metabolism in SVG-P12. In SVG-P12 cells, the disappearance of parent MJ04 post 96 h exposure was nearly 2-fold slower (85% of MJ04 remaining at 96 h), when compared to MJ02 (45% of MJ02 remaining at 96 h) and MJ03 (40% of MJ03 remaining at 96 h) (Figures IV.46, IV.47 and IV.48). In both cell lines, the metabolism of MJ04 resulted in the production of the chemotherapeutic agent, Leu-Dox. The involvement of MMPs was assessed by determining the degree of MJ04 metabolism by U87-MG cells in the presence of pan-MMP inhibitor Ilomastat (GM6001) and the MMP-10 selective inhibitor JJH-III-012A (developed by Dr Jonathan Harburn for a parallel project), at non-potent concentrations of 1 µM and 500 nM, respectively . Ilomastat resulted in a significant decrease in metabolism of MJ04 by U87-MG (t½ >96 h). Interestingly, MJ04 also displayed significantly slower metabolism in the presence of MMP-10 selective inhibitor (t½ = >96 h), when compared to the metabolism of MJ02 and MJ03 in the presence of this inhibitor (Figures IV.46, IV.47 and IV.48).
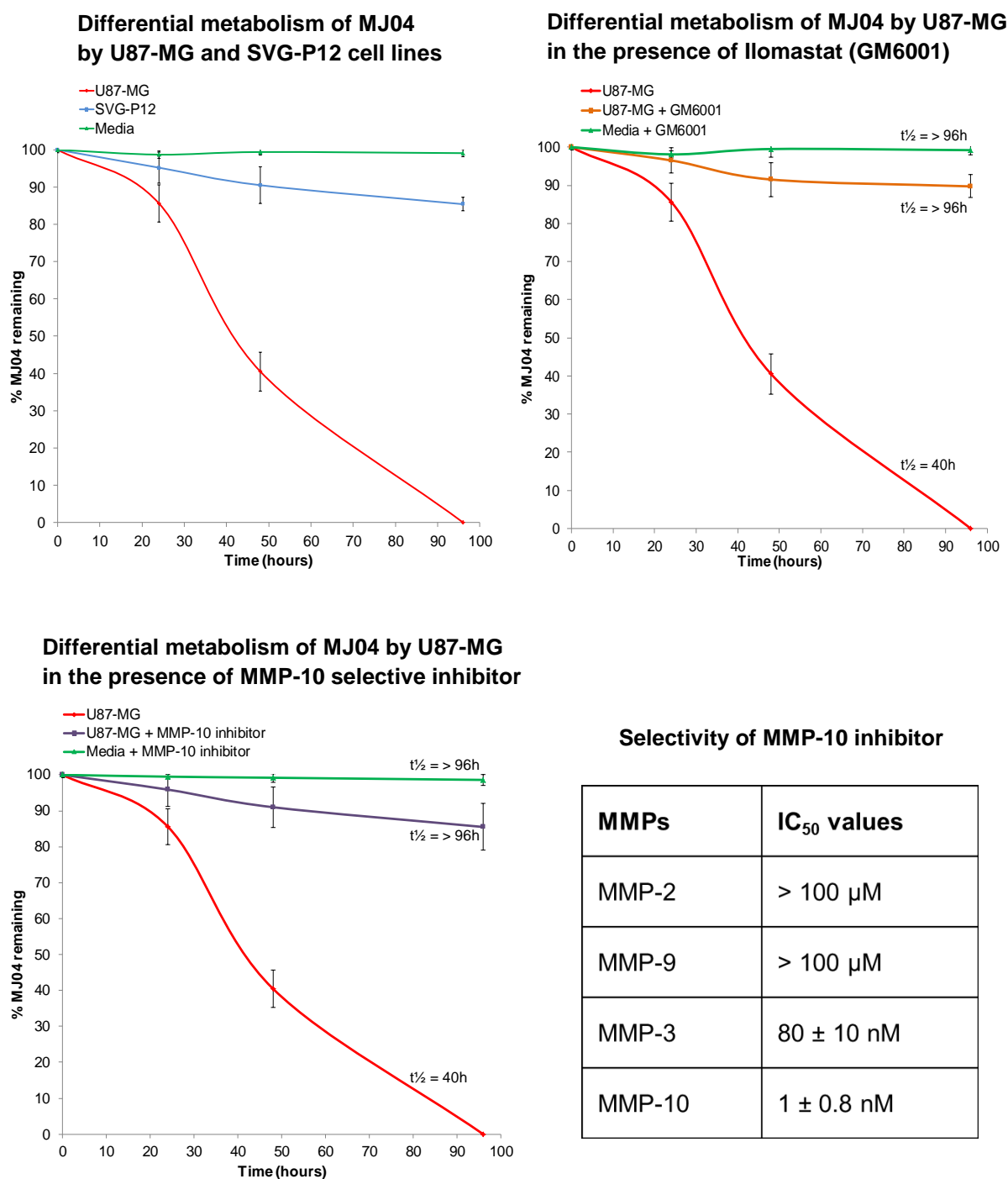
Figure IV.46: Differential metabolism of MJ04 by U87-MG (high MMP expressing) and SVG-P12 (low MMP expressing) cell lines. Cells in monolayer were assayed for their ability to metabolise MJ04 over 24 h, 48 h and 96 h time points, as detected by LCMS. Metabolism of MJ04 by cell lines representing 1×10^4 cells, demonstrated rapid metabolism by U87-MG relative to SVG-P12. In contrast, MJ04 demonstrated a decreased metabolism by U87-MG in the presence of pan-MMP inhibitor (Ilomastat, GM6001) and MMP-10 selective inhibitor (JJH-III-012A). Metabolism values are representative of average from two independent experiments. Each value of inhibition study represents the mean ± SE of three independent experiments.
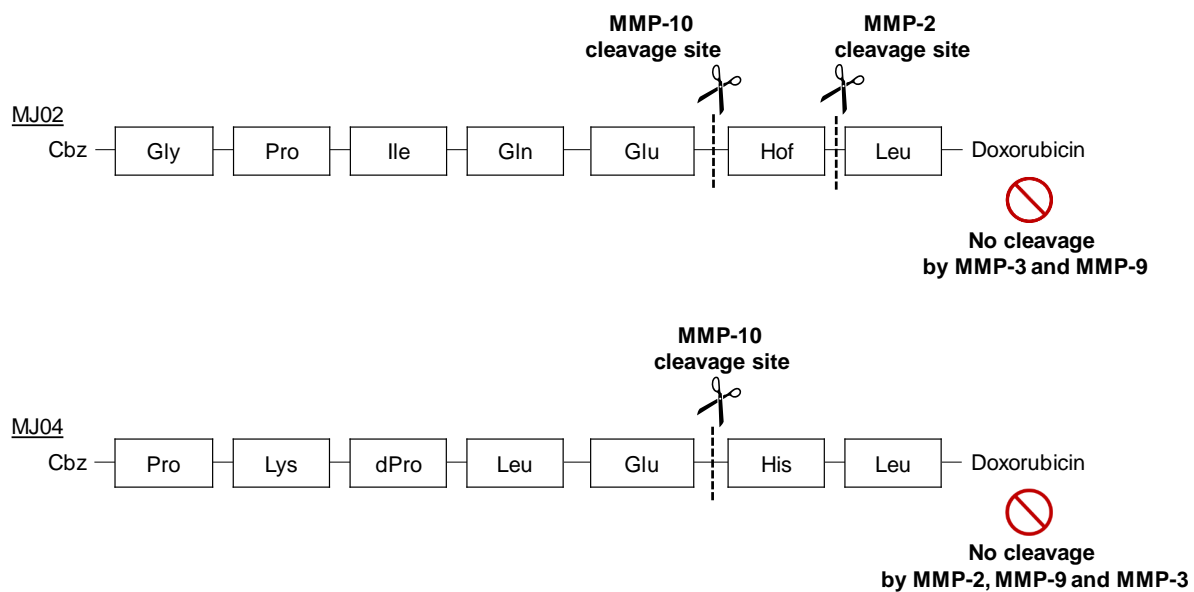
Figure IV.47: Differential MMP selectivity of rationally designed prodrugs of doxorubicin, MJ02 and MJ04.

Differential metabolism of MJ02 and MJ04 in U87-MG malignant glioma cell line

Differential metabolism of MJ02 and MJ04 in SVG-P12 normal glial cell line

Differential metabolism of MJ02 and MJ04 by U87-MG cell line in the presence of MMP-10 selective inhibitor

Comparison of MJ02 and MJ04 metabolism by glioma and normal glial cell lines

	MJ02 t½	MJ04 t½
U87-MG	40 ± 5.1 hours	40 ± 6.3 hours
SVG-P12	89 ± 2.5 hours	>> 96 hours
U87-MG + MMP-10 selective inhibitor	96 ± 6.5 hours	>> 96 hours

Figure IV.48: Comparison between metabolism of MJ02 and MJ04 in human glioma (U87-MG) and normal glial (SVG-P12) cell lines. MJ04 showed improved selective metabolism by U87-MG. Whereas, SVG-P12 demonstrated significantly lower metabolism of MJ04 than MJ02. Compared to MJ02, MJ04 was relatively stable in the presence of MMP-10 selective inhibitor (JJH-III-012A) demonstrating MMP-10 selective action of MJ04 to selectively release the chemotherapeutic Leu-dox within the human glioma cells.

Doxorubicin

MJ04

MJ04 in the presence of MMP inhibitors

IC$_{50}$ value of compounds

	Compound	U87-MG IC$_{50}$ (µM)	1321N1 IC$_{50}$ (µM)	SVG-P12 IC$_{50}$ (µM)
96 hours	Doxorubicin	0.3 ± 0.2	0.005 ± 0.002	0.7 ± 0.5
	Leu-Dox	0.6 ± 0.2	0.01 ± 0.02	0.9 ± 0.3
	MJ04	8 ± 0.5	1.2 ± 0.25	> 100

Compound	U87-MG IC$_{50}$ (µM)
MJ04	8 ± 0.5
MJ04 + GM6001	> 100
MJ04 + JJH-III-012A	> 100

Figure IV.49: Chemosensitivity of U87-MG, 1321N1 and SVG-P12 to Doxorubicin and MJ04. Assessed using MTT assay following 96 h drug exposure. Cell survival is represented as relative to solvent control and demonstrates sensitivity of U87-MG and 1321N1 cell lines to both Doxorubicin and MJ04 whilst SVG-P12 is sensitive only to Doxorubicin. Potency of compounds is reported as IC$_{50}$ values (the concentration of drug required to reduce cell viability by 50% relative to control).

IV.6   Discussion

Identification of endoproteases overexpressed in human tumours relative to normal tissues represent promising drug targets for development of specific inhibitors and proteolytically activated antitumour prodrugs. A crucial requirement for the design of peptide prodrugs is the recognition of amino acid sequence selectively cleaved by the protease to which it is targeted. Since Chapter-2 demonstrated a statistically significant overexpression of MMP-10 in preclinical and clinical tissues of glioma relative to normal brain, this section of work focussed on utilising the learning from *in silico* modelling, exploiting the differences between the MMP substrate binding sites and the rational design of anticancer prodrugs selectively activated by MMP-10.

Anticancer prodrugs selectively activated due to elevated endoproteases activity within the tumour microenvironment relative to surrounding normal tissues, are composed of three components; a potent chemotherapeutic drug (effector), a peptide sequence which inactivates the effector and possesses a cleavage site for the endoprotease of choice and a chemical endcap to prevent non-specific metabolism by exoproteases.[203] In this study, *in silico* proteolytic docking coupled to *in vitro* biochemical assessment have been applied to enable development of anticancer peptide prodrugs selectively activated by MMPs within the tumour, resulting in improved release of chemotherapeutic drug at the tumour site relative to normal tissues, thereby increasing the therapeutic index of the drug. In choosing the anticancer drug, we endeavoured to take advantage of the established antitumour activities of doxorubicin and the colchicine derivative (azademthylcolchicine) but avoid systemic toxicity by conjugating them to rationally designed MMP-cleavable peptides activated selectively at the tumour

site. The rational exploitation of stromelysin catalytic domains to identify the differences in their binding sites and design tumour selective prodrugs activated by MMP-10 over its close homologues, MMP-3 and gelatinases, is a novel and unreported approach to cancer treatment.

To achieve differential selectivity between structurally homologous MMPs, the initial efforts focused on developing MMP-subtype selective prodrugs. Considering a very similar catalytic structural homology between MMPs, it would be beneficial to differentiate between catalytic binding subsites and further attain better selectivity. The most crucial step in developing peptide prodrugs is the development of an amino acid sequence which allows for selective cleavage only by specific MMPs. But more often than not, the peptide sequence is also selective for non-specific homologous MMPs, rendering the drug targeting system ineffective. For this purpose, the 'Albright prodrug' sequence possessing pan-MMP selectivity was utilised as the template sequence.[207, 285] Derived from 'Albright prodrug', the modified MJ02 sequence consisted of amino acids which would selectively align into the active sites of MMP-2 and MMP-10, over MMP-3 and MMP-9. Using the MMP-2/MMP-9 cleavage site, Gly-Ser(OBenzyl), of the "Albright prodrug"; the replacements of the P1 Gly with a Hof residue, P2 Leu with a Glu residue and P3 Pro with a Gln residue, were induced to achieve MMP-2 selectivity over MMP-9. In terms of binding affinity, it was observed that the S1 and S3 subsites in MMP-2 have deeper cavity than MMP-9, suggesting MMP-2 can accommodate longer side chains than MMP-9 (Figures IV.50 and IV.51). The presence of small chain Ala165 residue in MMP-2 S1 subsite showed affinity for large aromatic residues, whereas Glu402 residue in MMP-9 causes the S1 pocket to become shallow in comparison. Therefore, Hof was able to tightly fit into S1

pocket of MMP-2 as demonstrated by strong hydrophobic interaction with Ala165 (Figures IV.50 and IV.51). However, Hof was unable to align into the shallow S1 pocket of MMP-9. Similarly, the presence of Gly204 residue in MMP-2 at S3 subsite accounts for a large neutrally charged pocket. Therefore the S3 pocket of MMP-2 was able to accommodate Gln residue at P3 position. Conversely, Asp410 present at the bottom of S3 subsite in MMP-9 accounted for a smaller pocket and was therefore unable to accept Gln at this subsite (Figures IV.50 and IV.51). Furthermore, MMP-2 and MMP-9 consisted of large S2 pockets with a difference in polarity. His205 in MMP-2 made the S2 pocket charged in nature and had affinity for acidic residues. Whereas, Phe192 residue in the S2 pocket of MMP-9 was hydrophobic in nature and possessed affinity for hydrophobic residues. Therefore, Glu residue at P2 position was able to strongly align into the S2 subsite of MMP-2, but not into MMP-9 (Figures IV.50 and IV.51). It is suggested that MMP-9 prefers an Arg at P2 whilst MMP-2 more efficiently cleaves small chain residues such as Leu.[286-288] In this study, however, the addition of Leu at P2 position caused relatively stronger interaction with MMP-9 when compared to Glu at this position. It was observed that the S1' specificity pocket of MMP-2 was larger in comparison to MMP-9. In MMP-2, the external wall of the S1' cavity if largely formed by Thr227 – Phe232 specificity residues, creating a deeper pocket. Whereas, Arg424 in MMP-9 is present at the bottom of S1' pocket and closes off the end, leading to a relatively smaller cavity.[134, 269] Despite, the affinity of S1' pocket in MMP-2 to accommodate long hydrophobic residues, small non-polar residue, Leu, was included at P1' position instead. This was due to longer residues leading to a negative effect on the predicted binding affinity, due to conformational change. The S1' cavity of MMP-9 was unable to accommodate Leu due to

steric/charge hindrances imposed by S1, S2 and S3 subsites of MMP-9 towards the MJ02 residues.
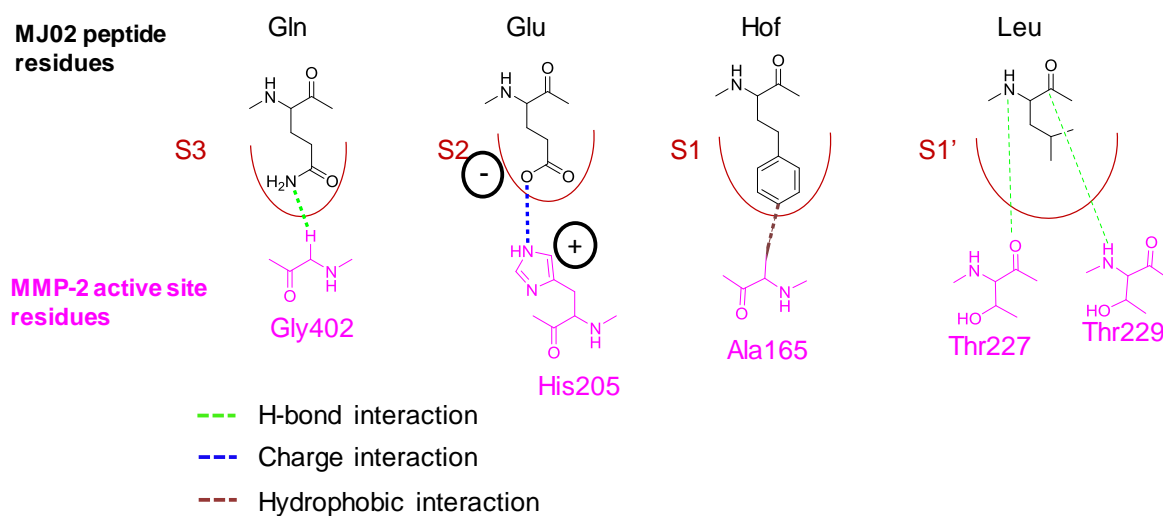
Figure IV.50: MMP-2 binding subsite demonstrates strong preference for MJ02 peptide residues
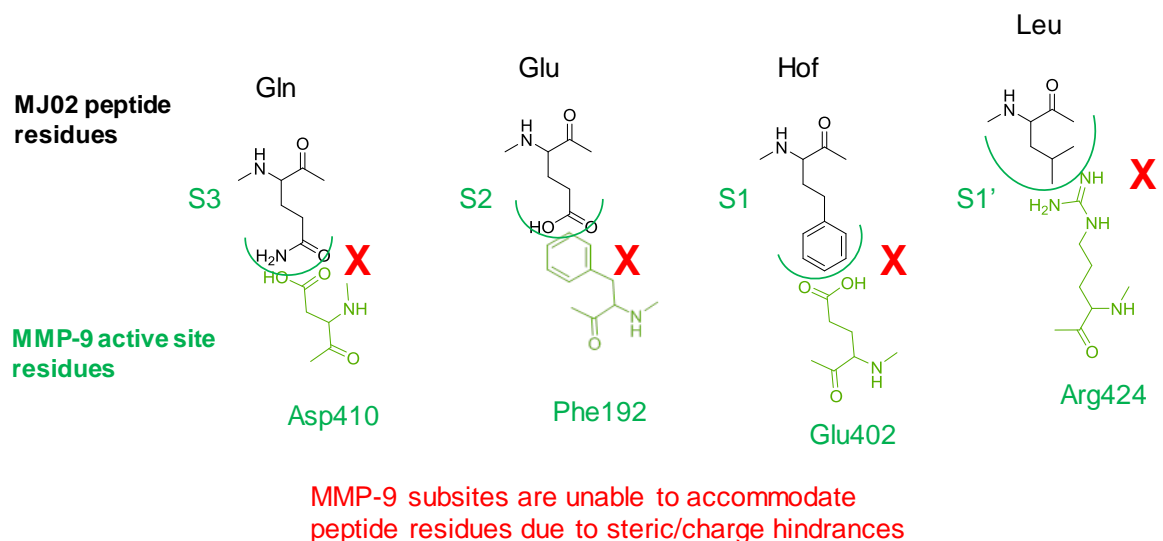
Figure IV.51: MMP-9 binding subsites do not show preference for MJ02 residues due to steric/charge hindrances, relative to MMP-2

Similarly, based on the MMP-3/MMP-10 cleavage site, Ser(OBenzyl)-Tyr, in the 'Albright prodrug' the replacements of the P1 Ser(OBenzyl) with a Glu residue, P2 Gly with a Gln residue, P5 Glu with a Gly residue and P1' Tyr with a Hof residue, were induced to achieve MMP-10 selectivity over MMP-3. In spite of identical substrate selectivity of MMP-3 and MMP-10, there were subtle but significant binding differences between the two. The difference in S2 and S3 pockets were important in rationalising the peptide selectivity between the two stromelysins. Ser179 and Leu180 residues, present on either sides of the S2 pocket in MMP-10 demonstrated affinity for both hydrophobic and hydrophilic residues. Whereas, the presence of Ile203 in MMP-3 caused the S2 pocket hydrophobic in nature. Therefore, the Gln at P2 position inserted into the S2 pocket was strongly coordinated by Ser179 and Leu180 residues present on either side of MMP-10 pocket (Figure IV.52). In MMP-3 however, the hydrophobic nature of S2 pocket demonstrated weaker affinity for Gln at this position. Similarly, Ala229 and His227 residues present on either side of the S3 pocket of MMP-10 demonstrated affinity for both polar and non-polar residues (Figure IV.52). On the other hand, the S3 pocket of MMP-3 contained His166 and was smaller in comparison to MMP-10. Therefore, the replacement of Ile at P3, was strongly coordinated by Ala 229 in MMP-10, but demonstrated weaker affinity for MMP-3. The small hydrophilic S3 pocket of MMP-3 possessed weaker interaction with the hydrophobic Ile residue. It was suggested that a peptide sequence must possess Glu at P1 position, for it to be selectively cleaved by stromelysins.[221, 284] Therefore, Glu was inserted at P1 position and its acidic nature indeed made significant contributions to the MJ02 binding energy. The presence of histidine-zinc complex in MMP-10, coordinated strongly with the Glu at P1 position. The Hof side-chain at P1' position was

inserted into the S1' pocket of MMP-10 and further coordinated by the wall-forming segment residues (at interatomic distances of 2.3 Å to 2.5 Å). The side-chains of Phe212, Leu213, Leu234 and Phe248 in MMP-10 make the hydrophobic cluster at the bottom of the pocket, suggesting a strong binding affinity towards MMP-10 compared to MMP-3.[271]
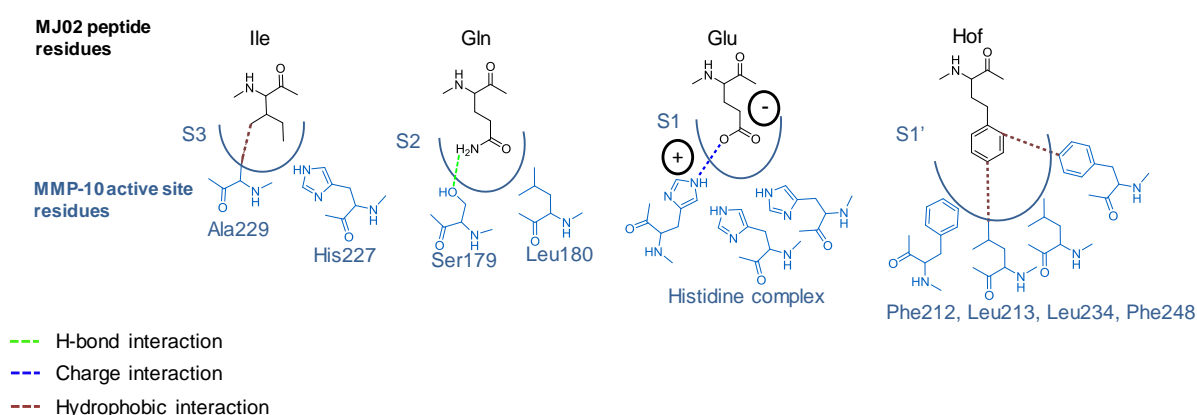
Figure IV.52: MMP-10 binding subsites demonstrating string preference for MJ02 peptide residues

This is the first study, to our knowledge, to detail the critical binding determinants of gelatinases and stromelysins. It has been suggested that the main functional difference between MMP subtypes is present in the specificity loop region (S1' subsite) of MMPs. Modifying substrate residues only at P1' position has proven in the past to improve MMP selectivity, but these substrates were also partially selective to other MMP family members.[201, 204, 285]

The modified peptide sequence of MJ02 demonstrated selective *in silico* proteolytic binding into the active sites of both MMP-2 and MMP-10, but displayed negligible binding with MMP-9 and MMP-3. The strong interaction of catalytic zinc with the carboxylate between the Hof-Leu bond in MMP-2 and the Glu-Hof bond in

MMP-10 suggested that the experimental cleavage must occur at these subsites by respective MMPs. It is proven that the catalytic zinc complex consisting of three histidine residues are responsible for efficiency of binding and hydrolysis by specific enzymes.[134] In agreement with the *in silico* prediction, the MMP-2 and MMP-10 targeted prodrug of doxorubicin, MJ02, displayed preferential cleavage by recombinant MMP-2 at the Hof-Leu bond and by recombinant MMP-10 at the Glu-Hof bond. This was an encouraging result because the utilisation of *in silico* approaches to exploit the differences in MMP binding sites, successfully lead to the development of MMP-subtype selective prodrugs.

Furthermore, MJ02 demonstrated relative stability in mouse liver homogenate, mouse plasma and mouse kidney homogenates whilst being rapidly metabolised by the HT1080 tumour homogenate to release free Dox. In order to assess the MMP-metabolism of MJ02 in preclinical models, the U87-MG human glioma cell line was selected as a positive control based on its expression of both MMP-2 and MMP-10 whilst SVG-P12 normal glial cell line was selected as a negative control since it demonstrated low expression of MMP-10, but does express MMP-2 at high levels. U87-MG demonstrated rapid metabolism of MJ02 to release Leu-Dox whilst relative stability of MJ02 was observed in SVG-P12 cell line. U87-MG displayed negligible metabolism of MJ02 in the presence of pan-MMP inhibitor (GM6001), strongly supporting an involvement of MMPs in the metabolism of MJ02. The metabolism of MJ02 by U87-MG decreased significantly in the presence of MMP-10 selective inhibitor, JJH-III-012A, (developed by Dr. JJ Harburn in a parallel project) suggestive of MMP-10 selective metabolism of MJ02. However, the differential metabolism between GM6001 and JJH-III-012A could be suggestive of MMP-2 involvement in MJ02 metabolism.

Following the successful demonstration of selective MJ02 metabolism by MMP-10 expressing preclinical model U87-MG, *in vitro* cytotoxicity of Dox, Leu-Dox (the chemotherapeutic released in preclinical cell models) and MJ02 were examined in U87-MG, 1321N1 and SVG-P12 cell lines. Selective cytotoxicity of MJ02 was observed in U87-MG and 1321N1 cell lines relative to the SVG-P12 cell line whilst all the cell lines demonstrated chemosensitivity to Dox. This data strongly supports the prodrug strategy of drug inactivation when attached to a peptide sequence, as demonstrated by a significantly decreased cytotoxicity of prodrug against the SVG-P12 cell line. The lack of MJ02 cytotoxicity against U87-MG in the presence of GM6001 also demonstrated MMP-selective chemotherapeutic action of prodrug.

To protect from metabolism by non-specific exoproteases, peptides were initially endcapped with Fmoc at the N-terminus. But the conjugation of anticancer drug at the C-terminus of the peptide eventually failed when the Fmoc proved to be chemically unstable in the presence of mild acidic conditions (data not shown). Therefore, Cbz non-polar group was employed as an endcap instead, providing improved stability during drug conjugation and in the reaction mixture.

The demonstration of MMP-10 as a viable target for treatment of glioma and the successful development of rationalised MMP-subtype selective anticancer prodrugs led to further evaluation of peptide sequence in an effort to make MMP-10 targeted prodrugs, and to eliminate metabolism by its close family homologues. Utilising the *in silico* docked complexes MJ02 and MMPs as a reference, we tried to engineer-out the MMP-2 selectivity, but it proved to be complicated. In the process of retaining MMP-10 selectivity, other MMP members also demonstrated marginal selectivity. Therefore, the focus shifted towards using the docked complexes of stromelysin-selective fluorescent substrate, M-2110, (discussed in

Chapter 3) and MMPs, as a template sequence. In agreement with the *in silico* prediction, M-2110 demonstrated preferential cleavage by MMP-3 and MMP-10 at Glu-Nva bond; and a relatively slower hydrolysis by MMP-9 at Pro-Val bond, whereas no cleavage by MMP-2 was detected. As mentioned earlier, that the design of peptide prodrugs selective for MMP-10, over MMP-3 (the closest MMP subfamily with 86% structural similarity) has not been reported.[209, 271] The *in silico* docking complex of M-2110 and MMPs provided a suitable model to rationally exploit the difference in stromeysin binding sites. The peptide sequence of M-2110 was modified towards MMP-10 selectivity by incorporating residues to fit the specificity pockets of MMP-10; but prevent binding with MMP-2, MMP-9 and MMP-3. Using the MMP-3/MMP-10 cleavage site, Glu-Nva, of M-2110 substrate; the replacements of the P2 Val with a Leu residue, P3 Pro with a D-Pro residue, P1' Nva with a His residue and P2' Trp with a Leu residue, were induced to achieve MMP-10 selectivity over other MMPs. It was suggested that in order for a substrate to be selectively cleaved by stromelysin family, it must possess a Glu residue in the P1 position. By keeping Glu as a constant residue at P1 position, the sequence of M-2110 was modified based on the learning from the *in silico* docked models. Rational design of MMP-10 selective peptide conjugate was achieved by incorporating residues into the peptide chain to fit S2, S1' and S2' pockets of MMP-10 which differed in size, charge and polar affinity compared to MMP-3 The following modifications were incorporated: branched non-polar residues in S2 subsite; basic residues in S1' subsite and branched non-polar residues in S2' subsite. The Val in M-2110 at P2 position was substituted by Leu to fit a relatively larger S2 pocket in MMP-10 than in MMP-3. MMP-10 demonstrated the lack in affinity for aromatic residues at S2' subsite and was

suitable for aliphatic side-chains instead. Therefore, Trp in M-2110 at P2' position was substituted by Leu to tightly fit into the pocket of MMP-10, a feature not observed in MMP-3 where aromatic residues are preferred. At S1' position, Nva residue was substituted by His to align well into the specificity pocket of MMP-10 but not into MMP-3. The modification of peptide sequence with His at S1' subsite and to adapt well into MMP-10 binding site was an unusual finding because like other MMPs, MMP-10 pocket is well suited to accommodate hydrophobic residues that may well provide better selectivity. However, the rationale for employing His at S1' subsite was that Glu218 (responsible for H_2O bonding with the catalytic zinc) side chain is present very close to the neck of S1' pocket in MMP-10, which further suggested the potential of S1' to also accommodate charged basic residues (Figure IV.53). In contrast, the same Glu202 side chain in MMP-3 is facing away from the S1' pocket suggesting a possibility of weaker interaction with the binding site in the presence of His at S1' subsite.
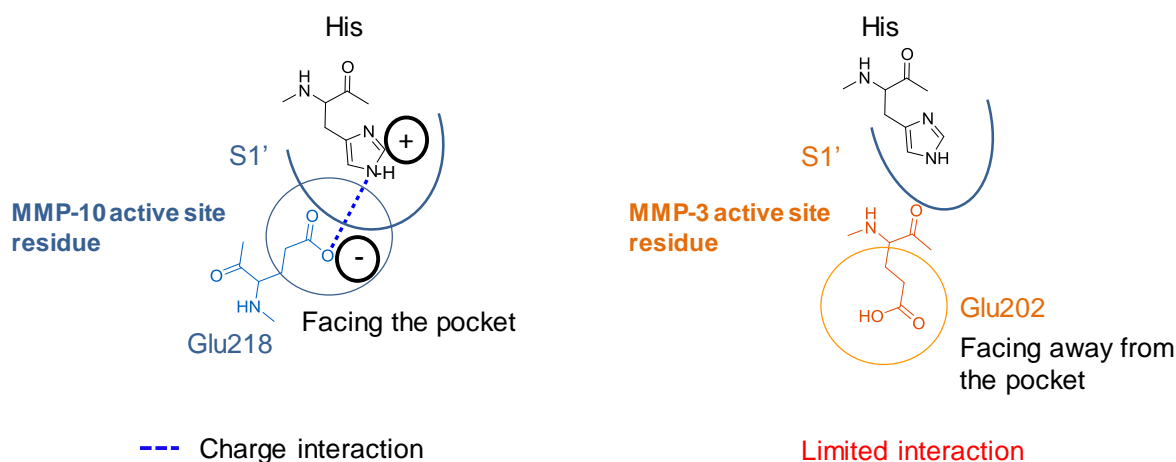
Figure IV.53: Differences possessed by the S1' binding cavities of MMP-10 and MMP-3. The position of Glu residues in both MMPs determine the type of peptide residue preference. His peptide residue was preferred by MMP-10 because Glu is facing towards the pocket and interacts with His. Whereas His aligned weakly into MMP-3 S1' pocket because the carboxylate side groups of Glu were facing away from the pocket.

In the flexible docking model the modified sequence: Pro-Lys-Pro-Leu-Glu-His-Leu aligned well into the MMP-10 sequence, but also showed a weaker selectivity towards MMP-3. His residue at P1' position was able to loosely fit into the S1' pocket of MMP-10 whereas in MMP-3 Pro~Lys residues formed the P1-P1' subsites, as determined by the presence of catalytic zinc ions. In order to engineer-out catalysis by MMP-3, the Pro at P3 position was replaced by its D-isomer, D-Pro; such that the peptide sequence adapted a moderate conformational change enough to eliminate its selectivity at Pro~Lys bond by MMP-3. The rationally designed peptide sequence Pro-Lys-DPro-Leu-Glu-His-Leu was further minimised and docked into the active sites of stromelysins and gelatinases.

The newly modified sequence demonstrated *in silico* proteolytic docking into the active site of MMP-10, but displayed negligible/negative binding with MMP-2, MMP-9 and MMP-3. The strong interaction of catalytic zinc with the carboxylate between the Glu-His bond in MMP-10 suggested that the experimental cleavage must occur at these subsites by respective MMPs. The MMP-10 targeted prodrug of doxorubicin, MJ04, displayed preferential cleavage by recombinant MMP-10 at the Glu-His bond, but displayed no cleavage by recombinant MMP-2, MMP-3 and MMP-9; thus confirming the *in silico* prediction. The assessment of MJ04 metabolism in preclinical cell models demonstrated rapid metabolism by MMP-10 positive U87-MG cell line compared to MMP-10 negative SVG-P12 cell line. Crucially, using MJ04 to release Leu-Dox resulted in a greatly reduced exposure of SVG-P12 normal glial cell line to the Leu-Dox intermediate, thus suggesting an increased therapeutic index compared to MJ02. The metabolism of MJ04 was 2-fold slower in SVG-P12 cell line compared to MJ02. Importantly, for this prodrug

strategy and targeted therapy of glioma, Leu-Dox was only detected after 96 h when dosed with MJ04 in the presence of MMP-10 selective inhibitor, which is in contrast to MJ02 where Leu-Dox was detected at 48 h. The positive result obtained with the significant decrease in MJ04 metabolism by U87-MG in the presence of JJH-III-012A, suggesting a total involvement of MMP-10 in metabolism of MJ04. Therefore, MJ04 cleavage was significantly retained in normal glial cells and also in the presence of MMP-10 selective inhibitor, with rapid cleavage demonstrated in U87-MG glioma cell line. In terms of glioma, this finding strongly support the development of MMP-10 activated prodrugs as a means for selectively delivering anticancer agents to the glioma tumour relative to normal brain tissue.

In monitoring the *in vitro* cellular metabolism of MMP-selective doxorubicin prodrugs designed in this study, doxorubicin was detected as an intermediate species, Leu-doxorubicin. This is in agreement to the limited published studies where prodrugs, usually of doxorubicin, are not efficiently metabolised following the initial MMP-selective cleavage step to release the cytotoxic agent. The MMP and PSA activated prodrugs of doxorubicin are activated to release Leu-doxorubicin and generally do not result in complete hydrolysis to produce doxorubicin directly.[207, 209, 289-292] Leu-doxorubicin is an active chemotherapeutic agent in its own right and was originally developed to increase the therapeutic efficacy of doxorubicin.[293] It is suggested that once released from the prodrug, Leu-doxorubicin is taken up efficiently into the cells and the Leu further removed is as yet an unidentified intracellular process.[293] In contrast to Leu-doxorubicin as intermediate species, release of free azademethylcolchicine was observed in the metabolism of azademethylcolchicine prodrugs. This is again, in agreement with

237

the reported literature that demonstrated a rapid degradation of prodrugs in the panel of tumour homogenates and cell lines to release free azademthylcolchicine.[203]

On the contrary, doxorubicin was detected as a free cytotoxic agent released after metabolism of MJ02 *ex vivo*. Despite the release of free doxorubicin, MJ02 displayed differential and selective metabolism in tumour homogenates relative to normal tissues. The presence of a high proportion of both extracellular and intracellular proteolytic enzymes in tumour homogenates, relative to tumour cell models, could have resulted in the rapid degradation of MJ02 to produce free doxorubicin. It will be valuable in the future to determine the exact cleavage pattern of metabolism by significantly slowing down the reaction.

In summary, these data indicate that it is possible to utilise *in silico* predictive approaches to rationally design prodrugs selectively metabolised by MMP-10 expressed in glioma tumours relative to normal brain. The prodrugs demonstrated tumour selective drug release with a significant reduction in exposure of normal glial cells to the released chemotherapeutic agents, as compared to administration of the active agent alone.

Chapter 5: Development and preclinical testing of graphene oxide tethered prodrug conjugates

V.1   Graphene oxide as a drug carrier

The development of nanoscale drug carriers has been an important focus in advanced drug delivery systems.[294] Recently approved drug delivery systems like polymer nanoparticles or liposomes, have led to many conventional drugs regaining the possibility of clinical use.[295] Since 2004, graphene has been recognised as one of the most promising materials for biomedical and life science applications. Graphene is a two-dimensional carbon material with enhanced mechanical strength, conductivity and gas barrier properties. Compared to other carrier materials used in advanced drug delivery systems, graphene oxide (GO) offers a high surface to weight ratio, high drug loading efficiency, high possibility for surface modification and photothermal effects.[296-300] Furthermore, functionalised GO can enter mammalian cells to deliver the therapeutic drug, rendering it a reasonable drug carrier.[298] Unlike the common poor aqueous dispersion problems observed with the use of other carbon nanomaterials like carbon nanotubes and fullerenes, GO has good water solubility because of abundant hydrophilic groups on either side of the GO surface. The functional groups such as epoxide, carboxylic and hydroxylic groups help to maintain stability in physiological solutions and increase the drug carrier efficiency.[301]

Currently, all the research applications of GO-drug binding are based on non-covalent interactions. For example, π-π stacking exists between GO and chemotherapeutic drugs possessing aromatic structures such as doxorubicin, SN-38 and camptothecin. This adsorption binding provide GO with high drug loading

efficiency.[302] Chen *et al.* used a chemical coprecipitation method to add Fe_3O_4 magnetic nanoparticles onto graphene. After linking the targeting ligand, the graphene selectively released doxorubicin to target breast cancer cells. Graphene can also be modified with polyvinyl alcohol for adsorption of doxorubicin for targeted anticancer delivery. Studies have also increased the GO pH-responsiveness with sulphonic acid to improve increased drug loading and delivery efficiency.[303]

In light of the current study, a major hindrance in the use of systemic chemotherapy for the treatment of glioma is the presence of the blood brain barrier (BBB). Therefore the clinical use of novel MMP-targeted prodrugs via systemic route would prove challenging for anti-glioma therapy.[304] In order to selectively target glioma tumour, one therapeutic strategy is to harness the activity of specific MMPs located in the glioma microenvironment for tumour-selective release of potent chemotherapeutics from functionalised GO nanostructured prodrug implants.

V.2   Aims and objectives

This chapter determines the feasibility of targeting MMP-selective anticancer prodrugs conjugated to graphene oxide as a local drug delivery approach for glioblastoma.

Specific objectives of this section include:

1. To design graphene tethered doxorubicin prodrug, with MJ02 peptide sequence nested between functionalised graphene oxide and doxorubicin.

2. To determine the selective cleavage of graphene oxide-prodrug by recombinant MMPs.

3. To assess metabolism of graphene oxide-prodrug in preclinical human glioma cell lines.

4. To assess specificity of prodrug cytotoxicity in human glioma cells relative to normal glial cells.

V.3   Materials and methods

V.3.1 Reagents and materials

GO was purchased from ACS Materials (Pasadena, CA, USA), as a starting material. N-Hydroxysulfosuccinimide (Sulfo-NHS), 1-ethyl-3-(3-dimethyl-aminopropyl) carbodiimide hydrochloride (EDC) and sodium chloroacetate ($ClCH_2COONa$) were purchased from Sigma Aldrich (Missouri, USA).

V.3.2 Preparation of graphene oxide (GO)-peptide conjugate

The GO suspension (in H_2O, ~1 mg/mL) was sonicated in a bath sonicator for 1 h. The resulting suspension was centrifuged at 12,000 rpm for 10 min, and the supernatant was taken for further carboxylation and peptide conjugation. In carboxylation of GO, 125 mM NaOH and 42.9 mM $ClCH_2COONa$ were added into 1.5 mL GO suspension and bath sonicated for 1 h to convert the hydroxyl and epoxide groups to COOH groups. The resulting reaction mixture was neutralized with diluted HCl, and purified by repeated centrifugation at 100,000 rpm for 30 min and rinsing with distilled water. The sediment was re-dispersed in 1.5 mL phosphate buffer (PB) (8 mM Na_2HPO_4, 2 mM KH_2PO_4, pH 7.4) to obtain the carboxylated GO suspension. In conjugation of GO with peptide, 5 mM Sulfo-NHS, 1 mM EDC were added into the carboxylated GO suspension, and the mixture was bath sonicated for 1 h. After the mixture adjusted to pH 8.0 with 1 mM NaOH, 1 mM side-chain protected MJ02 with free N-terminus, was added. The mixture was stirred vigorously at 37°C in the dark overnight. The product was purified by repeated centrifugation at 100,000 rpm for 30 min and rinsing with distilled water to remove unreacted peptides. The final product, GO−peptide conjugate, was dispersed in distilled water and stored in refrigerator at 4 ºC.

V.4   Results

V.4.1 Creation of graphene oxide tethered doxorubicin prodrug

Chapter-4 demonstrates the utilisation of *in silico* approaches to design anticancer prodrugs selectively activated by specific MMP-subtype members. In developing a graphene oxide (GO)-bound anticancer prodrug implant, we endeavoured to take advantage of MJ02's MMP-subtype selectivity and antitumour activity by catalytically hydrogenating the Cbz 'endcapping group' with Pd/C (10 wt. %) and attaching the carboxylated GO to the N-terminus of MJ02 peptide-Dox that is only cleaved at the tumour site by MMP-2 and MMP-10. The GO-conjugated MJ02 was developed systematically comprising of following reaction stages and analytic detection at each step: Development of MJ02 with preserved side-chain protecting groups, catalytic hydrogenation of Cbz endcapping group and conjugation of MJ02 peptide-Dox onto graphene oxide.

V.4.1.1   Development of MJ02 with side-chain protecting groups

The MJ02 peptide sequence containing a Cbz non-polar endcapping group was conjugated to doxorubicin warhead, as described in materials and methods (Chapter 4, section IV.4.4). The side chain protecting groups, Boc (tert-butyloxycarbonyl) of Gln and O^tBu (tert-butyl) of Glu, were preserved to avoid side-chain reactions while conjugation with the GO. MJ02, with protecting groups, was synthesised containing the amino acid sequence Gly-Pro-Ile-Gln(Boc)-Glu(O^tBu)-Hof-Leu which has doxorubicin at the C-terminus of the peptide and Cbz groups at the N-terminus.

V.4.1.2   Analytical detection of 'protected MJ02'

Protected MJ02 was analysed and its molecular mass confirmed using LCMS methods described in section IV.4.4 (Chapter 4). Preparative-HPLC gradient system with a C18 column was used to purify 'protected MJ02' at tR of 3.760 minutes ($^m/_z$ 1633.7 Da [M+H]$^+$) (Figures V.1 and V.2), to give a pale red solid.
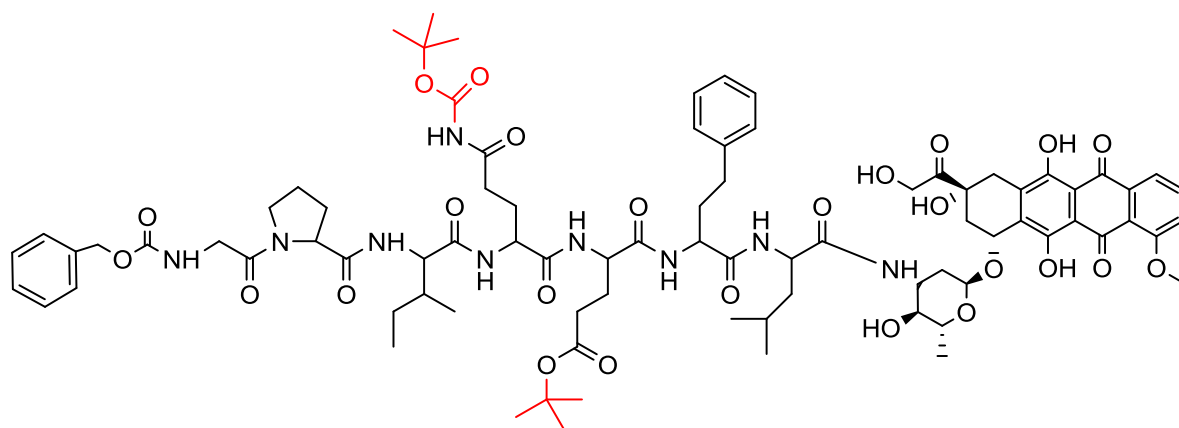
Chemical Formula: $C_{83}H_{109}N_9O_{25}$
Molecular Weight: 1632.8

Figure V.1: Purified 'Protected MJ02'. Sequence: Cbz – Gly-Pro-Ile-Gln(Boc)-Glu(O^{t}Bu)-Hof-Leu – Doxorubicin
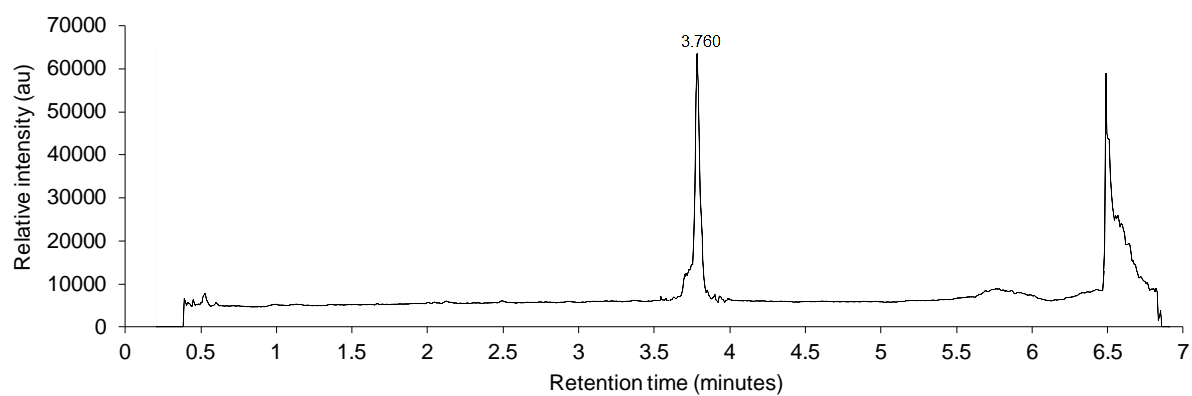
t_R = 3.760 minutes
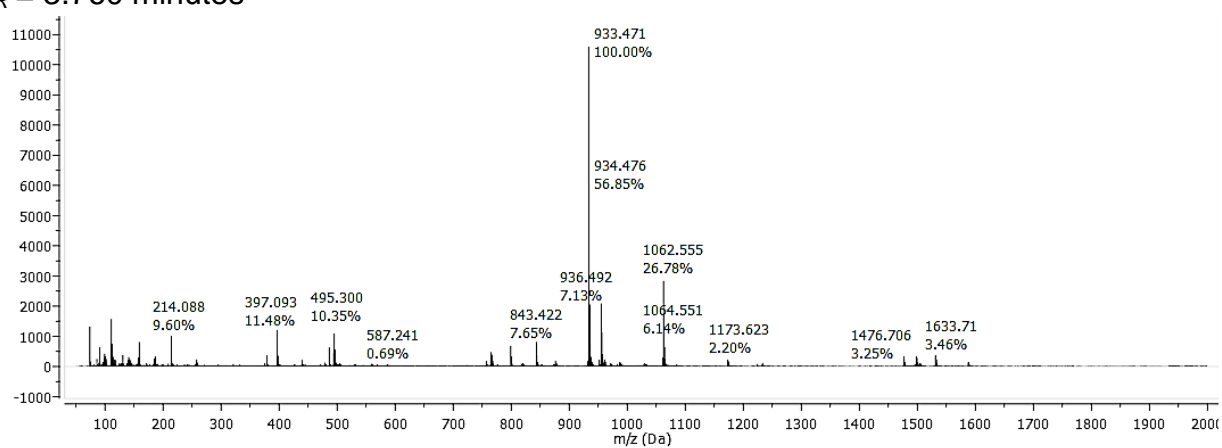
Figure V.2: Identification of MJ02 with side chain protecting groups at t_R 3.760 minutes ($^m/_z$: 1633.7 Da [M+H]$^+$) confirmed by LCMS

V.4.1.3 Catalytic hydrogenation of Cbz with Pd/C (10 wt. %)

Cbz, the endcapping group, of 'protected MJ02' was deprotected using catalytic hydrogenation reaction in the presence of palladium catalyst at room temperature. The hydrogenation reaction of Cbz was performed based on the literature.[305] It has been suggested that during hydrogenolysis of Cbz groups, the phenyl ring of the Cbz is simultaneously converted to toluene, thus cleaving from the N-terminus of the corresponding molecule.[306] 'Protected MJ02' was successfully converted into a free N-terminus peptide-Dox conjugate devoid of Cbz protecting group, containing the amino acid sequence NH_2-Gly-Pro-Ile-Gln(Boc)-Glu(O^tBu)-Hof-Leu which has doxorubicin at the C-terminus of the peptide (Figures V.3 and V.4).

Chemical Formula: $C_{75}H_{103}N_9O_{23}$
Molecular Weight: 1498.7
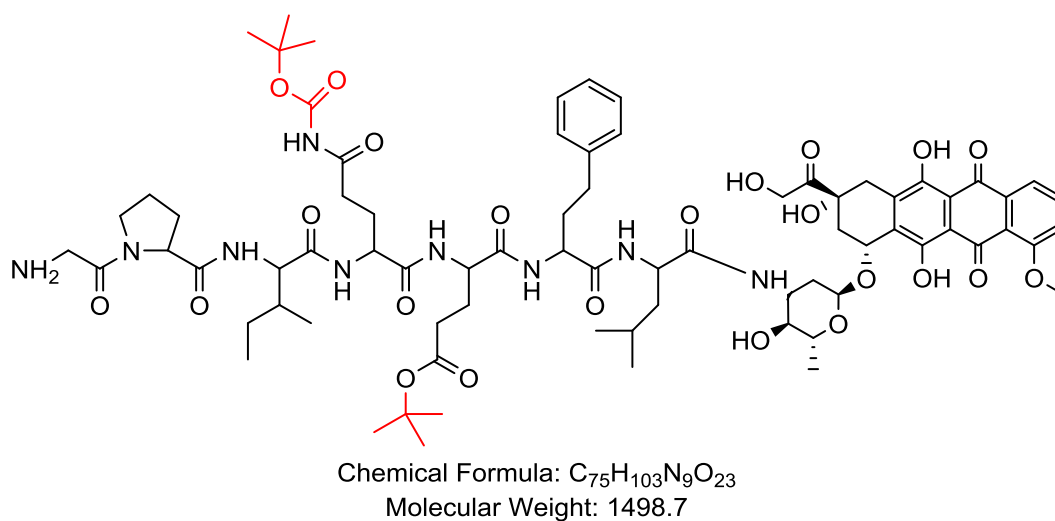
Figure V.3: 'Protected MJ02' with free N-terminus after catalytic hydrogenation of Cbz non-polar endcap. **Sequence:** NH_2-Gly-Pro-Ile-Gln(Boc)-Glu(O^tBu)-Hof-Leu – Doxorubicin
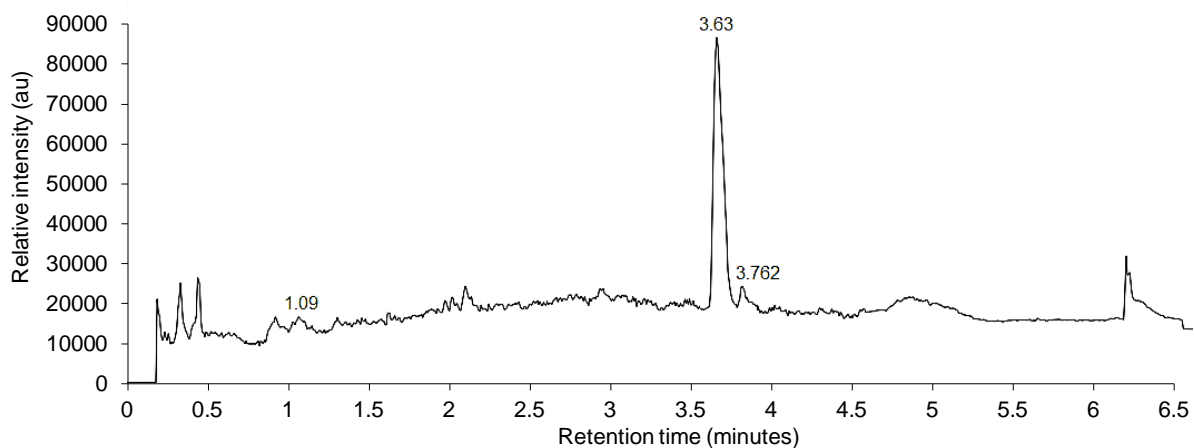
$t_R = 3.63$ minutes
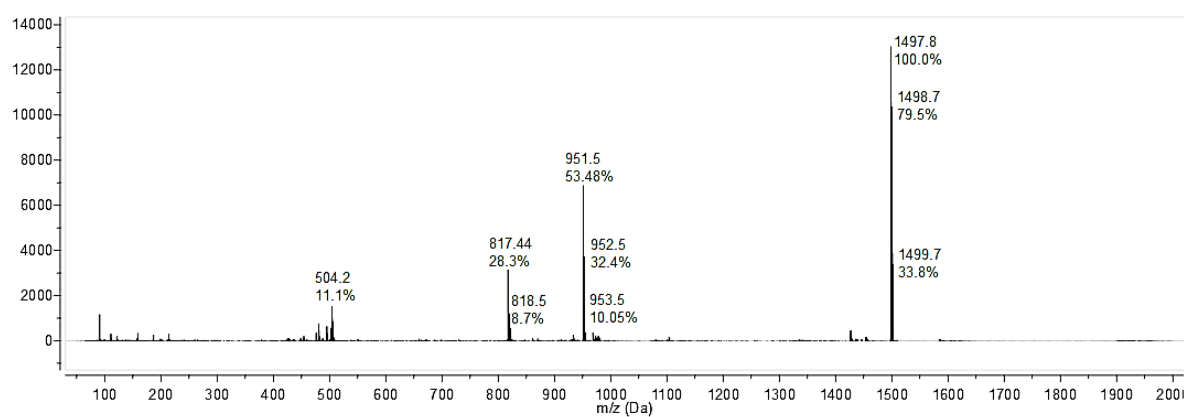
Figure V.4: LCMS Confirmation of Cbz deprotection from MJ02, leaving the N-terminus of MJ02 free. The metabolite detected at t_R 3.63 minutes ($^m/_z$: 1497.8 Da [M+H]$^+$). At t_R 3.762 minutes, $^m/_z$ 1633.7 Da [M+H]$^+$ (corresponds to the starting material i.e. the prodrug)

V.4.1.4   Development of GO-prodrug conjugate (MJ06)

The GO-peptide conjugate was prepared based on the method described in the literature.[307] Following its complete carboxylation, the COOH of GO was conjugated to free N-terminus of the peptide-Dox of MJ02. After completion of the GO-peptide-Dox conjugation reaction, the final product was purified by repeated centrifugation and rinsing with water to separate unreacted peptide-Dox (Figure V.5).

The resulting GO conjugated prodrug could not be detected by LCMS (as per previous samples). This was because the finished product presented as a suspension with a large particulate size that is unable to be passed through a MS column. In order to prove the success of conjugation in a step-wise manner, the separated unreacted peptide present in the supernatant, following centrifugation, was detected on LCMS to prove whether the 'N-terminus free' MJ02 peptide-Dox remained intact during the conjugation reaction (Figure V.6). The centrifugation was repeated until the free peptide-Dox in the supernatant was undetectable on LCMS.

The red-charcoal coloured GO-peptide-Dox precipitate, now potentially free of any unreacted peptide contaminants, was subjected to side-chain deprotection reaction with TFA:DCM (1:1) to selectively cleave Boc and O^tBu protecting groups. The reaction mixture was again centrifuged and the supernatant from this reaction mixture was analysed to ensure that no peptide-Dox had deprotected from the GO (Figure V.7). When analysed by LCMS, there was no presence of free peptide-Dox in the supernatant of deprotection reaction mixture, suggesting that the GO was successfully adhered or conjugated onto the peptide-Dox (Figure V.7).
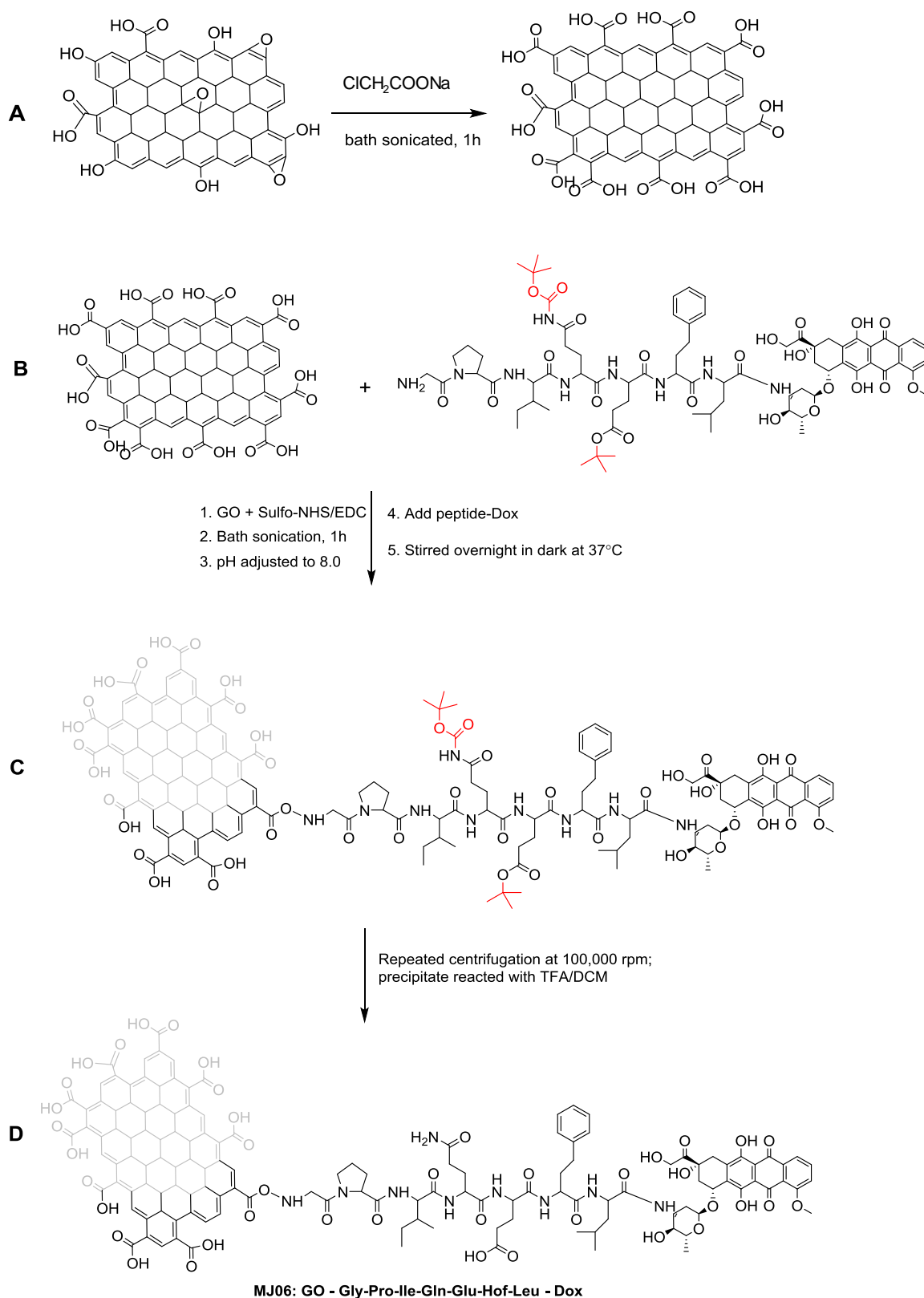
Figure V.5: Synthesis route of the GO-peptide-Dox conjugate (MJ06). A, carboxylation of GO to convert hydroxyl and epoxide groups to COOH groups. **B,** Reactions conditions required for the conjugation of 'protected MJ02' to the surface of GO. **C,** GO-conjugated to protected MJ02 purified by repeated centrifugation and deprotection of side-chain protecting groups. **D,** Production of purified MJ06
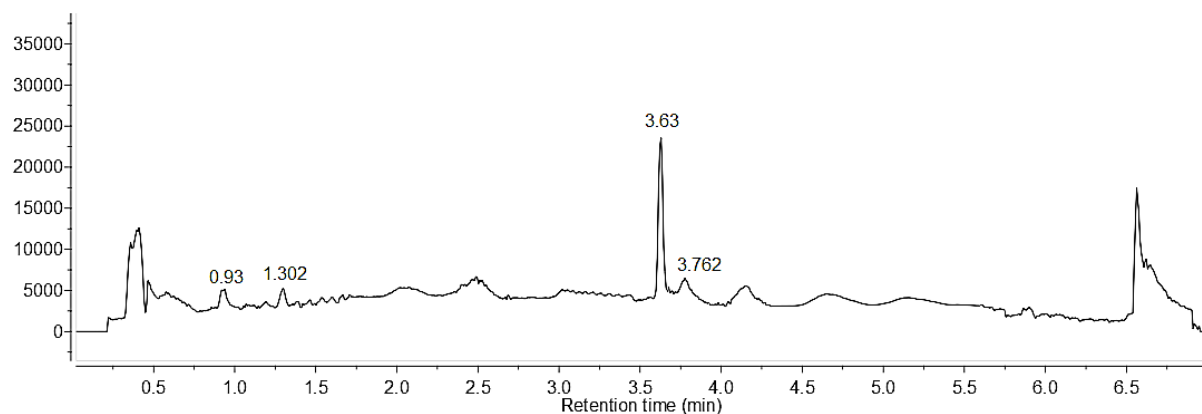
tR = 3.63 minutes
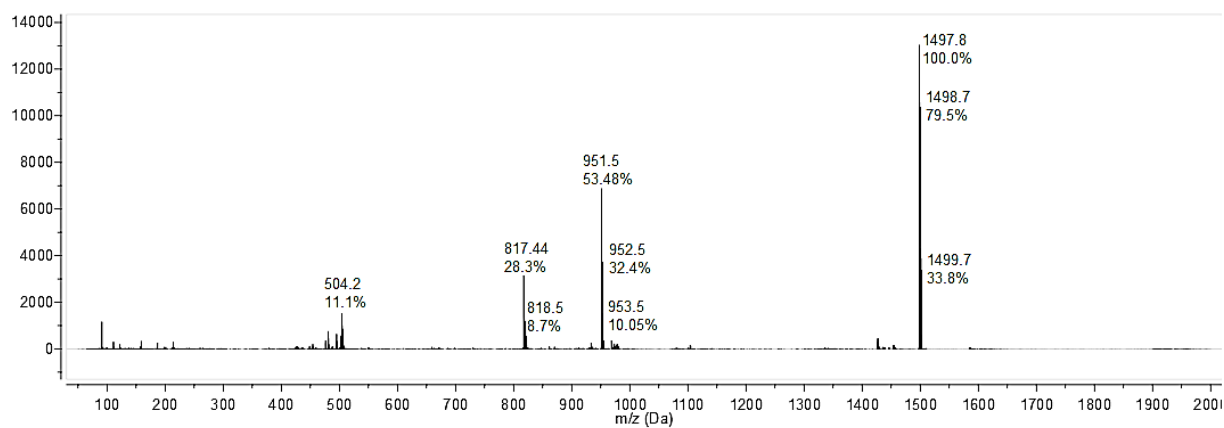
Figure V.6: LCMS detection of unreacted peptide-doxorubicin. Supernatant from the reaction mixture corresponding to the unreacted peptide-doxorubicin at tR of 3.63 minutes, $^m/_z$ 1497.8 Da $[M+H]^+$. At t_R 3.762, $^m/_z$ is 1633.7 Da $[M+H]^+$ corresponding to 'protected MJ02'.
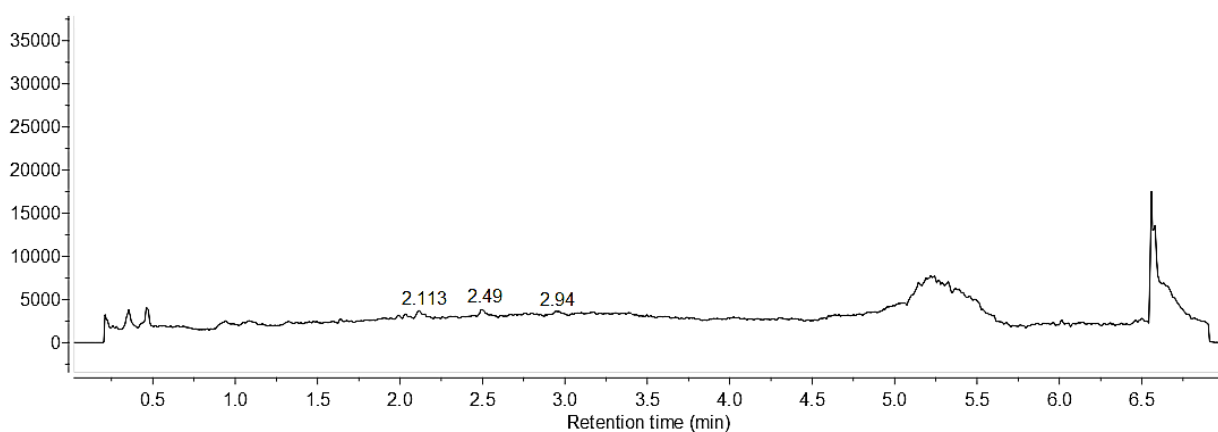
Figure V.7: LCMS analysis of supernatant from the TFA (50%)-DCM deprotection reaction mixture. Indicating the absence of unreacted peptide from the supernatant.

V.4.2 Analysis of MJ06 cleavage by recombinant MMP-2 and MMP-10

MJ02 was rationally designed to be preferentially cleaved by MMP-2 and MMP-10, over MMP-9 and MMP-3. Following complete energy minimisation the *in silico* modelling of GO-prodrug of doxorubicin (MJ06) demonstrated rigid molecular conformation. The peptide sequence, in the same rigid conformation, was docked into the active site of respective MMPs. Similar to the MJ02 flexible docking presented in section IV.5.3 (Chapter 4), the rigid peptide sequence demonstrated selective interaction with MMP-2 and MMP-10, whereas negligible interaction was observed with MMP-9 and MMP-3. This suggests that MJ06 should still be selectively activated by MMP-2 and MMP-10. In order to validate the *in silico* prediction, MJ06, containing the amino acid sequence of MJ02, was assessed for its cleavage by recombinant MMPs. Considering the limitation of MJ06 detection, only the Dox-half of the cleaved metabolites were detected on LCMS, whereas the GO-conjugated half of the peptide remained precipitated along with the enzyme buffer and recombinant MMP proteins, prior to analysis. Therefore, only one peak was detected, corresponding to Dox-half of MJ06, suggesting preferential cleavage by a particular MMP. However, MMP-3 and MMP-9 demonstrating lack of cleavage of MJ06 showed undetectable metabolites when analysed by LCMS.

MMP-2 cleaved MJ06 at the Hof-Leu bond whereas MMP-10 cleaved MJ06 at the Glu-Hof bond, as was predicted (Figures V.8, V.9, V.10 and V.11). MJ06 was preferentially cleaved by MMP-2 at Hof-Leu and one peak identified; corresponding to Leu-Doxorubicin at t_R of 2.078 minutes ($^m/_z$ 657.2Da, [M+H]$^+$) (Figures. V.8 and V.9). MJ06 was also cleaved by MMP-10 at Glu-Hof bond and one peak was identified; corresponding Hof-Leu-Doxorubicin at t_R of 2.996 minutes ($^m/_z$ 816.66 Da, [M+H]$^+$) (Figures V.10 and V.11). Conversely MMP-9 and

MMP-3 did not cleave MJ02 in the same timeframe, indicating that MJ06 is still

MMP-2 and MMP-10 selective, supporting the *in silico* prediction (Figure V.12).

GO – Gly-Pro-Ile-Gln-Glu-Hof-Leu – Doxorubicin

MMP-2
mediated cleavage

GO – Gly-Pro-Ile-Gln-Glu-Hof-
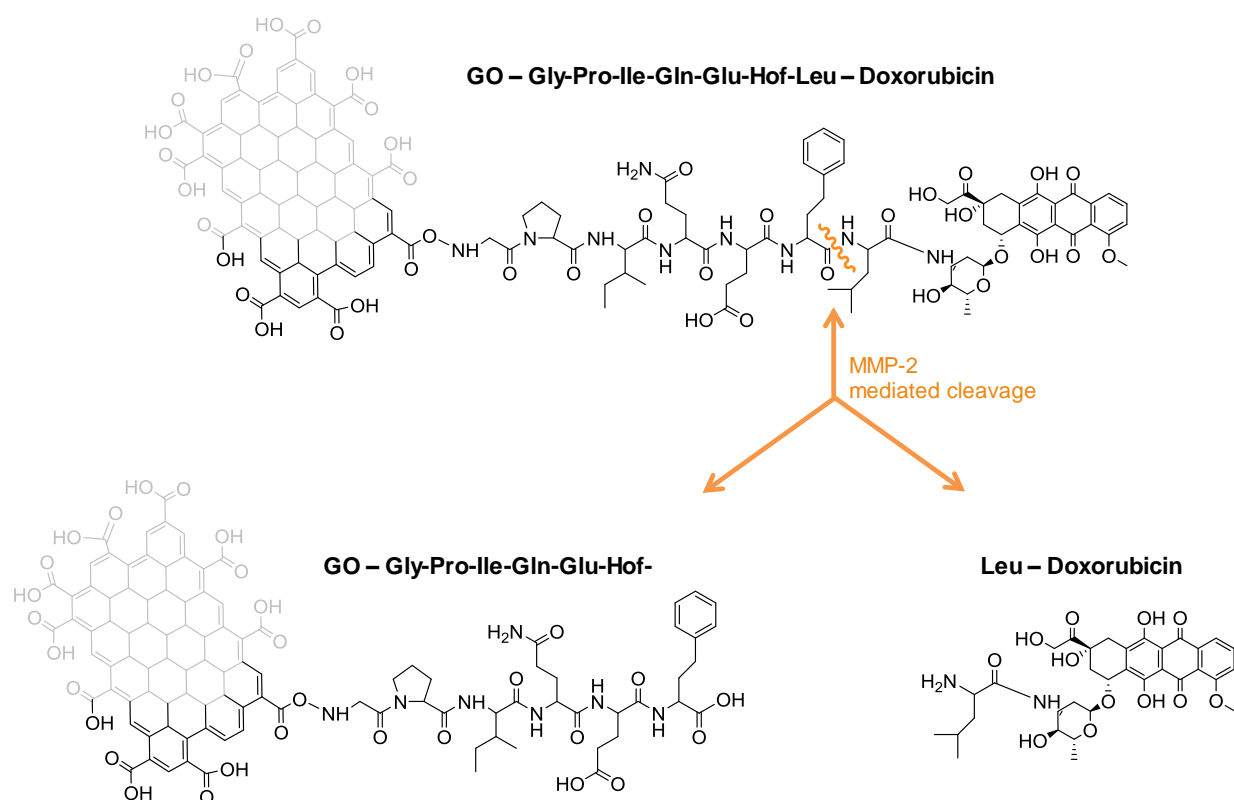
Leu – Doxorubicin

Figure V.8: Schematic representation of the cleavage of MJ06 by recombinant MMP-2. Indicating cleavage of MJ06 at the Homophe-Leu bond
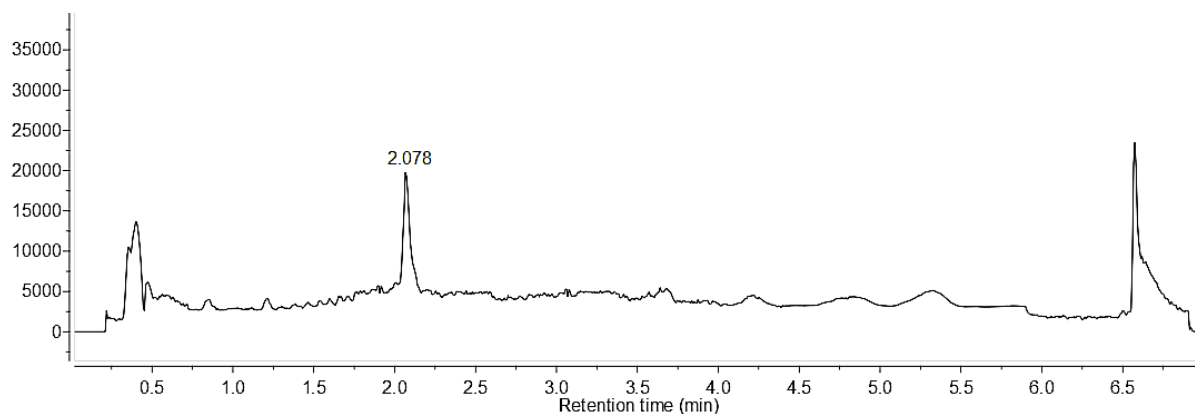
t$_R$ 2.078 minutes; peptide metabolite: Leu-Doxorubicin
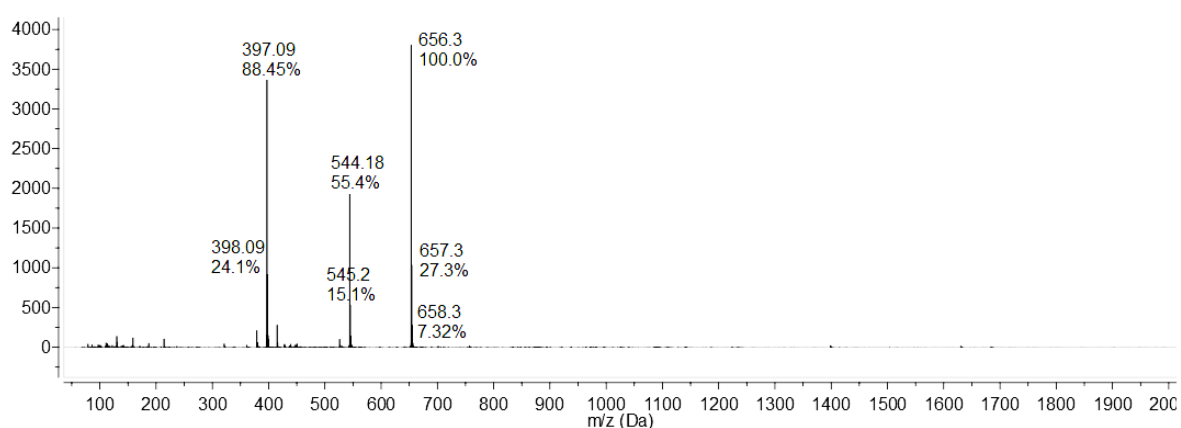
Figure V.9: Determination of MMP-2 cleavage site in MJ06 – Supernatant from the enzyme treated MJ06 mixture. Recombinant MMP-2 cleavage of MJ06 at the Homophe-Leu bond, as determined by LCMS analysis. HPLC trace of MJ06 metabolism following 12 h incubation with recombinant MMP-2 at 37°C, showing the cleaved metabolite at t$_R$ 2.078 minutes and the MS detection of metabolite as $^m/_z$ 658.2 Da [M+H]$^+$, corresponding to Leu-Doxorubicin

GO – Gly-Pro-Ile-Gln-Glu-Hof-Leu – Doxorubicin

MMP-10
mediated cleavage

GO – Gly-Pro-Ile-Gln-Glu-

Hof-Leu – Doxorubicin
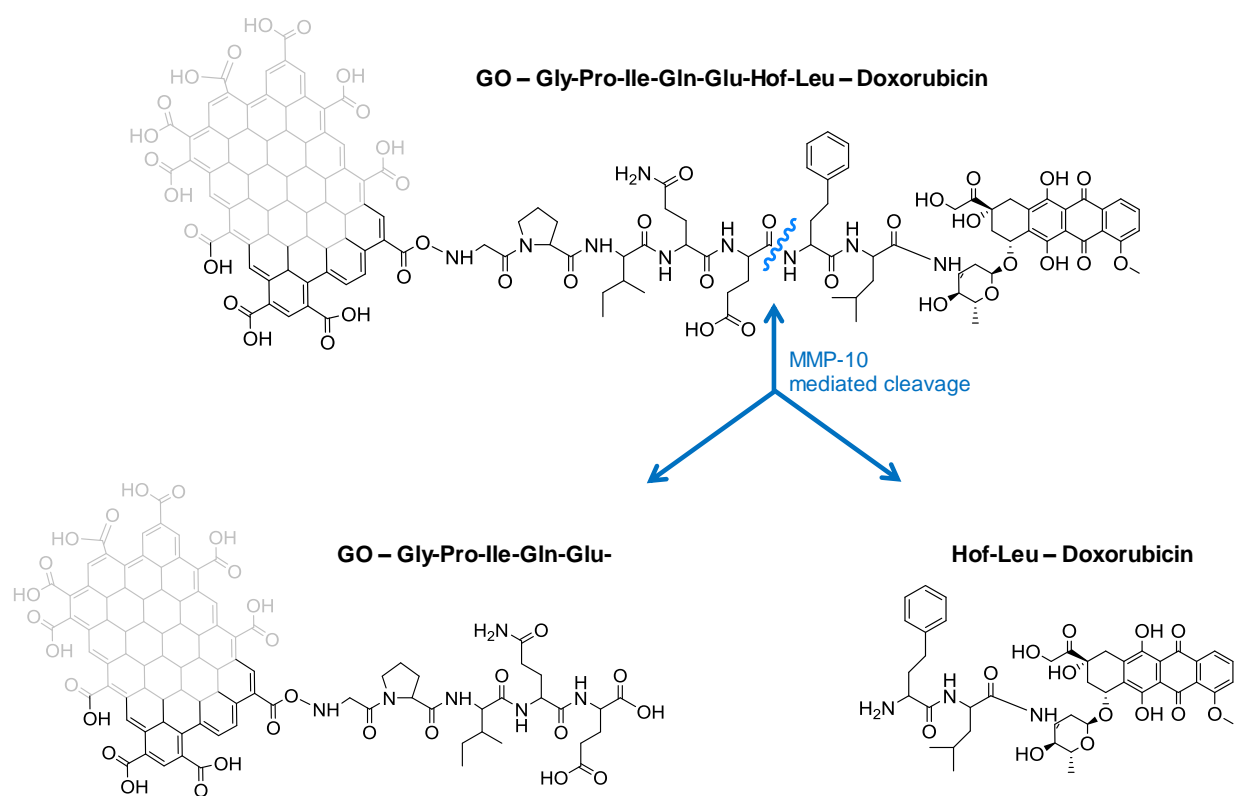
Figure V.10: Schematic representation of the cleavage of MJ06 by recombinant MMP-10. Indicating cleavage of MJ06 at the Glu-Homophe bond

255
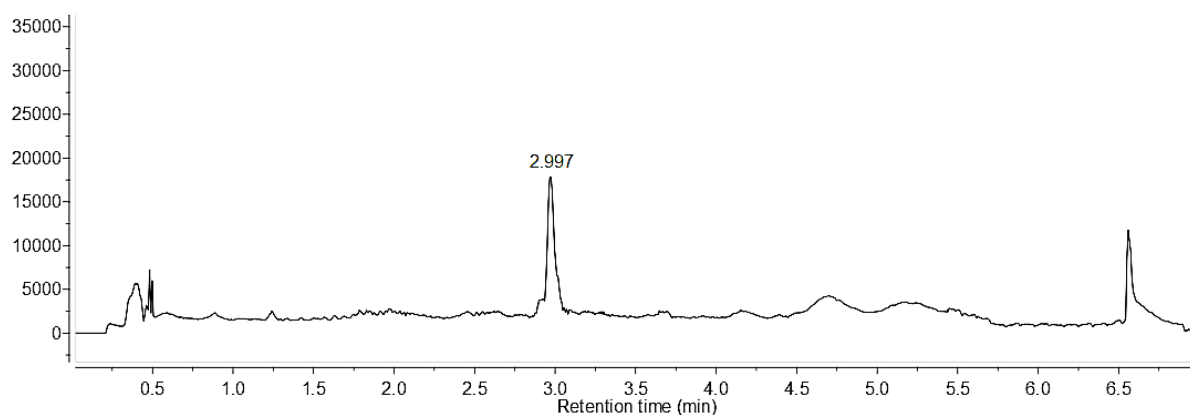
t$_R$ 2.997 minutes; peptide metabolite: Hof-Leu-Doxorubicin
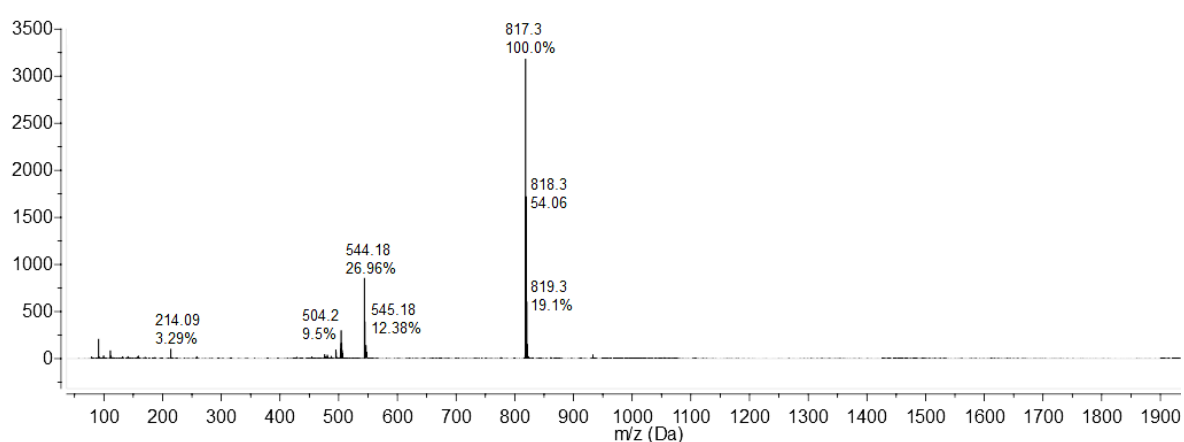
Figure V.11: Determination of MMP-10 cleavage site in MJ06 – Supernatant from the enzyme treated MJ06 mixture. Recombinant MMP-10 cleavage of MJ06 at the Glu-Hof bond, as determined by LCMS analysis. HPLC trace of MJ06 metabolism following 12 h incubation with recombinant MMP-10 at 37°C, showing the cleaved metabolite at t$_R$ 2.997 minutes and the MS detection of metabolite as $^m/_z$ 817.3 Da [M+H]$^+$, corresponding to Hof-Leu-Doxorubicin.

Incubation with MMP-9
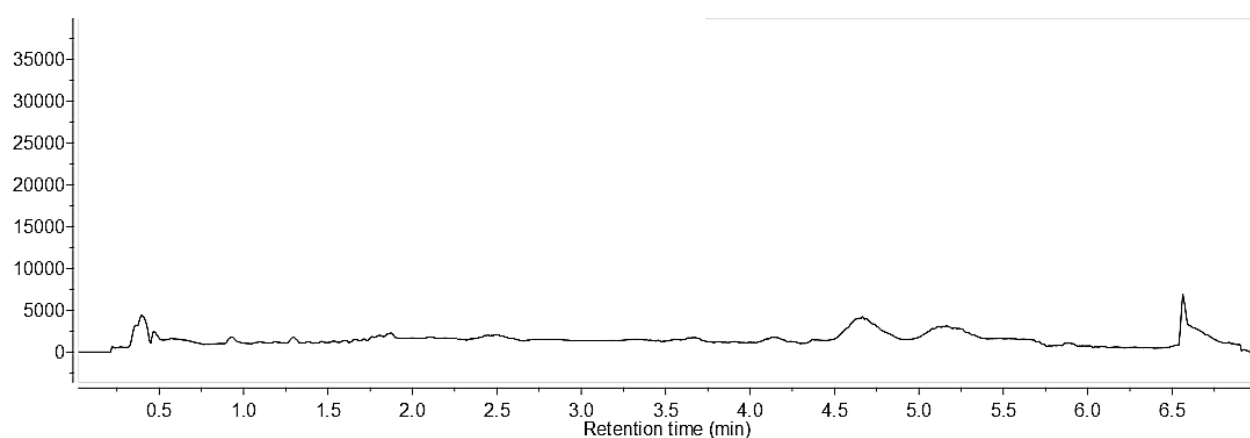
Incubation with MMP-3
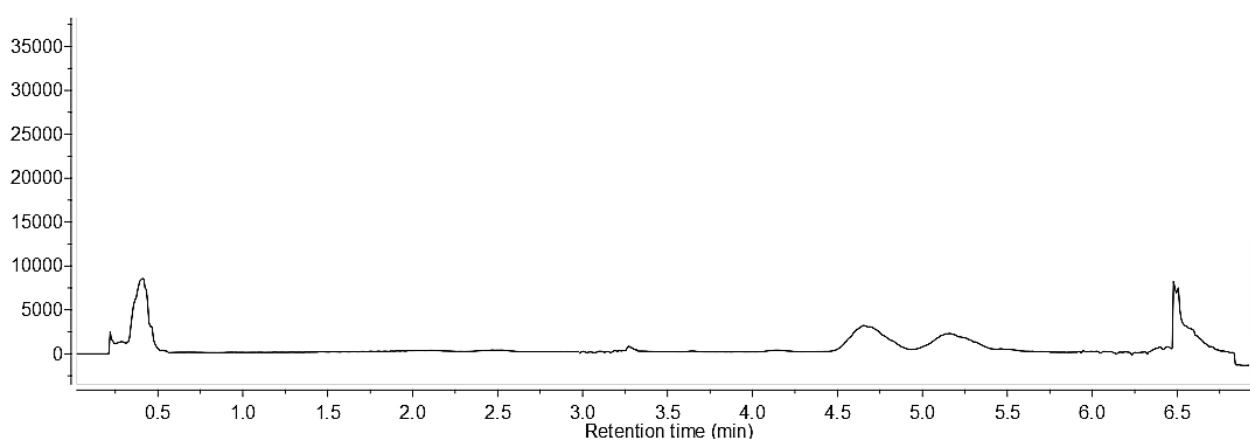
Figure V.12: Recombinant MMP-9 and MMP-3 do not cleave MJ06

V.4.3 Stability of MJ06 in MMP positive and MMP negative cell lines

Similar to the metabolism of MMP-selective prodrugs measured in Chapter-4, the selectivity of MJ06 was tested in human glioma U87-MG (MMP-10 positive) and SVG-P12 (MMP-10 negative) cell lines. Despite being negative for MMP-10, SVG-P12 cells do express MMP-2. These cell lines grown in monolayer were assayed for their ability to metabolise MJ06 and the appearance of compound Leu-Dox was analysed after 24 h, 48 h and 96 h prodrug exposures, determined by LCMS. In order to bypass the limitation of LCMS detection pertaining to parent MJ06, Leu-Dox was used as an 'internal standard' in a separate cell monolayer at equipotent dose of MJ06 (100 µM), to calculate the appearance of compound. Figure V.13 demonstrates that MJ06 was rapidly converted into Leu-Dox by U87-MG with a significantly slower conversion observed in SVG-P12. U87-MG demonstrated complete conversion of MJ06 at 96 h, compared to only 50% (± 3.4) of Leu-Dox detected in SVG-P12.

The involvement of MMPs was assessed by determining the degree of MJ06 metabolism by U87-MG cells in the presence of pan-MMP inhibitor Ilomastat (GM6001) and the MMP-10 selective inhibitor JJH-III-012A (developed by Dr Jonathan Harburn for a parallel project), at non-potent concentrations of 1 µM and 500 nM, respectively . Ilomastat resulted in a significant decrease in metabolism of MJ06 by U87-MG, measured by slow appearance rate of Leu-Dox. There was only 10% (±2.5) of Leu-Dox detected in the presence of Ilomastat, suggesting the MMP-selective action of MJ06. In contrast, MJ06 displayed relatively faster metabolism in the presence of MMP-10 selective inhibitor (inhibiting 50% of MMP-10 enzyme at 1 nM) (Figure V.13). It is interesting to note that there is a significant differential between the metabolisms by U87-MG alone and the one in the

presence of MMP-10 inhibitor, suggesting the involvement of MMP-10 enzyme to rapidly metabolise MJ02 in MMP-positive cells. Since MJ06 is selectively activated by both MMP-2 and MMP-10 (Figures V.13), the differential metabolism of MJ06 in the presence of MMP-10 inhibitor (compared to Ilomastat) could suggest a selective cleavage by MMP-2, which remains uninhibited at the treated dose.

Differential metabolism of MJ06 by U87-MG and SVG-P12 cell lines

Differential metabolism of MJ06 by U87-MG in the presence of Ilomastat (GM6001)

Differential metabolism of MJ06 by U87-MG in the presence of MMP-10 selective inhibitor

Selectivity of MMP-10 inhibitor

MMPs	IC_{50} values
MMP-2	> 100 µM
MMP-9	> 100 µM
MMP-3	80 ± 10 nM
MMP-10	1 ± 0.8 nM
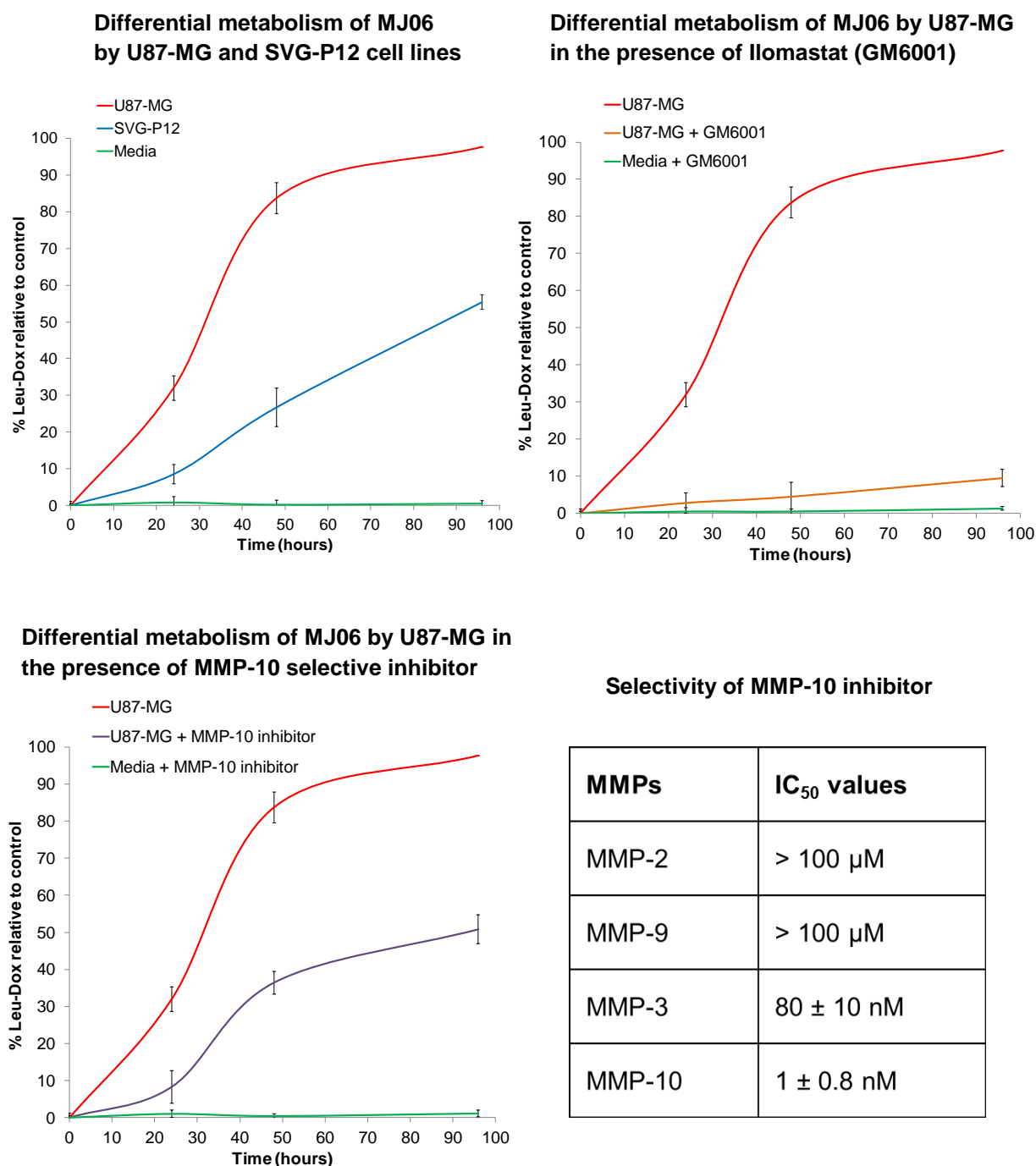
Figure V.13: Differential metabolism of MJ06 demonstrated by time-dependent release of compound Leu-Dox in U87-MG (high MMP expressing) and SVG-P12 (low MMP expressing) cell lines. Cells in monolayer were assayed for their ability to metabolise MJ06 over 24 h, 48 h and 96 h time points, as detected by LCMS. Appearance of Leu-Dox; demonstrating rapid metabolism of MJ06 in U87-MG relative to SVG-P12, and increased release of Leu-Dox. In contrast, MJ06 displayed a decreased metabolism by U87-MG in the presence of pan-MMP inhibitor (Ilomastat, GM6001) and MMP-10 selective inhibitor (JJH-III-012A), evidenced by relatively slower rate of MJ06 conversion to Leu-Dox. Metabolism values are representative of average from two independent experiments. Each value of inhibition study represents the mean ± SE of three independent experiments.

V.4.4 *In vitro* cytotoxicity of GO, Doxorubicin, Leu-Dox and MJ06

The response of the human glioma (U87-MG) and normal glial (SVG-P12) cell lines to the GO, doxorubicin, Leu-Dox and MJ06 was investigated using the MTT assay. The cytotoxicity of GO was carried out to prove their safety as a drug delivery vehicle. The GO sheets were dissolved in distilled H_2O and delivered into the cells at 3 mg/ml concentration. Drug responses of cell lines were analysed after 96 h exposures (Figure V.14).

All the cell lines were sensitive to doxorubicin and Leu-Dox at equipotent doses of doxorubicin, following 96 h exposure. In contrast, the treatment of GO into the cells proved to be non-toxic, verifying its application in this study as a safe drug carrier. As predicted, malignant human glioma cells (U87-MG and 1321N1) expressing MMP-10, were able to metabolise the prodrug efficiently and thus has a significantly lower IC_{50} for MJ06 compared to SVG-P12 (MMP-10 negative) at 96 h exposures. The differential cytotoxicity between doxorubicin and MJ06 against glioma models supports the requirement of MJ06 to be activated prior to inducing its effects. Furthermore, MJ06 remained inactive in the presence of a pan-MMP inhibitor (GM6001; Ilomastat), again demonstrating MMP-selective chemotherapeutic action of this prodrug. Whereas, in the presence of MMP-10 selective inhibitor (JJH-III-012A), MJ06 demonstrated a 40-fold weaker cytotoxicity against U87-MG suggesting MMP-10 selective chemotherapeutic action of MJ06. Similar to the metabolism study, the differential cytotoxicity of MJ02 between the two inhibitors could suggest the proteolytic activity of MMP-2 in U87-MG, causing MJ06 to metabolise faster in the presence of JJH-III-012A relative to Ilomastat.

	Compound	U87-MG IC$_{50}$ (µM)	1321N1 IC$_{50}$ (µM)	SVG-P12 IC$_{50}$ (µM)
96 hours	Doxorubicin	0.3 ± 0.2	0.005 ± 0.002	0.7 ± 0.5
	Leu-Dox	0.6 ± 0.2	0.01 ± 0.02	0.9 ± 0.3
	MJ06	2 ± 1.8	0.1 ± 0.32	> 100

Compound	U87-MG IC$_{50}$ (µM)
MJ06	2 ± 1.8
MJ06 + GM6001	> 100
MJ06 + JJH-III-012A	80 ± 7.5

Figure V.14: Chemosensitivity of U87-MG, 1321N1 and SVG-P12 to Doxorubicin and MJ06. Assessed using MTT assay following 96 h drug exposure. Cell survival is represented as relative to solvent control and demonstrates sensitivity of U87-MG and 1321N1 cell lines to both Doxorubicin and MJ06 whilst SVG-P12 is sensitive only to Doxorubicin. There is no significant difference between the MJ02 and MJ06 cytotoxicity. Potency of compounds is reported as IC$_{50}$ values (the concentration of drug required to reduce cell viability by 50% relative to control).

V.5   Discussion

Therapeutic options for glioblastoma are significantly restricted by the inability of systemic chemotherapy to reach the tumour, due to the presence of blood-brain barrier, and subsequent dose-limiting toxicity against normal tissues. To improve the concentration of drug reaching the glioma tumour, the implantation of Gliadel wafers into the tumour resection cavity is a currently employed strategy to overcome the pathophysiological barriers within the brain and locally target the tumour with a DNA alkylating chemotherapeutic, BCNU. Despite the median survival of patients has been reported to increase by 2-4 months, Gliadel wafers provide insignificant clinical benefit with adverse neurological side-effects reported in patients. This is therefore an area of significant unmet medical need and improved tumour-selective therapeutics are essential for the treatment of patients with glioma. Since this study attempted to rationally design anticancer peptide-prodrugs selectively activated by MMPs overexpressed in glioma relative to normal brain, this section of work focussed on the potential of utilising these tumour-selective anticancer prodrugs and converting them into nanostructured prodrug implants of functionalised graphene.

The biomedical applications of graphene oxide (GO), including drug delivery; have been extensively explored as one of the most promising biomaterials due to their unique properties: possibility of surface modification, 2D-planar surface, chemical stability, efficiency of drug loading and photothermal effects. However, the utility of GO as a 'base' for tumour-selective drug delivery has been largely unexplored.[308] Herein, we attempted to take advantage of the superior functional and mechanical properties of GO and report the proof-of-principle of novel tumour-targeted therapeutics based on the nanoconjugate of GO and MMP-selective prodrugs.

263

Because GO as a nanocarrier can intrinsically deliver peptide fluorophores and chemotherapeutics, like doxorubicin, inside the cells;[309, 310] the GO-conjugate of anticancer peptide prodrugs may be selectively activated by overexpressed MMPs to release the potent chemotherapeutic to glioma cells relative to normal brain cells. To test this hypothesis, the peptide-Dox sequence of MMP-2 and MMP-10 selective prodrug, MJ02, was chosen and the Cbz endcap was replaced with nanostructured carboxylated GO.

Essentially, GO, in this study, potentially functions as an endcap to protect from metabolism by non-specific exoproteases and also as a material to accommodate multiple peptide-Dox conjugated on single GO surface. Since GO is a material with large surface area, the analytic confirmation of chemical conjugation between GO and peptide-Dox could not be fully confirmed by LCMS. Instead, we relied on demonstrating the complete removal of unreacted peptide-Dox during multiple washes of conjugation reaction and analysing the cleavage of MJ06 by recombinant MMPs, thus liberating the Dox-half of the peptide for successful detection on LCMS. Thus, suggesting the conjugation of GO and peptide-Dox was potentially successful.

Similar to MJ02, MJ06 demonstrated preferential cleavage by recombinant MMP-2 at the Hof-Leu bond and by recombinant MMP-10 at the Glu-Hof bond, whereas no cleavage was detected by recombinant MMP-9 and MMP-3. MJ06 also displayed relative stability in SVG-P12 cells whilst being rapidly metabolised by U87-MG cells to release free Leu-Dox. The decreased metabolism of MJ06 in the presence of pan-MMP inhibitor and MMP-10 selective inhibitors demonstrated proof of MMPs involved in the metabolism of MJ06.

Following successful demonstration of selective MJ06 metabolism by MMP-10 expressing preclinical model U87-MG, *in vitro* cytotoxicity of doxorubicin, Leu-Dox and MJ06 were examined in human glioma cells, U87-MG and 1321N1; and normal glial cells, SVG-P12. Selective cytotoxicity of MJ06 was observed in U87-MG and 1321N1 cell lines relative to the SVG-P12 cell line whilst all the cell lines demonstrated chemosensitivity to Dox and Leu-Dox at equipotent doses. This data strongly proves the ability of GO to physically support the conjugated peptide-Dox on its functionalised surface, acting as a prodrug; and to allow selective delivery of chemotherapeutics into the tumour cells as demonstrated by significantly decreased cytotoxicity of MJ06 against SVG-P12 cell line. The lack of MJ06 cytotoxicity against U87-MG in the presence of GM6001 also demonstrated MMP-selective chemotherapeutic action of GO-prodrug.

One of the limitations in this study was the failure to successfully characterise the chemical conjugation of the peptide-prodrug to GO surface. Despite several washes performed during conjugation reaction in an effort to remove unreacted peptides and the successful analytical detection of MMP-mediated cleaved metabolites, corresponding to doxorubicin-half of the prodrug not attached to GO; there is a possibility that a significant proportion of peptide itself was adsorbed, rather than conjugated, to the surface of GO. According to the published studies, GO-peptide conjugates were confirmed using atomic forced microscopy (AFM), confocal microscopy and fluorescence spectrum detection of the GO-peptide fragments.[307, 311] Guaranteed, these detection techniques would provide the visual evidence of the drug carriers being loaded on to the GO surface, but does not prove whether the nature of encapsulation was chemical conjugation or just surface adsorption (through non-covalent interactions). It will be crucial in the

future studies to determine the nature of the conjugation between peptide and GO by analysing the chemical bonds using matrix-assisted laser desorption/ionisation (MALDI).

The observation that MJ06 is cleaved by MMP-2 and MMP-10; and demonstrated glioma selective release of chemotherapeutic agent, Leu-doxorubicin, compared to normal glial cells; is a promising and valuable result. MJ06 contains the amino acid sequence of MJ02, but with the GO as the endcap. In agreement with MJ02 cleavage, the ability of MMPs to metabolise MJ06 in a similar fashion suggests that molecular conformation of the peptide chain was retained causing the residues to fit into the active sites of MMP-2 and MMP-10, selectively. This offers the opportunity to further improve the GO-prodrug conjugate by the incorporation of GO matrix with larger surface area to accommodate several tumour-selective peptide prodrugs and utilisation of this superior chemotherapeutic drug as a post-operative brain tumour implant.

In summary, this study explored the strategy of exploiting the proteolytic activity of these specific endoproteases located in the glioma microenvironment for tumour selective-release of potent chemotherapeutics, from graphene oxide-bound prodrug nanostructure implants. During surgical resection, it is difficult to remove glioma tumours completely because these tumours infiltrate the normal brain tissue, and more often than not, gliomas recur at the same site in the brain, which further causes the increase in endoprotease activity and the vicious cycle of tumour angiogenesis and invasion is switched on with poor prognosis making it challenging for intervention by current therapies. Mechanistically, the implantation of GO-bound tumour-activated prodrug implants following tumour resection, are aimed to halt the recurrence of glioblastomas by exploring the proteolytic activity of

specific tumour endoproteases and safe release of the anticancer drug into the tumour. This therapeutic strategy will potentially improve the therapeutic efficacy of the drug and eliminate toxicity on normal tissues.
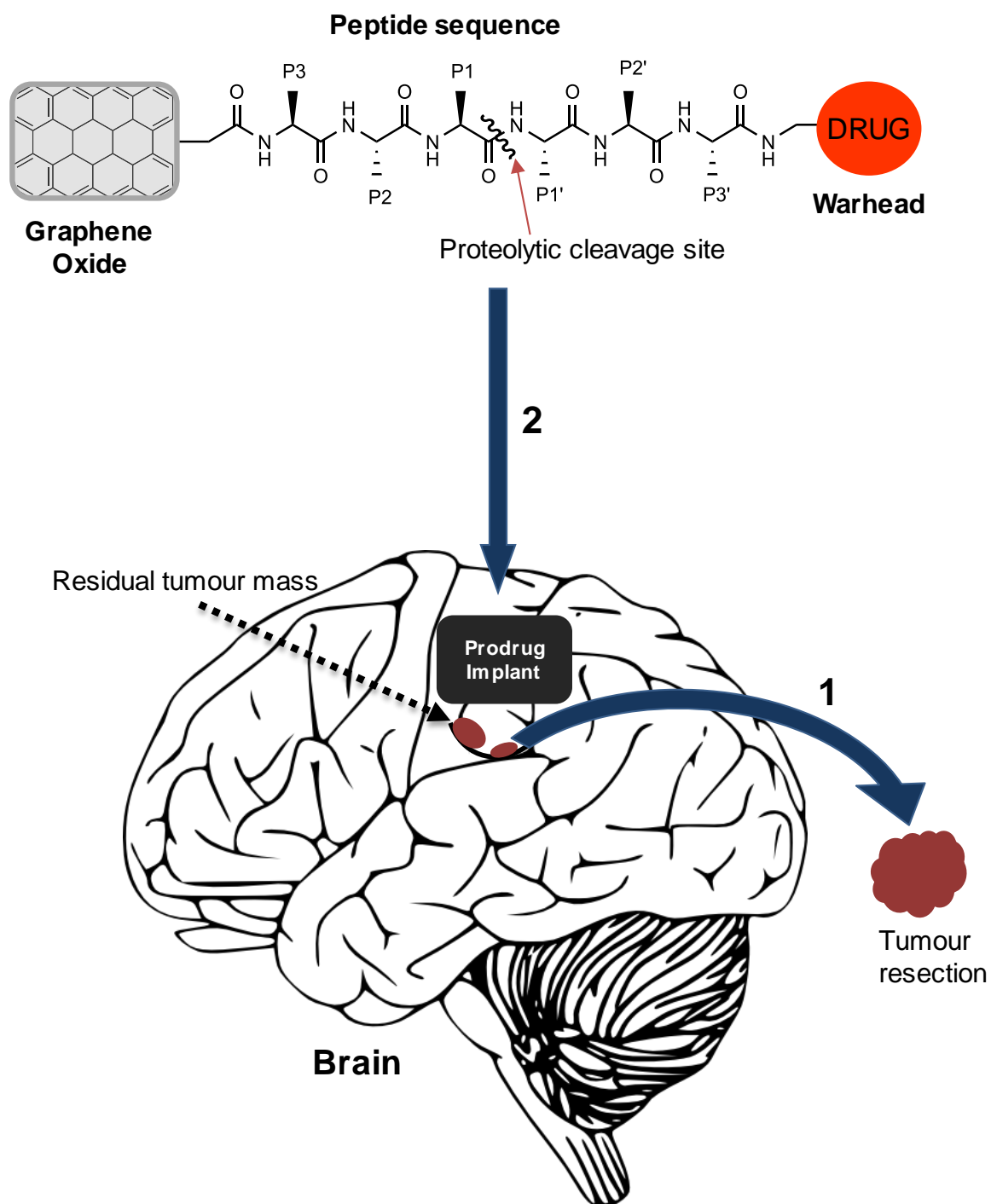
Figure V.15: Overview of therapeutic strategy. Post-operative introduction of Graphene-oxide 'tethered' MMP-activated prodrug

Chapter 6: Overall conclusion and discussion

Glioblastoma is one of the most aggressive human cancers. Despite recent advances in cancer biology and multimodality therapies, such as surgery, radiotherapy and chemotherapy, the outcome of patients with high grade glioma remains fatal.[312] A major limitation of current standard chemotherapeutics is their lack of tumour selectivity and consequent side effects, with inevitable glioma tumour recurrence within 30-32 weeks following surgery.[313] Rationalised drug design approaches represent an attempt to address this problem. This process involves the identification of tumour associated molecular targets followed by the assessment of their drugability and finally the design of tumour-selective therapies.[314] The main aims of this study was to assess the expression and activity of matrix metalloproteases in human glioma samples and preclinical glioma models, to examine substrate binding differences between homologues MMPs using *in silico* approaches, to rationally design anticancer prodrugs and evaluate MMP-mediated tumour-selective drug release, and finally to assess the conceivability of targeting tumour-specific MMPs with nanostructured anticancer prodrug implants of functionalised-graphene as a therapeutic strategy for localised drug delivery post glioma tumour resection.

MMPs are a family of zinc-dependent endoproteases with a causal and central role in cancer.[135] The overexpression and endoproteolytic activity of specific MMP members is a major contributor to tumour progression, invasion and metastasis, thus making them attractive targets for drug development. This study assessed the expression and activity profile of key MMPs in preclinical human glioma models; glioma and histologically normal brain samples. Significantly greater MMP-10 expression was observed in the analysed clinical samples of human gliomas

269

relative to histologically normal brain. Furthermore, MMP-10 gene expression as determined by RT-PCR was shown to display a strong correlation with the levels of active MMP-10 in preclinical models, suggesting a predominant role of MMP-10 in the growth and development of glioma tumours. Taken together, this data indicates that MMP-10 is overexpressed, proteolytically active and is a target for therapeutic intervention in human glioblastoma. Overexpression of MMP-10 has been shown in several malignancies including oral carcinoma, head and neck squamous cell carcinoma (HNSCC), skin cancer, oesophageal carcinoma and non-small cell lung carcinoma (NSCLC).[155, 223-226] However, the expression of MMP-10 protein in human glioblastoma had not been previously reported. To our knowledge, the present study is the first to address the overexpression and elevated proteolytic activity of MMP-10 in preclinical models of human glioma relative to normal glial cells.

Despite the involvement of MMP-10 in several human malignancies, the elucidation of therapeutics targeted against MMP-10 has remained unexplored and elusive. All MMPs share a marked structural similarity in their catalytic domains with MMP-3 and MMP-10 being the most homologous of the MMP family with 86% structural similarity.[271] The similarity in binding preferences and substrate complexity poses a significant problem in the generation of MMP subfamily selective prodrugs. A requirement for success in prodrug approaches is MMP selectivity through incorporation of MMP subtype selective peptide sequence and subsequence disease activation. In order to achieve this, reiterative approach using *in silico* proteolytic docking coupled to *in vitro* biochemical assessment methodology was employed. The available MMP X-ray crystal structures were carefully studied *in silico* and the substrate binding selectivity between close MMP

family homologues was analysed. The rationale for using a computer-aided drug design approach was to evaluate its potential as a guide to rationalise functional similarity between MMP catalytic domains for subsequent development of novel MMP-targeted prodrugs. The 3D-strutures of closely related MMP sub-families: gelatinases (MMP-2[268] and MMP-9[269]) and stromelysins (MMP-3[270] and MMP-10[271]) and their flexible docked complexes with MMP-substrates, provided valuable insights into the structural determinants of substrate selectivity of a particular MMP. According to the literature, M-2110 is hydrolysed rapidly by stromelysins and very slowly by MMP-9; whereas M-2055 is hydrolysed rapidly by MMP-9 and very slowly by gelatinase B (MMP-2) and stromelysins. The cleavage pattern reported in the literature[222] and observed via 3-D molecular docking (current study), demonstrated that MMP-9 strongly interacts with M-2055 at the Gly-Cys(Me) bond, and the present study confirmed this finding. However, the cleavage of this substrate by MMP-2 and Stromelysins is unknown. Based on 3-D molecular modelling and the respective zinc-chelation sites, it was predicted that MMP-2 interacts with the substrate at Gly-Cys(Me) bond and stromelysins interacts at Pro-β-cyclohexyl-Ala bond. This prediction data was experimentally confirmed by incubating M-2055 substrate with recombinant MMPs and analysing the cleaved metabolites via LCMS.

The cleavage of M-2110 reported in the literature[221] and observed in our 3-D molecular modelling indicated that stromelysins strongly interact with M-2110 at the Glu-Nva bond, which was confirmed by the *in vitro* cleavage assay. Again, as for the non-selective use of M-2110, the cleavage pattern of this substrate by MMP-9 is unknown/unreported. Based on 3-D molecular modelling and the respective zinc-chelation sites, it was predicted that MMP-9 interacts with the

substrate at the Pro-Val bond. This prediction was also experimentally confirmed highlighting that a suitable predictive model has been created for the determination of substrate cleavage sites by these MMPs.

This promising result demonstrated that it is possible to accurately predict the substrate binding differences between homologous MMPs without a substrate 'small molecule' crystal structure to guide molecular conformation. Furthermore, this approach proved to be of applicable value for the development of prodrugs to be selectively activated by specific MMP subtype such as MMP-10 and target tumours with the selective release of the chemotherapeutic agent.

In order to achieve MMP subtype selectivity, a known MMP-targeted peptide-prodrug of doxorubicin (Albright prodrug)[207, 285] was utilised as a template sequence as it is cleaved by MMP-2 and MMP-9 at the same subsite (Gly-Ser(OBenzyl)), presenting an excellent model for further modification. The *in silico* interaction of the Albright prodrug with MMP-2 and MMP-9 demonstrated zinc chelation between the known cleavage site, Gly and Ser(OBenzyl) bond, which was also confirmed by the *in vitro* cleavage assay with respective MMPs. However, the Albright prodrug also showed relatively weaker *in silico* interaction with MMP-3 and MMP-10 at a distinctive unknown subsite Ser(OBenzyl)–Tyr. The *in vitro* assessment confirmed cleavage of prodrug by MMP-3 and MMP-10 at the predicted subsite, supporting the predictability of the *in silico* model of anticancer prodrugs and providing a suitable template for the exploitation of MMP binding subsites and rational modification of peptide residues to produce prodrugs selective for specific MMP subtypes. Initial efforts focused on exploiting the

differences in peptide selectivity between homologous MMPs to produce a prodrug, termed MJ02, selective for MMP-2 and MMP-10, over MMP-3 and MMP-9. Based on the MMP-2/MMP-9 cleavage site, Gly-Ser(OBenzyl), rational design of a peptide sequence selective for MMP-2 over MMP-9 was achieved by incorporating residues into the peptide chain to fit S1, S2, S3 and S1' pockets of MMP-2 which differed in size and polar affinity compared to MMP-9. Modifications such as aromatic residue homophenylalanine (Hof) in S1 subsite, acidic residue Glu in S2 subsite, polar side chain Gln at S3 subsite and small nonpolar residue Leu in S1' subsite were incorporated. Similarly, based on the MMP-3/MMP-10 cleavage site, Ser(OBenzyl)-Tyr, in the 'Albright prodrug' the replacements of the P1 Ser(OBenzyl) with a Glu residue, P2 Gly with a Gln residue, P5 Glu with a Gly residue and P1' Tyr with a Hof residue, were induced to achieve MMP-10 selectivity over MMP-3. In spite of identical substrate selectivity of MMP-3 and MMP-10,[271] there were subtle but significant binding differences between the two. The difference in S2 and S3 pockets were important in rationalising the peptide selectivity between the two stromelysins. The modified peptide sequence demonstrated strong *in silico* zinc interaction with MMP-2 at the Hof-Leu bond, and with MMP-10 at the Glu-Hof bond, indicating the predicted cleavage sites. The interaction of peptide sequence was not detectable in MMP-3 and MMP-9, suggesting the modified peptide residues should give selectivity for MMP-2 and MMP-10, over MMP-3 and MMP-9. In order to confirm the *in vitro* prediction and assess the preferential MMP-selective activation, a rationally designed peptide conjugated prodrug, MJ02, was synthesised via solid phase chemistry with the chemotherapeutic drug doxorubicin conjugated to the C-terminus and the Cbz non-polar endcap linked to the N-terminus of the peptide. Both MMP-2 and MMP-

10 recombinant enzymes induced cleavage of MJ02, with cleavage occurring at the predicted subsites. Conversely, no MJ02 activation was observed by MMP-3 and MMP-9, indicating that MJ02 is MMP-2 and MMP-10 selective supporting the *in silico* prediction. The prodrug also displayed differentials in cytotoxicity and ability to metabolise between MMP positive glioma cell lines (U87-MG and 1321N1) and MMP-negative normal glial cell line (SVG-P12). Furthermore, MJ02 remained inactive in the presence of pan-MMP inhibitor, demonstrating MMP-selective action of this prodrug. However, MJ02 was metabolised slowly by both glioma and normal brain cell lines, in the presence of MMP-10 selective inhibitor, suggesting the involvement of MMP-2 in MJ02 metabolism, as evidenced by high proteolytic activity of MMP-2 in all the brain tumour and normal brain cells. The successful rationalised computer-aided development of MJ02 in this project provided valuable understanding for the progress towards specific investigation in the development of MMP-10 selective prodrug (rationally designed by Dr. Jonathan Harburn).

Even though strategies were directed towards MMP-10 selectivity for prodrug design, understanding and attainment of MMP-subtype selectivity, possessed by MJ02, was important because it allowed for a first-hand detailed exploitation of the differences within the same MMP subfamily. To achieve MMP-10 selectivity, efforts focused on utilising the *in silico* docked complexes of MJ02 and MMPs as a reference to engineer-out selectivity of close family homologues i.e. MMP-3 and gelatinases. However, in the process of retaining MMP-10 selectivity, other MMP members also demonstrated marginal selectivity. Therefore, focus shifted towards exploiting the docked complexes of M-2110 fluorescent substrate and MMPs. The peptide sequence of M-2110 was modified towards MMP-10 selectivity by

incorporating residues to fit the specificity pockets of MMP-10; but prevent binding with MMP-2, MMP-9 and MMP-3. Using the MMP-3/MMP-10 cleavage site, Glu-Nva, of M-2110 substrate; the replacements of the P2 Val with a Leu residue, P3 Pro with a D-Pro residue, P1' Nva with a His residue and P2' Trp with a Leu residue, were induced to achieve MMP-10 selectivity over other MMPs. The design of a peptide prodrug selective for MMP-10, termed MJ04, over MMP-3 (the closest MMP subfamily with 86% structural similarity) has yet been unreported and is the first study to our knowledge, to describe detailed differences between MMP-10 and MMP-3 binding subsites.

The MMP-10 targeted prodrug of doxorubicin, MJ04, displayed preferential cleavage by recombinant MMP-10 at the predicted subsite, but displayed no cleavage by recombinant MMP-2, MMP-3 and MMP-9; thus confirming the *in silico* prediction. The assessment of MJ04 metabolism in preclinical cell models demonstrated rapid metabolism by MMP-10 positive U87-MG cell line compared to MMP-10 negative SVG-P12 cell line. Crucially, using MJ04 to release Leu-Dox resulted in a greatly reduced exposure of SVG-P12 normal glial cell line to the Leu-Dox intermediate, thus suggesting an increased therapeutic index compared to MJ02. The metabolism of MJ04 was 2-fold slower (or negligible) in SVG-P12 cell line compared to MJ02.

Whilst these cell lines were selected for preclinical prodrug screening based on their differential levels of MMP expression, it would be worthwhile undertaking a more extensive screen of brain tumour xenograft models to allow for the selection of glioblastoma model systems for drug screening. If the progress and direction of this project could have been predicted from the outset, it would have been of great

value to produce fluorescently labelled substrates of these rationally designed peptides where the efficiency of MMP-mediated cleavage could be analysed by enzyme kinetics. The MMP-10 selective prodrug could prove potentially useful in the selective targeting of many cancers including glioblastoma, where MMP-10 is overexpressed and proteolytically active relative to normal surrounding tissues. It could also provide a valuable template for development of MMP-10 selective inhibitors and peptide probes for advanced diagnostic and prognostic applications.

With regards to glioblastoma, the systemic delivery of therapeutics has been a disadvantageous with poor outcome because of the limitations imposed by the blood brain barrier (BBB). Even with the application of localised post-surgical BCNU (Gliadel) wafers have proven ineffective in many cases because of lack of tumour-selective drug targeting with neurological side effects. In order to circumvent this problem, the final part of this study was aimed at developing nanostructured graphene oxide (GO)-tethered prodrug implants. With overexpression of specific MMPs in the glioma tumour microenvironment, the prodrugs conjugated to a stable "base" can get activated by tumour-associated MMPs and target the tumour selectively. This study was carried out only on a small scale to prove the *in vitro* application. The GO-conjugated prodrug (MJ06) was derived from MJ02 peptide sequence with GO sheets as the endcap and doxorubicin as the chemotherapeutic agent. MJ06 preparation underwent several washing steps to remove non-conjugated peptide impurities. Since the detection of GO material was difficult on LCMS due to size restrictions, only the 2nd half of the cleaved MMP-metabolites were detectable, whereas the first half linked to the GO was undetectable. A promising outcome from the *in vitro* cleavage assay was that MJ06 demonstrated cleavage by both MMP-2 and MMP-10 at the predicted

subsites. However this study faced shortcomings in examining whether the prodrug was chemically conjugated to the GO as a covalent bond or was it in fact only adsorbed or adhered on the surface. Non-chemical linkage of prodrug on GO is insufficient in tumour environment because the free non-conjugated N-terminus of the prodrug is prone to non-selective hydrolysis by exoproteases and subsequence release of toxic chemotherapeutic agent targeting the normal cells. Therefore it would be important to convincingly elucidate the type of conjugation between GO and the prodrug, before evaluating its potential for glioma targeted therapy. Our research team believed that the characterisation and development of GO-prodrug implants could become part of future research projects extensively concentrating on localised targeted therapy of cancers such as glioblastoma.

Following successful development and validation of GO-prodrug implants, this therapeutic can be implanted in the tumour resected site of glioblastoma to halt its recurrence. This localised prodrug-implant strategy could lead to dose intensification at the tumour site, avoid the accumulation of prodrug in the surrounding tissues, result in reduced side-effects and potentially improve the success rate of glioblastoma.

References

1. Lengauer, C.; Kinzler, K. W.; Vogelstein, B. Genetic instabilities in human cancers. *Nature* **1998,** 396, 643-649.

2. Bertram, J. S. The molecular biology of cancer. *Mol Aspects Med* **2000,** 21, 167-223.

3. Hanahan, D.; Weinberg, R. A. Hallmarks of cancer: the next generation. *Cell* **2011,** 144, 646-74.

4. Hanahan, D.; Weinberg, R. A. The hallmarks of cancer. *Cell* **2000,** 100, 57-70.

5. Kirsch, M.; Schackert, G.; Black, P. M. Metastasis and angiogenesis. *Cancer Treat Res* **2004,** 117, 285-304.

6. Folkman, J. Role of angiogenesis in tumor growth and metastasis. *Semin Oncol* **2002,** 29, 15-8.

7. Zetter, B. R. Angiogenesis and tumor metastasis. *Annu Rev Med* **1998,** 49, 407-24.

8. Meyer, T.; Hart, I. R. Mechanisms of tumour metastasis. *European Journal of Cancer* **1998,** 34, 214-221.

9. Martinez, J. D.; Parker, M. T.; Fultz, K. E.; Ignatenko, N. A.; Gerner, E. W. Molecular Biology of Cancer. In *Burger's Medicinal Chemistry and Drug Discovery*, John Wiley & Sons, Inc.: 2003.

10. Friedl, P.; Wolf, K. Tube travel: the role of proteases in individual and collective cancer cell invasion. *Cancer Res* **2008,** 68, 7247-9.

11. Yong, V. W.; Krekoski, C. A.; Forsyth, P. A.; Bell, R.; Edwards, D. R. Matrix metalloproteinases and diseases of the CNS. *Trends Neurosci* **1998,** 21, 75-80.

12.	Louis, D. N.; Ohgaki, H.; Wiestler, O. D.; Cavenee, W. K.; Burger, P. C.; Jouvet, A.; Scheithauer, B. W.; Kleihues, P. The 2007 WHO Classification of Tumours of the Central Nervous System. *Acta Neuropathol* **2007,** 114, 97-109.

13.	Hemmati, H. D.; Nakano, I.; Lazareff, J. A.; Masterman-Smith, M.; Geschwind, D. H.; Bronner-Fraser, M.; Kornblum, H. I. Cancerous stem cells can arise from pediatric brain tumors. *Proceedings of the National Academy of Sciences* **2003,** 100, 15178-15183.

14.	Riemenschneider, M. J.; Reifenberger, G. Molecular Neuropathology of Gliomas. *Int J Mol Sci* **2009,** 10, 184-212.

15.	Louis, D. N. Molecular pathology of malignant gliomas. *Annu Rev Pathol* **2006,** 1, 97-117.

16.	Miller, C. R.; Perry, A. Glioblastoma. *Arch Pathol Lab Med* **2007,** 131, 397-406.

17.	Hatanpaa, K. J.; Burma, S.; Zhao, D.; Habib, A. A. Epidermal Growth Factor Receptor in Glioma: Signal Transduction, Neuropathology, Imaging, and Radioresistance. *Neoplasia* **2010,** 12, 675-84.

18.	Shinojima, N.; Tada, K.; Shiraishi, S.; Kamiryo, T.; Kochi, M.; Nakamura, H.; Makino, K.; Saya, H.; Hirano, H.; Kuratsu, J.-i.; Oka, K.; Ishimaru, Y.; Ushio, Y. Prognostic Value of Epidermal Growth Factor Receptor in Patients with Glioblastoma Multiforme. *Cancer Research* **2003,** 63, 6962-6970.

19.	Yamasaki, F.; Kurisu, K.; Satoh, K.; Arita, K.; Sugiyama, K.; Ohtaki, M.; Takaba, J.; Tominaga, A.; Hanaya, R.; Yoshioka, H.; Hama, S.; Ito, Y.; Kajiwara, Y.; Yahara, K.; Saito, T.; Thohar, M. A. Apparent diffusion coefficient of human brain tumors at MR imaging. *Radiology* **2005,** 235, 985-91.

20.   Schulte, A.; Liffers, K.; Kathagen, A.; Riethdorf, S.; Zapf, S.; Merlo, A.; Kolbe, K.; Westphal, M.; Lamszus, K. Erlotinib resistance in EGFR-amplified glioblastoma cells is associated with upregulation of EGFRvIII and PI3Kp110delta. *Neuro Oncol* **2013,** 15, 1289-301.

21.   Heimberger, A. B.; Hlatky, R.; Suki, D.; Yang, D.; Weinberg, J.; Gilbert, M.; Sawaya, R.; Aldape, K. Prognostic effect of epidermal growth factor receptor and EGFRvIII in glioblastoma multiforme patients. *Clin Cancer Res* **2005,** 11, 1462-6.

22.   England, B.; Huang, T.; Karsy, M. Current understanding of the role and targeting of tumor suppressor p53 in glioblastoma multiforme. *Tumour Biol* **2013,** 34, 2063-74.

23.   Sidransky, D.; Mikkelsen, T.; Schwechheimer, K.; Rosenblum, M. L.; Cavanee, W.; Vogelstein, B. Clonal expansion of p53 mutant cells is associated with brain tumour progression. *Nature* **1992,** 355, 846-7.

24.   Burton, E. C.; Lamborn, K. R.; Forsyth, P.; Scott, J.; O'Campo, J.; Uyehara-Lock, J.; Prados, M.; Berger, M.; Passe, S.; Uhm, J.; O'Neill, B. P.; Jenkins, R. B.; Aldape, K. D. Aberrant p53, mdm2, and proliferation differ in glioblastomas from long-term compared with typical survivors. *Clin Cancer Res* **2002,** 8, 180-7.

25.   Kim, S. S.; Rait, A.; Kim, E.; Pirollo, K. F.; Nishida, M.; Farkas, N.; Dagata, J. A.; Chang, E. H. A nanoparticle carrying the p53 gene targets tumors including cancer stem cells, sensitizes glioblastoma to chemotherapy and improves survival. *ACS Nano* **2014,** 8, 5494-514.

26.   Srividya, M. R.; Thota, B.; Shailaja, B. C.; Arivazhagan, A.; Thennarasu, K.; Chandramouli, B. A.; Hegde, A. S.; Santosh, V. Homozygous 10q23/PTEN deletion and its impact on outcome in glioblastoma: a prospective translational

study on a uniformly treated cohort of adult patients. *Neuropathology* **2011,** 31, 376-83.

27. Groszer, M.; Erickson, R.; Scripture-Adams, D. D.; Dougherty, J. D.; Le Belle, J.; Zack, J. A.; Geschwind, D. H.; Liu, X.; Kornblum, H. I.; Wu, H. PTEN negatively regulates neural stem cell self-renewal by modulating G0-G1 cell cycle entry. *Proc Natl Acad Sci U S A* **2006,** 103, 111-6.

28. Xu, J.; Li, Z.; Wang, J.; Chen, H.; Fang, J. Y. Combined PTEN Mutation and Protein Expression Associate with Overall and Disease-Free Survival of Glioblastoma Patients. *Transl Oncol* **2014,** 7, 196-205.e1.

29. Noell, S.; Ritz, R.; Wolburg-Buchholz, K.; Wolburg, H.; Fallier-Becker, P. An allograft glioma model reveals the dependence of aquaporin-4 expression on the brain microenvironment. *PLoS One* **2012,** 7, e36555.

30. Daumas-Duport, C.; Scheithauer, B.; O'Fallon, J.; Kelly, P. Grading of astrocytomas. A simple and reproducible method. *Cancer* **1988,** 62, 2152-65.

31. Takano, S.; Yamashita, T.; Ohneda, O. Molecular therapeutic targets for glioma angiogenesis. *J Oncol* **2010,** 2010, 351908.

32. Dvorak, H. F. Rous-Whipple Award Lecture. How tumors make bad blood vessels and stroma. *Am J Pathol* **2003,** 162, 1747-57.

33. Bergers, G.; Benjamin, L. E. Tumorigenesis and the angiogenic switch. *Nat Rev Cancer* **2003,** 3, 401-10.

34. Shweiki, D.; Itin, A.; Soffer, D.; Keshet, E. Vascular endothelial growth factor induced by hypoxia may mediate hypoxia-initiated angiogenesis. *Nature* **1992,** 359, 843-5.

35.   Alves, T. R.; Lima, F. R.; Kahn, S. A.; Lobo, D.; Dubois, L. G.; Soletti, R.; Borges, H.; Neto, V. M. Glioblastoma cells: a heterogeneous and fatal tumor interacting with the parenchyma. *Life Sci* **2011,** 89, 532-9.

36.   van Tellingen, O.; Yetkin-Arik, B.; de Gooijer, M. C.; Wesseling, P.; Wurdinger, T.; de Vries, H. E. Overcoming the blood-brain tumor barrier for effective glioblastoma treatment. *Drug Resist Updat* **2015,** 19, 1-12.

37.   Westhouse, R. A. Safety assessment considerations and strategies for targeted small molecule cancer therapeutics in drug discovery. *Toxicol Pathol* **2010,** 38, 165-8.

38.   Walker, I.; Newell, H. Do molecularly targeted agents in oncology have reduced attrition rates? *Nat Rev Drug Discov* **2009,** 8, 15-6.

39.   Pardridge, W. M. The blood-brain barrier: bottleneck in brain drug development. *NeuroRx* **2005,** 2, 3-14.

40.   Pardridge, W. M. Drug transport across the blood-brain barrier. *J Cereb Blood Flow Metab* **2012,** 32, 1959-72.

41.   Pardridge, W. M. CSF, blood-brain barrier, and brain drug delivery. *Expert Opin Drug Deliv* **2016,** 13, 963-75.

42.   Sage, M. R.; Wilson, A. J.; Scroop, R. Contrast media and the brain. The basis of CT and MR imaging enhancement. *Neuroimaging Clin N Am* **1998,** 8, 695-707.

43.   Sage, M. R.; Wilson, A. J. The blood-brain barrier: an important concept in neuroimaging. *AJNR Am J Neuroradiol* **1994,** 15, 601-22.

44.   Larsson, H. B.; Stubgaard, M.; Frederiksen, J. L.; Jensen, M.; Henriksen, O.; Paulson, O. B. Quantitation of blood-brain barrier defect by magnetic

resonance imaging and gadolinium-DTPA in patients with multiple sclerosis and brain tumors. *Magn Reson Med* **1990,** 16, 117-31.

45.   Abbott, N. J.; Ronnback, L.; Hansson, E. Astrocyte-endothelial interactions at the blood-brain barrier. *Nat Rev Neurosci* **2006,** 7, 41-53.

46.   Alvarez, J. I.; Katayama, T.; Prat, A. Glial influence on the blood brain barrier. *Glia* **2013,** 61, 1939-58.

47.   Obermeier, B.; Daneman, R.; Ransohoff, R. M. Development, maintenance and disruption of the blood-brain barrier. *Nature medicine* **2013,** 19, 1584-96.

48.   Daneman, R.; Zhou, L.; Kebede, A. A.; Barres, B. A. Pericytes are required for blood-brain barrier integrity during embryogenesis. *Nature* **2010,** 468, 562-6.

49.   Mizee, M. R.; de Vries, H. E. Blood-brain barrier regulation: Environmental cues controlling the onset of barrier properties. *Tissue Barriers* **2013,** 1, e26882.

50.   Liebner, S.; Corada, M.; Bangsow, T.; Babbage, J.; Taddei, A.; Czupalla, C. J.; Reis, M.; Felici, A.; Wolburg, H.; Fruttiger, M.; Taketo, M. M.; von Melchner, H.; Plate, K. H.; Gerhardt, H.; Dejana, E. Wnt/beta-catenin signaling controls development of the blood-brain barrier. *J Cell Biol* **2008,** 183, 409-17.

51.   Daneman, R.; Agalliu, D.; Zhou, L.; Kuhnert, F.; Kuo, C. J.; Barres, B. A. Wnt/beta-catenin signaling is required for CNS, but not non-CNS, angiogenesis. *Proc Natl Acad Sci U S A* **2009,** 106, 641-6.

52.   Alvarez, J. I.; Dodelet-Devillers, A.; Kebir, H.; Ifergan, I.; Fabre, P. J.; Terouz, S.; Sabbagh, M.; Wosik, K.; Bourbonniere, L.; Bernard, M.; van Horssen, J.; de Vries, H. E.; Charron, F.; Prat, A. The Hedgehog pathway promotes blood-brain barrier integrity and CNS immune quiescence. *Science (New York, N.Y.)* **2011,** 334, 1727-31.

53. Rascher, G.; Fischmann, A.; Kroger, S.; Duffner, F.; Grote, E. H.; Wolburg, H. Extracellular matrix and the blood-brain barrier in glioblastoma multiforme: spatial segregation of tenascin and agrin. *Acta Neuropathol* **2002,** 104, 85-91.

54. Tamai, I.; Tsuji, A. Transporter-mediated permeation of drugs across the blood-brain barrier. *J Pharm Sci* **2000,** 89, 1371-88.

55. Cuddapah, V. A.; Robel, S.; Watkins, S.; Sontheimer, H. A neurocentric perspective on glioma invasion. *Nat Rev Neurosci* **2014,** 15, 455-465.

56. Zlokovic, B. V. Remodeling after stroke. *Nature medicine* **2006,** 12, 390-1.

57. Jones, P. M.; George, A. M. The ABC transporter structure and mechanism: perspectives on recent research. *Cell Mol Life Sci* **2004,** 61, 682-99.

58. Begley, D. J.; Brightman, M. W. Structural and functional aspects of the blood-brain barrier. *Prog Drug Res* **2003,** 61, 39-78.

59. Abbott, N. J.; Patabendige, A. A.; Dolman, D. E.; Yusof, S. R.; Begley, D. J. Structure and function of the blood-brain barrier. *Neurobiol Dis* **2010,** 37, 13-25.

60. Wolburg, H.; Lippoldt, A. Tight junctions of the blood-brain barrier: development, composition and regulation. *Vascul Pharmacol* **2002,** 38, 323-37.

61. Nagelhus, E. A.; Mathiisen, T. M.; Ottersen, O. P. Aquaporin-4 in the central nervous system: cellular and subcellular distribution and coexpression with KIR4.1. *Neuroscience* **2004,** 129, 905-13.

62. Verkman, A. S.; Anderson, M. O.; Papadopoulos, M. C. Aquaporins: important but elusive drug targets. *Nat Rev Drug Discov* **2014,** 13, 259-77.

63. Hunter, D. D.; Llinas, R.; Ard, M.; Merlie, J. P.; Sanes, J. R. Expression of s-laminin and laminin in the developing rat central nervous system. *J Comp Neurol* **1992,** 323, 238-51.

64.   Barber, A. J.; Lieth, E. Agrin accumulates in the brain microvascular basal lamina during development of the blood-brain barrier. *Dev Dyn* **1997,** 208, 62-74.

65.   Sanes, J. R.; Engvall, E.; Butkowski, R.; Hunter, D. D. Molecular heterogeneity of basal laminae: isoforms of laminin and collagen IV at the neuromuscular junction and elsewhere. *J Cell Biol* **1990,** 111, 1685-99.

66.   Ambudkar, S. V.; Lelong, I. H.; Zhang, J.; Cardarelli, C. O.; Gottesman, M. M.; Pastan, I. Partial purification and reconstitution of the human multidrug-resistance pump: characterization of the drug-stimulatable ATP hydrolysis. *Proc Natl Acad Sci U S A* **1992,** 89, 8472-6.

67.   Thiebaut, F.; Tsuruo, T.; Hamada, H.; Gottesman, M. M.; Pastan, I.; Willingham, M. C. Cellular localization of the multidrug-resistance gene product P-glycoprotein in normal human tissues. *Proc Natl Acad Sci U S A* **1987,** 84, 7735-8.

68.   Fung, K. L.; Pan, J.; Ohnuma, S.; Lund, P. E.; Pixley, J. N.; Kimchi-Sarfaty, C.; Ambudkar, S. V.; Gottesman, M. M. MDR1 synonymous polymorphisms alter transporter specificity and protein stability in a stable epithelial monolayer. *Cancer Res* **2014,** 74, 598-608.

69.   Bertossi, M.; Virgintino, D.; Maiorano, E.; Occhiogrosso, M.; Roncali, L. Ultrastructural and morphometric investigation of human brain capillaries in normal and peritumoral tissues. *Ultrastruct Pathol* **1997,** 21, 41-9.

70.   Hirano, A.; Matsui, T. Vascular structures in brain tumors. *Hum Pathol* **1975,** 6, 611-21.

71.   Wolburg, H.; Wolburg-Buchholz, K.; Kraus, J.; Rascher-Eggstein, G.; Liebner, S.; Hamm, S.; Duffner, F.; Grote, E. H.; Risau, W.; Engelhardt, B. Localization of claudin-3 in tight junctions of the blood-brain barrier is selectively

lost during experimental autoimmune encephalomyelitis and human glioblastoma multiforme. *Acta Neuropathol* **2003,** 105, 586-92.

72.   Liu, H. L.; Hua, M. Y.; Chen, P. Y.; Chu, P. C.; Pan, C. H.; Yang, H. W.; Huang, C. Y.; Wang, J. J.; Yen, T. C.; Wei, K. C. Blood-brain barrier disruption with focused ultrasound enhances delivery of chemotherapeutic drugs for glioblastoma treatment. *Radiology* **2010,** 255, 415-25.

73.   Warth, A.; Kroger, S.; Wolburg, H. Redistribution of aquaporin-4 in human glioblastoma correlates with loss of agrin immunoreactivity from brain capillary basal laminae. *Acta Neuropathol* **2004,** 107, 311-8.

74.   Pastan, I.; Gottesman, M. M. Multidrug resistance. *Annu Rev Med* **1991,** 42, 277-86.

75.   Juliano, R. L.; Ling, V. A surface glycoprotein modulating drug permeability in Chinese hamster ovary cell mutants. *Biochimica et biophysica acta* **1976,** 455, 152-62.

76.   Deeken, J. F.; Loscher, W. The blood-brain barrier and cancer: transporters, treatment, and Trojan horses. *Clin Cancer Res* **2007,** 13, 1663-74.

77.   Cheshier, S. H.; Kalani, M. Y.; Lim, M.; Ailles, L.; Huhn, S. L.; Weissman, I. L. A neurosurgeon's guide to stem cells, cancer stem cells, and brain tumor stem cells. *Neurosurgery* **2009,** 65, 237-49; discussion 249-50; quiz N6.

78.   Gladson, C. L. Expression of integrin alpha v beta 3 in small blood vessels of glioblastoma tumors. *J Neuropathol Exp Neurol* **1996,** 55, 1143-9.

79.   Candelario-Jalil, E.; Yang, Y.; Rosenberg, G. A. Diverse roles of matrix metalloproteinases and tissue inhibitors of metalloproteinases in neuroinflammation and cerebral ischemia. *Neuroscience* **2009,** 158, 983-94.

80. Hardee, M. E.; Zagzag, D. Mechanisms of Glioma-Associated Neovascularization. *Am J Pathol* **2012,** 181, 1126-41.

81. Plate, K. H.; Scholz, A.; Dumont, D. J. Tumor angiogenesis and anti-angiogenic therapy in malignant gliomas revisited. *Acta Neuropathol* **2012,** 124, 763-75.

82. Korfel, A.; Thiel, E. Targeted Therapy and Blood-Brain Barrier. In *Targeted Therapies in Cancer*, Dietel, M., Ed. Springer Berlin Heidelberg: Berlin, Heidelberg, 2007; pp 123-133.

83. Juillerat-Jeanneret, L. The targeted delivery of cancer drugs across the blood-brain barrier: chemical modifications of drugs or drug-nanoparticles? *Drug Discov Today* **2008,** 13, 1099-106.

84. Nishio, S.; Ohta, M.; Abe, M.; Kitamura, K. Microvascular abnormalities in ethylnitrosourea (ENU)-induced rat brain tumors: structural basis for altered blood-brain barrier function. *Acta Neuropathol* **1983,** 59, 1-10.

85. Ningaraj, N. S.; Rao, M.; Hashizume, K.; Asotra, K.; Black, K. L. Regulation of blood-brain tumor barrier permeability by calcium-activated potassium channels. *J Pharmacol Exp Ther* **2002,** 301, 838-51.

86. Lin, F.; de Gooijer, M. C.; Roig, E. M.; Buil, L. C.; Christner, S. M.; Beumer, J. H.; Wurdinger, T.; Beijnen, J. H.; van Tellingen, O. ABCB1, ABCG2, and PTEN determine the response of glioblastoma to temozolomide and ABT-888 therapy. *Clin Cancer Res* **2014,** 20, 2703-13.

87. Stupp, R.; Mason, W. P.; van den Bent, M. J.; Weller, M.; Fisher, B.; Taphoorn, M. J.; Belanger, K.; Brandes, A. A.; Marosi, C.; Bogdahn, U.; Curschmann, J.; Janzer, R. C.; Ludwin, S. K.; Gorlia, T.; Allgeier, A.; Lacombe, D.; Cairncross, J. G.; Eisenhauer, E.; Mirimanoff, R. O. Radiotherapy plus

concomitant and adjuvant temozolomide for glioblastoma. *N Engl J Med* **2005,** 352, 987-96.

88.   Keles, G. E.; Anderson, B.; Berger, M. S. The effect of extent of resection on time to tumor progression and survival in patients with glioblastoma multiforme of the cerebral hemisphere. *Surg Neurol* **1999,** 52, 371-9.

89.   Stupp, R.; Hegi, M. E.; Gilbert, M. R.; Chakravarti, A. Chemoradiotherapy in malignant glioma: standard of care and future directions. *Journal of clinical oncology : official journal of the American Society of Clinical Oncology* **2007,** 25, 4127-36.

90.   Hegi, M. E.; Diserens, A. C.; Gorlia, T.; Hamou, M. F.; de Tribolet, N.; Weller, M.; Kros, J. M.; Hainfellner, J. A.; Mason, W.; Mariani, L.; Bromberg, J. E.; Hau, P.; Mirimanoff, R. O.; Cairncross, J. G.; Janzer, R. C.; Stupp, R. MGMT gene silencing and benefit from temozolomide in glioblastoma. *N Engl J Med* **2005,** 352, 997-1003.

91.   Esteller, M.; Garcia-Foncillas, J.; Andion, E.; Goodman, S. N.; Hidalgo, O. F.; Vanaclocha, V.; Baylin, S. B.; Herman, J. G. Inactivation of the DNA-repair gene MGMT and the clinical response of gliomas to alkylating agents. *N Engl J Med* **2000,** 343, 1350-4.

92.   Villalva, C.; Cortes, U.; Wager, M.; Tourani, J. M.; Rivet, P.; Marquant, C.; Martin, S.; Turhan, A. G.; Karayan-Tapon, L. O6-Methylguanine-methyltransferase (MGMT) promoter methylation status in glioma stem-like cells is correlated to temozolomide sensitivity under differentiation-promoting conditions. *Int J Mol Sci* **2012,** 13, 6983-94.

93.   Beier, D.; Rohrl, S.; Pillai, D. R.; Schwarz, S.; Kunz-Schughart, L. A.; Leukel, P.; Proescholdt, M.; Brawanski, A.; Bogdahn, U.; Trampe-Kieslich, A.;

Giebel, B.; Wischhusen, J.; Reifenberger, G.; Hau, P.; Beier, C. P. Temozolomide preferentially depletes cancer stem cells in glioblastoma. *Cancer Res* **2008,** 68, 5706-15.

94.   Wick, A.; Pascher, C.; Wick, W.; Jauch, T.; Weller, M.; Bogdahn, U.; Hau, P. Rechallenge with temozolomide in patients with recurrent gliomas. *J Neurol* **2009,** 256, 734-41.

95.   Kleinberg, L. Polifeprosan 20, 3.85% carmustine slow release wafer in malignant glioma: patient selection and perspectives on a low-burden therapy. *Patient Prefer Adherence* **2016,** 10, 2397-2406.

96.   Westphal, M.; Hilt, D. C.; Bortey, E.; Delavault, P.; Olivares, R.; Warnke, P. C.; Whittle, I. R.; Jaaskelainen, J.; Ram, Z. A phase 3 trial of local chemotherapy with biodegradable carmustine (BCNU) wafers (Gliadel wafers) in patients with primary malignant glioma. *Neuro Oncol* **2003,** 5, 79-88.

97.   Valtonen, S.; Timonen, U.; Toivanen, P.; Kalimo, H.; Kivipelto, L.; Heiskanen, O.; Unsgaard, G.; Kuurne, T. Interstitial chemotherapy with carmustine-loaded polymers for high-grade gliomas: a randomized double-blind study. *Neurosurgery* **1997,** 41, 44-8; discussion 48-9.

98.   Brem, H.; Piantadosi, S.; Burger, P. C.; Walker, M.; Selker, R.; Vick, N. A.; Black, K.; Sisti, M.; Brem, S.; Mohr, G.; et al. Placebo-controlled trial of safety and efficacy of intraoperative controlled delivery by biodegradable polymers of chemotherapy for recurrent gliomas. The Polymer-brain Tumor Treatment Group. *Lancet* **1995,** 345, 1008-12.

99.   Brem, H.; Ewend, M. G.; Piantadosi, S.; Greenhoot, J.; Burger, P. C.; Sisti, M. The safety of interstitial chemotherapy with BCNU-loaded polymer followed by

radiation therapy in the treatment of newly diagnosed malignant gliomas: phase I trial. *J Neurooncol* **1995,** 26, 111-23.

100.   Westphal, M.; Ram, Z.; Riddle, V.; Hilt, D.; Bortey, E. Gliadel wafer in initial surgery for malignant glioma: long-term follow-up of a multicenter controlled trial. *Acta Neurochir (Wien)* **2006,** 148, 269-75; discussion 275.

101.   De Bonis, P.; Anile, C.; Pompucci, A.; Fiorentino, A.; Balducci, M.; Chiesa, S.; Maira, G.; Mangiola, A. Safety and efficacy of Gliadel wafers for newly diagnosed and recurrent glioblastoma. *Acta Neurochir (Wien)* **2012,** 154, 1371-8.

102.   Bota, D. A.; Desjardins, A.; Quinn, J. A.; Affronti, M. L.; Friedman, H. S. Interstitial chemotherapy with biodegradable BCNU (Gliadel) wafers in the treatment of malignant gliomas. *Ther Clin Risk Manag* **2007,** 3, 707-15.

103.   Fleming, A. B.; Saltzman, W. M. Pharmacokinetics of the carmustine implant. *Clin Pharmacokinet* **2002,** 41, 403-19.

104.   Palanichamy, K.; Erkkinen, M.; Chakravarti, A. Predictive and prognostic markers in human glioblastomas. *Curr Treat Options Oncol* **2006,** 7, 490-504.

105.   Carlsson, S. K.; Brothers, S. P.; Wahlestedt, C. Emerging treatment strategies for glioblastoma multiforme. *EMBO Mol Med* **2014,** 6, 1359-70.

106.   Ferrara, N.; Hillan, K. J.; Novotny, W. Bevacizumab (Avastin), a humanized anti-VEGF monoclonal antibody for cancer therapy. *Biochem Biophys Res Commun* **2005,** 333, 328-35.

107.   Hosokawa, T.; Tokita, H.; Matsuyama, T.; Sakamoto, K.; Nishida, K.; Iwao, Y.; Koshiishi, H.; Okamura, T.; Koshinaga, T. [Two cases of venous thrombosis confirmed during the bevacizumab combination chemotherapy for colorectal cancer]. *Gan To Kagaku Ryoho* **2010,** 37, 2520-2.

108.   Hamblett, K. J.; Kozlosky, C. J.; Siu, S.; Chang, W. S.; Liu, H.; Foltz, I. N.; Trueblood, E. S.; Meininger, D.; Arora, T.; Twomey, B.; Vonderfecht, S. L.; Chen, Q.; Hill, J. S.; Fanslow, W. C. AMG 595, an Anti-EGFRvIII Antibody-Drug Conjugate, Induces Potent Antitumor Activity against EGFRvIII-Expressing Glioblastoma. *Mol Cancer Ther* **2015,** 14, 1614-24.

109.   Yu, J. S.; Liu, G.; Ying, H.; Yong, W. H.; Black, K. L.; Wheeler, C. J. Vaccination with tumor lysate-pulsed dendritic cells elicits antigen-specific, cytotoxic T-cells in patients with malignant glioma. *Cancer Res* **2004,** 64, 4973-9.

110.   Prins, R. M.; Soto, H.; Konkankit, V.; Odesa, S. K.; Eskin, A.; Yong, W. H.; Nelson, S. F.; Liau, L. M. Gene expression profile correlates with T-cell infiltration and relative survival in glioblastoma patients vaccinated with dendritic cell immunotherapy. *Clin Cancer Res* **2011,** 17, 1603-15.

111.   Fueyo, J.; Gomez-Manzano, C.; Alemany, R.; Lee, P. S.; McDonnell, T. J.; Mitlianga, P.; Shi, Y. X.; Levin, V. A.; Yung, W. K.; Kyritsis, A. P. A mutant oncolytic adenovirus targeting the Rb pathway produces anti-glioma effect in vivo. *Oncogene* **2000,** 19, 2-12.

112.   Pol, J. G.; Marguerie, M.; Arulanandam, R.; Bell, J. C.; Lichty, B. D. Panorama from the oncolytic virotherapy summit. *Mol Ther* **2013,** 21, 1814-8.

113.   Muldoon, L. L.; Soussain, C.; Jahnke, K.; Johanson, C.; Siegal, T.; Smith, Q. R.; Hall, W. A.; Hynynen, K.; Senter, P. D.; Peereboom, D. M.; Neuwelt, E. A. Chemotherapy delivery issues in central nervous system malignancy: a reality check. *Journal of clinical oncology : official journal of the American Society of Clinical Oncology* **2007,** 25, 2295-305.

114.   Moghimi, S. M.; Hunter, A. C.; Murray, J. C. Long-circulating and target-specific nanoparticles: theory to practice. *Pharmacol Rev* **2001,** 53, 283-318.

115. Kreuter, J. Influence of the surface properties on nanoparticle-mediated transport of drugs to the brain. *J Nanosci Nanotechnol* **2004,** 4, 484-8.

116. Provenzale, J. M.; Mukundan, S.; Dewhirst, M. The role of blood-brain barrier permeability in brain tumor imaging and therapeutics. *AJR Am J Roentgenol* **2005,** 185, 763-7.

117. Bhowmik, A.; Khan, R.; Ghosh, M. K. Blood brain barrier: a challenge for effectual therapy of brain tumors. *Biomed Res Int* **2015,** 2015, 320941.

118. Wolburg, H.; Noell, S.; Fallier-Becker, P.; Mack, A. F.; Wolburg-Buchholz, K. The disturbed blood-brain barrier in human glioblastoma. *Mol Aspects Med* **2012,** 33, 579-89.

119. Dubois, L. G.; Campanati, L.; Righy, C.; D'Andrea-Meira, I.; Spohr, T. C.; Porto-Carreiro, I.; Pereira, C. M.; Balca-Silva, J.; Kahn, S. A.; DosSantos, M. F.; Oliveira Mde, A.; Ximenes-da-Silva, A.; Lopes, M. C.; Faveret, E.; Gasparetto, E. L.; Moura-Neto, V. Gliomas and the vascular fragility of the blood brain barrier. *Front Cell Neurosci* **2014,** 8, 418.

120. Azad, T. D.; Pan, J.; Connolly, I. D.; Remington, A.; Wilson, C. M.; Grant, G. A. Therapeutic strategies to improve drug delivery across the blood-brain barrier. *Neurosurg Focus* **2015,** 38, E9.

121. Blakeley, J. Drug delivery to brain tumors. *Curr Neurol Neurosci Rep* **2008,** 8, 235-41.

122. Verhaak, R. G.; Hoadley, K. A.; Purdom, E.; Wang, V.; Qi, Y.; Wilkerson, M. D.; Miller, C. R.; Ding, L.; Golub, T.; Mesirov, J. P.; Alexe, G.; Lawrence, M.; O'Kelly, M.; Tamayo, P.; Weir, B. A.; Gabriel, S.; Winckler, W.; Gupta, S.; Jakkula, L.; Feiler, H. S.; Hodgson, J. G.; James, C. D.; Sarkaria, J. N.; Brennan, C.; Kahn, A.; Spellman, P. T.; Wilson, R. K.; Speed, T. P.; Gray, J. W.; Meyerson, M.; Getz,

G.; Perou, C. M.; Hayes, D. N. Integrated genomic analysis identifies clinically relevant subtypes of glioblastoma characterized by abnormalities in PDGFRA, IDH1, EGFR, and NF1. *Cancer cell* **2010,** 17, 98-110.

123.   Weller, M.; Stupp, R.; Hegi, M.; Wick, W. Individualized targeted therapy for glioblastoma: fact or fiction? *Cancer J* **2012,** 18, 40-4.

124.   Stupp, R.; Hegi, M. E.; Mason, W. P.; van den Bent, M. J.; Taphoorn, M. J.; Janzer, R. C.; Ludwin, S. K.; Allgeier, A.; Fisher, B.; Belanger, K.; Hau, P.; Brandes, A. A.; Gijtenbeek, J.; Marosi, C.; Vecht, C. J.; Mokhtari, K.; Wesseling, P.; Villa, S.; Eisenhauer, E.; Gorlia, T.; Weller, M.; Lacombe, D.; Cairncross, J. G.; Mirimanoff, R. O. Effects of radiotherapy with concomitant and adjuvant temozolomide versus radiotherapy alone on survival in glioblastoma in a randomised phase III study: 5-year analysis of the EORTC-NCIC trial. *Lancet Oncol* **2009,** 10, 459-66.

125.   Vehlow, A.; Cordes, N. Invasion as target for therapy of glioblastoma multiforme. *Biochimica et biophysica acta* **2013,** 1836, 236-44.

126.   Giese, A.; Bjerkvig, R.; Berens, M. E.; Westphal, M. Cost of migration: invasion of malignant gliomas and implications for treatment. *Journal of clinical oncology : official journal of the American Society of Clinical Oncology* **2003,** 21, 1624-36.

127.   Rao, J. S. Molecular mechanisms of glioma invasiveness: the role of proteases. *Nat Rev Cancer* **2003,** 3, 489-501.

128.   Mentlein, R.; Hattermann, K.; Held-Feindt, J. Lost in disruption: role of proteases in glioma invasion and progression. *Biochimica et biophysica acta* **2012,** 1825, 178-85.

129. Levicar, N.; Nuttall, R. K.; Lah, T. T. Proteases in brain tumour progression. *Acta Neurochir (Wien)* **2003,** 145, 825-38.

130. Nakada, M.; Okada, Y.; Yamashita, J. The role of matrix metalloproteinases in glioma invasion. *Front Biosci* **2003,** 8, e261-9.

131. Cathcart, J.; Pulkoski-Gross, A.; Cao, J. Targeting matrix metalloproteinases in cancer: Bringing new life to old ideas. *Genes & Diseases* **2015,** 2, 26-34.

132. Seiki, M. Membrane-type 1 matrix metalloproteinase: a key enzyme for tumor invasion. *Cancer Lett* **2003,** 194, 1-11.

133. Vandenbroucke, R. E.; Libert, C. Is there new hope for therapeutic matrix metalloproteinase inhibition? *Nat Rev Drug Discov* **2014,** 13, 904-927.

134. Maskos, K. Crystal structures of MMPs in complex with physiological and pharmacological inhibitors. *Biochimie* **2005,** 87, 249-63.

135. Egeblad, M.; Werb, Z. New functions for the matrix metalloproteinases in cancer progression. *Nat Rev Cancer* **2002,** 2, 161-74.

136. Curran, S.; Murray, G. I. Matrix metalloproteinases: molecular aspects of their roles in tumour invasion and metastasis. *European journal of cancer (Oxford, England : 1990)* **2000,** 36, 1621-30.

137. Westermarck, J.; Kahari, V. M. Regulation of matrix metalloproteinase expression in tumor invasion. *Faseb j* **1999,** 13, 781-92.

138. Sternlicht, M. D.; Werb, Z. How matrix metalloproteinases regulate cell behavior. *Annu Rev Cell Dev Biol* **2001,** 17, 463-516.

139. Fanjul-Fernández, M.; Folgueras, A. R.; Cabrera, S.; López-Otín, C. Matrix metalloproteinases: Evolution, gene regulation and functional analysis in mouse

models. *Biochimica et Biophysica Acta (BBA) - Molecular Cell Research* **2010,** 1803, 3-19.

140.   Uria, J. A.; Werb, Z. Matrix metalloproteinases and their expression in mammary gland. *Cell Res* **1998,** 8, 187-94.

141.   Overall, C. M.; Lopez-Otin, C. Strategies for MMP inhibition in cancer: innovations for the post-trial era. *Nat Rev Cancer* **2002,** 2, 657-72.

142.   John, A.; Tuszynski, G. The role of matrix metalloproteinases in tumor angiogenesis and tumor metastasis. *Pathol Oncol Res* **2001,** 7, 14-23.

143.   McCawley, L. J.; Matrisian, L. M. Matrix metalloproteinases: multifunctional contributors to tumor progression. *Mol Med Today* **2000,** 6, 149-56.

144.   Stetler-Stevenson, W. G.; Yu, A. E. Proteases in invasion: matrix metalloproteinases. *Semin Cancer Biol* **2001,** 11, 143-52.

145.   Wilson, C. L.; Heppner, K. J.; Labosky, P. A.; Hogan, B. L.; Matrisian, L. M. Intestinal tumorigenesis is suppressed in mice lacking the metalloproteinase matrilysin. *Proc Natl Acad Sci U S A* **1997,** 94, 1402-7.

146.   Itoh, T.; Tanioka, M.; Yoshida, H.; Yoshioka, T.; Nishimoto, H.; Itohara, S. Reduced angiogenesis and tumor progression in gelatinase A-deficient mice. *Cancer Res* **1998,** 58, 1048-51.

147.   Itoh, T.; Tanioka, M.; Matsuda, H.; Nishimoto, H.; Yoshioka, T.; Suzuki, R.; Uehira, M. Experimental metastasis is suppressed in MMP-9-deficient mice. *Clin Exp Metastasis* **1999,** 17, 177-81.

148.   Gialeli, C.; Theocharis, A. D.; Karamanos, N. K. Roles of matrix metalloproteinases in cancer progression and their pharmacological targeting. *Febs j* **2011,** 278, 16-27.

149. Suzuki, M.; Raab, G.; Moses, M. A.; Fernandez, C. A.; Klagsbrun, M. Matrix metalloproteinase-3 releases active heparin-binding EGF-like growth factor by cleavage at a specific juxtamembrane site. *The Journal of biological chemistry* **1997,** 272, 31730-7.

150. Bergers, G.; Brekken, R.; McMahon, G.; Vu, T. H.; Itoh, T.; Tamaki, K.; Tanzawa, K.; Thorpe, P.; Itohara, S.; Werb, Z.; Hanahan, D. Matrix metalloproteinase-9 triggers the angiogenic switch during carcinogenesis. *Nat Cell Biol* **2000,** 2, 737-44.

151. Hojilla, C. V.; Mohammed, F. F.; Khokha, R. Matrix metalloproteinases and their tissue inhibitors direct cell fate during cancer development. *Br J Cancer* **2003,** 89, 1817-21.

152. Plaisier, M.; Kapiteijn, K.; Koolwijk, P.; Fijten, C.; Hanemaaijer, R.; Grimbergen, J. M.; Mulder-Stapel, A.; Quax, P. H.; Helmerhorst, F. M.; van Hinsbergh, V. W. Involvement of membrane-type matrix metalloproteinases (MT-MMPs) in capillary tube formation by human endometrial microvascular endothelial cells: role of MT3-MMP. *J Clin Endocrinol Metab* **2004,** 89, 5828-36.

153. Abraham, R.; Schafer, J.; Rothe, M.; Bange, J.; Knyazev, P.; Ullrich, A. Identification of MMP-15 as an anti-apoptotic factor in cancer cells. *The Journal of biological chemistry* **2005,** 280, 34123-32.

154. Hoekstra, R.; Eskens, F. A.; Verweij, J. Matrix metalloproteinase inhibitors: current developments and future perspectives. *Oncologist* **2001,** 6, 415-27.

155. Gill, J. H.; Kirwan, I. G.; Seargent, J. M.; Martin, S. W.; Tijani, S.; Anikin, V. A.; Mearns, A. J.; Bibby, M. C.; Anthoney, A.; Loadman, P. M. MMP-10 is overexpressed, proteolytically active, and a potential target for therapeutic intervention in human lung carcinomas. *Neoplasia* **2004,** 6, 777-85.

156.   Jiang, R.; Yu, S. Expression of MMP-13 and its correlation with prognosis in non-small cell lung cancer. *The Chinese-German Journal of Clinical Oncology* **2008,** 7, 142-144.

157.   Sunami, E.; Tsuno, N.; Osada, T.; Saito, S.; Kitayama, J.; Tomozawa, S.; Tsuruo, T.; Shibata, Y.; Muto, T.; Nagawa, H. MMP-1 is a prognostic marker for hematogenous metastasis of colorectal cancer. *Oncologist* **2000,** 5, 108-14.

158.   Brinckerhoff, C. E.; Rutter, J. L.; Benbow, U. Interstitial collagenases as markers of tumor progression. *Clin Cancer Res* **2000,** 6, 4823-30.

159.   Wick, W.; Platten, M.; Weller, M. Glioma cell invasion: regulation of metalloproteinase activity by TGF-beta. *J Neurooncol* **2001,** 53, 177-85.

160.   Bhoopathi, P.; Chetty, C.; Gogineni, V. R.; Gujrati, M.; Dinh, D. H.; Rao, J. S.; Lakka, S. S. MMP-2 mediates mesenchymal stem cell tropism towards medulloblastoma tumors. *Gene Ther* **2011,** 18, 692-701.

161.   Tews, D. S.; Nissen, A. Expression of adhesion factors and degrading proteins in primary and secondary glioblastomas and their precursor tumors. *Invasion Metastasis* **1998,** 18, 271-84.

162.   Nakagawa, T.; Kubota, T.; Kabuto, M.; Sato, K.; Kawano, H.; Hayakawa, T.; Okada, Y. Production of matrix metalloproteinases and tissue inhibitor of metalloproteinases-1 by human brain tumors. *J Neurosurg* **1994,** 81, 69-77.

163.   Sawaya, R. E.; Yamamoto, M.; Gokaslan, Z. L.; Wang, S. W.; Mohanam, S.; Fuller, G. N.; McCutcheon, I. E.; Stetler-Stevenson, W. G.; Nicolson, G. L.; Rao, J. S. Expression and localization of 72 kDa type IV collagenase (MMP-2) in human malignant gliomas in vivo. *Clin Exp Metastasis* **1996,** 14, 35-42.

164.   Nakada, M.; Nakamura, H.; Ikeda, E.; Fujimoto, N.; Yamashita, J.; Sato, H.; Seiki, M.; Okada, Y. Expression and tissue localization of membrane-type 1, 2,

and 3 matrix metalloproteinases in human astrocytic tumors. *Am J Pathol* **1999,** 154, 417-28.

165.   Forsyth, P. A.; Wong, H.; Laing, T. D.; Rewcastle, N. B.; Morris, D. G.; Muzik, H.; Leco, K. J.; Johnston, R. N.; Brasher, P. M.; Sutherland, G.; Edwards, D. R. Gelatinase-A (MMP-2), gelatinase-B (MMP-9) and membrane type matrix metalloproteinase-1 (MT1-MMP) are involved in different aspects of the pathophysiology of malignant gliomas. *Br J Cancer* **1999,** 79, 1828-35.

166.   Esteve, P. O.; Tremblay, P.; Houde, M.; St-Pierre, Y.; Mandeville, R. *In vitro* expression of MMP-2 and MMP-9 in glioma cells following exposure to inflammatory mediators. *Biochimica et biophysica acta* **1998,** 1403, 85-96.

167.   Rooprai, H. K.; Van Meter, T.; Rucklidge, G. J.; Hudson, L.; Everall, I. P.; Pilkington, G. J. Comparative analysis of matrix metalloproteinases by immunocytochemistry, immunohistochemistry and zymography in human primary brain tumours. *Int J Oncol* **1998,** 13, 1153-7.

168.   Vince, G. H.; Wagner, S.; Pietsch, T.; Klein, R.; Goldbrunner, R. H.; Roosen, K.; Tonn, J. C. Heterogeneous regional expression patterns of matrix metalloproteinases in human malignant gliomas. *Int J Dev Neurosci* **1999,** 17, 437-45.

169.   Raithatha, S. A.; Muzik, H.; Muzik, H.; Rewcastle, N. B.; Johnston, R. N.; Edwards, D. R.; Forsyth, P. A. Localization of gelatinase-A and gelatinase-B mRNA and protein in human gliomas. *Neuro Oncol* **2000,** 2, 145-50.

170.   Matsuzawa, K.; Fukuyama, K.; Dirks, P. B.; Hubbard, S.; Murakami, M.; Becker, L. E.; Rutka, J. T. Expression of stromelysin 1 in human astrocytoma cell lines. *J Neurooncol* **1996,** 30, 181-8.

171. Kachra, Z.; Beaulieu, E.; Delbecchi, L.; Mousseau, N.; Berthelet, F.; Moumdjian, R.; Del Maestro, R.; Beliveau, R. Expression of matrix metalloproteinases and their inhibitors in human brain tumors. *Clin Exp Metastasis* **1999,** 17, 555-66.

172. Van Wart, H. E. Human neutrophil collagenase. *Matrix Suppl* **1992,** 1, 31-6.

173. Nuttall, R. K.; Pennington, C. J.; Taplin, J.; Wheal, A.; Yong, V. W.; Forsyth, P. A.; Edwards, D. R. Elevated membrane-type matrix metalloproteinases in gliomas revealed by profiling proteases and inhibitors in human cancer cells. *Mol Cancer Res* **2003,** 1, 333-45.

174. Lettau, I.; Hattermann, K.; Held-Feindt, J.; Brauer, R.; Sedlacek, R.; Mentlein, R. Matrix metalloproteinase-19 is highly expressed in astroglial tumors and promotes invasion of glioma cells. *J Neuropathol Exp Neurol* **2010,** 69, 215-23.

175. Zhang, H.; Kelly, G.; Zerillo, C.; Jaworski, D. M.; Hockfield, S. Expression of a cleaved brain-specific extracellular matrix protein mediates glioma cell invasion In vivo. *J Neurosci* **1998,** 18, 2370-6.

176. Hu, B.; Kong, L. L.; Matthews, R. T.; Viapiano, M. S. The proteoglycan brevican binds to fibronectin after proteolytic cleavage and promotes glioma cell motility. *The Journal of biological chemistry* **2008,** 283, 24848-59.

177. Silveira Correa, T. C.; Massaro, R. R.; Brohem, C. A.; Taboga, S. R.; Lamers, M. L.; Santos, M. F.; Maria-Engler, S. S. RECK-mediated inhibition of glioma migration and invasion. *J Cell Biochem* **2010,** 110, 52-61.

178. Nakano, A.; Tani, E.; Miyazaki, K.; Yamamoto, Y.; Furuyama, J. Matrix metalloproteinases and tissue inhibitors of metalloproteinases in human gliomas. *J Neurosurg* **1995,** 83, 298-307.

179. Groft, L. L.; Muzik, H.; Rewcastle, N. B.; Johnston, R. N.; Knauper, V.; Lafleur, M. A.; Forsyth, P. A.; Edwards, D. R. Differential expression and localization of TIMP-1 and TIMP-4 in human gliomas. *Br J Cancer* **2001,** 85, 55-63.

180. Aaberg-Jessen, C.; Christensen, K.; Offenberg, H.; Bartels, A.; Dreehsen, T.; Hansen, S.; Schroder, H. D.; Brunner, N.; Kristensen, B. W. Low expression of tissue inhibitor of metalloproteinases-1 (TIMP-1) in glioblastoma predicts longer patient survival. *J Neurooncol* **2009,** 95, 117-28.

181. Lu, K. V.; Jong, K. A.; Rajasekaran, A. K.; Cloughesy, T. F.; Mischel, P. S. Upregulation of tissue inhibitor of metalloproteinases (TIMP)-2 promotes matrix metalloproteinase (MMP)-2 activation and cell invasion in a human glioblastoma cell line. *Lab Invest* **2004,** 84, 8-20.

182. Lamfers, M. L.; Gianni, D.; Tung, C. H.; Idema, S.; Schagen, F. H.; Carette, J. E.; Quax, P. H.; Van Beusechem, V. W.; Vandertop, W. P.; Dirven, C. M.; Chiocca, E. A.; Gerritsen, W. R. Tissue inhibitor of metalloproteinase-3 expression from an oncolytic adenovirus inhibits matrix metalloproteinase activity in vivo without affecting antitumor efficacy in malignant glioma. *Cancer Res* **2005,** 65, 9398-405.

183. Whittaker, M.; Floyd, C. D.; Brown, P.; Gearing, A. J. Design and therapeutic application of matrix metalloproteinase inhibitors. *Chem Rev* **1999,** 99, 2735-76.

184. Drummond, A. H.; Beckett, P.; Brown, P. D.; Bone, E. A.; Davidson, A. H.; Galloway, W. A.; Gearing, A. J.; Huxley, P.; Laber, D.; McCourt, M.; Whittaker, M.; Wood, L. M.; Wright, A. Preclinical and clinical studies of MMP inhibitors in cancer. *Ann N Y Acad Sci* **1999,** 878, 228-35.

185.   Macaulay, V. M.; O'Byrne, K. J.; Saunders, M. P.; Braybrooke, J. P.; Long, L.; Gleeson, F.; Mason, C. S.; Harris, A. L.; Brown, P.; Talbot, D. C. Phase I study of intrapleural batimastat (BB-94), a matrix metalloproteinase inhibitor, in the treatment of malignant pleural effusions. *Clin Cancer Res* **1999,** 5, 513-20.

186.   Sparano, J. A.; Bernardo, P.; Stephenson, P.; Gradishar, W. J.; Ingle, J. N.; Zucker, S.; Davidson, N. E. Randomized phase III trial of marimastat versus placebo in patients with metastatic breast cancer who have responding or stable disease after first-line chemotherapy: Eastern Cooperative Oncology Group trial E2196. *Journal of clinical oncology : official journal of the American Society of Clinical Oncology* **2004,** 22, 4683-90.

187.   Steward, W. P.; Thomas, A. L. Marimastat: the clinical development of a matrix metalloproteinase inhibitor. *Expert Opin Investig Drugs* **2000,** 9, 2913-22.

188.   Toth, M.; Bernardo, M. M.; Gervasi, D. C.; Soloway, P. D.; Wang, Z.; Bigg, H. F.; Overall, C. M.; DeClerck, Y. A.; Tschesche, H.; Cher, M. L.; Brown, S.; Mobashery, S.; Fridman, R. Tissue inhibitor of metalloproteinase (TIMP)-2 acts synergistically with synthetic matrix metalloproteinase (MMP) inhibitors but not with TIMP-4 to enhance the (Membrane type 1)-MMP-dependent activation of pro-MMP-2. *The Journal of biological chemistry* **2000,** 275, 41415-23.

189.   Hirte, H.; Vergote, I. B.; Jeffrey, J. R.; Grimshaw, R. N.; Coppieters, S.; Schwartz, B.; Tu, D.; Sadura, A.; Brundage, M.; Seymour, L. A phase III randomized trial of BAY 12-9566 (tanomastat) as maintenance therapy in patients with advanced ovarian cancer responsive to primary surgery and paclitaxel/platinum containing chemotherapy: A National Cancer Institute of Canada Clinical Trials Group Study. *Gynecologic Oncology* **2006,** 102, 300-308.

190.   Fisher, J. F.; Mobashery, S. Recent advances in MMP inhibitor design. *Cancer and Metastasis Reviews* **2006,** 25, 115-136.

191.   Groves, M. D.; Puduvalli, V. K.; Hess, K. R.; Jaeckle, K. A.; Peterson, P.; Yung, W. K. A.; Levin, V. A. Phase II Trial of Temozolomide Plus the Matrix Metalloproteinase Inhibitor, Marimastat, in Recurrent and Progressive Glioblastoma Multiforme. *Journal of Clinical Oncology* **2002,** 20, 1383-1388.

192.   Dufour, A.; Overall, C. M. Missing the target: matrix metalloproteinase antitargets in inflammation and cancer. *Trends Pharmacol Sci* **2013,** 34, 233-42.

193.   Overall, C. M.; Kleifeld, O. Towards third generation matrix metalloproteinase inhibitors for cancer therapy. *Br J Cancer* **2006,** 94, 941-6.

194.   Overall, C. M.; Kleifeld, O. Tumour microenvironment - opinion: validating matrix metalloproteinases as drug targets and anti-targets for cancer therapy. *Nat Rev Cancer* **2006,** 6, 227-39.

195.   Jacobsen, J. A.; Major Jourden, J. L.; Miller, M. T.; Cohen, S. M. To bind zinc or not to bind zinc: An examination of innovative approaches to improved metalloproteinase inhibition. *Biochimica et Biophysica Acta (BBA) - Molecular Cell Research* **2010,** 1803, 72-94.

196.   Georgiadis, D.; Dive, V. Phosphinic peptides as potent inhibitors of zinc-metalloproteases. *Top Curr Chem* **2015,** 360, 1-38.

197.   Coussens, L. M.; Fingleton, B.; Matrisian, L. M. Matrix metalloproteinase inhibitors and cancer: trials and tribulations. *Science (New York, N.Y.)* **2002,** 295, 2387-92.

198.   Chuang, C. H.; Chuang, K. H.; Wang, H. E.; Roffler, S. R.; Shiea, J. T.; Tzou, S. C.; Cheng, T. C.; Kao, C. H.; Wu, S. Y.; Tseng, W. L.; Cheng, C. M.; Hou, M. F.; Wang, J. M.; Cheng, T. L. In vivo positron emission tomography imaging of

protease activity by generation of a hydrophobic product from a noninhibitory protease substrate. *Clin Cancer Res* **2012,** 18, 238-47.

199.   Heal, W. P.; Wickramasinghe, S. R.; Tate, E. W. Activity based chemical proteomics: profiling proteases as drug targets. *Curr Drug Discov Technol* **2008,** 5, 200-12.

200.   Ansari, C.; Tikhomirov, G. A.; Hong, S. H.; Falconer, R. A.; Loadman, P. M.; Gill, J. H.; Castaneda, R.; Hazard, F. K.; Tong, L.; Lenkov, O. D.; Felsher, D. W.; Rao, J.; Daldrup-Link, H. E. Development of novel tumor-targeted theranostic nanoparticles activated by membrane-type matrix metalloproteinases for combined cancer magnetic resonance imaging and therapy. *Small (Weinheim an der Bergstrasse, Germany)* **2014,** 10, 566-75, 417.

201.   Choi, K. Y.; Swierczewska, M.; Lee, S.; Chen, X. Protease-activated drug development. *Theranostics* **2012,** 2, 156-78.

202.   Vandooren, J.; Opdenakker, G.; Loadman, P. M.; Edwards, D. R. Proteases in cancer drug delivery. *Adv Drug Deliv Rev* **2016,** 97, 144-55.

203.   Atkinson, J. M.; Falconer, R. A.; Edwards, D. R.; Pennington, C. J.; Siller, C. S.; Shnyder, S. D.; Bibby, M. C.; Patterson, L. H.; Loadman, P. M.; Gill, J. H. Development of a novel tumor-targeted vascular disrupting agent activated by membrane-type matrix metalloproteinases. *Cancer Res* **2010,** 70, 6902-12.

204.   Atkinson, J. M.; Siller, C. S.; Gill, J. H. Tumour endoproteases: the cutting edge of cancer drug delivery? *Br J Pharmacol* **2008,** 153, 1344-52.

205.   Vartak, D. G.; Gemeinhart, R. A. Matrix metalloproteases: underutilized targets for drug delivery. *J Drug Target* **2007,** 15, 1-20.

206.   Van Valckenborgh, E.; Mincher, D.; Di Salvo, A.; Van Riet, I.; Young, L.; Van Camp, B.; Vanderkerken, K. Targeting an MMP-9-activated prodrug to

multiple myeloma-diseased bone marrow: a proof of principle in the 5T33MM mouse model. *Leukemia* **2005,** 19, 1628-33.

207.   Albright, C. F.; Graciani, N.; Han, W.; Yue, E.; Stein, R.; Lai, Z.; Diamond, M.; Dowling, R.; Grimminger, L.; Zhang, S. Y.; Behrens, D.; Musselman, A.; Bruckner, R.; Zhang, M.; Jiang, X.; Hu, D.; Higley, A.; Dimeo, S.; Rafalski, M.; Mandlekar, S.; Car, B.; Yeleswaram, S.; Stern, A.; Copeland, R. A.; Combs, A.; Seitz, S. P.; Trainor, G. L.; Taub, R.; Huang, P.; Oliff, A. Matrix metalloproteinase-activated doxorubicin prodrugs inhibit HT1080 xenograft growth better than doxorubicin with less toxicity. *Mol Cancer Ther* **2005,** 4, 751-60.

208.   Kline, T.; Torgov, M. Y.; Mendelsohn, B. A.; Cerveny, C. G.; Senter, P. D. Novel antitumor prodrugs designed for activation by matrix metalloproteinases-2 and -9. *Mol Pharm* **2004,** 1, 9-22.

209.   Mansour, A. M.; Drevs, J.; Esser, N.; Hamada, F. M.; Badary, O. A.; Unger, C.; Fichtner, I.; Kratz, F. A new approach for the treatment of malignant melanoma: enhanced antitumor efficacy of an albumin-binding doxorubicin prodrug that is cleaved by matrix metalloproteinase 2. *Cancer Res* **2003,** 63, 4062-6.

210.   Kratz, F.; Drevs, J.; Bing, G.; Stockmar, C.; Scheuermann, K.; Lazar, P.; Unger, C. Development and *in vitro* efficacy of novel MMP2 and MMP9 specific doxorubicin albumin conjugates. *Bioorganic & medicinal chemistry letters* **2001,** 11, 2001-6.

211.   Timar, F.; Botyanszki, J.; Suli-Vargha, H.; Babo, I.; Olah, J.; Pogany, G.; Jeney, A. The antiproliferative action of a melphalan hexapeptide with collagenase-cleavable site. *Cancer Chemother Pharmacol* **1998,** 41, 292-8.

212. Chau, Y.; Dang, N. M.; Tan, F. E.; Langer, R. Investigation of targeting mechanism of new dextran-peptide-methotrexate conjugates using biodistribution study in matrix-metalloproteinase-overexpressing tumor xenograft model. *J Pharm Sci* **2006,** 95, 542-51.

213. Tauro, J. R.; Gemeinhart, R. A. Matrix metalloprotease triggered delivery of cancer chemotherapeutics from hydrogel matrixes. *Bioconjug Chem* **2005,** 16, 1133-9.

214. Chau, Y.; Tan, F. E.; Langer, R. Synthesis and characterization of dextran-peptide-methotrexate conjugates for tumor targeting via mediation by matrix metalloproteinase II and matrix metalloproteinase IX. *Bioconjug Chem* **2004,** 15, 931-41.

215. Gill, J. H.; Loadman, P. M.; Shnyder, S. D.; Cooper, P.; Atkinson, J. M.; Ribeiro Morais, G.; Patterson, L. H.; Falconer, R. A. Tumor-targeted prodrug ICT2588 demonstrates therapeutic activity against solid tumors and reduced potential for cardiovascular toxicity. *Mol Pharm* **2014,** 11, 1294-300.

216. Davies, N. M.; Jamali, F. COX-2 selective inhibitors cardiac toxicity: getting to the heart of the matter. *J Pharm Pharm Sci* **2004,** 7, 332-6.

217. Kohrmann, A.; Kammerer, U.; Kapp, M.; Dietl, J.; Anacker, J. Expression of matrix metalloproteinases (MMPs) in primary human breast cancer and breast cancer cell lines: New findings and review of the literature. *BMC Cancer* **2009,** 9, 188.

218. Uhlen, M.; Fagerberg, L.; Hallstrom, B. M.; Lindskog, C.; Oksvold, P.; Mardinoglu, A.; Sivertsson, A.; Kampf, C.; Sjostedt, E.; Asplund, A.; Olsson, I.; Edlund, K.; Lundberg, E.; Navani, S.; Szigyarto, C. A.; Odeberg, J.; Djureinovic, D.; Takanen, J. O.; Hober, S.; Alm, T.; Edqvist, P. H.; Berling, H.; Tegel, H.;

Mulder, J.; Rockberg, J.; Nilsson, P.; Schwenk, J. M.; Hamsten, M.; von Feilitzen, K.; Forsberg, M.; Persson, L.; Johansson, F.; Zwahlen, M.; von Heijne, G.; Nielsen, J.; Ponten, F. Proteomics. Tissue-based map of the human proteome. *Science (New York, N.Y.)* **2015,** 347, 1260419.

219. Uhlen, M.; Oksvold, P.; Fagerberg, L.; Lundberg, E.; Jonasson, K.; Forsberg, M.; Zwahlen, M.; Kampf, C.; Wester, K.; Hober, S.; Wernerus, H.; Bjorling, L.; Ponten, F. Towards a knowledge-based Human Protein Atlas. *Nature biotechnology* **2010,** 28, 1248-50.

220. Uhlen, M.; Bjorling, E.; Agaton, C.; Szigyarto, C. A.; Amini, B.; Andersen, E.; Andersson, A. C.; Angelidou, P.; Asplund, A.; Asplund, C.; Berglund, L.; Bergstrom, K.; Brumer, H.; Cerjan, D.; Ekstrom, M.; Elobeid, A.; Eriksson, C.; Fagerberg, L.; Falk, R.; Fall, J.; Forsberg, M.; Bjorklund, M. G.; Gumbel, K.; Halimi, A.; Hallin, I.; Hamsten, C.; Hansson, M.; Hedhammar, M.; Hercules, G.; Kampf, C.; Larsson, K.; Lindskog, M.; Lodewyckx, W.; Lund, J.; Lundeberg, J.; Magnusson, K.; Malm, E.; Nilsson, P.; Odling, J.; Oksvold, P.; Olsson, I.; Oster, E.; Ottosson, J.; Paavilainen, L.; Persson, A.; Rimini, R.; Rockberg, J.; Runeson, M.; Sivertsson, A.; Skollermo, A.; Steen, J.; Stenvall, M.; Sterky, F.; Stromberg, S.; Sundberg, M.; Tegel, H.; Tourle, S.; Wahlund, E.; Walden, A.; Wan, J.; Wernerus, H.; Westberg, J.; Wester, K.; Wrethagen, U.; Xu, L. L.; Hober, S.; Ponten, F. A human protein atlas for normal and cancer tissues based on antibody proteomics. *Molecular & cellular proteomics : MCP* **2005,** 4, 1920-32.

221. Nagase, H.; Fields, C. G.; Fields, G. B. Design and characterization of a fluorogenic substrate selectively hydrolyzed by stromelysin 1 (matrix metalloproteinase-3). *The Journal of biological chemistry* **1994,** 269, 20952-7.

222. Bickett, D. M.; Green, M. D.; Berman, J.; Dezube, M.; Howe, A. S.; Brown, P. J.; Roth, J. T.; McGeehan, G. M. A high throughput fluorogenic substrate for interstitial collagenase (MMP-1) and gelatinase (MMP-9). *Anal Biochem* **1993,** 212, 58-64.

223. Cho, N. H.; Hong, K. P.; Hong, S. H.; Kang, S.; Chung, K. Y.; Cho, S. H. MMP expression profiling in recurred stage IB lung cancer. *Oncogene* **2003,** 23, 845-851.

224. Kerkela, E.; Ala-aho, R.; Lohi, J.; Grenman, R.; V, M. K.; Saarialho-Kere, U. Differential patterns of stromelysin-2 (MMP-10) and MT1-MMP (MMP-14) expression in epithelial skin cancers. *Br J Cancer* **2001,** 84, 659-69.

225. Polette, M.; Clavel, C.; Muller, D.; Abecassis, J.; Binninger, I.; Birembaut, P. Detection of mRNAs encoding collagenase I and stromelysin 2 in carcinomas of the head and neck by in situ hybridization. *Invasion Metastasis* **1991,** 11, 76-83.

226. Impola, U.; Uitto, V. J.; Hietanen, J.; Hakkinen, L.; Zhang, L.; Larjava, H.; Isaka, K.; Saarialho-Kere, U. Differential expression of matrilysin-1 (MMP-7), 92 kD gelatinase (MMP-9), and metalloelastase (MMP-12) in oral verrucous and squamous cell cancer. *J Pathol* **2004,** 202, 14-22.

227. Mathew, R.; Khanna, R.; Kumar, R.; Mathur, M.; Shukla, N. K.; Ralhan, R. Stromelysin-2 overexpression in human esophageal squamous cell carcinoma: potential clinical implications. *Cancer Detect Prev* **2002,** 26, 222-8.

228. Deraz, E. M.; Kudo, Y.; Yoshida, M.; Obayashi, M.; Tsunematsu, T.; Tani, H.; Siriwardena, S. B.; Keikhaee, M. R.; Qi, G.; Iizuka, S.; Ogawa, I.; Campisi, G.; Lo Muzio, L.; Abiko, Y.; Kikuchi, A.; Takata, T. MMP-10/stromelysin-2 promotes invasion of head and neck cancer. *PLoS One* **2011,** 6, e25438.

229. Frederick, L. A.; Matthews, J. A.; Jamieson, L.; Justilien, V.; Thompson, E. A.; Radisky, D. C.; Fields, A. P. Matrix metalloproteinase-10 is a critical effector of protein kinase Ciota-Par6alpha-mediated lung cancer. *Oncogene* **2008,** 27, 4841-53.

230. Lathia, J. D.; Mack, S. C.; Mulkearns-Hubert, E. E.; Valentim, C. L. L.; Rich, J. N. Cancer stem cells in glioblastoma. *Genes Dev* **2015,** 29, 1203-17.

231. Plaks, V.; Kong, N.; Werb, Z. The Cancer Stem Cell Niche: How Essential is the Niche in Regulating Stemness of Tumor Cells? *Cell Stem Cell* **2015,** 16, 225-38.

232. Justilien, V.; Regala, R. P.; Tseng, I. C.; Walsh, M. P.; Batra, J.; Radisky, E. S.; Murray, N. R.; Fields, A. P. Matrix Metalloproteinase-10 Is Required for Lung Cancer Stem Cell Maintenance, Tumor Initiation and Metastatic Potential. *PLoS One* **2012,** 7.

233. Jaiswal, R.; Luk, F.; Dalla, P. V.; Grau, G. E.; Bebawy, M. Breast cancer-derived microparticles display tissue selectivity in the transfer of resistance proteins to cells. *PLoS One* **2013,** 8, e61515.

234. Chen, J.; Kesari, S.; Rooney, C.; Strack, P. R.; Chen, J.; Shen, H.; Wu, L.; Griffin, J. D. Inhibition of Notch Signaling Blocks Growth of Glioblastoma Cell Lines and Tumor Neurospheres. *Genes Cancer* **2010,** 1, 822-35.

235. Sullivan, J. P.; Spinola, M.; Dodge, M.; Raso, M. G.; Behrens, C.; Gao, B.; Schuster, K.; Shao, C.; Larsen, J. E.; Sullivan, L. A.; Honorio, S.; Xie, Y.; Scaglioni, P. P.; DiMaio, J. M.; Gazdar, A. F.; Shay, J. W.; Wistuba, II; Minna, J. D. Aldehyde dehydrogenase activity selects for lung adenocarcinoma stem cells dependent on notch signaling. *Cancer Res* **2010,** 70, 9937-48.

236.   Fan, X.; Khaki, L.; Zhu, T. S.; Soules, M. E.; Talsma, C. E.; Gul, N.; Koh, C.; Zhang, J.; Li, Y. M.; Maciaczyk, J.; Nikkhah, G.; Dimeco, F.; Piccirillo, S.; Vescovi, A. L.; Eberhart, C. G. NOTCH pathway blockade depletes CD133-positive glioblastoma cells and inhibits growth of tumor neurospheres and xenografts. *Stem Cells* **2010,** 28, 5-16.

237.   Yu, J. M.; Jun, E. S.; Jung, J. S.; Suh, S. Y.; Han, J. Y.; Kim, J. Y.; Kim, K. W.; Jung, J. S. Role of Wnt5a in the proliferation of human glioblastoma cells. *Cancer Lett* **2007,** 257, 172-81.

238.   Ramos-DeSimone, N.; Hahn-Dantona, E.; Sipley, J.; Nagase, H.; French, D. L.; Quigley, J. P. Activation of matrix metalloproteinase-9 (MMP-9) via a converging plasmin/stromelysin-1 cascade enhances tumor cell invasion. *The Journal of biological chemistry* **1999,** 274, 13066-76.

239.   Nakamura, H.; Fujii, Y.; Ohuchi, E.; Yamamoto, E.; Okada, Y. Activation of the precursor of human stromelysin 2 and its interactions with other matrix metalloproteinases. *Eur J Biochem* **1998,** 253, 67-75.

240.   van den Oord, J. J.; Paemen, L.; Opdenakker, G.; de Wolf-Peeters, C. Expression of gelatinase B and the extracellular matrix metalloproteinase inducer EMMPRIN in benign and malignant pigment cell lesions of the skin. *Am J Pathol* **1997,** 151, 665-70.

241.   Huggins, D. J.; Sherman, W.; Tidor, B. Rational approaches to improving selectivity in drug design. *J Med Chem* **2012,** 55, 1424-44.

242.   Lee, C. H.; Huang, H. C.; Juan, H. F. Reviewing ligand-based rational drug design: the search for an ATP synthase inhibitor. *Int J Mol Sci* **2011,** 12, 5304-18.

243.   Cavasotto, C. N.; Phatak, S. S. Homology modeling in drug discovery: current trends and applications. *Drug Discov Today* **2009,** 14, 676-83.

244. Sleno, L.; Emili, A. Proteomic methods for drug target discovery. *Curr Opin Chem Biol* **2008,** 12, 46-54.

245. Moon, J. B.; Howe, W. J. Computer design of bioactive molecules: a method for receptor-based de novo ligand design. *Proteins* **1991,** 11, 314-28.

246. Drews, J. Drug discovery: a historical perspective. *Science (New York, N.Y.)* **2000,** 287, 1960-4.

247. Langer, T.; Hoffmann, R. D. Virtual screening: an effective tool for lead structure discovery? *Curr Pharm Des* **2001,** 7, 509-27.

248. Tintori, C.; Manetti, F.; Botta, M. Pharmacophoric models and 3D QSAR studies of the adenosine receptor ligands. *Curr Top Med Chem* **2010,** 10, 1019-35.

249. van Drie, J. H. Pharmacophore discovery--lessons learned. *Curr Pharm Des* **2003,** 9, 1649-64.

250. Mattos, C.; Ringe, D. Locating and characterizing binding sites on proteins. *Nature biotechnology* **1996,** 14, 595-9.

251. Smyth, M. S.; Martin, J. H. J. x Ray crystallography. *Mol Pathol* **2000,** 53, 8-14.

252. Gernert, K. M.; Smith, R.; Carter, D. C. A simple apparatus for controlling nucleation and size in protein crystal growth. *Anal Biochem* **1988,** 168, 141-7.

253. Carter, C. W., Jr.; Carter, C. W. Protein crystallization using incomplete factorial experiments. *The Journal of biological chemistry* **1979,** 254, 12219-23.

254. Hampel, A.; Labanauskas, M.; Connors, P. G.; Kirkegard, L.; RajBhandary, U. L.; Sigler, P. B.; Bock, R. M. Single crystals of transfer RNA from formylmethionine and phenylalanine transfer RNA's. *Science (New York, N.Y.)* **1968,** 162, 1384-7.

255. Rossmann, M. G.; Arnold, E.; Erickson, J. W.; Frankenberger, E. A.; Griffith, J. P.; Hecht, H. J.; Johnson, J. E.; Kamer, G.; Luo, M.; Mosser, A. G.; et al. Structure of a human common cold virus and functional relationship to other picornaviruses. *Nature* **1985,** 317, 145-53.

256. Smyth, M.; Tate, J.; Hoey, E.; Lyons, C.; Martin, S.; Stuart, D. Implications for viral uncoating from the structure of bovine enterovirus. *Nat Struct Biol* **1995,** 2, 224-31.

257. Hope, H. Crystallography of biological macromolecules at ultra-low temperature. *Annu Rev Biophys Biophys Chem* **1990,** 19, 107-26.

258. Jones, T. A.; Zou, J. Y.; Cowan, S. W.; Kjeldgaard, M. Improved methods for building protein models in electron density maps and the location of errors in these models. *Acta Crystallogr A* **1991,** 47 (Pt 2), 110-9.

259. Arnold, E.; Rossmann, M. G. Effect of errors, redundancy, and solvent content in the molecular replacement procedure for the structure determination of biological macromolecules. *Proc Natl Acad Sci U S A* **1986,** 83, 5489-93.

260. Ahmed, M. A.; Azam, F.; Rghigh, A. M.; Gbaj, A.; Zetrini, A. E. Structure-based design, synthesis, molecular docking, and biological activities of 2-(3-benzoylphenyl) propanoic acid derivatives as dual mechanism drugs. *J Pharm Bioallied Sci* **2012,** 4, 43-50.

261. Durrant, J. D.; McCammon, J. A. Molecular dynamics simulations and drug discovery. *BMC Biol* **2011,** 9, 71.

262. Mackerell, A. D., Jr. Empirical force fields for biological macromolecules: overview and issues. *J Comput Chem* **2004,** 25, 1584-604.

263. Tuckerman, M. E.; Martyna, G. J. Understanding Modern Molecular Dynamics: Techniques and Applications. *The Journal of Physical Chemistry B* **2000,** 104, 159-178.

264. MacKerell, A. D.; Bashford, D.; Bellott, M.; Dunbrack, R. L.; Evanseck, J. D.; Field, M. J.; Fischer, S.; Gao, J.; Guo, H.; Ha, S.; Joseph-McCarthy, D.; Kuchnir, L.; Kuczera, K.; Lau, F. T.; Mattos, C.; Michnick, S.; Ngo, T.; Nguyen, D. T.; Prodhom, B.; Reiher, W. E.; Roux, B.; Schlenkrich, M.; Smith, J. C.; Stote, R.; Straub, J.; Watanabe, M.; Wiorkiewicz-Kuczera, J.; Yin, D.; Karplus, M. All-atom empirical potential for molecular modeling and dynamics studies of proteins. *J Phys Chem B* **1998,** 102, 3586-616.

265. Oostenbrink, C.; Villa, A.; Mark, A. E.; van Gunsteren, W. F. A biomolecular force field based on the free enthalpy of hydration and solvation: the GROMOS force-field parameter sets 53A5 and 53A6. *J Comput Chem* **2004,** 25, 1656-76.

266. Cornell, W. D.; Cieplak, P.; Bayly, C. I.; Gould, I. R.; Merz, K. M.; Ferguson, D. M.; Spellmeyer, D. C.; Fox, T.; Caldwell, J. W.; Kollman, P. A. A Second Generation Force Field for the Simulation of Proteins, Nucleic Acids, and Organic Molecules J. Am. Chem. Soc. 1995, 117, 5179−5197. *Journal of the American Chemical Society* **1996,** 118, 2309-2309.

267. Rappe, A. K.; Casewit, C. J.; Colwell, K. S.; Goddard, W. A.; Skiff, W. M. UFF, a full periodic table force field for molecular mechanics and molecular dynamics simulations. *Journal of the American Chemical Society* **1992,** 114, 10024-10035.

268. Dhanaraj, V.; Williams, M. G.; Ye, Q. Z.; Molina, F.; Johnson, L. L.; Ortwine, D. F.; Pavlovsky, A.; Rubin, J. R.; Skeean, R. W.; White, A. D.; Humblet, C.; Hupe,

D. J.; Blundell, T. L. X-ray Structure of Gelatinase A Catalytic Domain Complexed with a Hydroxamate Inhibitor. *Croatica Chemica Acta* **1999,** 72, 575-591.

269.   Rowsell, S.; Hawtin, P.; Minshull, C. A.; Jepson, H.; Brockbank, S. M.; Barratt, D. G.; Slater, A. M.; McPheat, W. L.; Waterson, D.; Henney, A. M.; Pauptit, R. A. Crystal structure of human MMP9 in complex with a reverse hydroxamate inhibitor. *J Mol Biol* **2002,** 319, 173-81.

270.   Pavlovsky, A. G.; Williams, M. G.; Ye, Q. Z.; Ortwine, D. F.; Purchase, C. F., 2nd; White, A. D.; Dhanaraj, V.; Roth, B. D.; Johnson, L. L.; Hupe, D.; Humblet, C.; Blundell, T. L. X-ray structure of human stromelysin catalytic domain complexed with nonpeptide inhibitors: implications for inhibitor selectivity. *Protein science : a publication of the Protein Society* **1999,** 8, 1455-62.

271.   Bertini, I.; Calderone, V.; Fragai, M.; Luchinat, C.; Mangani, S.; Terni, B. Crystal structure of the catalytic domain of human matrix metalloproteinase 10. *J Mol Biol* **2004,** 336, 707-16.

272.   Wang, L.; Hermans, J. Reaction Field Molecular Dynamics Simulation with Friedman's Image Charge Method. *The Journal of Physical Chemistry* **1995,** 99, 12001-12007.

273.   Tosco, P.; Stiefl, N.; Landrum, G. Bringing the MMFF force field to the RDKit: implementation and validation. *Journal of Cheminformatics* **2014,** 6, 37.

274.   Brooks, B. R.; Brooks, C. L., 3rd; Mackerell, A. D., Jr.; Nilsson, L.; Petrella, R. J.; Roux, B.; Won, Y.; Archontis, G.; Bartels, C.; Boresch, S.; Caflisch, A.; Caves, L.; Cui, Q.; Dinner, A. R.; Feig, M.; Fischer, S.; Gao, J.; Hodoscek, M.; Im, W.; Kuczera, K.; Lazaridis, T.; Ma, J.; Ovchinnikov, V.; Paci, E.; Pastor, R. W.; Post, C. B.; Pu, J. Z.; Schaefer, M.; Tidor, B.; Venable, R. M.; Woodcock, H. L.;

Wu, X.; Yang, W.; York, D. M.; Karplus, M. CHARMM: the biomolecular simulation program. *J Comput Chem* **2009,** 30, 1545-614.

275. Lopez-Otin, C.; Overall, C. M. Protease degradomics: a new challenge for proteomics. *Nat Rev Mol Cell Biol* **2002,** 3, 509-19.

276. Puente, X. S.; Sanchez, L. M.; Overall, C. M.; Lopez-Otin, C. Human and mouse proteases: a comparative genomic approach. *Nat Rev Genet* **2003,** 4, 544-58.

277. Schilling, O.; Overall, C. M. Proteomic discovery of protease substrates. *Curr Opin Chem Biol* **2007,** 11, 36-45.

278. Turk, B. E.; Huang, L. L.; Piro, E. T.; Cantley, L. C. Determination of protease cleavage site motifs using mixture-based oriented peptide libraries. *Nature biotechnology* **2001,** 19, 661-7.

279. Welch, A. R.; Holman, C. M.; Huber, M.; Brenner, M. C.; Browner, M. F.; Van Wart, H. E. Understanding the P1' specificity of the matrix metalloproteinases: effect of S1' pocket mutations in matrilysin and stromelysin-1. *Biochemistry* **1996,** 35, 10103-9.

280. Nagase, H.; Fields, G. B. Human matrix metalloproteinase specificity studies using collagen sequence-based synthetic peptides. *Biopolymers* **1996,** 40, 399-416.

281. Niedzwiecki, L.; Teahan, J.; Harrison, R. K.; Stein, R. L. Substrate specificity of the human matrix metalloproteinase stromelysin and the development of continuous fluorometric assays. *Biochemistry* **1992,** 31, 12618-23.

282. Nagai, Y.; Masui, Y.; Sakakibara, S. Substrate specificity of vetebrate collagenase. *Biochimica et biophysica acta* **1976,** 445, 521-4.

283. Netzel-Arnett, S.; Sang, Q. X.; Moore, W. G.; Navre, M.; Birkedal-Hansen, H.; Van Wart, H. E. Comparative sequence specificities of human 72- and 92-kDa gelatinases (type IV collagenases) and PUMP (matrilysin). *Biochemistry* **1993,** 32, 6427-32.

284. Schlage, P.; Kockmann, T.; Sabino, F.; Kizhakkedathu, J. N.; Auf dem Keller, U. Matrix Metalloproteinase 10 Degradomics in Keratinocytes and Epidermal Tissue Identifies Bioactive Substrates With Pleiotropic Functions. *Molecular & cellular proteomics : MCP* **2015,** 14, 3234-46.

285. Hu, Z.; Jiang, X.; Albright, C. F.; Graciani, N.; Yue, E.; Zhang, M.; Zhang, S. Y.; Bruckner, R.; Diamond, M.; Dowling, R.; Rafalski, M.; Yeleswaram, S.; Trainor, G. L.; Seitz, S. P.; Han, W. Discovery of matrix metalloproteases selective and activated peptide-doxorubicin prodrugs as anti-tumor agents. *Bioorganic & medicinal chemistry letters* **2010,** 20, 853-6.

286. Minond, D.; Lauer-Fields, J. L.; Cudic, M.; Overall, C. M.; Pei, D.; Brew, K.; Moss, M. L.; Fields, G. B. Differentiation of secreted and membrane-type matrix metalloproteinase activities based on substitutions and interruptions of triple-helical sequences. *Biochemistry* **2007,** 46, 3724-33.

287. Chen, E. I.; Li, W.; Godzik, A.; Howard, E. W.; Smith, J. W. A residue in the S2 subsite controls substrate selectivity of matrix metalloproteinase-2 and matrix metalloproteinase-9. *The Journal of biological chemistry* **2003,** 278, 17158-63.

288. Kridel, S. J.; Chen, E.; Kotra, L. P.; Howard, E. W.; Mobashery, S.; Smith, J. W. Substrate hydrolysis by matrix metalloproteinase-9. *The Journal of biological chemistry* **2001,** 276, 20572-8.

289. Wong, B. K.; DeFeo-Jones, D.; Jones, R. E.; Garsky, V. M.; Feng, D. M.; Oliff, A.; Chiba, M.; Ellis, J. D.; Lin, J. H. PSA-specific and non-PSA-specific

conversion of a PSA-targeted peptide conjugate of doxorubicin to its active metabolites. *Drug metabolism and disposition: the biological fate of chemicals* **2001,** 29, 313-8.

290. Kratz, F.; Mansour, A.; Soltau, J.; Warnecke, A.; Fichtner, I.; Unger, C.; Drevs, J. Development of albumin-binding doxorubicin prodrugs that are cleaved by prostate-specific antigen. *Archiv der Pharmazie* **2005,** 338, 462-72.

291. DiPaola, R. S.; Rinehart, J.; Nemunaitis, J.; Ebbinghaus, S.; Rubin, E.; Capanna, T.; Ciardella, M.; Doyle-Lindrud, S.; Goodwin, S.; Fontaine, M.; Adams, N.; Williams, A.; Schwartz, M.; Winchell, G.; Wickersham, K.; Deutsch, P.; Yao, S. L. Characterization of a novel prostate-specific antigen-activated peptide-doxorubicin conjugate in patients with prostate cancer. *Journal of clinical oncology : official journal of the American Society of Clinical Oncology* **2002,** 20, 1874-9.

292. DeFeo-Jones, D.; Garsky, V. M.; Wong, B. K.; Feng, D. M.; Bolyar, T.; Haskell, K.; Kiefer, D. M.; Leander, K.; McAvoy, E.; Lumma, P.; Wai, J.; Senderak, E. T.; Motzel, S. L.; Keenan, K.; Van Zwieten, M.; Lin, J. H.; Freidinger, R.; Huff, J.; Oliff, A.; Jones, R. E. A peptide-doxorubicin 'prodrug' activated by prostate-specific antigen selectively kills prostate tumor cells positive for prostate-specific antigen in vivo. *Nature medicine* **2000,** 6, 1248-52.

293. Breistol, K.; Hendriks, H. R.; Berger, D. P.; Langdon, S. P.; Fiebig, H. H.; Fodstad, O. The antitumour activity of the prodrug N-L-leucyl-doxorubicin and its parent compound doxorubicin in human tumour xenografts. *European journal of cancer (Oxford, England : 1990)* **1998,** 34, 1602-6.

294. Chithrani, B. D.; Ghazani, A. A.; Chan, W. C. Determining the size and shape dependence of gold nanoparticle uptake into mammalian cells. *Nano letters* **2006,** 6, 662-8.

295. Moses, M. A.; Brem, H.; Langer, R. Advancing the field of drug delivery: taking aim at cancer. *Cancer cell* **2003,** 4, 337-41.

296. Yang, K.; Zhang, S.; Zhang, G.; Sun, X.; Lee, S. T.; Liu, Z. Graphene in mice: ultrahigh in vivo tumor uptake and efficient photothermal therapy. *Nano letters* **2010,** 10, 3318-23.

297. Lu, C. H.; Yang, H. H.; Zhu, C. L.; Chen, X.; Chen, G. N. A graphene platform for sensing biomolecules. *Angewandte Chemie (International ed. in English)* **2009,** 48, 4785-7.

298. Liu, Z.; Robinson, J. T.; Sun, X.; Dai, H. PEGylated nanographene oxide for delivery of water-insoluble cancer drugs. *Journal of the American Chemical Society* **2008,** 130, 10876-7.

299. Compton, O. C.; Nguyen, S. T. Graphene oxide, highly reduced graphene oxide, and graphene: versatile building blocks for carbon-based materials. *Small (Weinheim an der Bergstrasse, Germany)* **2010,** 6, 711-23.

300. Novoselov, K. S.; Geim, A. K.; Morozov, S. V.; Jiang, D.; Zhang, Y.; Dubonos, S. V.; Grigorieva, I. V.; Firsov, A. A. Electric field effect in atomically thin carbon films. *Science (New York, N.Y.)* **2004,** 306, 666-9.

301. Sun, X.; Liu, Z.; Welsher, K.; Robinson, J. T.; Goodwin, A.; Zaric, S.; Dai, H. Nano-Graphene Oxide for Cellular Imaging and Drug Delivery. *Nano research* **2008,** 1, 203-212.

302. Wang, Y.; Shi, Z.; Huang, Y.; Ma, Y.; Wang, C.; Chen, M.; Chen, Y. Supercapacitor Devices Based on Graphene Materials. *The Journal of Physical Chemistry C* **2009,** 113, 13103-13107.

303.   Zhang, L.; Wang, Z.; Xu, C.; Li, Y.; Gao, J.; Wang, W.; Liu, Y. High strength graphene oxide/polyvinyl alcohol composite hydrogels. *Journal of Materials Chemistry* **2011,** 21, 10399-10406.

304.   Drean, A.; Goldwirt, L.; Verreault, M.; Canney, M.; Schmitt, C.; Guehennec, J.; Delattre, J. Y.; Carpentier, A.; Idbaih, A. Blood-brain barrier, cytotoxic chemotherapies and glioblastoma. *Expert review of neurotherapeutics* **2016,** 16, 1285-1300.

305.   Felpin, F.-X.; Fouquet, E. A Useful, Reliable and Safer Protocol for Hydrogenation and the Hydrogenolysis of O-Benzyl Groups: The In Situ Preparation of an Active Pd0/C Catalyst with Well-Defined Properties. *Chemistry – A European Journal* **2010,** 16, 12440-12445.

306.   Decristoforo, M. Reaction of organic compounds with low amounts of hydrogen. In Google Patents: 2014.

307.   Wang, H.; Zhang, Q.; Chu, X.; Chen, T.; Ge, J.; Yu, R. Graphene Oxide– Peptide Conjugate as an Intracellular Protease Sensor for Caspase-3 Activation Imaging in Live Cells. *Angewandte Chemie International Edition* **2011,** 50, 7065-7069.

308.   Lu, Y.-J.; Yang, H.-W.; Hung, S.-C.; Huang, C.-Y.; Li, S.-M.; Ma, C.-C. M.; Chen, P.-Y.; Tsai, H.-C.; Wei, K.-C.; Chen, J.-P. Improving thermal stability and efficacy of BCNU in treating glioma cells using PAA-functionalized graphene oxide. *International Journal of Nanomedicine* **2012,** 7, 1737-1747.

309.   Patel, S. C.; Lee, S.; Lalwani, G.; Suhrland, C.; Chowdhury, S. M.; Sitharaman, B. Graphene-based platforms for cancer therapeutics. *Therapeutic Delivery* **2016,** 7, 101-116.

310.   Yao, V. J.; D'Angelo, S.; Butler, K. S.; Theron, C.; Smith, T. L.; Marchiò, S.; Gelovani, J. G.; Sidman, R. L.; Dobroff, A. S.; Brinker, C. J.; Bradbury, A. R. M.; Arap, W.; Pasqualini, R. Ligand-targeted theranostic nanomedicines against cancer. *Journal of Controlled Release* **2016,** 240, 267-286.

311.   Qin, X. C.; Guo, Z. Y.; Liu, Z. M.; Zhang, W.; Wan, M. M.; Yang, B. W. Folic acid-conjugated graphene oxide for cancer targeted chemo-photothermal therapy. *Journal of photochemistry and photobiology. B, Biology* **2013,** 120, 156-62.

312.   Lima, F. R.; Kahn, S. A.; Soletti, R. C.; Biasoli, D.; Alves, T.; da Fonseca, A. C.; Garcia, C.; Romao, L.; Brito, J.; Holanda-Afonso, R.; Faria, J.; Borges, H.; Moura-Neto, V. Glioblastoma: therapeutic challenges, what lies ahead. *Biochimica et biophysica acta* **2012,** 1826, 338-49.

313.   Roy, S.; Lahiri, D.; Maji, T.; Biswas, J. Recurrent Glioblastoma: Where we stand. *South Asian Journal of Cancer* **2015,** 4, 163-73.

314.   Garrett, M. D.; Workman, P. Discovering novel chemotherapeutic drugs for the third millennium. *European journal of cancer (Oxford, England : 1990)* **1999,** 35, 2010-30.

Appendix 1: Human cell line origin

Cell line	Tissue of origin	Cell morphology	Culture medium
U87-MG	Brain; Grade-IV glioblastoma astrocytoma	Epithelial-like	EMEM + 1% NEAA
1321N1	Brain; Grade-II astrocytoma	Glial	DMEM
SVG-P12	Brain; Foetal glial cells	Fibroblasts	EMEM + 1% NEAA
H460	Lung cancer	Epithelial	RPMI
MCF7	Breast cancer	Epithelial	RPMI

Note: 10% fetal bovine serum (FBS) and 2 mM L-glutamine were added to each culture medium prior to supplementation

Appendix 2: Composition of Buffer RLT

According to the manufacturer, the exact composition of Buffer RLT is confidential. Buffer RLT contains a high concentration of guanidine isothiocycanate, which supports the binding of RNA to the silica membrane (Qiagen, Hilden, Germany).

Note: note that ß-mercaptoethanol should be added to Buffer RLT before use to effectively inactivate RNAses in the lysate (10 µl ß-Mercaptoethanol per 1 ml Buffer RLT).

Appendix 3: Composition of Buffer RW1

According to the manufacturer, the exact composition of Buffer RW1 is confidential. Buffer RW1 contains a guanidine salt, as well as ethanol, and is used as a stringent washing buffer that efficiently removes biomolecules such as carbohydrates, proteins, fatty acids etc., that are non-specifically bound to the silica membrane. At the same time, RNA molecules larger than 200 bases remain bound to the column (Qiagen, Hilden, Germany).

Note: Buffer RW1 should not be used for isolation of small RNAs, for example, microRNAs or fragmented RNA from formalin-fixed tissues, as these smaller fragments will be washed away. Buffer RWT should be used instead.

Appendix 4: Composition of Buffer RPE

According to the manufacturer, the exact composition of Buffer RPE is confidential. Buffer RPE is a mild washing buffer, and proprietary component of RNeasy Kits. Its main function is to remove traces of salts, which are still on the column due to buffers used in the protocol. Ethanol is an important ingredient of Buffer RPE (Qiagen, Hilden, Germany).

Appendix 5: Composition of 1X Master Mix

- 10 mM Tris-HCl
- 50 mM KCl
- 1.5 mM MgCl$_2$
- 0.2 mM dNTPs
- 5% Glycerol
- 0.08% IGEPAL CA-630
- 0.05% Tween 20
- 25 units/ml *Taq* DNA Polymerase
- pH 8.6 at 25°C

Storage temperature: -20°C

Provided by the manufacturer (New England Biolabs, USA) as '*Taq* 2X Master Mix'.

Note: IGEPAL CA-630 is a non-ionic, non-denaturing detergent with IUPAC name as octylphenoxypolyethoxyethanol.

Appendix 6: PhD publications

1. Jain *et al., J. Med. Chem.* 2017, 60, 4496-4502

Rationalized Computer-Aided Design of Matrix-Metalloprotease-Selective Prodrugs

Mohit Jain,[†] J. Jonathan Harburn,[†] Jason H. Gill,[†] Paul M. Loadman,[‡] Robert A. Falconer,[‡] Caitlin A. Mooney,[§] Steven L. Cobb,[§] and David J. Berry*[†]

[†]School of Medicine, Pharmacy and Health, Durham University, Queen's Campus, Stockton on Tees, TS17 6BH, U.K.
[‡]Institute of Cancer Therapeutics, ICT Building, University of Bradford, Bradford, BD7 1DP, U.K.
[§]Department of Chemistry, Durham University, Lower Mountjoy, South Road, Durham, DH1 3LE, U.K.

*s Supporting Information

ABSTRACT: Matrix metalloproteinases (MMPs) are central to cancer development and metastasis. They are highly active in the tumor environment and absent or inactive in normal tissues; therefore they represent viable targets for cancer drug discovery. In this study we evaluated in silico docking to develop MMP-subtype-selective tumor-activated prodrugs. Proof of principle for this therapeutic approach was demonstrated in vitro against an aggressive human glioma model, with involvement of MMPs confirmed using pharmacological inhibition.
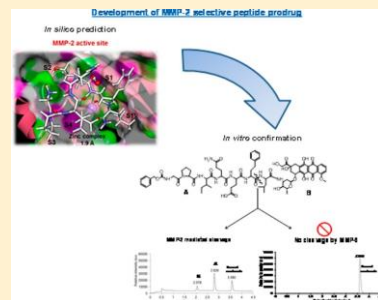
INTRODUCTION

Matrix metalloproteinases (MMPs) are zinc-dependent endoproteases central to digestion of extracellular matrix (ECM) and pericellular proteins involved in regulation of many normal physiological processes including tissue growth and embryogenesis.[1−5] Their activity is regulated by postsecretion zymogenic activation and inhibition by endogenous inhibitors termed TIMPs (tissue inhibitor of metalloproteinase).[6] However, dysregulation of MMP expression and unbalanced endoproteolytic activity of specific MMPs are a major contributor to many degradative diseases including arthritis, cancer, cardiovascular disease, inflammatory disorders, and neurodegeneration,[5,7−9] thus making them attractive drug targets.[2,10,11]

In the past 2 decades significant drug discovery effort was focused on inhibition of MMPs as a strategy to prevent tumor invasion and subsequent tumor metastases.[12] As a result, the pharmaceutical industry produced a number of well tolerated orally active MMP inhibitors (MMPi).[13] These agents were largely peptidomimetic zinc-binding hydroxamates, based upon an MMP peptide substrate.[2,14,15] Although many of these inhibitors progressed to late stage clinical trials against metastatic cancer, limited clinical success was seen due to a lack of inhibitor MMP-subtype specificity and insufficient knowledge about the complexity of the disease biology.[2,16,17] Several additional strategies have been evaluated over recent years, including development of inhibitors exploiting the enzymatic transition state,[2,18] inhibitors binding enzyme cavity subsites,[19] or alternative zinc chelation groups.[2] Generation of

MMP subfamily selective inhibitors still proves mostly elusive, however, because of the broad structural similarity of their active site, substrate complexity, and identification of specific MMPs as antitargets.[2,17]

In contrast to inhibition of MMP function, exploitation of the MMP-mediated proteolysis within diseased tissues has also been investigated as a diagnostic and prognostic approach. These studies used activity-based probes comprising a "broad-spectrum" or selective MMP-cleavable peptide labeled with a quenched fluorophore or imaging moiety.[20,21] In this approach, elevated MMP activity in the diseased tissue results in activation of the probe via selective cleavage of the peptide and release of the contrast agent, facilitating imaging and quantification of MMP activity.[20,21]

In line with the MMP-activated probe-based approaches, elevated activity of MMPs within diseased tissue has also been explored as a strategy for conversion of a nontoxic peptide-conjugated prodrug into a potent therapeutic entity within the disease site. The advantage of this approach is dose intensification and reduced systemic drug exposure.[1,22−26] A requirement for success in activity probes, prodrugs, or theranostic approaches is MMP selectivity through incorporation of MMP-subtype unique (e.g., MMP-2, MMP-9, or MMP-14) peptide sequences and subsequent disease-selective activation.

The rationale for this study is to exploit the MMP binding subsites and modify the substrate residues to produce a prodrug selective for MMP-2 over MMP-9 and MMP-14 and create a robust approach that could be exploited for development of endoprotease-activated diagnostic probes and therapeutics. Visualizing and quantifying binding preferences and motifs can provide valuable insight into the structural determinants of substrate selectivity and enable MMP-targeted drug development.[27] In order to achieve this, the following steps were undertaken: definition of the catalytic domains within the relevant MMPs through in silico study, docking of known MMP-selective sequences to highlight key catalytic binding determinants, subsequent rational design of novel MMP-selective prodrugs, and in vitro confirmation of MMP selectivity and therapeutic proof-of-concept. In this work a reiterative approach using in silico proteolytic docking coupled to in vitro biochemical assessment has been applied to enable the development of prodrugs that are selectively activated by MMP-2 over MMP-9, the closely related gelatinase family members, and over MMP-14, the endogenous activator of MMP-2. The availability of three-dimensional crystal structures of MMPs allowed us to critically examine the differences existing between the catalytic domains of the MMP-2 (PDB code 1QIB), MMP-9 (PDB code 1GKC), and MMP-14 (PDB code 1BQQ).[28−30] This allowed for successful development of in silico models of MMPs. The in silico model was able to accurately predict known cleavage sites on substrates and prodrugs by MMPs, thus enabling rationalized design of an MMP-2 selective peptide.

RESULTS AND DISCUSSION

The catalytic domain of MMPs consists of five β-sheet strands and three α-helixes. The catalytic center comprises a catalytic zinc ion coordinated by three histidine residues and a glutamic acid.[28] The specificity loop within the catalytic site of MMPs shows the largest structural differences, as visualized for MMP-2 and MMP-9 in Figure S1 in Supporting Information. The overall folding of MMP-2 and MMP-9 resembles those of other MMPs, which is expected based on their structural similarity (Figure S1).[31] The cavity of S1′ pockets in MMPs is well-suited to accommodate a wide range of hydrophobic residues, with the main functional difference between MMP subtypes lying in this region. In MMP-9, residues 421−423 form the wall of the binding pocket and the specificity loop is formed by the residues 424−430. Arg424 is present at the bottom of S1′ pocket and closes off the end. Arg424 is therefore responsible for making the pocket cavity smaller in MMP-9 than in MMP2 (Figure S1), whereas in MMP-2, the external wall of the S1′ pocket is largely formed by Thr227-Phe232 specificity residues, creating a deeper pocket. These differences can potentially be exploited for rational design of MMP-selective substrates/conjugates.

To probe the selective binding of potential substrates, the peptide sequence of the nonspecific gelatinase substrate 1 Dnp-Pro-β-cyclohexyl-Ala-Gly-Cys(Me)-His-Ala-Lys(N-Me-Abz)-NH2 (M-2055)[32] was input into BIOVIA Discovery Studio 4.0, minimized with respect to its geometry, and then docked into the MMPs. In order to validate modeling work, attempts at crystallization of this and other substrates were undertaken to determine the X-ray crystal structure. Crystallization experiments failed to yield suitable crystals for structure determination; therefore only force field (CHARMM) minimized

geometries of the substrates were employed throughout this study.

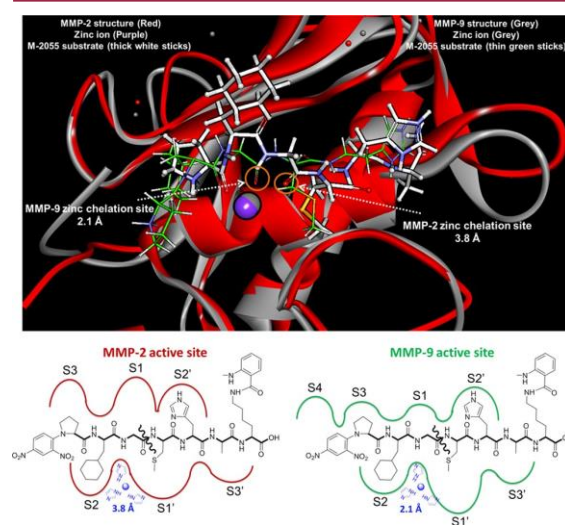Figure 1 shows the interaction of 1 peptide sequence with human MMP-2 and MMP-9. In both MMPs the zinc ion

Figure 1. (Top) Docked complexes of 1 substrate and the catalytic domain of human MMP-2 (PDB code 1QIB) and MMP-9 (PDB code 1GKC). The MMP-substrate docked complexes are merged with zinc as the same point of view. MMP-2 structure is shown in red, zinc as purple, and 1 substrate (white sticks) docked within MMP-2 active site. MMP-9 is shown in gray, zinc as green, and 1 substrate (thin green sticks) docked within its active site. (Bottom) Schematic representation of 1: active site binding interaction in human MMP-2 and MMP-9. MMP-2 and MMP-9 enzyme binding pockets are shown in red and green, respectively. Substrate chemical structure and its scissile bond are shown in black. The zinc ion is indicated in blue.

interacts with the Gly and Cys(Me) bond, the known cleavage site according to Bickett et al.[32] MMP-9 is able to bind tightly with the substrate residues compared to MMP-2, as determined by differences in their predicted interatomic zinc distances and overall binding energies. The substrate bound MMP complexes provided crucial insight into the differences in their subsite interactions, as S1 and S3 subsites in MMP-2 demonstrated affinity to accommodate longer side chains than MMP-9. The charged nature of the S2 subsite (presence of His205) in MMP-2 lends affinity for acidic residues, whereas this feature is not observed in MMP-9. In the MMP-9 structure, the carboxylic acid between Gly and Cys(Me) chelates the zinc ion (2.1 Å) and is involved in a strong H-bond to the carboxylate O of Glu402. The zinc ion is further coordinated by three histidine residues, namely, His401, His405, and His411 present in Helix αβ segment of the protein. Only the P1′ amino acid is involved in strong H-bonds with Arg424 (2.2 Å), which creates the wall-forming segment. The strong binding of Arg424 with the P1′ residue is an important determinant of the specificity pocket. Remaining substrate residues are involved in strong interactions with the bulge-edge segment molecules (Gly186 to His190) with interatomic distances ranging from 2.5 to 3.1 Å. The docked complex of 1 and MMP-9 has an overall binding energy of 706 kcal/mol (Figures 1, S2, S3, and S4).

Consideration of the interaction of 1 with the active site of MMP-2 shows a marked reduction in affinity in energetic

326

terms; the predicted interaction is 7 times weaker than that of 1 and MMP-9 (binding energy of 101 kcal/mol). Gly forms the P1 subsite and Cys(Me) forms the P1′ subsite, and the presence of a zinc ion, chelated by the carboxylic acid between P1 and P1′ residues (3.8 Å), further confirms this. The P1′ residue, although favorable for the MMP-2 specificity pocket, is not involved in any significant interaction with MMP-2 residues. The remaining substrate residues have weak H-bond interactions with wall-forming and bulge-edge segments of MMP-2 with interatomic distances ranging from 3.1 to 5.1 Å. This is expected as 1 residues are oriented away from further MMP-2 binding pockets (Figures 1, S2, S3, and S4). Key observed differences between the binding affinity of MMP-2 and MMP-9 with 1 are S1 and S3 subsites in MMP-2 that can accommodate longer side chains than MMP-9. Charged nature of S2 subsite in MMP-2 has affinity for acidic residues, whereas this feature is not observed in MMP-9. Refer to Figure S5 for in silico binding of 1 with the active site of MMP-14, also demonstrating zinc interaction between Gly-Cys(Me) bond.

To experimentally validate the predictability of this model and confirm the in vitro cleavage position of 1, hydrolysis of the substrate by recombinant MMP-2 and MMP-9 was assessed over a 12 h period. The resultant products were analyzed by LCMS using a reverse phase gradient system to separate the substrate 1 and proteolytic products. The identification of these species was confirmed by retention time and mass spectrometry (MS) data. 1 demonstrated a retention time (t_R) of 2.8 min (Figure S6), and rapid cleavage by MMP-9 at Gly-Cys(Me) bond was confirmed by LCMS, two peaks corresponding to Dnp-Pro-β-cyclohexyl-Ala-Gly at t_R of 2.3 min (m/z 491.5 Da, [M + H]$^+$) and Cys(Me)-His-Ala-Lys(N-Me-Abz)-NH$_2$ at t_R of 2.47 min (m/z 604.7 Da, [M + H]$^+$) (Figures 2 and S7). Slow
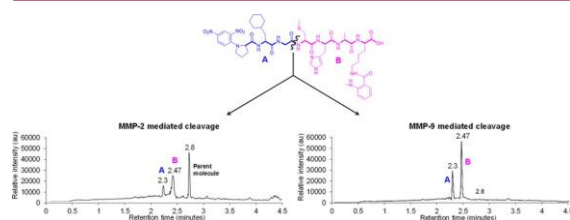

Figure 2. Schematic representation of the cleavage of 1 substrate by recombinant MMP-2 and MMP-9 enzymes at Gly-Cys(Me).

hydrolysis of 1 by MMP-2 (compared to MMP-9) at Gly-Cys(Me) bond was confirmed by two peaks at t_R of 2.3 min and t_R of 2.47 min. MMP-2 cleavage experiments displayed a parent peak of 1, detected at t_R of 2.8 min (m/z 1077.5 Da, [M + H]$^+$), suggesting that MMP-2 metabolized 1 at a slower rate than MMP-9 (Figures 2 and S8). Recombinant MMP-14 also cleaved 1 at the Gly-Cys(Me), confirming the in silico prediction (Figure S9). This in vitro assessment supports the validity of the predicted in silico model of substrate and MMP interactions and was subsequently used for further design of MMP-targeted therapeutics.

The next phase of the study was to design a prodrug (substrate and warhead) that would be selectively activated by a specific MMP over a close family homologue, i.e., cleaved by MMP-2 and not by MMP-9 or MMP-14. A known MMP-targeted peptide-conjugated doxorubicin prodrug[33,34] was evaluated as it is cleaved by MMP-2, MMP-9, and MMP-14, presenting an excellent model for further modification. MMP-

targeted peptide conjugates were synthesized via solid phase chemistry and purified by reverse phase HPLC, the chemotherapeutic drug doxorubicin conjugated to the C-terminus (Scheme S10). In silico interaction of the 2 (reference compound) with MMP-2 and MMP-9 shows the zinc ions are chelated by the carboxylate between Gly-Ser(O-benzyl) bond (2.6 and 2.8 Å, respectively), the known cleavage site.[31,32] Figure S11 shows that the binding pockets of MMP-2 are larger and deeper than MMP-9, S1 subsite allowing for larger aromatic residues. Compound 2 aligns tightly into the active site of both MMPs as shown by their predicted interatomic zinc distances and binding energies (555 and 492 kcal/mol) in MMP-2 and MMP-9 docked complexes, respectively. Active site residues interact with the compound in a similar way to that previously explained. His205 in MMP-2 αβ-helix loop makes the S2 pocket charged in nature and could potentially accommodate acidic residues (Figures S11 and S12). Similar to MMP-2 and MMP-9, MMP-14 also demonstrated selective interaction with 2 (Figure S13) To experimentally validate the in silico docking of 2[33,34] and confirm the in vitro cleavage site, the lysis of this prodrug by recombinant MMP-2 and MMP-9 was assessed over a 12 h period, with the resultant products being assessed by LCMS. HPLC (reverse phase gradient) was used to separate 2 (Cbz-Glu-Pro-Leu-Gly-Ser(O-benzyl)-Tyr-Leu-doxorubicin),[33,34] identification confirmed by mass spectrometry (MS) with a retention time of 3.63 min (Figure S14). Cleavage of 2 by MMP-2 and MMP-9 at Gly-Ser(O-benzyl) bond was confirmed by LCMS, two peaks corresponding to Cbz-Glu-Pro-Leu-Gly at t_R of 2.87 min (m/z 547.2 Da, [M + H]$^+$) and Ser(O-benzyl)-Tyr-Leu-doxorubicin at t_R of 3.23 min (m/z 997.4, [M + H]$^+$) (Figures 3, S15, and S16). A parent
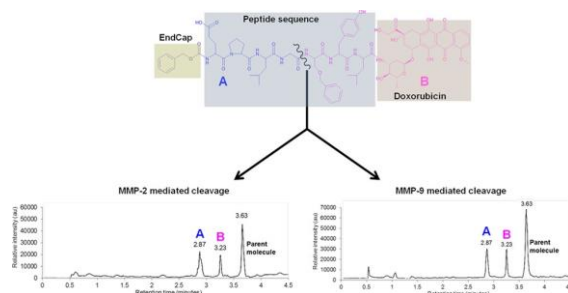

Figure 3. Schematic representation of the cleavage of 2 by recombinant MMP-2 and MMP-9 enzymes at the Gly-Ser(O-Bn) bond.

peak was also detected at t_R of 3.63 min (m/z 1525.8 Da, [M + H]$^+$). Similarly, MMP-14 also displayed hydrolysis of 2 at the Gly-Ser(O-Benzyl) bond (Figure S17). This in vitro assessment supports the predictability of the in silico model of anticancer therapeutics with MMPs for further design of MMP-2 selective prodrugs.

Rational design of a peptide conjugate selective for MMP-2 over MMP-9 was achieved by incorporating residues into the peptide chain to fit S1, S2, S3, and S1′ pockets of MMP-2 which differ in size and polar affinity compared to MMP-9. The following modifications were incorporated: aromatic residues in S1 subsite; acidic side chain in S2 subsite, and a polar side chain at the S3 subsite. Small nonpolar residues were included at the S1′ subsite despite S1′s potential to accommodate longer hydrophobic residues. This was due to longer residues leading

to a negative effect on the predicted binding affinity, due to conformational alteration.

The zinc ion in MMP-2 demonstrated interaction with 3 at carboxylate between homophenylalanine (Hof)-Leu bond (1.9 Å), indicating the predicted cleavage site. Residues of MMP-2 tightly bind with 3 as demonstrated by strong interactions with the bulge-edge segment molecules (Gly162 to His166) and the wall-forming segment molecules (Tyr223 to Thr229) with interatomic distances ranging from 1.8 to 2.8 Å. The docked complex of 3 and MMP-2 has an overall binding energy of 805 kcal/mol. In MMP-9 the zinc interaction is not detectable and the predicted binding energy is negative (-107 kcal/mol), suggesting the modified peptide residues should give selectivity of MMP-2 over MMP-9 (Figures 4, S18, and S19). Similarly,
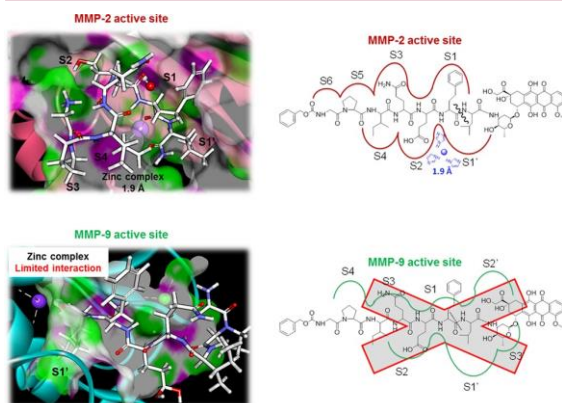

Figure 4. (Left) Docked complexes of 3 (white sticks), catalytic domain of human MMP-2 (PDB code 1QIB) (red), and MMP-9 (PDB code 1GKC) (green). Catalytic and structural zinc ions are shown as purple spheres, and active-site cleft residues (αβ-helix loop and the specificity loop) are shown as green. (Right) Schematic representation of 3 substrate active site binding interactions in MMP-2 and MMP-9 are shown in red and green, respectively. Substrate chemical structure and its scissile bond are shown in black, and zinc ion coordinated by histidine is indicated in blue.

on the basis of the peptide modifications for MMP-14 selectivity suggested in the literature,[35,36] the zinc interaction between 3 and MMP-14 was nondetectable and the binding energy was negative (Figure S20). The hydrolysis of 3 by recombinant MMP-2, MMP-9, and MMP-14 was assessed over a 12 h period and analyzed by LCMS. Reverse phase HPLC identified 3 at t_R of 3.58 min (Figure S21). 3 was preferentially cleaved by MMP-2 at Hof-Leu, and two peaks were identified corresponding to Leu-doxorubicin at t_R of 2.078 min (m/z 657.2 Da, [M + H]$^+$) and Cbz-Gly-Pro-Ile-Gln-Glu-Hof at t_R of 2.826 min (m/z 821.4 Da, [M + H]$^+$) (Figures S22 and S23). Conversely MMP-9 and MMP-14 did not cleave 3 in the same time frame, indicating that 3 is MMP-2 selective supporting the in silico prediction (Figures S22 and S24).

In order to assess activity and demonstrate proof-of-concept for the developing approach, the effects of 3 were assessed against the U87-MG malignant human glioma cell line. This cell line is derived from a highly aggressive glioma tumor and expresses MMP-2 and MMP-9 (Figure 5). Cytotoxicity was observed in this cell line with doxorubicin, leucine-doxorubicin (Leu-Dox), and 3, with IC$_{50}$ values of 0.3 ± 0.2 μM, 0.6 ± 0.2 μM, and 5.0 ± 1.2 μM, respectively. The differential
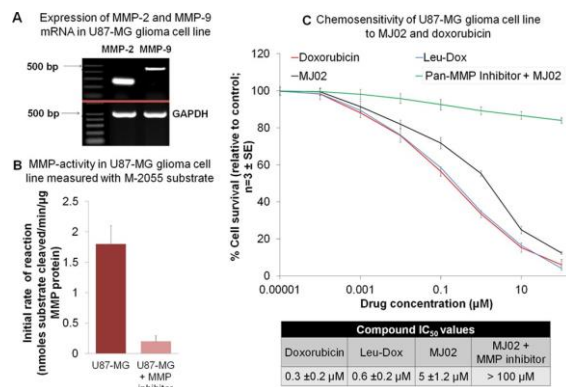

Figure 5. Therapeutic activity of 3 against human cancer. (A) expression of MMP-2 and MMP-9 mRNA in the U87-MG glioma cell line; (B) MMP activity in the U87-MG cell line, as demonstrated by activation of 1 substrate Dnp-Pro-β-cyclohexyl-Ala-Gly-Cys(Me)-His-Ala-Lys(N-Me-Abz)-NH$_2$; (C) cytotoxicity of doxorubicin, Leu-Dox, and 3 against U87-MG cell line. MMP-selective activation of 3 in the presence of a pan-MMP inhibitor (Ilomastat).

cytotoxicity between doxorubicin and 3 supports the requirement for 3 to be activated prior to inducing its effects. Furthermore, 3 remained inactive in the presence of a pan-MMP inhibitor, (2R)-N'-hydroxy-N-[(2S)-3-(1H-indol-3-yl)-1-(methylamino)-1-oxopropan-2-yl]-2-(2-methylpropyl)-butanediamide (GM6001, ilomastat/galardin),[37] demonstrating MMP-selective chemotherapeutic action of this prodrug.

In order to further determine the tumor-selective activation of 3, its metabolism was studied ex vivo using MMP-expressing HT1080 human tumor xenograft,[33] mouse plasma, and homogenized murine liver and kidney tissues (Figure S25). Rapid metabolism of 3 was observed in the HT1080 xenograft homogenate ($t_{1/2} \geq 8.8$ min). In comparison, 3 was relatively stable in plasma ($t_{1/2} \gg 90$ min), murine liver ($t_{1/2} \geq 17.0$ min), and murine kidney ($t_{1/2} \geq 38.1$ min). The liver homogenate is a "worse case scenario" for 3's stability due to a high proportion of extracelluar and intracellular proteases. 3 displayed relative stability in mouse plasma and liver and kidney homogenates and associated rapid metabolism in tumor homogenates.

CONCLUSIONS

Targeted cancer therapies offer the potential of reduced side effects along with benefits of prolonging drug exposure to cancerous tissues, enabling improved tumor response and survival rates.[38,39] Harnessing the elevated enzymatic activity of MMPs within the tumor microenvironment to selectively convert a nontoxic prodrug into a potent chemotherapeutic agent is one such approach with significant potential therapeutic scope.[40,41] In this study a reiterative approach using in silico docking coupled to in vitro biochemical proteolytic assessment has been applied to enable the development of anticancer prodrugs selectively activated by MMP-2 but not by dose family homologue MMP-9 or the MMP-2 activator MMP-14. Proof-of-concept for this therapeutic approach was demonstrated against a glioma cell line in vitro, with the involvement of MMPs confirmed using pharmacological inhibition and by tumor-selective activation with ex vivo tumor xenografts. This study has shown that it is feasible to utilize in silico predictive approaches to rationally

328

design MMP-selective prodrugs with possible utility in the treatment of cancer.

EXPERIMENTAL SECTION

3D Molecular Modeling. Refer to method S30.

Synthesis of MMP-Targeted Peptide Conjugates. Custom designed peptide sequences with Cbz (benzyloxycarbonyl) as the chemical endcap were supplied (Bachem, Switzerland) or synthesized using solid phase strategy. Activation of the preloaded 2-chlorotrityl resin was carried out in a fritted polypropylene reaction chamber. 0.1 mmol of resin was weighed into the reaction chamber and 2 mL of dry DCM added. The reaction vessel was shaken for 45 min. After this time, DCM was removed and the resin washed further with DCM. Single couplings were carried out using 5 equiv of peptide (compared to resin), 5 equiv of benzotriazol-1-yloxytripyrrolidinophosphonium hexafluorophosphate (PyBOP), 10 equiv of *N,N*-diisopropyl-ethylamine (DIPEA), and 2 mL of DMF under agitation for 45 min. Double peptide couplings were carried out (2 × 45 min couplings for each residue addition), the reaction was drained after each coupling, and fresh reagents were added. After each set of coupling reactions, the reaction solution was drained and resin washed with 5 portions of 2 mL of DMF. Removal of the Fmoc group was carried out using 5 mL of a solution of 20% piperidine in DMF for 5 under agitation. Piperidine solution was drained and fresh solution added for a further 10 min under agitation. Piperidine solution was drained and the resin rinsed using 5 portions of 2 mL of DMF. Peptide-resin was treated with a solution of 20% hexafluoroisopropanol in DCM for 1 h. The resin was removed by filtration and the solvent removed from the filtrate under reduced pressure before precipitation using ether and decanting of the liquid (followed by subsequent ether washes). The resulting solid peptide (Cbz-GPIQ(Trt)-E(tBu)-hPhe-L-OH) was dissolved in deionized water and acetonitrile mix and lyophilized. Purification of peptides was carried out using Perking Elmer HPLC. Samples were injected into a column and a gradient of 0−100% solvent B (solvent A = 95% H_2O, 5% MeCN, 0.01% TFA, solvent B = 95% MeCN, 5% H_2O, 0.01% TFA) over 95 min with a flow rate of 2.0 mL/min. Doxorubicin was conjugated to the peptide C-terminus as follows: doxorubicin·HCl (0.0012 g, 0.002 mol, 1 equiv), peptide (0.0022 g, 0.002 mol, 1 equiv), PyBOP (0.0015 g, 0.003 mol, 1.3 equiv), and hydroxybenzotriazole hydrate (0.0073 g, 0.0054 mol, 2.6 equiv) were added together under nitrogen in anhydrous DMF (2 mL). DIPEA (8 equiv, 0.016 mol) was added, and the reaction mixture was stirred overnight in the absence of light. Solvent was removed in vacuo and the mixture triturated with cold Et_2O (5 mL) to precipitate the crude peptide which was then obtained through centrifugation to obtain the crude solid peptide conjugate. The product was then purified using a C18 column and reverse phase HPLC (H_2O/MeCN) gradient system using mass spectrometry as confirmation of molecular mass to give a pale red solid (0.0021 g, 70% yield).

Liquid Chromatography and Mass Spectrometry (LCMS) Detection of Substrates. *LC Conditions.* High-purity HPLC-grade solvents (Sigma-Aldrich), analytical grade chemicals (Sigma-Aldrich), and triple distilled water were used throughout. Reverse-phase chromatographic separation of substrates was performed using an Acquity UPLC comprising a BEH C18 1.7 μm column (2.1 mm × 100 mm) (Waters, U.K.). Mobile phases were as follows: Mobile phase A consisted of 90% HPLC grade water, 10% HPLC grade MeCN, and 0.1% HCO_2H. Mobile phase B consisted of 40% HPLC grade water, 60% MeCN, and 0.1% HCO_2H.

MS Conditions. A Micromass ZMD single quadrupole electrospray MS was used in positive mode (Micromass, Manchester, U.K.), and MassLynx software was used to identify substrates and anticipated metabolites. MS source parameters were optimized to desolvation gas 375 L/h, cone gas 33 L/h, capillary 2.9 kV, sample cone 16 V, extraction cone 5 V, fR lens 0.1 V, source block temperature 150 °C, and desolvation temperature 200 °C. Parent compounds and metabolites were detected as singularly charged ions using selected ion readings (SIRs).

Cleavage of Substrates by Recombinant MMPs. Refer to method S31.

Determination of MMP mRNA Expression by Semiquantitative RT-PCR Analysis. Refer to method S32.

MTT Assay. Refer to method S33.

Metabolism of 3 in Tissues ex Vivo. Refer to method S34.

ASSOCIATED CONTENT

* Supporting Information

The Supporting Information is available free of charge on the ACS Publications website at DOI: 10.1021/acs.jmedchem.6b01472.

Structural analysis of MMP 2 and MMP 9, Figure S1; chemical interaction of MMPs with 1 and 3D docking of MMP-14 with 1, Figures S2−S5; electrospray ionization liquid chromatography−mass spectrometry (ESI-LCMS) identification of 1 and its metabolites, Figures S6−S9; synthetic scheme for the production of the peptide doxorubicin conjugates, Figure S10; 3D and chemical interaction of 2 with MMPs, Figures S11−S13; LCMS analysis of 2 cleavage by MMPs, Figures S14−S17; chemical and 3D interaction of 3 with MMPs, Figures S18−S20; LCMS detection of 3 and analysis of its cleavage by MMP-2, MMP-9, and MMP-14, Figures S21−S24; metabolism of 3 in tissues ex vivo, Figure S25; superimposition of MMP-9 docked with 1, presented with zinc in the same point of view, Figure S26; description of in silico and in vitro methods, sections S27−S31 (PDF)

Molecular formula strings (CSV)

AUTHOR INFORMATION

Corresponding Author

*E-mail: d.j.berry@durham.ac.uk. Phone: (0044) 1913 340817.

ORCID

David J. Berry: 0000-0001-6321-7379

Notes

The authors declare no competing financial interest.

ACKNOWLEDGMENTS

ABBREVIATIONS USED

DCM, dichloromethane; DIPEA, *N,N*-diisopropylethylamine; DMF, dimethylformamide; Et_2O, diethyl ether; HCO_2H, formic acid; HPLC, high performance liquid chromatography; HT1080, human fibrosarcoma; LCMS, liquid chromatography−mass spectrometry; MeCN, acetonitrile; MMP, matrix metalloprotease; MTT, 3-(4,5-Ddimethylthiazol-2-yl)-2,5-diphenyltetrazolium bromide; PyBOP, benzotriazol-1-yloxy-tripyrrolidinophosphonium hexafluorophosphate; TFA, trifluoroacetic acid; U87-MG, human malignant glioma

REFERENCES

(1) Atkinson, J. M.; Siller, C. S.; Gill, J. H. Tumour endoproteases: the cutting edge of cancer drug delivery? *Br. J. Pharmacol.* 2008, *153*, 1344−1352.

(2) Vandenbroucke, R. E.; Libert, C. Is there new hope for therapeutic matrix metalloproteinase inhibition? *Nat. Rev. Drug Discovery* 2014, *13*, 904−927.

(3) Brown, P. D. Matrix metalloproteinase inhibitors in the treatment of cancer. *Med. Oncol.* 1997, *14*, 1−10.

329

(4) Bourboulia, D.; Stetler-Stevenson, W. G. Matrix metalloproteinases (MMPs) and tissue inhibitors of metalloproteinases (TIMPs): Positive and negative regulators in tumor cell adhesion. *Semin. Cancer Biol.* 2010, *20*, 161−168.

(5) Khokha, R.; Murthy, A.; Weiss, A. Metalloproteinases and their natural inhibitors in inflammation and immunity. *Nat. Rev. Immunol.* 2013, *13*, 649−665.

(6) Visse, R.; Nagase, H. Matrix metalloproteinases and tissue inhibitors of metalloproteinases: structure, function, and biochemistry. *Circ. Res.* 2003, *92*, 827−839.

(7) Clark, I. A.; Swingler, T. E.; Sampieri, C. L.; Edwards, D. R. The regulation of matrix metalloproteinases and their inhibitors. *Int. J. Biochem. Cell Biol.* 2008, *40*, 1362−1378.

(8) Nagase, H.; Visse, R.; Murphy, G. Structure and function of matrix metalloproteinases and TIMPs. *Cardiovasc. Res.* 2006, *69*, 562−573.

(9) Shay, G.; Lynch, C. C.; Fingleton, B. Moving targets: Emerging roles for MMPs in cancer progression and metastasis. *Matrix Biol.* 2015, *44−46*, 200−206.

(10) Hu, J.; Van den Steen, P. E.; Sang, Q. X.; Opdenakker, G. Matrix metalloproteinase inhibitors as therapy for inflammatory and vascular diseases. *Nat. Rev. Drug Discovery* 2007, *6*, 480−498.

(11) Pirard, B. Insight into the structural determinants for selective inhibition of matrix metalloproteinases. *Drug Discovery Today* 2007, *12*, 640−646.

(12) Overall, C. M.; Kleifeld, O. Tumour microenvironment - opinion: validating matrix metalloproteinases as drug targets and anti- targets for cancer therapy. *Nat. Rev. Cancer* 2006, *6*, 227−239.

(13) Mccullagh, K.; Wadsworth, H.; Hann, M. Carboxyalkyl peptide derivatives. EP 0126974 A1, 1985.

(14) De, B.; Natchus, M. G.; Cheng, M.; Pikul, S.; Almstead, N. G.; Taiwo, Y. O.; Snider, C. E.; Chen, L.; Barnett, B.; Gu, F.; Dowty, M. The next generation of MMP inhibitors. Design and synthesis. *Ann. N. Y. Acad. Sci.* 1999, *878*, 40−60.

(15) Overall, C. M.; Kleifeld, O. Towards third generation matrix metalloproteinase inhibitors for cancer therapy. *Br. J. Cancer* 2006, *94*, 941−946.

(16) Coussens, L. M.; Fingleton, B.; Matrisian, L. M. Matrix metalloproteinase inhibitors and cancer: Trials and tribulations. *Science* 2002, *295*, 2387−2392.

(17) Dufour, A.; Overall, C. M. Missing the target: matrix metalloproteinase antitargets in inflammation and cancer. *Trends Pharmacol. Sci.* 2013, *34*, 233−242.

(18) Georgiadis, D.; Dive, V. Phosphinic peptides as potent inhibitors of zinc-metalloproteases. *Top. Curr. Chem.* 2014, *360*, 1−38.

(19) Jacobsen, J. A.; Major Jourden, J. L.; Miller, M. T.; Cohen, S. M. To bind zinc or not to bind zinc: an examination of innovative approaches to improved metalloproteinase inhibition. *Biochim. Biophys. Acta, Mol. Cell Res.* 2010, *1803*, 72−94.

(20) Heal, W. P.; Wickramasinghe, S. R.; Tate, E. W. Activity based chemical proteomics: profiling proteases as drug targets. *Curr. Drug Discovery Technol.* 2008, *5*, 200−212.

(21) Chuang, C. H.; Chuang, K. H.; Wang, H. E.; Roffler, S. R.; Shiea, J. T.; Tzou, S. C.; Cheng, T. C.; Kao, C. H.; Wu, S. Y.; Tseng, W. L.; Cheng, C. M.; Hou, M. F.; Wang, J. M.; Cheng, T. L. In vivo positron emission tomography imaging of protease activity by generation of a hydrophobic product from a noninhibitory protease substrate. *Clin. Cancer Res.* 2012, *18*, 238−247.

(22) Atkinson, J. M.; Falconer, R. A.; Edwards, D. R.; Pennington, C. J.; Siller, C. S.; Shnyder, S. D.; Bibby, M. C.; Patterson, L. H.; Loadman, P. M.; Gill, J. H. Development of a novel tumor-targeted vascular disrupting agent activated by membrane-type matrix metalloproteinases. *Cancer Res.* 2010, *70*, 6902−6912.

(23) Vandooren, J.; Opdenakker, G.; Loadman, P. M.; Edwards, D. R. Proteases in cancer drug delivery. *Adv. Drug Delivery Rev.* 2016, *97*, 144−155.

(24) Choi, K. Y.; Swierczewska, M.; Lee, S.; Chen, X. Protease-activated drug development. *Theranostics* 2012, *2*, 156−178.

(25) Ansari, C.; Tikhomirov, G. A.; Hong, S. H.; Falconer, R. A.; Loadman, P. M.; Gill, J. H.; Castaneda, R.; Hazard, F. K.; Tong, L.; Lenkov, O. D.; Felsher, D. W.; Rao, J.; Daldrup-Link, H. E. Development of novel tumor-targeted theranostic nanoparticles activated by membrane-type matrix metalloproteinases for combined cancer magnetic resonance imaging and therapy. *Small* 2014, *10*, 566−575.

(26) Wang, Y.; Pu, L.; Li, Z.; Hu, X.; Jiang, L. Hypoxia-inducible factor-1alpha gene expression and apoptosis in ischemia-reperfusion injury: a rat model of early-stage pressure ulcer. *Nurs. Res.* 2016, *65*, 35−46.

(27) Huggins, D. J.; Sherman, W.; Tidor, B. Rational approaches to improving selectivity in drug design. *J. Med. Chem.* 2012, *55*, 1424−1444.

(28) Rowsell, S.; Hawtin, P.; Minshull, C. A.; Jepson, H.; Brockbank, S. M.; Barratt, D. G.; Slater, A. M.; McPheat, W. L.; Waterson, D.; Henney, A. M.; Pauptit, R. A. Crystal structure of human MMP9 in complex with a reverse hydroxamate inhibitor. *J. Mol. Biol.* 2002, *319*, 173−181.

(29) Dhanaraj, V.; Ye, Q.-Z.; Johnson, L. L.; Hupe, D. J.; Ortwine, D. F.; Dunbar, J. B.; Rubin, J. R.; Pavlovsky, A.; Humblet, C.; Blundell, T. L. X-ray structure of gelatinase A catalytic domain complexed with a hydroxamate inhibitor. *Croat. Chem. Acta* 1999, *72*, 575−591.

(30) Fernandez-Catalan, C.; Bode, W.; Huber, R.; Turk, D.; Calvete, J.J.; Lichte, A.; Tschesche, H.; Maskos, K. Crystal structure of the complex formed by the membrane type 1-matrix metalloproteinase with the tissue inhibitor of metalloproteinase-2, the soluble progelatinase A receptor. *EMBO J.* 1998, *17*, 5238−5248.

(31) Maskos, K. Crystal structures of MMPs in complex with physiological and pharmacological inhibitors. *Biochimie* 2005, *87*, 249−263.

(32) Bickett, D. M.; Green, M. D.; Berman, J.; Dezube, M.; Howe, A. S.; Brown, P. J.; Roth, J. T.; McGeehan, G. M. A high throughput fluorogenic substrate for interstitial collagenase (MMP-1) and gelatinase (MMP-9). *Anal. Biochem.* 1993, *212*, 58−64.

(33) Albright, C. F.; Graciani, N.; Han, W.; Yue, E.; Stein, R.; Lai, Z.; Diamond, M.; Dowling, R.; Grimminger, L.; Zhang, S. Y.; Behrens, D.; Musselman, A.; Bruckner, R.; Zhang, M.; Jiang, X.; Hu, D.; Higley, A.; Dimeo, S.; Rafalski, M.; Mandlekar, S.; Car, B.; Yeleswaram, S.; Stern, A.; Copeland, R. A.; Combs, A.; Seitz, S. P.; Trainor, G. L.; Taub, R.; Huang, P.; Oliff, A. Matrix metalloproteinase-activated doxorubicin prodrugs inhibit HT1080 xenograft growth better than doxorubicin with less toxicity. *Mol. Cancer Ther.* 2005, *4*, 751−760.

(34) Hu, Z.; Jiang, X.; Albright, C. F.; Graciani, N.; Yue, E.; Zhang, M.; Zhang, S. Y.; Bruckner, R.; Diamond, M.; Dowling, R.; Rafalski, M.; Yeleswaram, S.; Trainor, G. L.; Seitz, S. P.; Han, W. Discovery of matrix metalloproteases selective and activated peptide-doxorubicin prodrugs as anti-tumor agents. *Bioorg. Med. Chem. Lett.* 2010, *20*, 853−856.

(35) Atkinson, J. M.; Falconer, R. A.; Edwards, D. R.; Pennington, C. J.; Siller, C. S.; Shnyder, S. D.; Bibby, M. C.; Patterson, L. H.; Loadman, P. M.; Gill, J. H. Development of a novel tumor-targeted vascular disrupting agent activated by MT-MMPs. *Cancer Res.* 2010, *70*, 6902−6912.

(36) Kridel, S. J.; Sawai, H.; Ratnikov, B. I.; Chen, E. I.; Li, W.; Godzik, A.; Strongin, A. Y.; Smith, J. W. A unique substrate binding mode discriminates membrane type-I matrix metalloproteinase from other matrix metalloproteinases. *J. Biol. Chem.* 2002, *277*, 23788−23793.

(37) McClellan, M.; Benner, J.; Schilsky, R.; Epstein, D.; Woosley, R.; Friend, S.; Sidransky, D.; Geoghegan, C.; Kessler, D. An accelerated pathway for targeted cancer therapies. *Nat. Rev. Drug Discovery* 2011, *10*, 79−80.

(38) Santiskulvong, C.; Rozengurt, E. Galardin (GM6001), a broad-spectrum matrix metalloproteinase inhibitor, blocks bombesin- and LPA-induced EGF receptor transactivation and DNA synthesis in rat-1 cells. *Exp. Cell Res.* 2003, *290*, 437−446.

330

(39)Wang, H.; Xu, T.; Jiang, Y.; Xu, H.; Yan, Y.; Fu, D.; Chen, J. The challenges and the promise of molecular targeted therapy in malignant gliomas. *Neoplasia* 2015, *17*, 239−255.

(40)Vartak, D. G.; Gemeinhart, R. A. Matrix metalloproteases: underutilized targets for drug delivery. *J. Drug Target* 2007, *15*, 1−20.

(41) Cathcart, J.; Pulkoski-Gross, A.; Cao, J. Targeting matrix metalloproteinases in cancer: bringing new life to old ideas. *Genes Dis.* 2015, *2*, 26−34.

331

Dalton Transactions

Pyridylphosphinate metal complexes: synthesis, structural characterisation and biological activity†

Jasmine M. Cross,[a] Natalie Gallagher,[b] Jason H. Gill,[b] Mohit Jain,[b] Archibald W. McNeillis,[a] Kimberly L. Rockley,[b] Fiona H. Tscherny,[a] Natasha J. Wirszycz,[a] Dmitry S. Yufit[a] and James W. Walton*[a]

For the first time, a series of 25 pseudo-octahedral pyridylphosphinate metal complexes (Ru, Os, Rh, Ir) has been synthesised and assessed in biological systems. Each metal complex incorporates a pyridylphosphinate ligand, a monodentate halide and a capping η^6-bound aromatic ligand. Solid- and solution-state analyses of two complexes reveal a structural preference for one of a possible two diastereomers. The metal chlorides hydrolyse rapidly in D_2O to form a 1 : 1 equilibrium ratio between the aqua and chloride adducts. The pK_a of the aqua adduct depends upon the pyridyl substituent and the metal but has little dependence upon the phosphinate R' group. Toxicity was measured *in vitro* against non-small cell lung carcinoma H460 cells, with the most potent complexes reporting IC_{50} values around 50 μM. Binding studies with selected amino acids and nucleobases provide a rationale for the variation in toxicity observed within the series. Finally, an investigation into the ability of the chelating amino acid L-His to displace the phosphinate O–metal bond shows the potential for phosphinate complexes to act as prodrugs that can be activated in the intracellular environment.

Introduction

In the field of bioinorganic chemistry, platinum group metal complexes have found application in cellular imaging,[1] in enzyme inhibition[2] and as molecular probes of biological activity.[3] The therapeutic anticancer activity of these complexes is also often probed both *in vitro* and *in vivo*.[4] In the context of therapeutics, the advantages that metal complexes offer over purely organic species include: a variety of metal geometries and coordination numbers, allowing access to intricate 3-dimensional structures; numerous metal oxidation states, allowing redox-activated drugs; tuneable ligands to vary sterics and electronics about the metal centre; exchangeable ligands, for *in situ* activation and binding to biomolecules; simple and modular syntheses, allowing rapid determination of structure to activity relationships. Despite the wide-spread clinical use of the platinum-based drugs, cisplatin, oxaliplatin and carboplatin,[5] there remains issues associated with side-effects, including dose-limiting systemic toxicities[6] and acquisition of drug resistance, which reduce the efficacy and clinical utility of these drugs.[7]

[a]*Department of Chemistry, Durham University, South Road, Durham, DH1 3LE, UK. E-mail: james.walton@durham.ac.uk*
[b]*School of Medicine, Pharmacy and Health, Durham University, Wolfson Research Institute, Queen's Campus, Stockton on Tees, TS17 6BH, UK*

One class of metal complexes that has shown great promise as alternatives to Pt drugs are the pseudo-octahedral piano stool complexes,[8] in which a low-spin d^6 metal ion is capped by an η^6-phenyl or η^5-cyclopentadienyl ligand, with the remaining 3 coordination sites occupied by tri- bi- or mono-dentate ligands.

Over the past decades, many examples of piano stool metal complexes have been reported that show excellent *in vitro*[9] and *in vivo*[10] activity against cancers (Fig. 1). Variation of each component of the piano stool arrangement alters the activity of the complex. For example, in the series [(η^6-arene)Ru(en)Cl]PF$_6$ a
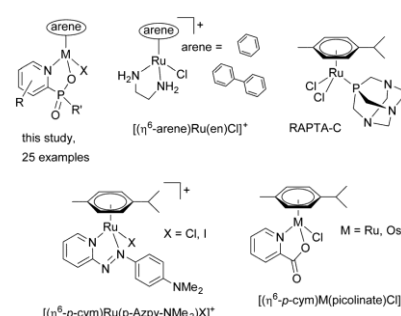

Fig. 1 Examples of metal complexes assessed for their anticancer activity.

3-fold increase in activity against human ovarian cancer cell line A2780 is observed when the arene is varied from benzene to biphenyl.[11] Similarly, modulation of the mono-dentate halide in the series [(η[6]-p-cym)Ru(p-Azpy-NMe₂)X]PF₆ from chloride to iodide results in a decrease in IC₅₀, the concentration of complex required to inhibit cell proliferation by 50%, from 13 μM to 0.69 μM in the A2780 cell line.[12] Finally, complexes with the same ligand can vary in activity, depending upon the central metal. In the [(η[6]-p-cym)M(picolinate)Cl] series, IC₅₀ values (A2780 cell line) of 45 μM (ref. 13) and 4.5 μM (ref. 14) were reported for the Ru and Os complexes, respectively. Beyond Ru(II) and Os(II), there are also a host of Ir(III) and Rh(III) piano-stool complexes, whose activity often surpasses that of related Ru(II) complexes.[15] Although often not well understood, the mechanism of action of these complexes may involve DNA binding,[16] interactions with histone proteins,[17] redox modulation[18] or enzyme inhibition.[19]

The vast majority of reported piano stool complexes in the bioinorganic chemistry field incorporate polypyridyl, carboxylate or halide ligands. Only rarely are ligands explored that include elements other than C, N and O. However, there are a host of alternatives that may offer significant advantages over the more traditional ligand systems. In this study we present a novel ligand for platinum group metal complexes: the pyridylphosphinates. We report the synthesis, structural characterisation, aqueous properties and biological activities, including *in vitro* cytotoxicities, of a series of piano stool metal complexes incorporating the pyridylphosphinate ligand (Fig. 1). Lanthanide complexes incorporating this ligand have found application in cellular imaging.[20] However, the piano stool pyridylphosphinate complexes have never been studied. Advantages of the pyridylphosphinate ligand include: biocompatibility; the presence of a ^{31}P-NMR spectroscopic handle; control over lipophilicity at phosphorus; modular synthesis allowing rapid structure–activity relationship profile and, finally, the presence a stereogenic phosphorus, which

presents an opportunity to develop enantiomerically pure metal-based complexes.[21]

Despite the host of piano stool complexes that have been reported, there is often a lack of information on biological behaviour, such as interactions between biologically relevant molecules (amino acids, proteins and nucleobases) and the metal complexes. This information is needed as the changes in structure of the complexes that take place in the cellular environment will have a profound effect upon the biological activity. Herein, we interrogate the behaviour of the novel pyridylphosphinate complexes in biological systems, by monitoring metal-halide hydrolysis, measuring pK_a values of the resultant aqua complexes and carrying out detailed binding studies with selected biomolecules.

Synthesis and structural characterisation

A series of complexes were synthesised in order to assess the factors that determine aqueous biological behaviour. Systematic variation in the metal–arene combination, the metal-bound halide, the phosphorus R′ group and the pyridyl R group led to a library of 25 new compounds (Scheme 1). Synthesis involves Pd-catalysed coupling of the phosphinate (HPO(OEt)R′) and bromo-pyridyl precursors.[22] Quantitative hydrolysis of the phosphinate ester was followed by neutralisation with NaOMe and complexation with the appropriate metal dimer [(arene)MX₂]₂. Purification by recrystallisation from CHCl₃/Et₂O gave the final complexes with 30–50% yields.†

The synthesis of complexes 7 and 8 (Scheme 2) proceeds *via* the 4-fluoropyridylphosphinate intermediate L1, which undergoes nucleophilic aromatic substitution to form the electron-rich 4-OCD₃- or electron-poor 4-Cl-pyridylphosphinate ligand, depending upon hydrolysis conditions.

Single crystals suitable for X-ray diffraction studies were grown of complexes 3 and 20 (Fig. 2A and 3). Complex 3 crystallises in the monoclinic crystal system and the $P2_1/c$ space group and displays the expected pseudo-tetrahedral geometry,
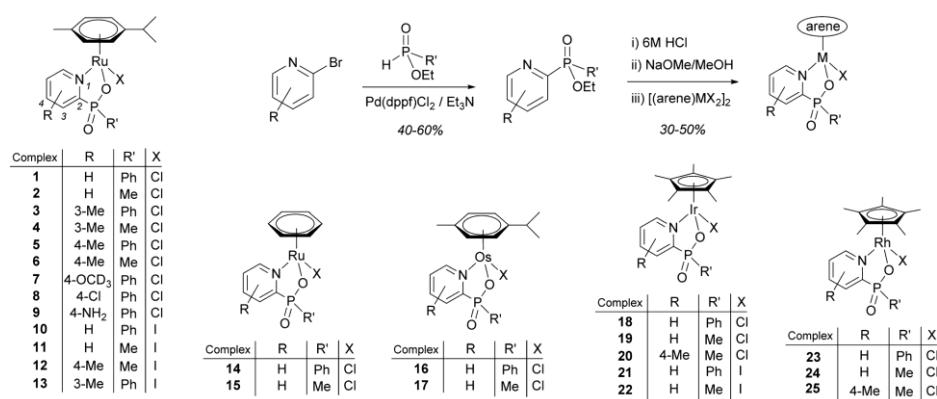
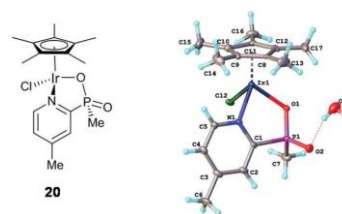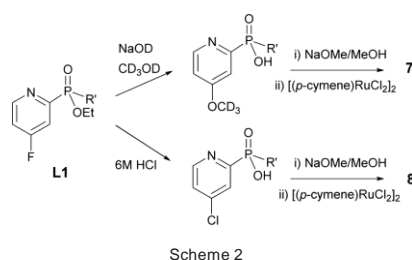Scheme 1 General synthetic pathway and list of new complexes.

333

Dalton Transactions

Paper

Scheme 2

Fig. 3 X-ray crystal structures of Ir complex 20.

with the η^6-p-cymene occupying one vertex. Ru–Cl (2.4155(6) Å), Ru–O (2.0809(14) Å) and Ru–N (2.1109(17) Å) bond lengths are almost identical to those reported for the analogous picolinate complex [(η^6-p-cym)Ru(picolinate)Cl],[13] however, the N–Ru–O bite angle is slightly larger in complex 3, at 80.50(6)° (bite angle in picolinate complex is 77.95(7)°), reflecting the larger size of the phosphinate group. Intriguingly, of the four possible stereoisomers (R or S at Ru and P, denoted $Ru_{R/S}$ and $P_{R/S}$, respectively), only one enantiomeric pair is observed in the solid state structure – Ru_SP_R and Ru_RP_S. ^{1}H-NMR indicates that a single diastereomer is also present in solution, evidenced by one set of diastereotopic p-cymene protons in the region 5–6 ppm (Fig. 2B). The origin of this stereoselectivity, which has also been observed in lanthanide pyridylphosphinate complexes,[23] can be rationalised in terms of the steric interactions between the p-cymene ligand and the P-phenyl group, which are minimised in the observed diastereomer. Weak intramolecular hydrogen bonds between the P=O and p-cymene methyl-H (2.587 Å) and the P-phenyl and pyridyl methyl-H (3.065 Å) may also influence the observed stereochemistry. In solution, slight broadening of the pyridyl Me peak reflects its proximity to the P-phenyl aromatic system, but the presence of a sharp singlet peak for the p-cymene Me

group suggests free rotation of the p-cymene ligand, as is expected for η^6-arene–metal bonds.[24]

The solid state structure of the Cp*–Ir complex 20 (Fig. 3) shows several differences from complex 3, including a Cc space group, longer bond lengths between the central metal and coordinated ligands and a wider N–metal–O bite angle of 82.00(11)°. Despite the presence of the less sterically challenging P-methyl phosphinate ligand, once again only a single diastereoisomer is observed – Ir_SP_R and Ir_RP_S. No intramolecular H-bond interactions can be observed in the crystal structure, which presents further questions over the origin of this stereoselectivity. It may be that stereoselectivity originates from the initial attack of the phosphinate ligand on the metal dimer, during the formation of the complex.

Aqueous behaviour of the complexes

To gain an understanding of the intracellular behaviour of metal complexes with biological application, it is essential to have an appreciation of the aqueous behaviour of new compounds. Upon dissolving complex 1 in a D_2O: CD_3OD (9 : 1) mix, equilibrium is established between the chloride (complex 1) and aqua (complex 1a) species (Fig. 4). ^{1}H-NMR of the p-cymene protons indicates that an approximate 1 : 1 (chloride : aqua) equilibrium is reached within 5 min and does
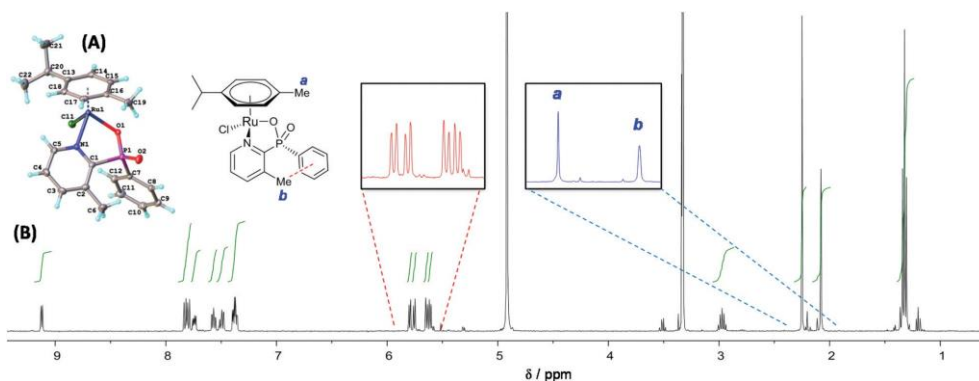

Fig. 2 (A) X-ray crystal structure of complex 3 and (B) ^{1}H-NMR spectrum (CD_3OD, 298 K, 400 MHz,), with expansions of the single set of diastereotopic p-cymene protons and of the two methyl groups.
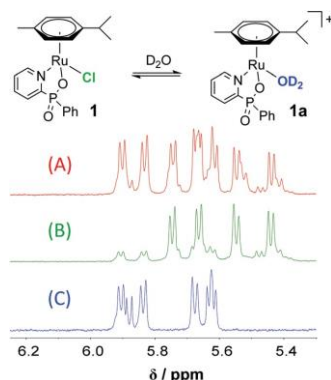
Paper

Fig. 4 ^{1}H-NMR spectra (D$_2$O: CD$_3$OD 9 : 1, 298 K, 400 MHz) of (A) complex 1 and 1a at approximately 1 : 1 equilibrium ratio, (B) chloride complex 1, following addition of 100 mM NaCl and (C) aqua complex 1a, following addition of AgNO$_3$ and filtration of AgCl.

Fig. 5 Measurement of the pK_a of aqua complex 5a by monitoring the ^{31}P-NMR spectrum (D$_2$O: CD$_3$OD 9 : 1, 298 K, 162 MHz) as a function of pH*. For Ru complexes, at approx. pH* >11 formation of the hydroxy-bridged dimer D1 is observed.

not shift over the course of 24 h (Fig. 4A). To confirm that the observed species are the chloride and aqua adducts, the complex was dissolved in 100 mM NaCl (Fig. 4B) and in aqueous AgNO$_3$, followed by filtration of AgCl (Fig. 4C), leading to the selective formation of the chloride and aqua adducts, respectively, each showing a characteristic set of diastereotopic protons. The analogous Ru–iodide complex also undergoes rapid hydrolysis with around 60% of the complex remaining as the intact iodide species.

At the extracellular chloride concentration (approx. 100 mM), the pyridylphosphinate complexes remains intact as the chloride adduct, but at lower intracellular chloride concentration (approx. 20 mM in cytoplasm)[25] significant amounts of the aqua adduct are present. With this in mind, we sought to measure the pK_a of the bound water molecule and to establish how the pK_a varies with the choice of central metal and coordinated ligands. pK_a^* (pK_a measured in D$_2$O) values were measured by monitoring the ^{31}P- and ^{1}H-NMR spectra of selected aqua complexes in D$_2$O : CD$_3$OD (9 : 1) as a function of pH* (pH values in D$_2$O solution, Fig. 5), according to established procedures[25] (see ESI† for full details). pK_a^* values were converted to pK_a values using the equation pK_a ¼ 0.929pK_a^* þ 0.42.[26] By comparing pK_a values of selected aqua complexes (Table 1), it is apparent that a more electron donating pyridyl ligand leads to a higher pK_a. This is shown by the increase in values in the order 5a < 3a < 7a for complexes with 4-Me, 3-Me and OCD$_3$ pyridyl substituents, respectively. This order reflects the higher pH required to deprotonate H$_2$O bound to a more electron-rich metal centre. The phosphorus-bound R′ group has little effect on pK_a, as can be seen by comparing values for 3a and 4a. Finally, as expected, the pK_a value for the Ir complex 20a is lower than that of the equivalent Rh complex 25a, reflecting the increased metal–oxygen bond strength of the heavier congener.[27] For each of the studied Ru complexes, the hydroxyl-bridged dimer D1 (Fig. 5) forms at
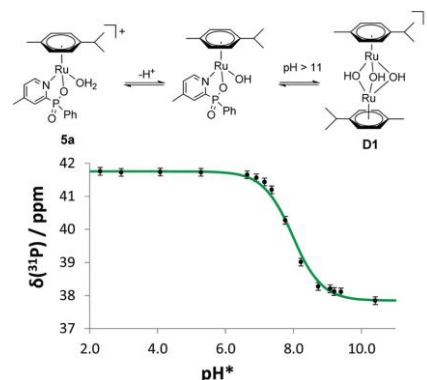
Table 1 pK_a values for selected aqua complexes (D$_2$O: CD$_3$OD 9 : 1, 298 K). pK_a values were measured by monitoring changes in ^{31}P-NMR and ^{1}H-NMR spectra and converted to pK_a using the equation pK_a ¼ 0.929pK_a^* þ 0.42 [26]

Complex	R	R′	{M(arene)}	pK_a
3a	3-Me	Ph	{Ru(p-cymene)}	9.34 ± 0.04
4a	3-Me	Me	{Ru(p-cymene)}	9.18 ± 0.19
5a	4-Me	Ph	{Ru(p-cymene)}	7.76 ± 0.13
7a	4-OCD$_3$	Ph	{Ru(p-cymene)}	10.08 ± 0.05
20a	4-Me	Me	{Ir(Cp*)}	9.31 ± 0.07
25a	4-Me	Me	{Rh(Cp*)}	10.95 ± 0.04

strongly basic pH (typically >pH 11), with concomitant loss of the pyridylphosphinate ligand.† The formation of this dimeric species from Ru piano stool complexes at elevated pH has been observed previously and the dimer is known to be non-cytotoxic.[28] NMR experiments indicate that dimer formation is partially reversible upon lowering the pH, but that complete regeneration of the starting complex does not take place.

Cytotoxicity studies

The toxicity of each complex was assessed against non-small cell lung carcinoma H460 cells. Each complex was incubated with H460 cells for 96 h at concentrations ranging from 0.1 to 200 μM (aqueous media containing 0.1% DMSO) and IC$_{50}$ values were measured using the MTT assay (see ESI† for details). The solubility of complexes at these concentrations was assessed to ensure the compounds are fully dissolved (see ESI† for details). Selected results are shown in Table 2 and represent the mean value for data from at least three experiments. All Ru complexes incorporating chloride ligands are non-toxic up to 200 μM. The most cytotoxic species are the iridium–Cp* complexes 21 and 22, each with IC$_{50}$ values of 50 ± 5 μM, respectively. The presence of the iodide ligand appears to play

Table 2 IC$_{50}$ values for selected complexes measured using the MTT assay (96 h) against the non-small cell lung carcinoma H460 cell line. Entries are the mean value for data from at least three experiments. Complexes not included were found to have IC$_{50}$ > 200 μM

Complex	R	R′	M	Arene	X	IC$_{50}$/μM
1	H	Ph	Ru	cym	Cl	>200
10	H	Ph	Ru	cym	I	65 ± 12
11	H	Me	Ru	cym	I	>200
18	H	Ph	Ir	Cp*	Cl	>200
19	H	Me	Ir	Cp*	Cl	>200
20	4-Me	Me	Ir	Cp*	Cl	140 ± 40
21	H	Ph	Ir	Cp*	I	52 ± 2
22	H	Me	Ir	Cp*	I	53 ± 4
25	4-Me	Me	Rh	Cp*	Cl	135 ± 17
Cisplatin	—	—	—	—	—	0.80 ± 0.01

an important role in the observed toxicity, as the analogous chloride complexes, 18 and 19, gave IC$_{50}$ values >200 μM. Comparing complexes 21 (*P*-phenyl) and 22 (*P*-methyl), it would appear that the phosphorus-R group has little influence upon the toxicity. However, this is not the case when comparing the Ru-*p*-cymene complexes 10 and 11, for which the *P*-phenyl analogue has significantly greater cytotoxicity than the *P*-methyl complex. A comparison with cisplatin (IC$_{50}$ = 0.80 ± 0.01 under the experimental conditions), shows that in general this class of complexes have low cytotoxicity. While ineffective as cytotoxic agents, this feature may bode well for uses in applications such as enzyme inhibitors.

A general feature within this series is that the complexes incorporating monodentate iodide ligands have higher toxicities than the corresponding chloride complexes. The extent of hydrolysis of the iodide complexes is less than that of the chloride complexes, leading to the conclusion that a mechanism of action involving hydrolysis and DNA binding, as is often proposed for piano stool metal complexes, may not be the main mechanism of action operating for this series of complexes. Whatever the mechanism, the observation of higher toxicity for iodide complexes is consistent with previously published reports[12,29] for both Ru- and Os-based anticancer complexes. Studies are ongoing to elucidate a potential mechanism of action for these species.

Binding studies

In general, the Ru complexes herein have IC$_{50}$ values greater than 200 μM. In an attempt to understand this low cytotoxicity, binding studies were carried out with several biomolecules. Addition of AgNO$_3$ to complex 1 dissolved in D$_2$O, followed by filtration of the resulting AgCl precipitate, gave the aqua adduct, 1a. Mass spectrometry and NMR spectroscopy (^{1}H and ^{31}P) were used to identify the presence and extent of biomolecule binding after addition of one and two equivalents of biomolecule to 1a, at 1 h and 16 h time-points (Fig. 6 and Table 3). The biomolecules selected for investigation were L-alanine (L-Ala), L-threonine (L-Thr), L-histidine (L-His), imidazole and 9-ethylguanine (9-EtG). No evidence for binding between 1a and 1 equivalent of amino acids L-Ala and L-Thr
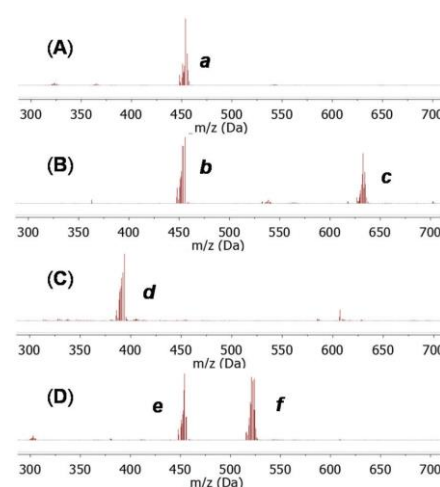

Fig. 6 Mass spectra for complex 1a in the presence of (A) L-alanine, (B) 9-ethylguanine, (C) L-histidine and (D) imidazole. Peaks labelled a–f correlate to peaks in Table 3.

Table 3 Proposed species that give rise to mass peaks in Fig. 6, upon addition of selected biomolecules. Tabulated *m/z* values a–f correspond to mass peaks in Fig. 6

Biomolecule	*m/z*	Species
L-Ala	*a*: 454.3	[1a − H$_2$O]$^+$
L-Thr	454.6	[1a − H$_2$O]$^+$
9-EtG	*b*: 453.8	[1a − H$_2$O]$^+$
	c: 632.9	1b
L-His	*d*: 390.6	1c
Imidazole	*e*: 454.0	[1a − H$_2$O]$^+$
	f: 522.4	1d

was observed after 1 h. In contrast, addition of 1 equivalent of 9-EtG led to a peak in the mass spectrum corresponding to the 9-EtG adduct of 1a, following loss of H$_2$O. ^{1}H-NMR analysis indicated the formation of a bond between Ru and N7 on
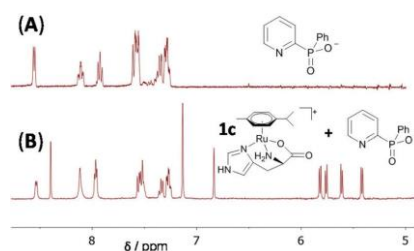
336

Paper

View Article Online

Dalton Transactions

Fig. 7 ^{1}H-NMR spectra (D$_2$O: CD$_3$OD 9 : 1, 298 K, 400 MHz) of (A) uncomplexed pyridylphosphinate ligand and (B) products of addition of 2 equivalents of L-His to complex 1a, showing the decomplexation of the pyridylphosphinate ligand and the formation of L-His complex, 1c.

9-EtG, with around 50% bound complex in solution. This mode of binding is consistent with previous reports that have proposed a mechanism of action for the anticancer behaviour of Ru complexes to involve DNA binding, leading to apoptosis.[16]

Upon addition of 1 equivalent of L-His, an adduct was observed, consistent with replacement of H$_2$O for L-His, binding though an imidazole N. When the sample was subjected to a second equivalent of L-His and left to equilibrate over 16 h, a species formed in which the pyridylphosphinate ligand is displaced and the L-His binds κ^3 (Fig. 7). The observed Ru–(L-His) complex, 1c, is known to be non-cytotoxic[30] and its formation presents a potential explanation of the low cytotoxicity of Ru chloride complexes described in this report. It follows that the higher cytotoxicity of the iodide-complexes, 10, 21 and 22, is due to the metal–iodide bond being less labile towards aquation and therefore less likely to undergo decomplexation by chelating biomolecules. It should be noted that the only tested biomolecule able to displace the pyridylphosphinate ligand was L-His. Addition of 2 equivalents of imidazole (16 h) leads to 1 : 1 adduct formation, with loss of H$_2$O, but no ligand displacement. The cytotoxicity of the displaced ligand of complex 1 (shown in Fig. 7A) was assessed using the MTT assay and found to by non-cytotoxic up to 200 μM. In future studies it may be possible to tune the lability of pyridylphosphinate ligands, so that the complexes remain intact in the high chloride concentration of the extracellular medium but are able to release some useful payload within the cell where the chloride concentration is lower.

Conclusions

A series of 25 new piano-stool pyridylphosphinate complexes has been synthesised, characterised and assessed in biologically-relevant systems. The properties of the complexes depend upon their various components – metal ion, arene, pyridyl substituent and *P*-alkyl group – which can be varied with relative ease. Aqueous solubility and stability is good. Ru–Cl complexes are non-toxic up to 200 μM, which bodes well for their use as a scaffold for metal-based enzyme inhibitors. Ir–I complexes are

more toxic to cells, so may have the potential to act as anticancer agents, although toxicity remains low compared to cisplatin. It was discovered that decomplexation of the ligand from complex 1 occurs in the presence of excess L-His, following hydrolysis of the Ru–Cl bond. This has the potential to be exploited in the form of complexes that deliver and release useful payloads to the cell. The rate of aquation and the pK_a of the resulting aqua species can be tuned by varying the pyridyl substituent and the judicious choice of metal–halide combination. Studies are ongoing to investigate the cell uptake, localisation and any potential antimetastatic behaviour of these exciting new complexes and to exploit the lability of the phenylphosphinate Ru bond to design responsive biologically active complexes.

Notes and references

1 (*a*) S. W. Botchway, M. Charnley, J. W. Haycock, A. W. Parker, D. L. Rochester, J. A. Weinstein and J. A. G. Williams, *Proc. Natl. Acad. Sci. U. S. A.*, 2008, 105, 16071; (*b*) D. Lloyd, M. P. Coogan and S. J. A. Pope, *Rev. Fluoresc.*, 2012, 2010, 15.

2 (*a*) M. Dorr and E. Meggers, *Curr. Opin. Chem. Biol.*, 2014, 19, 76; (*b*) D. Hu, Y. Liu, Y.-T. Lai, K.-C. Tong, Y.-M. Fung, C.-N. Lok and C.-M. Che, *Angew. Chem., Int. Ed.*, 2016, 55, 1387.

3 (*a*) F. E. Poynton, J. P. Hall, P. M. Keane, C. Schwarz, I. V. Sazanovich, M. Towrie, T. Gunnlaugsson, C. J. Cardin, D. J. Cardin, S. J. Quinn, C. Long and J. M. Kelly, *Chem. Sci.*, 2016, 7, 3075; (*b*) K. K. W. Lo, T. K. M. Lee, J. S. Y. Lau, W. L. Poon and S. H. Cheng, *Inorg. Chem.*, 2008, 47, 200; (*c*) K. K.-W. Lo, *Acc. Chem. Res.*, 2015, 48, 2985.

4 For recent reviews of metal-based anticancer agents see. (a) G. Gasser, I. Ott and N. Metzler-Nolte, *J. Med. Chem.*, 2011, 54, 3; (*b*) I. Ott and R. Gust, *Arch. Pharm.*, 2007, 340, 117; (*c*) S. Medici, M. Peana, V. M. Nurchi, J. I. Lachowicz, G. Crisponi and M. A. Zoroddu, *Coord. Chem. Rev.*, 2015, 329; (*d*) N. Muhammad and Z. Guo, *Curr. Opin. Chem. Biol.*, 2014, 19, 144.

5 (*a*) B. Rosenberg, L. van Camp and T. Krigas, *Nature*, 1965, 205, 698; (*b*) Y. Kidani, K. Inagaki, M. Iigo, A. Hoshi and K. Kuretani, *J. Med. Chem.*, 1978, 21, 1315; (*c*) K. R. Harrap, *Cancer Treat. Rev.*, 1985, 12, 21.

6 (*a*) H. Matsushima, K. Yonemura, K. Ohishi and A. Hishida, *J. Lab. Clin. Med.*, 1998, 131, 518; (*b*) N. E. Madias and J. T. Harrington, *Am. J. Med.*, 1978, 65, 307.

7 (*a*) M. Kartalou and J. M. Essigmann, *Mutat. Res.*, 2001, 478, 23; (*b*) K. J. Mellish, L. R. Kelland and K. R. Harrap, *Br. J. Cancer*, 1993, 68, 240.

8 A. A. Nazarov, C. G. Hartinger and P. J. Dyson, *J. Organomet. Chem.*, 2014, 751, 251.

9 (*a*) R. E. Morris, R. E. Aird, P. Del Socorro-Murdoch, H. Chen, J. Cummings, N. D. Hughes, S. Parsons, A. Parkin, G. Boyd, D. I. Jodrell and P. J. Sadler, *J. Med. Chem.*, 2001, 44, 3616; (*b*) M. Pernot, T. Bastogne, N. P. E. Barry, B. Therrien, G. Koellensperger, S. Hann, V. Reshetov and M. Barberi-Heyob, *J. Photochem. Photobiol., B*, 2012, 117, 80; (*c*) A. A. Nazarov, S. M. Meier, O. Zava, Y. N. Nosova, E. R. Milaeva, C. G. Hartinger and P. J. Dyson, *Dalton Trans.*, 2015, 44, 3614; (*d*) S. M. Meier, M. Hanif, Z. Adhireksan, V. Pichler, M. Novak, E. Jirkovsky, M. A. Jakupec, V. B. Arion, C. A. Davey, B. K. Keppler and C. G. Hartinger, *Chem. Sci.*, 2013, 4, 1837; (*e*) B. S. Murray, L. Menin, R. Scopelliti and P. J. Dyson, *Chem. Sci.*, 2014, 5, 2536.

10 (*a*) C. Scolaro, A. Bergamo, L. Brescacin, R. Delfino, M. Cocchietto, G. Laurenczy, T. J. Geldbach, G. Sava and P. J. Dyson, *J. Med. Chem.*, 2005, 48, 4161; (*b*) A. Weiss, R. H. Berndsen, M. Dubois, C. Müller, R. Schibli, A. W. Griffioen, P. J. Dyson and P. Nowak-Sliwinska, *Chem. Sci.*, 2014, 5, 4742; (*c*) X. Meng, M. L. Leyva, M. Jenny, I. Gross, S. Benosman, B. Fricker, S. Harlepp, P. Hébraud, A. Boos, P. Wlosik, P. Bischoff, C. Sirlin, M. Pfeffer, J. P. Loeffler and C. Gaiddon, *Cancer Res.*, 2009, 69, 5458.

11 (*a*) O. Novakova, H. Chen, O. Vrana, A. Rodger, P. J. Sadler and V. Brabec, *Biochemistry*, 2003, 42, 11544; (*b*) R. E. Morris, R. E. Aird, P. Del Socorro-Murdoch, H. Chen, J. Cummings, N. D. Hughes, S. Parsons, A. Parkin, G. Boyd, D. I. Jodrell and P. J. Sadler, *J. Med. Chem.*, 2001, 44, 3616.

12 S. H. Van Rijt, I. Romero-Canelón, Y. Fu, S. D. Shnyder and P. J. Sadler, *Metallomics*, 2014, 6, 1014.

13 K. D. Camm, A. El-Sokkary, A. L. Gott, P. G. Stockley, T. Belyaevab and P. C. McGowan, *Dalton Trans.*, 2009, 48, 10914.

14 A. F. A. Peacock, S. Parsons and P. J. Sadler, *J. Am. Chem. Soc.*, 2007, 129, 3348.

15 (*a*) Z. Liu, A. Habtemariam, A. M. Pizarro, S. A. Fletcher, A. Kisova, O. Vrana, L. Salassa, P. C. A. Bruijnincx, G. J. Clarkson, V. Brabec and P. J. Sadler, *J. Med. Chem.*, 2011, 54, 3011; (*b*) Z. Liu, I. Romero-Canelón, B. Qamar, J. M. Hearn, A. Habtemariam, N. P. E. Berry, A. M. Pizarro, G. J. Clarkson and P. J. Sadler, *Angew. Chem., Int. Ed.*, 2014, 53, 3941; (*c*) Z. Liu and P. J. Sadler, *Acc. Chem. Res.*, 2014, 47, 1174; (*d*) M. Grasa, B. Therrien, G. Süss-Fink, A. Casini, F. Edafe and P. J. Dyson, *J. Organomet. Chem.*, 2010, 695, 1119; (*e*) L. C. Sudding, R. Payne, P. Govender, F. Edafe, C. M. Clavel, P. J. Dyson, B. Therrien and G. S. Smith, *J. Organomet. Chem.*, 2014, 774, 79.

16 H. Chen, J. A. Parkinson, S. Parsons, R. A. Coxall, R. O. Gould and P. J. Sadler, *J. Am. Chem. Soc.*, 2002, 124, 3064.

17 Z. Adhireksan, G. E. Davey, P. Campomanes, M. Groessl, C. M. Clavel, H. Yu, A. A. Nazarov, C. Hui Fang Yeo, W. Han Ang, P. Dröge, U. Rothlisberger, P. J. Dyson and C. A. Davey, *Nat. Commun.*, 2014, 5, 3462.

18 (*a*) I. Romero-Canelón and P. J. Sadler, *Inorg. Chem.*, 2013, 52, 12276; (*b*) K. Suntharalingam, Y. Song and S. J. Lippard, *Chem. Commun.*, 2014, 50, 2465.

19 (*a*) A. de Almeida, B. L. Oliveira, J. D. G. Correia, G. Soveral and A. Casini, *Coord. Chem. Rev.*, 2013, 257, 2689; (*b*) L. Feng, Y. Geisselbrecht, S. Blanck, A. Wilbuer, G. E. Atilla-Gokcumen, P. Filippakopoulos, K. Kräling, M. A. Celik, K. Harms, J. Maksimoska, R. Marmorstein, G. Frenking, S. Knapp, L.-O. Essen and E. Meggers, *J. Am. Chem. Soc.*, 2011, 133, 5976; (*c*) E. Meggers, G. E. Atilla-Gokcumen, K. Gründler, C. Frias and A. Prokop, *Dalton Trans.*, 2009, 10882.

20 (*a*) S. J. Butler, M. Delbianco, L. Lamarque, B. K. McMahon, E. R. Neil, R. Pal, D. Parker, J. W. Walton and J. M. Zwier, *Dalton Trans.*, 2015, 44, 4791; (*b*) M. Soulié, F. Latzko, E. Bourrier, V. Placide, S. J. Butler, R. Pal, J. W. Walton, P. L. Baldeck, B. Le Guennic, C. Andraud, J. M. Zwier, L. Lamarque, D. Parker and O. Maury, *Chem. – Eur. J.*, 2014, 20, 8636; (*c*) A. J. Palmer, S. H. Ford, S. J. Butler, T. J. Hawkins, P. J. Hussey, R. Pal, J. W. Walton and D. Parker, *RSC Adv.*, 2014, 4, 9356.

21 Examples of enantiomerically pure anticancer metal complexes include. (*a*) G. E. Atilla-Gokcumen, L. Di Costanzo and E. Meggers, *J. Biol. Inorg. Chem.*, 2011, 16, 45; (*b*) E. Menéndez-Pedregal, Á. Manteca, J. Sánchez, J. Díez, M. P. Gamasa and E. Lastra, *Eur. J. Inorg. Chem.*, 2015, 1424.

22 (*a*) J. W. Walton, L. Di Bari, D. Parker, G. Pescitelli, H. Puschmann and D. S. Yufit, *Chem. Commun.*, 2011, 47, 12289; (*b*) J. W. Walton, R. Carr, N. H. Evans, A. M. Funk, A. M. Kenwright, D. Parker, D. S. Yufit, M. Botta, S. De Pinto and K.-L. Wong, *Inorg. Chem.*, 2012, 51, 8042.

23 (*a*) J. W. Walton, A. Bourdolle, S. J. Butler, M. Soulie, M. Delbianco, B. K. McMahon, R. Pal, H. Puschmann, J. M. Zwier, L. Lamarque, O. Maury, C. Andraud and D. Parker, *Chem. Commun.*, 2013, 49, 1600; (*b*) S. J. Butler, R. Pal, B. K. McMahon, D. Parker and J. W. Walton, *Chem. – Eur. J.*, 2013, 19, 9511.

24 C. Gossens, I. Tavernelli and U. Rothlisberger, *J. Phys. Chem. A*, 2009, 113, 11888.

25 S. H. Van Rijt, A. F. A. Peacock, R. D. L. Johnstone, S. Parsons and P. J. Sadler, *Inorg. Chem.*, 2009, 48, 1753.

26 A. Krezel and W. J. Bal, *Inorg. Biochem.*, 2004, 98, 161.

27 P. Moore, in *Inorganic Reaction Mechanisms*, ed. A. McAuley, CRC Press, Boca Raton, 1988, vol. 4, p. 129.

28 (*a*) M. Melchart, A. Habtemariam, S. Parsons, S. A. Moggach and P. J. Sadler, *Inorg. Chim. Acta*, 2006, 359, 3020; (*b*) W. Kandioller, C. Hartinger, A. A. Nazarov, M. L. Kuznetsov, R. John, C. Bartel, M. A. Jakupec, V. B. Arion and B. K. Keppler, *Organometallics*, 2009, 28, 4249.

29 I. Romero-Canelón, L. Salassa and P. J. Sadler, *J. Med. Chem.*, 2013, 56, 1291.

30 T. G. Scrase, M. J. O'Neill, A. J. Peel, P. W. Senior, P. D. Matthews, H. Shi, S. R. Boss and P. D. Barker, *Inorg. Chem.*, 2015, 54, 3118.

338